ABSTRACT

Computational Study of Glycopeptide Antibiotics Interactions with *Staphylococcus aureus* Peptidoglycan

Olatunde P. Olademehin, Ph.D.

Mentor: Kevin. L. Shuford, Ph.D.

Staphylococcus aureus is generally known for its ability to acquire resistance to any antibiotic. Methicillin-resistant *S. aureus* is one of the leading etiological agents responsible for the hospital- and community-acquired infections. Due to the rise of multi-drug resistant bacteria, there is a great need for continuous discovery and development of new antibiotics to overcome the inevitable emergence of antibiotic resistance in pathogens. Numerous classes of antibiotics, including glycopeptide antibiotics, target bacterial cell wall biosynthesis, where the cell wall plays an essential role in maintaining the structural integrity and morphology of bacteria. The major component of the cell wall is peptidoglycan (PG), a unique feature found in all bacteria. Inhibition of PG biosynthesis during cell growth results in bacterial cell lysis. This dissertation examines the glycopeptide antibiotics interactions with PG by molecular dynamics simulations to provide insight into modifying existing therapeutics or developing novel pharmacological therapeutics. Steered molecular dynamics simulations and umbrella sampling were also applied, when necessary, to characterize the thermodynamic properties and the dynamics of select glycopeptide-PG complexes. Our simulations provide insights into the role of

amino acid residues, which are not directly involved in the dipeptide binding of glycopeptides, in improving the binding of the glycopeptides to PG. We also reveal computational evidence of a secondary-binding site contributing to the enhancement in the binding of oritavancin to PG compared to other glycopeptide antibiotics lacking the additional binding interactions.

Computational Study of Glycopeptide Antibiotics Interactions with *Staphylococcus aureus* Peptidoglycan

by

Olatunde P. Olademehin, B.S., M.S.

A Dissertation

Approved by the Department of Chemistry and Biochemistry

_____

Patrick J. Farmer, Ph.D., Chairperson

Submitted to the Graduate Faculty of
Baylor University in Partial Fulfillment of the
Requirements for the Degree
of

Doctor of Philosophy

Approved by the Dissertation Committee

_____

Kevin L. Shuford, Ph.D., Chairperson

_____

Carlos E. Manzanares, Ph.D.

_____

Darrin J. Bellert, Ph.D.

_____

Bryan F. Shaw, Ph.D.

_____

Bessie Kebaara, Ph.D.

Accepted by the Graduate School

August 2021

_____

J. Larry Lyon, Ph.D., Dean

Page bearing signatures is kept on file in the Graduate School.

TABLE OF CONTENTS

LIST OF FIGURES

LIST OF TABLES

LIST OF ABBREVIATIONS

AFE:	Alchemical Free Energy
CGenFF:	CHARMM General Forcefield
COM:	Center-of-Mass
DFT:	Density Functional Theory
DNA:	Deoxyribonucleic acid
DR:	Distance Restraint
FDA:	Food and Drug Administration
FDASIA:	Food and Drug Administration Safety and Innovation Act
FEP:	Free Energy of Perturbation
GAIN:	Generating Antibiotics Incentives Now
GlcNAc:	N-Acetylglucosamine
LC-MS:	Liquid Chromatography-Mass Spectrometry
LIE:	Linear Integration Energy
LINCS:	Linear Constraint Solver
MD:	Molecular Dynamics
MIC:	Minimum Inhibitory Concentration
MM:	Molecular Mechanics
MM/GBSA:	Molecular Mechanics Generalized Born Surface Area
MM/PBSA:	Molecular Mechanics Poisson-Boltzmann Surface Area
MRSA:	Methicillin-Resistant *Staphylococcus aureus*

MurNAc:	N-Acetylmuramic acid
NMR:	Nuclear Magnetic Resonance
NOE:	Nuclear Overhauser Effect
NPT:	Constant Number of Particles, Pressure and Temperature
NVE:	Constant Number of Particles, Volume and Energy
NVT:	Constant Number of Particles, Volume and Temperature
PB:	Poisson-Boltzmann
PBPs:	Penicillin-Binding Proteins
PDB:	Protein Data Bank
PG:	Peptidoglycan
PME:	Particle Mesh Ewald
PMF:	Potential of Mean Force
PR:	Position Restraint
Rg:	Radius of Gyration
RMSD:	Root-Mean-Square Deviation
SA:	Surface Area
SASA:	Solvent-Accessible Surface Area
SAV:	Solvent-Accessible Volume
SMD:	Steered Molecular Dynamics
TI:	Thermodynamic Integration
TIP3P:	Transferable Intermolecular Potential with 3 Points
UDP:	Uridine Diphosphate
UMP:	Uridine Monophosphate

US: Umbrella Sampling

VRE: Vancomycin-Resistant Enterococci

VRSA: Vancomycin-Resistant *S. aureus*

WHAM: Weighted Histogram Analysis Method

ACKNOWLEDGMENTS

Thanks be to God who makes all things beautiful in His time. My profound appreciation goes to Dr. Sung Joon Kim and Dr. Kevin Shuford. Both have contributed immensely to my graduate school journey. I have been privileged to learn from these two outstanding mentors, whose counsel and guidance have shaped me as a learner, teacher, and researcher. Special thanks to Dr. Shuford for taking me under his wings when Dr. Kim moved to Howard University. I am also immensely grateful to Dr. Carlos Manzanares, Dr. Darrin Bellert, Dr. Bryan Shaw, and Dr. Bessie Kebaara for serving on my dissertation committee. Thank you all for your time, advisement, and kindness. I would also like to thank the Department of Chemistry and Biochemistry for providing support and a conducive environment to help graduate students thrive. Also, thanks for trusting and nominating me as a Postdoctoral Teaching Fellow. Thanks to Baylor University for providing me with financial support and access to the high-performance computing cluster, Kodiak. My appreciation to Baylor Graduate School for providing financial resources to help me present my research at academic conferences and for making available diverse resources to help graduate students complete their degrees.

During my Ph.D. program, many friends and colleagues made my time at Baylor memorable and joyous. Thanks to Dr. Emvia Calixte, Dr. Thomas Ellington, Paapa Nkrumah-Ababio, Daniel Agu, Idorenyin Udoetok, Paul Akula, Dr. Uchenna Peters, Dr. Dimuthu Weerawardene, Dr. Justina Ogodo, Dr. James Chang, Dr. Nathaniel Adegboyega, Dr. Mieke Lahousse, Binayak Rimal, Frank Liu, Ricardo Francis, Uvin De Alwis, Daniel

Devore, Kirk French, and the many undergraduate students with whom I shared my joy of teaching and learning. Thanks to my writing partner, Miriel Reneau, for keeping me accountable in the dissertation writing process. Also, special thanks to Melanie Briscoe for the opportunity to teach at the Baylor Tutoring Center. Thanks to the Baylor International Office for the opportunity to serve as one of their ambassadors to help international students transition smoothly to life in the U.S. I am also grateful to my church community at Antioch Waco.

Special thanks to my parents for their prayers and sacrifices to help me achieve the dreams in my heart. To my siblings, Titilayo, Oladunni, Afolabi, Segun, and Mojisola, thank you for supporting me through this journey.

This acknowledgment would not be complete without a special recognition to my wife, Sarah. Just like the peptidoglycan maintains the structural integrity and morphology of bacteria, you are the backbone upon which I achieved this remarkable feat of completing my Ph.D. program. Heaven smiled on me when you walked into my life. To our son, Josiah, thanks for enduring so many nights without seeing your dad. You are a precious gift from God to Sarah and me.

For my parents, Chief and Mrs. Olademehin; Though you never had a college education, you encouraged me to get to the peak of my academic pursuit.

CHAPTER ONE

Introduction

1.1 Motivation

*Staphylococcus aureu*s, a Gram-positive bacterium, is generally known for its ability to acquire resistance to any antibiotic. Infections resulting from antibiotic-resistant strains of *S. aureus* have reached epidemic proportions globally[1]. Staphylococci are among the most common bacteria that cause post-surgical infections in U.S. hospitals. Methicillin-resistant *S. aureus* (MRSA) strains are currently one of the leading causes of hospital-acquired and community-acquired infections, causing more deaths in the USA than tuberculosis and AIDS combined[2-3]. A fundamental biological property of *S. aureus* is the ability to colonize normal people asymptomatically. Approximately 30% of humans are asymptomatic nasal carriers of *S. aureus*[4-5].

The development of resistance by pathogenic bacteria, such as *S. aureus*, against antibiotics is inevitable[6], given the large number of bacteria in an infection cycle, the rapid generation time, and the intrinsic rate of mutation. The resistance could arise due to the mutation of a single gene, or multiple mutations may accumulate before remarkable growth advantage and resistance occurs. The rising prevalence of MRSA infections led to more usage of vancomycin and other similar glycopeptides, considered as drugs of last resort. Despite its high potency, vancomycin-resistant pathogens emerged from improper and frequent use. The stakes could not be higher. Without the development of new therapeutically viable antibiotics, we face a bleak future of returning to the pre-antibiotic

era plagued by misery, suffering, and death caused by infectious disease. Generating Antibiotics Incentives Now (GAIN) was passed in 2012 as part of the Food and Drug Administration Safety and Innovation Act (FDASIA) to combat the public health threat of antibacterial drug resistance by encouraging the development and approval of new antibacterial and antifungal drugs[7].

The bacterial cell wall is one of the main targets of antibiotics. Bacteria are remarkably able to change their cell wall structure depending on their individual needs. This change in the cell wall also enables the bacterial cell to better adapt to changing and often challenging environmental conditions. Understanding the changes that occur on bacterial cell wall structures in the presence of antibiotics and the interactions between the bacterial cell wall structures and selected antibiotics are crucial in the redesign of existing antibiotics or the development of novel antibiotics against emerging resistant pathogens. Our approach is to use computational analysis to gain more insight into the interactions of bacterial cell wall structures with glycopeptide antibiotics at the atomic level. The effects of different modifications of the selected antibiotics on our simulations are also considered.

1.2 Antibiotics

Antibiotics are molecules that can stop bacterial growth (bacteriostatic) or kill them outright (bactericidal). They are either human-made synthetic chemicals, semisynthetic or natural products designed to block crucial processes in bacterial cells selectively. Most antibiotics approved for clinical use in the past 70 years have been through natural product screening[8]. Although there are many promising prospects for antibiotics from natural products, many microbes are unculturable in the laboratory. Research is ongoing for better

ways of culturing microbes in their natural habitat to discover novel antibiotics[9-10]. The natural products antibiotics are chemical weapons from one species of microbe (bacteria or fungi) produced to kill off other microbes within its microenvironment to wade off competition for space and/or nutrients. Alexander Fleming discovered the first antibiotic, penicillin, in 1928. This discovery marked the beginning of an unprecedented era of man's immunity from bacterial infections.

Antibiotics are classified based on their targets at the bacterial cell surface or inside the cell. The four major targets of antibiotics include (i) Bacterial cell wall biosynthesis. This is inhibited by β-lactam antibiotics and the vancomycin class of glycopeptides. (ii) Bacterial protein biosynthesis. Bacterial ribosomes are selectively hindered at the 30S subunits by aminoglycosides and tetracyclines and at the 50S subunits by the macrolide family of antibiotics. (iii) Bacterial DNA replication and repair. The antibacterial drugs belonging to the quinolone family, such as ciprofloxacin, act to block bacterial DNA replication via inhibition of DNA gyrase. (iv) The folate coenzyme biosynthetic pathway. The sulfa drugs and trimethoprim block folate synthesis, which is essential for providing monomer units for DNA synthesis[11]. Table 1.1 shows examples of different antibiotics classified based on their target systems.

The emergent of resistant pathogens to all the important groups of antibiotics is an urgent reminder for the development of new antibiotics. Most chemical scaffolds from which the current antibiotics are derived were introduced between the mid-1930s and the early 1960s[12] (Figure 1.1). Bacterial infections that were once routinely treatable are no longer responsive to the standard antibiotic therapy. Effective mechanisms of resistance in bacterial pathogens include the destruction of the antibiotic, active extrusion of antibiotics

by transmembrane pumps and modification of target structures to antibiotic insensitivity. Antibiotics represented 5% of the global pharmaceutical market and provided about $42 billion in annual sales in 2009. Cephalosporin class of antibiotics was the largest in terms of sales, generating $11.9 billion in the same year[13]. In spite of the enormous market and pressing need for antibiotics, only a few antibiotic developments have made it to clinical approval over the past thirty years. This is because antibiotics are used in smaller quantities than other drugs, and their prescription only lasts for weeks, whereas prescription for chronic illnesses can last years or decades. Also, the use of a newly approved antibiotic is probably more restricted to the treatment of serious bacterial infections, limiting the amount of revenue that can be generated. The resultant effect is a continual increase of resistant pathogens while the development of novel antibiotics is on the decline.

Table 1.1. Classification of antibiotics

Target Systems	Classes of Antibiotics
Cell Wall Synthesis	β-lactams (Penicillin, Carbapenems, Cephalosporins, Monobactams, etc.)
	Bacitracin
	Cycloserines
	Fosfomycin
	Glycopeptides (Vancomycin, Teicoplanin, Dalbavancin, Oritavancin, etc.)
	Lipsidomycin B
	Lantibiotics (Mersacidine)
	Moenomycin
	Ramoplanin
	Tunicamycin
Protein Synthesis Inhibitors	Aminoglycosides (gentamicin)
	Tetracyclines
	Chloramphenicol
	Clindamycin
	Linezolid
	Streptogramins
	Macrolides (Erthromycins)
	Oxazolidinones
	Lincomycin
DNA Synthesis Inhibitors	Fluoroquinolones
	Metronidazole
	Nitrofurantoin
Folic Acid Synthesis Inhibitors	Sulfonamides
	Trimethoprim

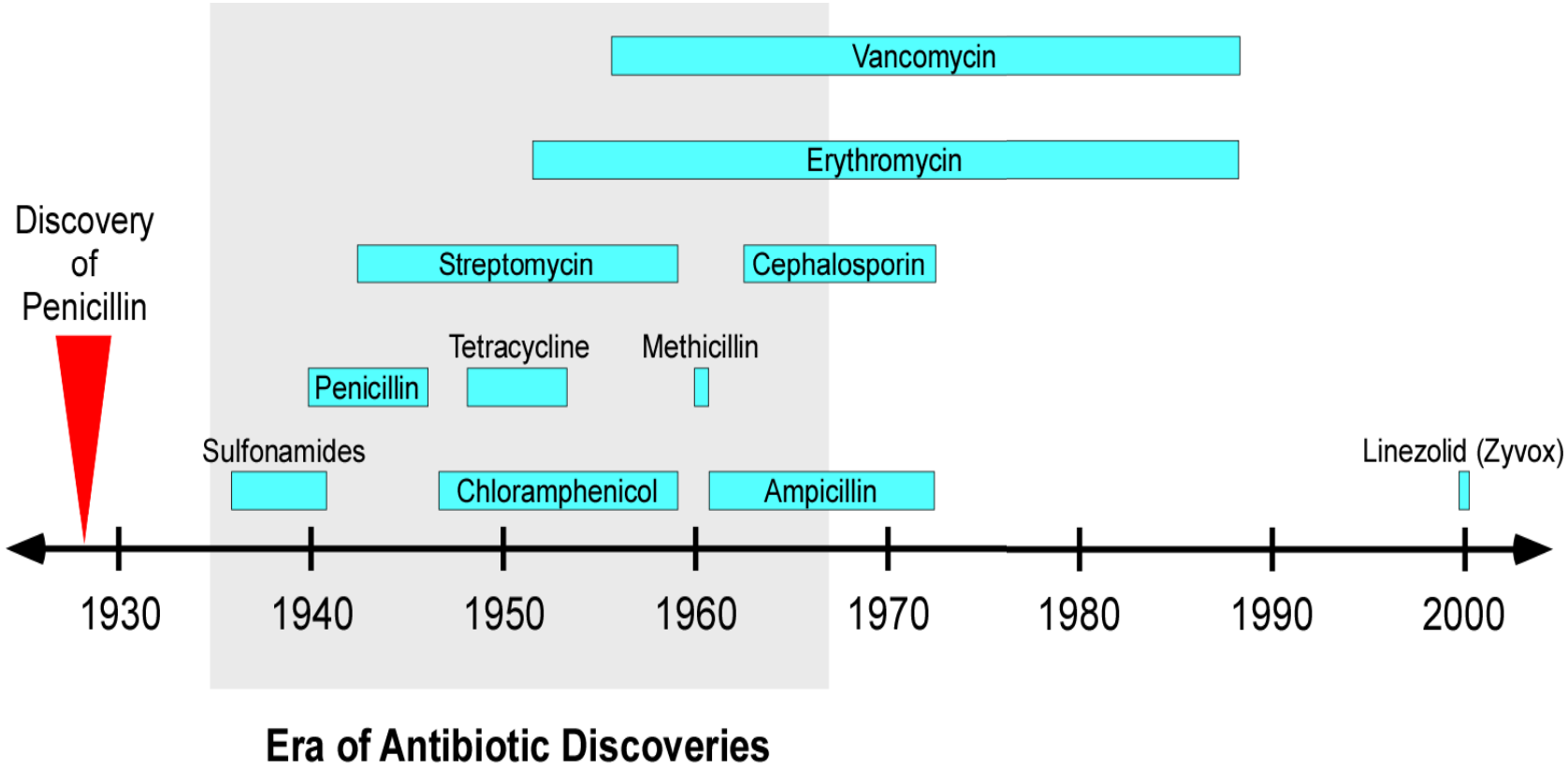

Figure 1.1. Timeline of antibiotics discovery and the appearance of resistance. The green rectangular boxes represent the length of time before the emergence of resistance for a specific antibiotic. The gray area is referred to as the era of antibiotic discovery[12].

1.3 Bacterial Cell Wall

The bacterial cell wall is a structural unit of variable thickness, which is situated outside the plasma membrane and completely covers the cell. It provides shape to the bacterial cell and also serves as a protective barrier against the external environment. The cell wall is elastic and strong, thereby preventing cell rupture due to intracellular osmotic pressure. Gram-positive bacteria, due to the thickness of their cell wall ranging from 20 to 40 nm, can withstand osmotic pressure up to 20 atm. The cell wall of Gram-negatives is comparatively thinner, about 6-8 nm in exponentially growing cells and 10-11 nm in stationary phase cells, and can protect the bacteria up to 2-5 atm. The major stress-bearing part of the bacterial cell wall is the peptidoglycan (murein). The peptidoglycan (PG) is common to both Gram-positive and Gram-negative bacteria, making its biosynthesis a vital target for antibiotics. The cell walls of Gram-positive bacteria are further strengthened by teichoic and lipoteichoic acids interwoven into the peptidoglycan layers (Figure 1.2).

The bacterial cell wall is related to antibiotic resistance. Glycopeptides such as vancomycin, for example, cannot penetrate the outer membrane of Gram-negative bacteria to reach the PG, making it only effective against Gram-positive pathogens. Both Gram-negative and Gram-positive bacteria have proteins that are covalently bonded to peptide chains of the PG layer[14]. The surface carbohydrates and proteins can serve many roles, such as protection against killing from host-cell, providing specific ligand for attachment to biotic and abiotic surfaces, and aiding interconversion between planktonic forms and biofilm communities of bacteria[11]. The alteration in PG structure affects the anchoring of the cell wall proteins and thus the pathogenicity of the bacteria.

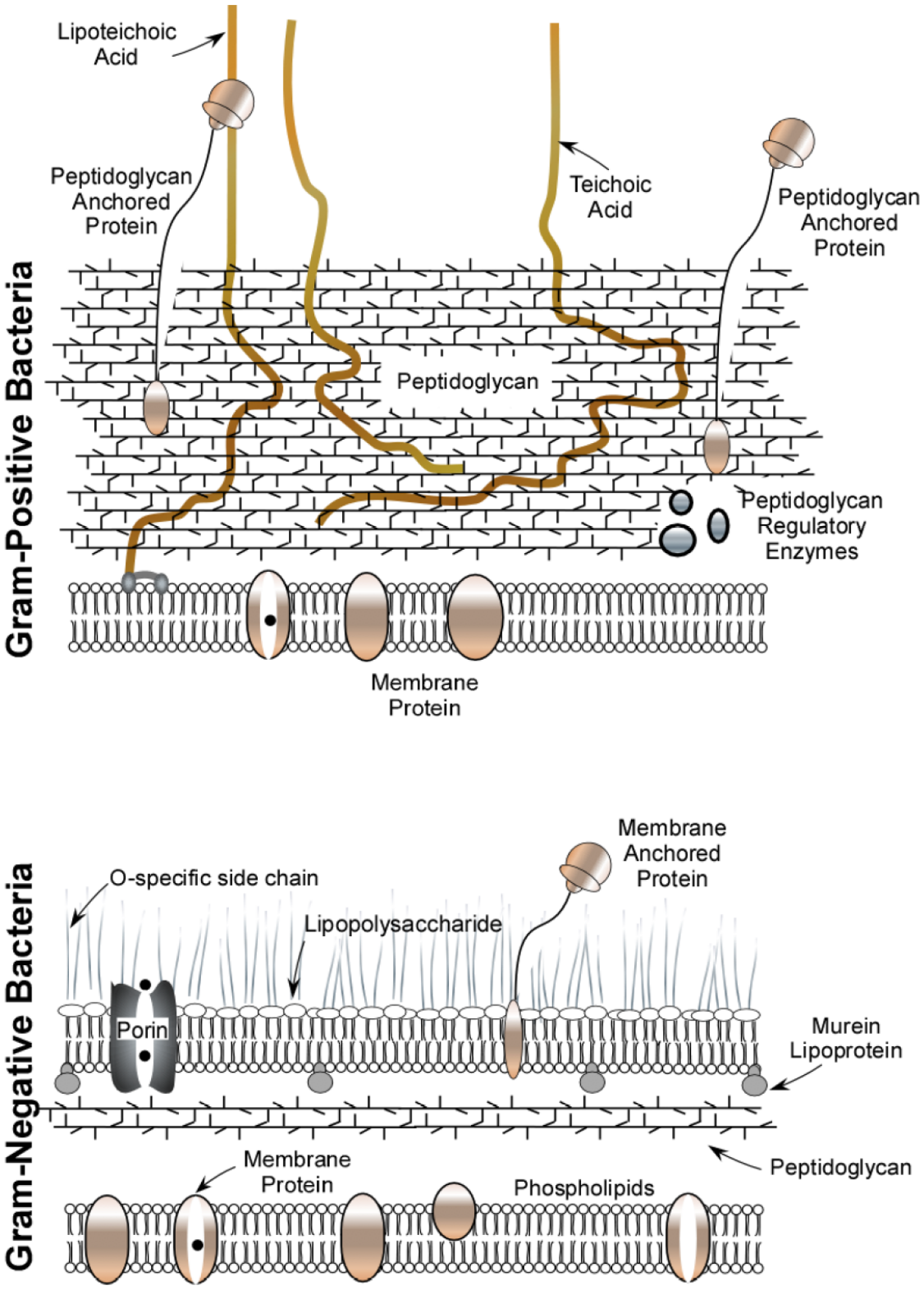

Figure 1.2. The cell wall structures of Gram-positive and Gram-negative bacteria[15]

The *S. aureus* cell walls contain organelles within. The organelles are made up of autolytic enzymes, which are strategically located to perform the concerted events of cell wall modifications during cell division, cell wall turnover and growth as a result of selective PG degradation. These organelles are localized within the cell but not covalently linked. The location of the organelles and PG structure determine the correlation between PG biosynthesis and degradation mechanisms, making it possible for the bacteria to cope and adapt to the surrounding environment. The disruption of this delicate balance is caused by antibiotics, which may lead to bacterial cell rupture due to excessive PG degradation or stunted growth driven by the over-production of PG. In spite of the fact that the chemical compositions of the components of the bacterial cell wall are well known, the majority of its structural organization and the structure of the cell wall components are not well established.

1.3.1 Peptidoglycan Structure in S. aureus

The cell wall of *S. aureus* comprises more than 20% of the entire dry weight of the bacteria, with the peptidoglycan (PG) making up more than half. The PG of *S. aureus* is a stress-bearing polymer of a disaccharide of N-acetylmuramic acid and N-acetylglucosamine (MurNAc and GlcNAc), linked by β(1➔4) bonds. The lactic moiety of MurNAc is bonded to a short pentapeptide-stem that is bridged to neighboring stems via a pentaglycyl segment. Cell envelope proteins are covalently anchored to the PG through the peptide stem[16]. The pentapeptide stem is comprised of L-alanine, D-iso-glutamine, L-lysine, D-alanine, and D-alanine. The amide bond formed by the pentaglycyl-bridge is referred to as the "bridge-link" (Figure 1.3). A new amide bond known as a "cross-link" is formed in a mature PG between the N-terminus of the terminal glycine of the pentaglycyl-

bridge from one glycan strand and the 4th amino acid of the pentapeptide stem of the adjacent glycan strand. The last D-Ala residue is being lost after cross-linking to form a matured macromolecule.

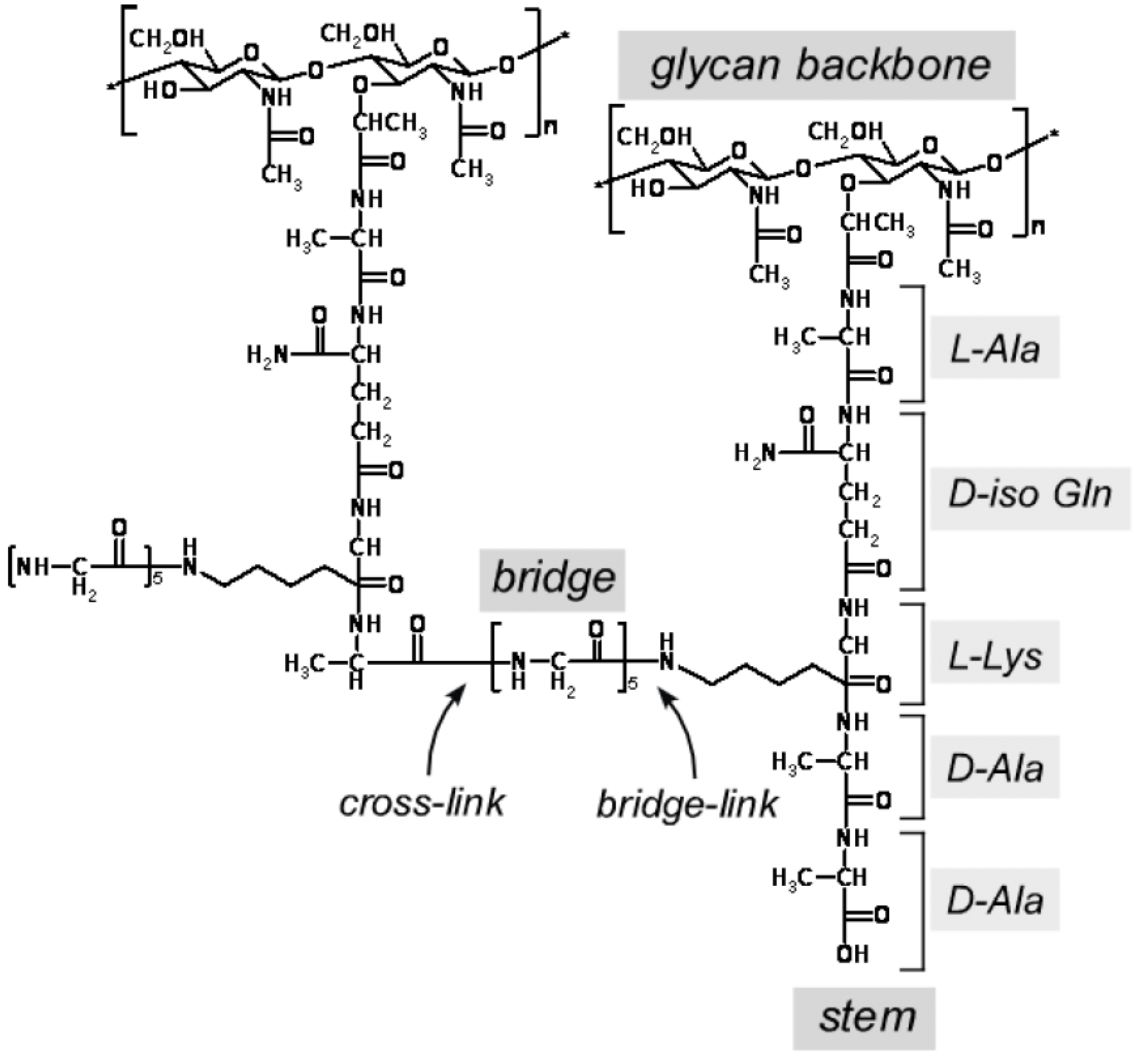

Figure 1.3. Chemical structure of *S. aureus* peptidoglycan[17]

The long glycan chain, formed from the polymerization of the disaccharide sugars, makes up the backbone of a mature PG (Figure 1.4). Remarkably, 85-90% of the glycan chains of *S. aureus* are only 3 to 10 disaccharide units long with an average length of 6 units. Longer glycan chain lengths of more than 26 units or longer constitute about 10-15%

of all the glycan materials[18]. Surprisingly, the average chain length of the glycan does not correspond to the thickness of the PG layer[19]. In addition to the cell wall of *S. aureus* conferring strength, it can expand up to 400% of its volume under osmotic pressure because of the ability of the pentaglycyl-bridge to stretch[20].

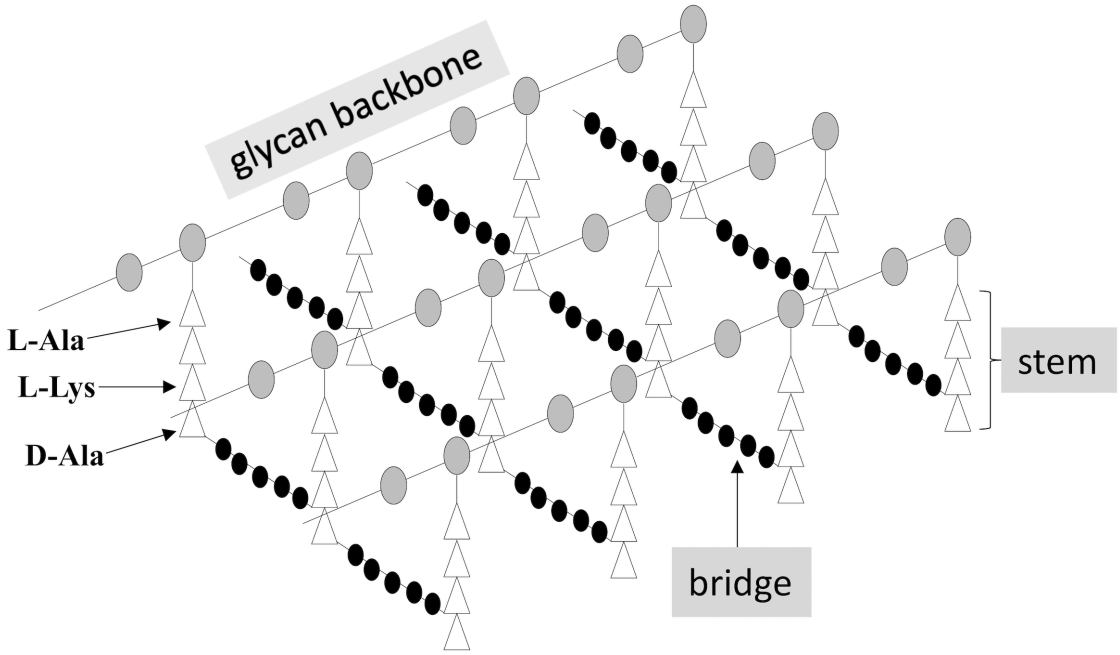

Figure 1.4. Mature peptidoglycan lattice representation. The dark circles indicate cross-linking between glycans through pentaglycyl bridges. The four-unit peptide step having the sequence L-Ala-D-Glu-L-Lys-D-Ala is shown by the triangles, while the sugars of the glycan backbone are represented by the light gray circles.

1.3.2 Peptidoglycan Biosynthesis in S. aureus

The biosynthesis of the peptidoglycan starts in the cytoplasm and ends outside the cytoplasmic membrane on the cell wall. The first stage of the PG biosynthesis in the cytoplasm leads to the formation of cytosolic monosaccharide PG precursor called Park's Nucleotide. This begins with the formation of UDP-GlcNAc-enolpyruvate, which is then reduced to UDP-MurNAc. The reduction is followed by sequential addition of the amino

acids L-Ala, D-isoGlu, L-Lys and D-Ala-D-Ala to form the Park's Nucleotide (UDP-MurNAc-L-Ala-D-isoGlu-L-Lys-D-Ala-D-Ala) catalyzed by the following enzymes: MurC, MurD, MurE and MurF[21-22].

The second stage of the PG biosynthesis in the cytoplasm converts Park's Nucleotide to lipid II (MurNAc-pentapeptide-pyrophosphoryl-undecaprenol). This conversion begins with the addition of the lipid transporter undecaprenyl phosphate (C_{55}) to Park's Nucleotide forming lipid I (MurNAc-pentapeptide-pyrophosphoryl-undecaprenol). The addition of the lipid transporter is catalyzed by MurY and leads to the liberation of UMP (uridine monophosphate) from Park's Nucleotide with the MurNAc-pentapeptide bound to the membrane. This is followed by the catalyzed addition of GlcNAc to lipid I by MurG, leading to the conversion of lipid I to immature lipid II. The mature lipid II is formed by the addition of a pentaglycyl bridge starting with the putative enzyme FemX, which adds the first glycine, then FemA and FemB, each adding two glycines. The mature lipid II is then translocated outside the cytoplasmic membrane by an unknown lipid II flippase for incorporation into the PG.

The third and final stage of the PG biosynthesis occurs on the cell wall outside the cytoplasmic membrane with two key enzymatic steps. The first step involves the addition of lipid II into the nascent PG by transglycosylase, and the second step is the incorporation of the nascent PG into the mature PG of the cell wall by transpeptidase. Carboxypeptidase removes the terminal D-Ala of uncross-linked peptidoglycan (Figure 1.5). The nascent PG is the growing chain of glycan bound to the membrane by the lipid transporter C_{55} and yet to be incorporated into the cell wall. The mechanism of transglycosylation results in the formation of a β(1➔4) glycosidic bond between GlcNAc from one unit to the MurNAc of

another. The action of transglycosylases leads to the dephosphorylation of the lipid transporter C_{55} forming undecaprenyl phosphate, which is then released for recycling. The C_{55} transporters are then flipped back through an unknown mechanism into the cytoplasm, ready to accept Park's Nucleotide and repeat the cycle. Few copies of C_{55} are found in bacteria. The low concentration of lipid II suggests that the rapid regeneration of C_{55} (or formation of lipid II) is the limiting factor in the PG biosynthesis[23]. The transpeptidases catalyze the cross-linking of the nascent PG to the mature PG by covalently linking the N-terminus of glycine from the pentaglycine bridge to the 4th D-Ala amino acid of an adjacent glycan stem. This cross-linking results in the cleavage of the 5th amino acid D-Ala, leading to the formation of a tetrapeptide stem.

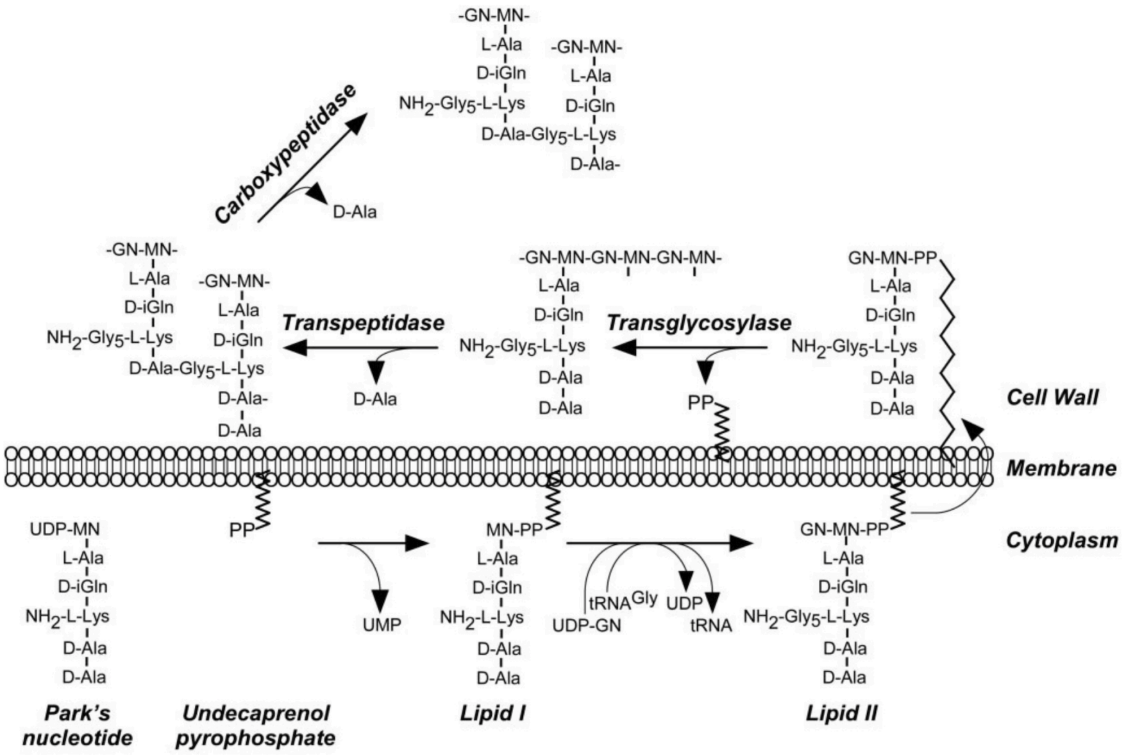

Figure 1.5. Peptidoglycan Biosynthesis in *S. aureus*[24]

1.4 Mode of Action of Bacterial Cell Wall Antibiotics

The mechanical strength conferred by the bacterial cell wall is vital for bacterial survival in environmental conditions that may alter the prevailing osmotic pressure. A well-formed PG layer preserves the bacterial cell integrity to enable survival and persistence in infection of pathogens. Any inhibition of the PG biosynthesis during bacterial cell growth leaves the cell wall mechanically weak and prone to lysis on osmotic pressure changes. Both β-lactams and glycopeptides are among the classes of antibiotics that exert their antimicrobial effects by inhibiting PG biosynthesis. Successful treatment of *S. aureus* bacterial infection with a PG biosynthesis inhibitor can lead to changes in cell shape and size, induction of cellular stress responses, and culminate in bacterial cell lysis[25].

β-lactam antibiotics are antibiotics that contain a 4-member, nitrogen-containing, β-lactam ring at the core of their molecular structure. The β-lactam ring mimics the D-Ala-D-Ala dipeptide terminal of the PG stem and acts as pseudosubstrate to acylate the active sites of transpeptidases involved in PG cross-linking (Figure 1.6). These transpeptidases are generally called penicillin-binding proteins (PBPs) because of their affinity for and binding of β-lactams such as penicillin. The acylation of the catalytic serine residue at the active sites of the PBPs makes them unavailable for the synthesis of new PG. The inhibition of the PG biosynthesis by β-lactam antibiotics leads to the bacterial cell lysis from osmotic instability or from the digestion of existing PG by autolytic hydrolases triggered by the build-up of PG precursors without the production of new PG.

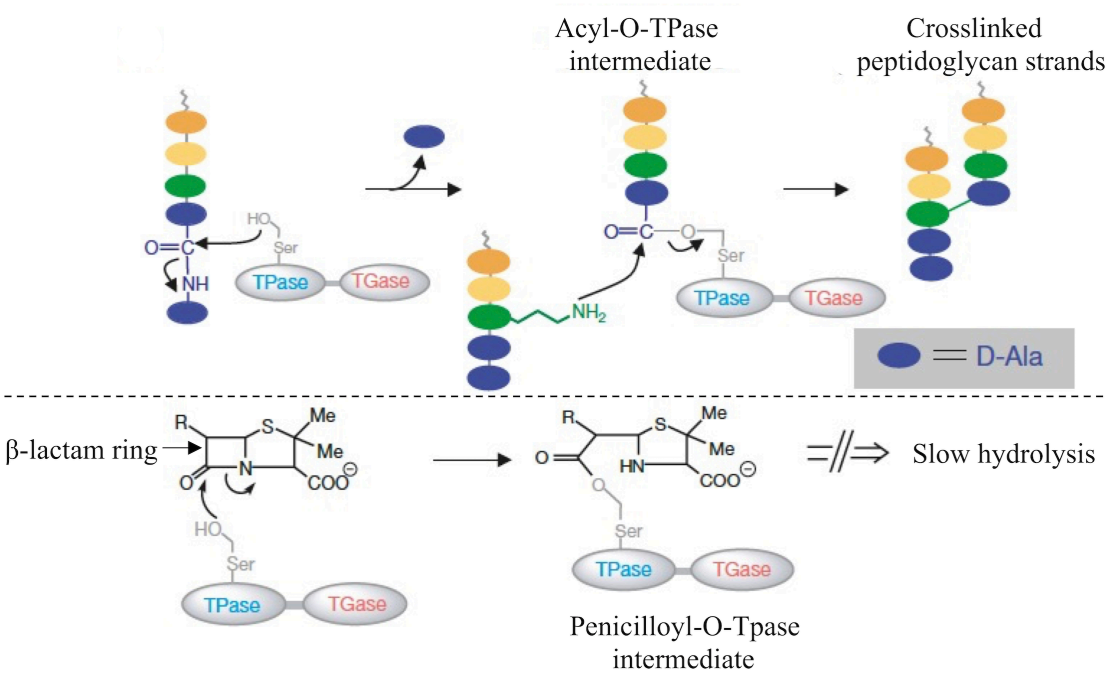

Figure 1.6. Mechanism of action of β-lactam antibiotics. Normal cross-linking of the PG pentapeptide stem by transpeptidases without any inhibition (top) and inhibition of the activity of transpeptidases by β-lactam antibiotic leading to acylation and slow hydrolysis of the enzyme complex intermediate (bottom)[8].

Resistance to β-lactam antibiotics may come in one of three pathways: The bacterial cell (i) may produce β-lactamase enzymes that destroy the β-lactam ring and prevent the antibiotics from interfering with the biosynthesis of PG by PBPs; (ii) may acquire different PBPs that have low affinity for or do not bind β-lactams sufficiently to inhibit the PG biosynthesis process; (iii) decrease the uptake of the β-lactam antibiotics by decreasing the number of channels through which they gain access to the bacterial cell (for Gram-negative bacteria).

Glycopeptides are antibiotics that have a characteristic heptapeptide core (aglycon) structure comprised of seven amino acids made through a series of phenolic oxidative couplings and various sugars attached to the aglycon. Glycopeptide antibiotics such as vancomycin do not inhibit the PG biosynthesis by targeting the transpeptidases (PBPs), but

rather they bind to the D-Ala-D-Ala of lipid II and prevent the incorporation of the PG precursors into the growing nascent PG[26] (Figure 1.7), interfering with the transglycosylase step[27]. Vancomycin binds to lipid II by forming five hydrogen bonds between the heptapeptide core and the lipid II mimic N-acetyl-D-Ala-D-Ala. The binding of vancomycin to lipid II is an effective way of sequestering the lipid transporter C_{55} and making it unavailable to the polymerase enzymes. The C_{55} transporter being a limiting factor in PG biosynthesis, since the numbers are conserved and only regenerated from lipid II during the transglycosylation step, demonstrates why vancomycin is highly potent. The depletion of the C_{55} transporter by vancomycin affects the ability of the bacteria to transport PG precursors to the exterior of the cytoplasmic membrane from the cytoplasm. This lack of translocation of the PG precursors from the cytoplasm leads to the dramatic reduction of lipid-associated PG precursors regardless of the accumulation of Park's nucleotide in the cytoplasm.

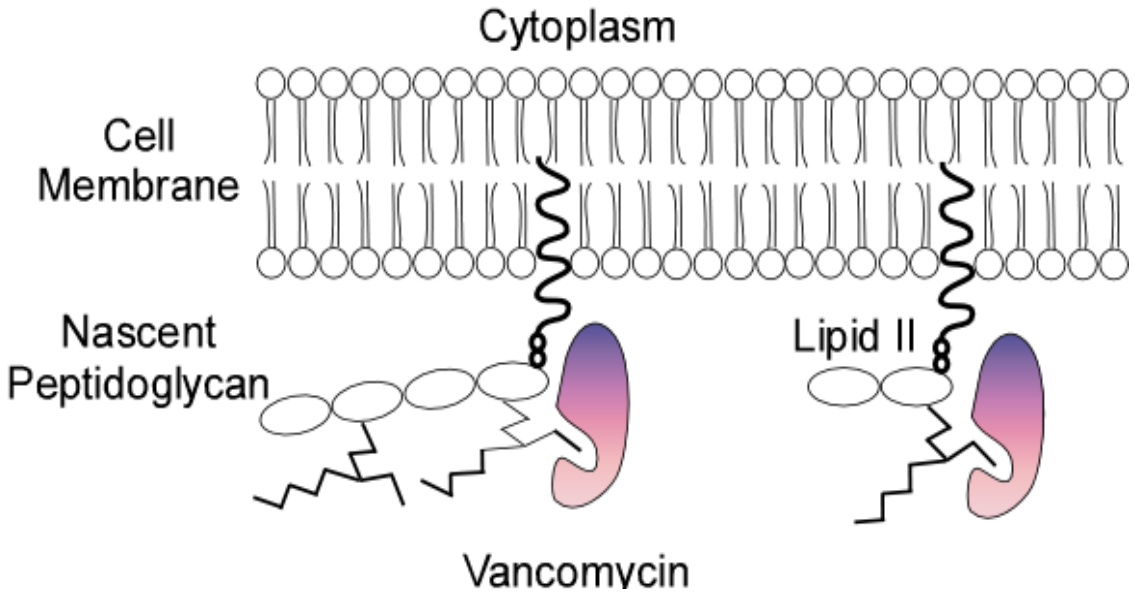

Figure 1.7. Mode of action of vancomycin[28]

The inhibition of PG biosynthesis by glycopeptides also leads to cell death by osmotic lysis due to the perturbation of the intricate balance between cell wall biosynthesis and cell wall turnover by autolytic enzymes. Glycopeptide resistance emerges through the divergent synthesis of lipid II terminating in D-Ala-D-Lac (*vanA, vanB, vanD*) or D-Ala-D-Ser (*vanC, vanE, vanG*) phenotype instead of the normal D-Ala-D-Ala dipeptide terminal. The lipid II terminating in D-Ala-D-Lac causes a 1000-fold decrease in glycopeptide binding affinity by removal of a key hydrogen bond interaction (Figure 1.8). The effect is less dramatic for D-Ala-D-Ser terminating muropeptide, which only leads to a 7-fold less binding affinity.

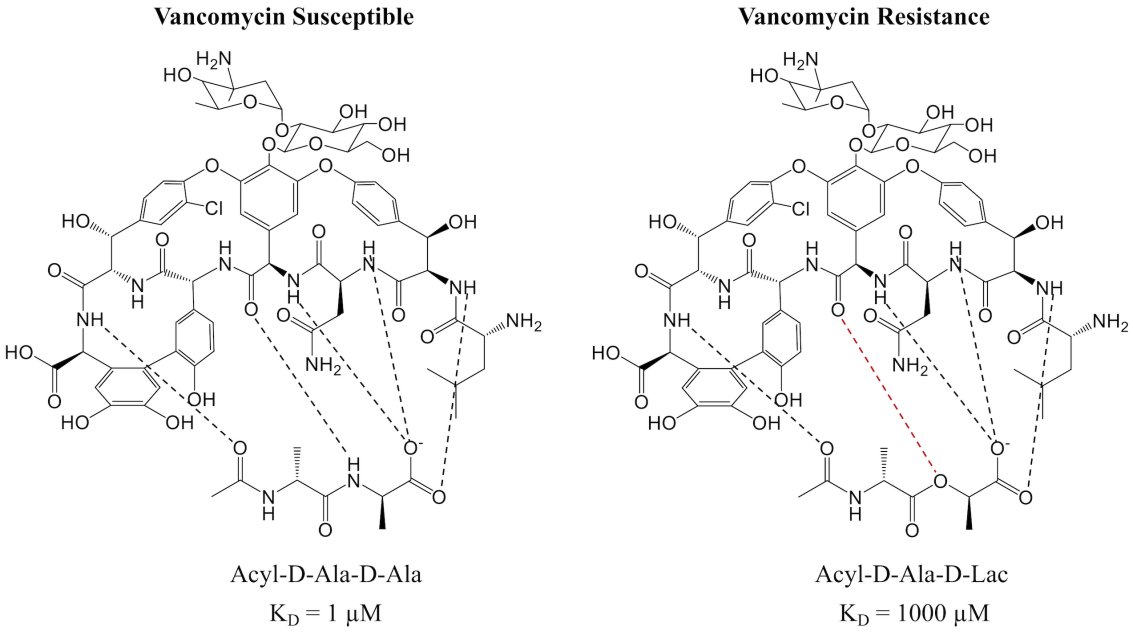

Figure 1.8. Mechanism of vancomycin resistance in *S. aureus.* Schematic representations of vancomycin bound to Acyl-D-Ala-D-Ala (left) and to Acyl-D-Ala-D-Lac (right). The dotted lines represent H-bonds. The red dotted line represents electrostatic repulsion.

1.5 Scope of Thesis

In this thesis, computational methods are used to investigate the interaction of glycopeptide antibiotics with bacterial cell wall structures of *S. aureus*. Chapter two provides details of the computational methods used. The computational study is by classical molecular dynamics simulations. In chapters three, four, and five, molecular dynamics simulations were used to elucidate the interactions and conformational changes occurring between select glycopeptides and peptidoglycan precursors. Chapter three focuses on characterization of the role of N-methylleucine, the first amino acid residue of vancomycin which is not directly involved in the binding of the glycopeptide to PG, in vancomycin binding to PG. Chapter four is an investigation into the role of the third amino acid residue of vancomycin, asparagine, in the dipeptide binding. Chapter five is an investigation of the secondary binding site of oritavancin through a comparison of the binding of vancomycin, chloroeremomycin, oritavancin, and their desleucyl analogues with PG acyl-L-Lys(Gly_5)-D-Ala-D-Ala. Chapter six gives a summary of the findings for the different projects carried out and suggestions for future work.

1.6 Attributions

Chapter Three: Sung Joon Kim and Peng Tao designed the experiment. Feng Wang, Hongyu Zhou, and Olatunde P. Olademehin carried out the MD simulations. All authors contributed to the data analyses and writing of the manuscript.

Chapter Four: Kevin L. Shuford, Sung Joon Kim, and Olatunde P. Olademehin designed the experiment. Olatunde P. Olademehin carried out the MD simulations. All authors contributed to the data analyses and writing of the manuscript.

CHAPTER TWO

Computational Methods

2.1 Molecular Dynamics Simulation

The computational procedure used in this work is based on classical molecular dynamics (MD) simulations. Typical MD simulations are used to predict the physical motions of atoms and molecules during a period of time for a system having a fixed number of particles, in order to gain molecular insight into the behavior of the system[29]. The atoms are treated as single point masses with partial charges representing the distribution of electronic charge on the molecule calculated from quantum methods, and the evolution of the atoms over time gives the trajectories of the simulation. Classical MD simulations are based on Newton's second law of motion (i.e., F = ma), where acceleration (a) of a particle i is determined by a net force (F) acting on the atom divided by the atom's mass (m). The forces are obtained from changes in potential energy which depend on the separation distances between the atoms. Improvements in simulation speed, accuracy, and accessibility, coupled with the varieties of available experimental structural data, have made MD simulations more appealing to study important biomolecular processes, including ligand binding, conformational changes, and protein folding at atomic level[30].

Molecular dynamics simulations are performed in an iterative fashion, where the output from one iteration becomes the input to the next. The sequence of steps is typically repeated for millions of steps before the pre-set time scale is achieved. Figure 2.1 shows the flowchart of MD simulation. The most computationally demanding step is the force calculation, which is obtained from the gradient of the potential U, that is, $F_i = -\nabla_i U(r)$. The

main idea in MD simulation is to generate structures from a natural ensemble through the calculation of potential functions and integration of Newton's equations of motions. The structures are then used to evaluate the equilibrium properties of the system. A time step shorter than the fastest movements in the molecule is needed as the integration of movement is done numerically to avoid instability. A typical time step ranks between 1 and 2 fs.

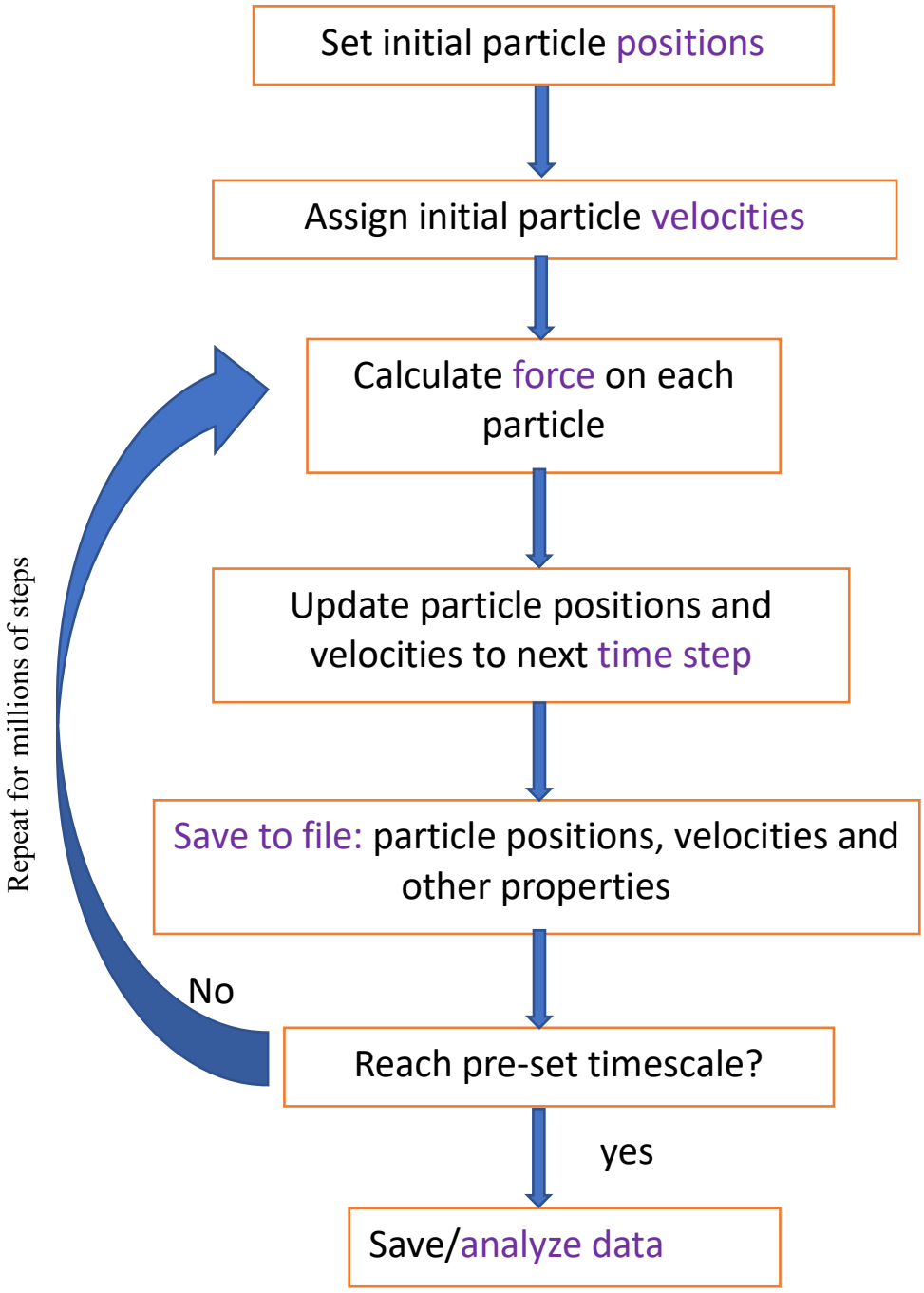

Figure 2.1. Flowchart of a typical MD simulation

2.1.1 Molecular Dynamics Input Files

Besides the coordinates and velocities changing with each step, the MD simulations also needs input files with a static description of all atoms and interactions in the system, known as topology. The input files normally contain the forcefield parameters, the description of the system, and the necessary simulation details.

2.1.1.1 Structure files. The starting point of MD simulation is the structure of the system of interest. These files are usually obtained from the PDB (Protein Data Bank) database and contain the spatial coordinates of every atom in the system at time $t = 0$. In most cases, the initial PDB files are not ideal, and modifications are made to get the correct structure representation. The solvent choice can be an explicit or implicit solvation model to approximate the thermodynamics properties of liquids. Though the use of implicit solvent help reduces computation time, explicit solvation is more reliable when the solvent plays an important role in the simulation process.

2.1.1.2 Topology and forcefield files. The topology file defines the connectivity between atoms in the MD simulation system. It contains information about the bonds, angles, and dihedrals present in the system, as well as atomic masses and partial charges (Figure 2.2). An appropriate force field is needed to better represent the interactions within the system and yield accurate results. The force field in MD simulation refers to the set of equations and parameters used to describe the energy of the system as a function of its atomic coordinates. The force field estimates the interatomic forces acting between atoms within the system. The parameters are usually developed from *ab initio* or semi-empirical

quantum mechanical calculations for small molecules, which can serve as building blocks in developing the force field for larger biomolecules[31].

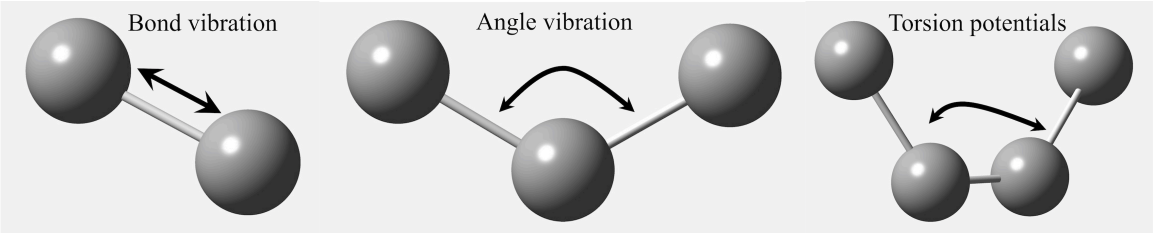

Figure 2.2. Examples of bonded interaction functions in a typical force field. The interactions shown include covalent bond-stretching, angle-bending, and torsion rotation around bonds.

The type of system being studied determines the choice of force field used. Ideally, the force field must be simple enough to be evaluated quickly but well detailed to reproduce the properties of interest in the system studied. For biomolecules studied in this work, the CHARMM force field was used. The initial stream file, which contains the starting guess for the topology, charges, and parameters, was produced using the Paramchem interface[32-33] (https://www.paramchem.org). The CHARMM force field has the following form of the potential energy function, U(r):

$$\begin{aligned} U = & \sum_{bonds} k_b\,(b - b_0)^2 + \sum_{angles} k_\theta\,(\theta - \theta_0)^2 \\ & + \sum_{dihedrals} k_\phi\,[1 + cos(n\phi - \delta)] \\ & + \sum_{impropers} k_\omega\,(\omega - \omega_0)^2 + \sum_{Urey-Bradley} k_u\,(u - u_0)^2 \\ & + \sum_{nonbonded} \epsilon \left[\left(\frac{R_{min_{ij}}}{r_{ij}}\right)^{12} - \left(\frac{R_{min_{ij}}}{r_{ij}}\right)^{6}\right] + \frac{q_i q_j}{\epsilon r_{ij}} \end{aligned} \tag{2.1}$$

The first five terms in equation 2.1 refer to intramolecular or local contributions to the total potential energy. The intramolecular interactions include terms for the bonds, angles, torsion or dihedral angles, improper dihedral angles and an Urey-Bradley 1,3-term. The constants b_0, θ_0, ω_0 and u_0 are the bond, angle, improper and Urey-Bradley equilibrium terms, respectively, while n and δ are the dihedral multiplicity and phase shift. The respective force constants are the k's. The last two terms describe the nonbonded interactions represented by the Lennard-Jones repulsion and attraction (Figure 2.3), as well as Coulomb electrostatics, where r_{ij} is the distance between particles i and j, $R_{min_{ij}}$ is the point where the Lennard-Jones potential is zero. The depth of the well for the interaction between two atoms is given by ϵ, and q_i and q_j is the partial atomic charge of atom i and j, respectively. The nonbonded interactions are only applied to atom pairs separated by at least three bonds.

The end goal of a force field is to describe in classical terms all the quantum mechanical facts, considering all the contributions to the total electronic energy. Unfortunately, it is extremely difficult to fully capture the intricate electronic effects[34], so significant physical approximations are done to describe in a useful way the intermolecular interactions, thereby limiting the accuracy of the result. Therefore, force fields used in classical MD simulations are called empirical potentials or empirical force fields. Each force field has its specific strengths and weaknesses in relation to the data and procedure used in its parametrization. Empirical force fields have some inherent limitations, which include their inability to provide information about electronic structure, and thus unable to capture reactions such as bond breaking and formation, charge transfers, electron excitations, etc. Their predictive power is also largely dependent on their application to

systems containing the functional groups added in the development of the force field, and the quality of their parametrization determine their accuracy.

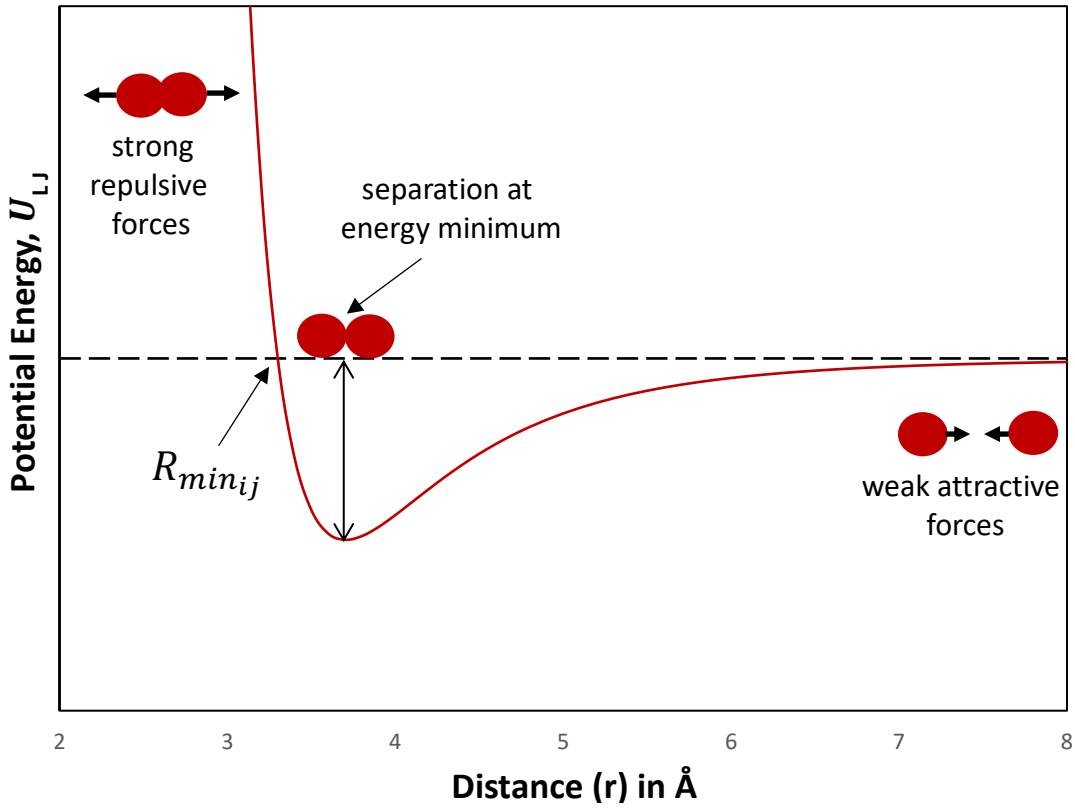

Figure 2.3. The Lennard-Jones potential describing the interaction between two neutral molecules

2.1.1.3 Position and Distance Restraints. Two types of restraints are utilized in the course of the MD simulations presented in this thesis. These are position and distance restraints. The position restraints (pr) are used to fix the reference position of heavy atoms during equilibration to avoid drastic rearrangements of critical parts and maintain the integrity of the system. Harmonic position restraints are based on the following potential:

$$U_{pr}(r_i) = \frac{1}{2} k_{pr} |r_i - R_i|^2 \tag{2.2}$$

The potential can be rewritten as

$$U_{pr}(r_i) = \frac{1}{2}\left[k_{pr}^{x}(x_i - X_i)^2\hat{\mathrm{x}} + k_{pr}^{y}(y_i - Y_i)^2\hat{\mathrm{y}} + k_{pr}^{z}(z_i - Z_i)^2\hat{\mathrm{z}}\right] \quad (2.3)$$

with forces:

$$F_i^x = -k_{pr}^{x}(x_i - X_i) \quad (2.4)$$

$$F_i^y = -k_{pr}^{y}(y_i - Y_i) \quad (2.5)$$

$$F_i^z = -k_{pr}^{z}(z_i - Z_i) \quad (2.6)$$

Using three different force constants means the position restraints can be turned on or off in each spatial dimension.

The distance restraints (dr) are based on knowledge from experimental data. In this work, distance restraints from solid state Nuclear Magnetic Resonance (NMR) experiments are incorporated as part of the input files to impose a penalty on the potential when the distance between specified atom pairs exceeds a threshold value. A measure of the distance that pairs of atoms have with respect to each other is obtained from the intensity of the Nuclear Overhauser Effect (NOE) peaks in selected NMR spectra. The potential used to impose distance restraints are flat-bottom potentials (Figure 2.4) which is implemented in the GROMACS package[35]. The potential form for distance restraints, as shown in equation 2.7, is quadratic (harmonic function) below a specified lower bound (low) and between two specified upper bounds (up1 and up2), and linear beyond the largest bound. In the area linking low and up1, the potential is zero and no extra force is exerted on the atom.

$$U_{dr}(r_{ij}) = \begin{cases} \frac{1}{2}k_{dr}(r_{ij} - r_0)^2 & \text{for} \quad r_{ij} < r_0 \\ 0 & \text{for} \quad r_{ij} < r_0 < r_1 \\ \frac{1}{2}k_{dr}(r_{ij} - r_1)^2 & \text{for} \quad r_1 < r_{ij} < r_2 \\ \frac{1}{2}k_{dr}(r_2 - r_1)(2r_{ij} - r_2 - r_1) & \text{for} \quad r_2 < r_{ij} \end{cases} \tag{2.7}$$

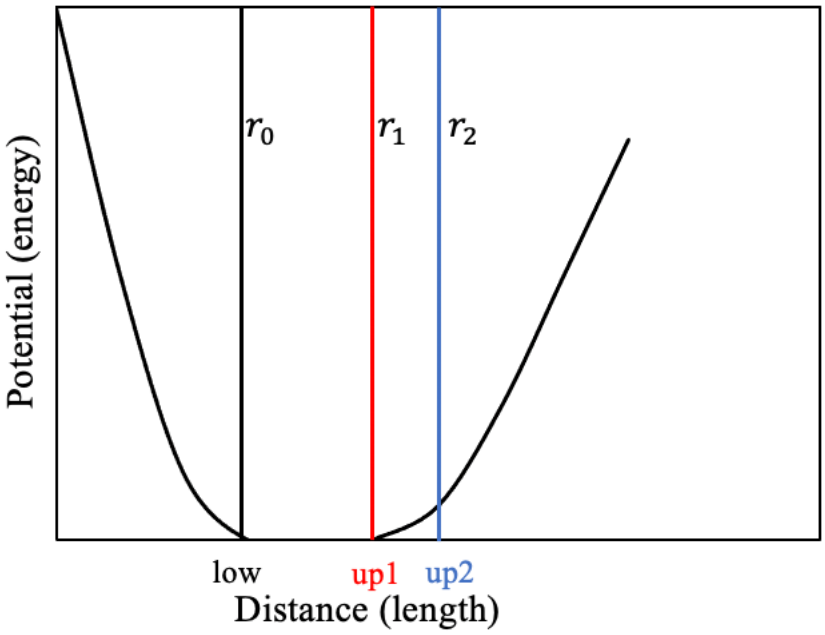

Figure 2.4. Distance restraint potential

2.1.2 Selection of Parameters for MD Simulation

There are extensive parameters available for MD simulation, and a good selection of parameters is vital for effectively running a simulation and making optimal use of

available computing resources. Few of such parameters include; timestep, velocities, integration algorithm, number of steps for duration of simulation, periodic boundary condition, etc.

2.1.2.1 Selection of the timestep. The timestep, Δt, is the time taken before the coordinate of the next step in the simulation is updated. The proper selection of timestep for MD simulation is necessary to prevent instability in the motion of particles due to truncation error in the integration process. A timestep shorter than the fastest movements in our system (biomolecule) is required for a stable motion of particles. Also, the timestep should not be too small for efficient use of computing resources. In most instances, a timestep between 1 and 2 fs are used for atomistic simulation.

2.1.2.2 Assignment of velocities. The velocities, v_i, $(i = 1 \ldots 3N)$ can be assigned to the atoms from a Maxwell-Boltzmann or Gaussian distribution at a given temperature. Equation 2.8 gives the probability that an atom i has a velocity v_x, in the x direction for the temperature, T.

$$p(v_{ix}) = \left(\frac{m_i}{2\pi k_B T}\right)^{\frac{1}{2}} exp\left[-\frac{m_i v_{ix}^2}{2k_B T}\right] \tag{2.8}$$

where k_B is the Boltzmann's constant. When the temperature achieved is not exact, the assignment of velocities is corrected through the removal of the center of mass motion and scaling the velocities by a factor $\sqrt{T_B/T(t)}$, where T_B is the desired temperature and $T(t)$ is the instantaneous temperature of the system before scaling. The velocities can be used to calculated the temperature from the relation in equation 2.9.

$$T = \frac{1}{3Nk_B}\sum_i \frac{p_i^2}{m_i} \tag{2.9}$$

where N is the total number of atoms in the simulation system.

2.1.2.3 Integration algorithm. To solve classical equation of motion numerically step by step, a good algorithm is required over small timestep for a satisfactory simulation. An immediate apparent solution would have been to use a simple Taylor expansion shown in equation 2.10, but the algorithm is inaccurate and unstable.

$$r_i(t_0 + \Delta t) = r_i(t_0) + \frac{dr_i(t_0)}{dt}\Delta t + \frac{1}{2}\frac{d^2 r_i(t_0)}{dt^2}\Delta t^2 + O(\Delta t^3) \tag{2.10}$$

The Verlet algorithm is a better solution than the Taylor expansion as it combines the Taylor expansion for $+\Delta t$ and $-\Delta t$, thus canceling the terms in $\Delta t, \Delta t^3$, etc. to obtain:

$$r_i(t_0 + \Delta t) = r_i(t_0 - \Delta t) + 2r_i(t_0) + a_i(t_0)\Delta t^2 + O(\Delta t^4) \tag{2.11}$$

The local error truncation is of $O(\Delta t^4)$. Two similar algorithms producing same trajectory as the Verlet integrator are the leap-frog algorithm (equation 2.12) and the velocity-Verlet algorithm (equation 2.13).

$$r_i(t_0 + \Delta t) = r_i(t_0) + v_i(t_0 + \frac{\Delta t}{2})\Delta t \tag{2.12}$$

$$r_i(t_0 + \Delta t) = r_i(t_0) + v_i(t_0)\Delta t + \frac{1}{2}a_i(t_0)\Delta t^2 \tag{2.13}$$

These three algorithms constitute a good choice for an MD simulation because they are efficient, stable and reasonably accurate.

2.1.2.4 Periodic boundary condition. There is need to impose some boundary conditions since, in most MD simulation, we are interested in the bulk properties of a liquid or solid system. The periodic boundary conditions replicate the small, simulated system to infinity to better reflect bulk properties of a macroscopic system (Figure 2.5). In applying

the boundary conditions, only the N atoms inside the main cell (yellow in figure 2.5) are explicitly considered, but as soon as a particle leaves the cell, an image particle from the opposite cell enters to replace it. The minimum image convention that a particle should never see its periodic image is put into consideration when specifying a solute-box distance. Care must be taken in choosing the cutoff radius when considering any property that depends on long-range corrections. The differences amongst truncation methods are less obvious for larger cut off radii.

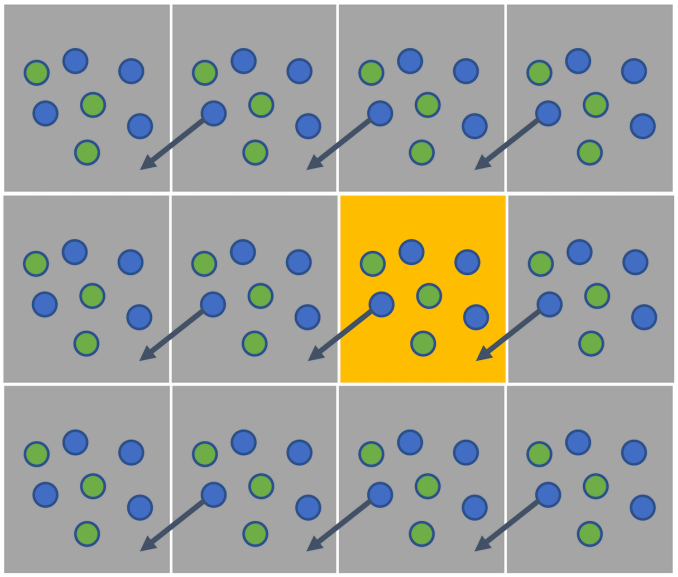

Figure 2.5. Illustration of Periodic Boundary Conditions applied to a simulation box

2.1.2.5 Choice of ensemble. The thermodynamic ensembles typically used for MD simulations are microcanonical or NVE ensemble, canonical or NVT ensemble, and constant isothermal-isobaric or NPT ensemble. In order to attain a desired ensemble, algorithms are normally used to control the temperature, pressure or volume of the system. There are several available thermostats or barostats to keep the temperature or pressure, or

a combination of both constant. To control the temperature, available thermostats include the Berendsen, Nosé-Hoover and v-rescale[36-39]. The Berendsen thermostat consist of a weak coupling of the system to a heat bath. The equation is obtained by modifying the equation of motion to give:

$$a_i = \frac{F_i}{m_i} + \frac{1}{2\tau_T}\left(\frac{T_B}{T(t)} - 1\right) v_i \tag{2.14}$$

The additional term acts as a frictional force and the coupling constant τ_T determines the strength of the coupling. The desired temperature can be achieved rapidly with this method and it is very flexible. The Nosé-Hoover thermostat gives a more rigorous way to control the temperature as it makes the heat bath an integral part of the system by adding an artificial variable with an associated effective mass. The methods to control the pressure of the system are similar to those used for the temperature. For the pressure, the virial takes the role of the temperature and the pressure is controlled by scaling the volume of the system. Some algorithms for pressure coupling are Berendsen and Parrinello-Rahman barostats[36, 40-41].

2.1.3 Molecular Dynamics Simulation Process

After preparing all the structures and parameters files, the next step is to perform the MD simulation. There are four major steps in the simulation process. This includes energy minimization, equilibration, production and Analysis.

2.1.3.1 Energy minimization. When all the input files are ready, including the structure rightly placed in a box, solvated and appropriate number of ions added to neutralize the charges, the next step is to relax the structure through energy minimization. The minimization of the energy helps to ensure there are no steric clashes or inappropriate

geometry that can cause large forces on particular atoms/molecules. A typical energy minimization is done in about 50,000 steps or less to guarantee the maximum force acting on each atom do not exceed a threshold value (mostly 1000 kJ/mol/nm) and there is the convergence of energy. The most common algorithm used for energy minimization is the Steepest Descent algorithm. The Steepest Descent is a simple method for obtaining local stationary points of a multi-dimensional function. In the Steepest Descent algorithm, the forces F and potential energy are first calculated, then new positions are assigned based on the equation 2.15.

$$r_{n+1} = r_n + \frac{\boldsymbol{F}_n}{\max(|\boldsymbol{F}_n|)} h_n \tag{2.15}$$

where h_n is the maximum displacement and $\boldsymbol{F}_n$ is the force which is calculated from the negative gradient of the potential U. The notation $(|\boldsymbol{F}_n|)$ implies the largest scalar force on any atom. The forces and energy are computed for the new positions again[35].

2.1.3.2 Equilibration. Energy minimization ensures we have an acceptable starting structure, but to begin real dynamics we need to equilibrate the solvent and ions around our biomolecule. This involves using the right thermostat and barostats to bring the system to the temperature and pressure required for our simulation. In this work, the equilibration of temperature is done using NVT ensemble while the equilibration of pressure is carried out with NPT ensemble. To ensure we have achieved equilibrium state, it is important to monitor the equilibration of the system by following the temperature, pressure, density and energy components which should fluctuate about some average value.

2.1.3.3 Production MD. After completion of the equilibration phases, the system is well equilibrated at our desired temperature and pressure, and the production MD can be run for data collection. The production run is the major step of interest for performing analysis and determining thermodynamic averages. The procedure for production MD is similar to that in the equilibration stage in that the algorithm used follow the phase-space trajectory and stores data on properties of the system. The timescale for the production run is dependent on the thermodynamic properties of interest, as enough time is needed to sample all the conformational transitions involved. The simulation time should be significantly long to validate the ergodic hypothesis, that is, the time average of a given property should coincide with the ensemble average. The nanosecond timescale is sufficient to study protein-ligand binding interactions, while dynamics for normal protein folding is in the microsecond timescale.

2.1.3.4 Analysis. The final stage of the MD simulation process is the data analysis, where the simulated trajectory is analyzed to extract the desired properties. After completing the production MD, we have access to the atomic positions, velocities, and forces as a function of time. It is easy to compute mechanical properties that can be expressed in terms of these variables. After an MD simulation, measurable properties include the root-mean-squared deviation (RMSD), the radius of gyration (R_g), protein-ligand interaction energy, hydrogen bond analysis, binding free energy computations, etc.

1. *Root-mean-squared deviation (RMSD).* The root-mean-square deviation (rmsd) compares the conformational difference between a stable structure, considered as the reference structure, and a dynamic structure along the trajectories during MD simulations

to estimate their structural similarities. The rmsd is achievable through the least-squares fitting of the dynamic structure to the reference structure. The rmsd equation for a molecular structure given by a cartesian coordinate vector $\mathbf{r}_i$ $(i = 1 - N)$ of N atoms is expressed as

$$\text{RMSD} = [\tfrac{1}{\text{M}} \sum_{i=1}^{N} m_i(\mathbf{r}_i^t - \mathbf{r}_i^0)^2]^{1/2} \tag{2.16}$$

where $\text{M} = \sum_{i=1}^{N} m_i$, $\mathbf{r}_i^t$ is the position of atom i along the trajectory at time t, $\mathbf{r}_i^0$ is the position of atom i for the stable reference structure, and m_i is the mass of atom i.

2. Hydrogen bond analysis. The average number of hydrogen bonds can predict the degree of interactions and stability between a glycopeptide and PG during MD simulation. The hydrogen bond is directional but flexible. It is predominantly electrostatic, which leads to pronounced flexibility in the bond length and angle. Depending on the bond length and angle, the hydrogen bond can be considered as weak (about 3.2 to 4.0 Å and < 4 kcal/mol), moderate (about 2.5 to 3.2 Å and between 4 – 15 kcal/mol) or strong (about 2.2 to 2.5 Å and between 14 – 40 kcal/mol). In this study, the hydrogen bond profiles for the interaction of the glycopeptide and PG are obtained using the g_hbond utility in GROMACS, with all the possible hydrogen bond donors and acceptors taken into consideration.

3. Free energy of binding, ΔG_{bind}. The free energy of binding, which refers to the amount of internal energy of a system available to do work, is an essential thermodynamic parameter for predicting the binding strength between a protein and ligand. The accurate determination of free energy is a vital task in biomolecular studies. The two most popular computational methods used for binding free energy determination in MD simulations are the alchemical free energy (AFE)[42-43] methods, referred to as the pathway methods, and the

end-point free energy methods. The alchemical methods require the interconversion of the biomolecular complex from an initial state to a final state through infinitesimal alchemical changes of the energy function. The alchemical methods are computationally expensive but accurate. Examples of widely utilized alchemical methods include free energy perturbation (FEP)[44-45], thermodynamic integration (TI)[46-47], and umbrella sampling (US)[48-50]. The end-point free energy methods, though less accurate than the pathway methods but can be effective for ranking similar ligands binding to a substrate[51], are based on the sampling of the final states of a system and computationally cheaper to use. The most commonly used end-point free energy methods are molecular mechanics Poisson-Boltzmann surface area (MM/PBSA), molecular mechanics generalized Born surface area (MM/GBSA), and linear interaction energy (LIE)[52-55]. In this work, the MM/PBSA and umbrella sampling techniques of binding free energy determination are utilized.

A. Molecular mechanics Poisson-Boltzmann surface area (MM/PBSA) free energy method. In the MM/PBSA method, the free energy of binding of a ligand (PG) to the receptor (glycopeptide or gly) to form a complex (com) is given by equation 2.17

$$\Delta G_{bind} = G_{com} - G_{gly} - G_{PG} \tag{2.17}$$

The ΔG_{bind} can be decomposed into the contributions from the different interactions occurring within the system (equation 2.18).

$$\Delta G_{bind} = \Delta H - T\Delta S = \Delta E_{MM} + \Delta G_{sol} - T\Delta S \tag{2.18}$$

in which

$$\Delta E_{MM} = \Delta E_{int} + \Delta E_{elec} + \Delta E_{vdW} \tag{2.19}$$

$$\Delta G_{sol} = \Delta G_{polar} + \Delta G_{nonpolar} \quad (2.20)$$

and

$$\Delta G_{polar} = \Delta G_{PB} \quad (2.21)$$

$$\Delta G_{nonpolar} = \Delta G_{SA} = \gamma . SASA + b \quad (2.22)$$

where ΔE_{MM}, ΔG_{sol}, and $-T\Delta S$ are the changes for the gas phase molecular mechanics (MM) energy, solvation free energy, and conformational entropy upon binding of the ligand, respectively. ΔE_{MM} comprises of the changes in the internal energies ΔE_{int} (bond, angle, and dihedral energies), electrostatic energies ΔE_{elec}, and the van der Waals energies ΔE_{vdW}. The ΔG_{sol} is the sum of the polar (electrostatic) solvation energy ΔG_{PB} and the nonpolar contribution ΔG_{SA} between the solute and the continuum solvent. The polar contribution is calculated with the Poisson-Boltzmann model, while the nonpolar part is estimated with the solvent-accessible surface area (SASA), with the correction constant designated as b. The nonpolar contribution can also be estimated with the solvent-accessible volume (SAV) model.

The MM/PBSA free energy method is implemented with MD simulations using implicit or explicit solvation. The explicit solvation method is widely used as the implicit solvation simulations have been shown to produce less accurate results[56]. The MM/PBSA free energy method can be implemented using a single trajectory or separate trajectory approach (called 3A-MM/PBSA and 1A-MM/PBSA, respectively by Genheden and Ryde[57]) (Figure 2.6). Different simulations are carried out in the separate trajectory approach for the ligand (PG), protein (glycopeptide or gly), and complex to compute the free energy of binding. On the other hand, in the single trajectory protocol, a single MD simulation of the complex is performed, and the free protein or ligand structures are

obtained by deleting the ligand or protein from each snapshot of the simulations of the complex. The single trajectory is more commonly used as it requires fewer simulations and gives more precise results.

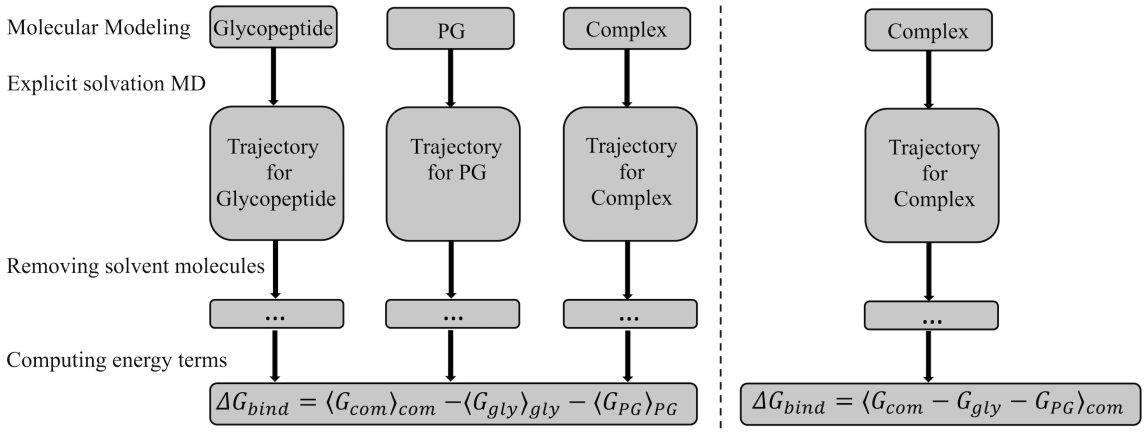

Figure 2.6. Schematic diagram of binding free energy calculation using separate trajectory (left) and single trajectory (right) approach

B. Umbrella sampling (US) free energy method. The umbrella sampling free energy technique, developed by Torrie and Valleau[58] in 1977, is used to obtain free energy profiles and other thermodynamic information through adequate conformational sampling along a reaction coordinate. It is commonly performed, following an explicit solvent MD simulation and a steered MD simulation (SMD), as an effective way to obtain the potential of mean force (PMF) along a reaction coordinate. In SMD, sometimes referred to as the center-of-mass (COM) pulling simulations, a constant harmonic force is applied to the COM of the PG (ligand) along a reaction coordinate (the z-axis) to pull it away from the glycopeptide, with a continuous propagation of the PG at constant velocity. Umbrella sampling utilizes a series of independent windows along a chosen reaction coordinate to model the conformational transitions (Figure 2.7). For each of the windows, the biasing

force applied is shown in equation 2.23. The windows must allow for slight overlap of the PG positions for adequate reconstruction of the PMF curve.

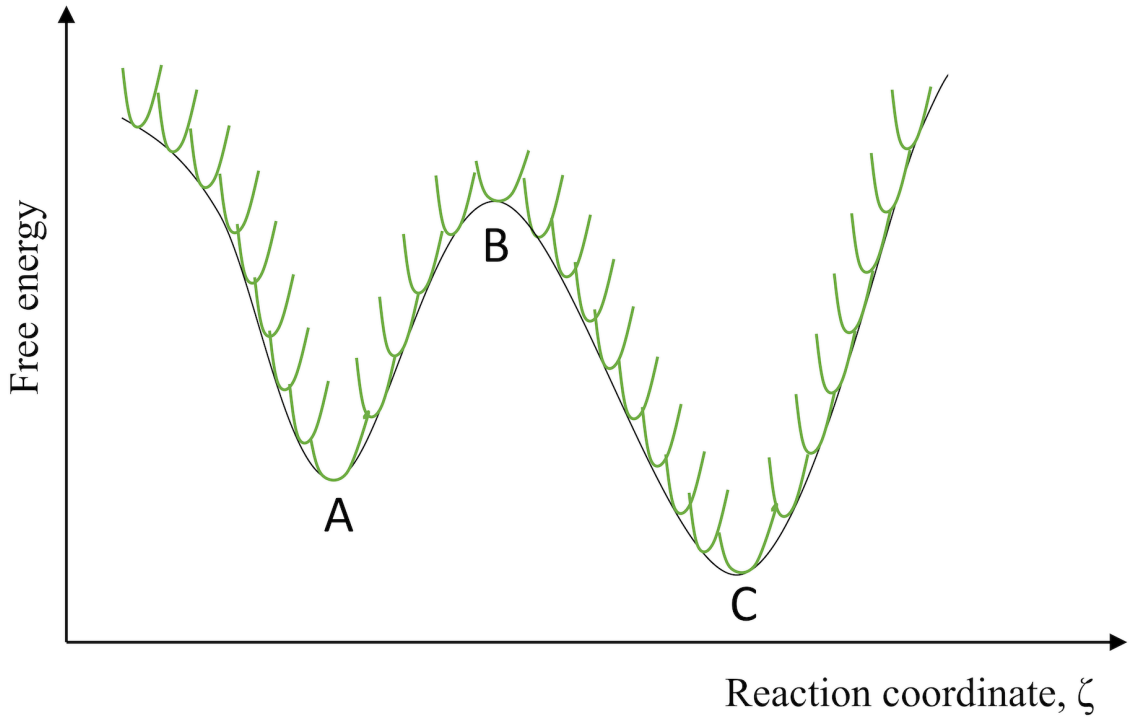

Figure 2.7. Schematic illustration of umbrella sampling method. The green color represents the harmonic bias potentials added at different reaction coordinate points (windows).

$$F = \frac{k}{2}[\zeta - (\zeta_0 + vt)] \tag{2.23}$$

where v is the pulling velocity, t is time, ζ_0 is a reference coordinate point, and k is the force constant. The work done by the force is represented as:

$$W = \int F ds \tag{2.24}$$

Although the method proposed by Jarzynski[59] (equation 2.25) can be used to extract equilibrium data (free energies) from the nonequilibrium pulling simulation trajectories, the weighted histogram analysis method (WHAM)[60] is more commonly applied.

$$e^{-\Delta G/k_B T} = \langle e^{-W/k_B T} \rangle \tag{2.25}$$

The WHAM approach calculates ΔG from several simulations carried out on the various configurations obtained from a single SMD simulation. The PMFs obtained as output from WHAM are calculated for the situation where a simulation is done with the desired set of coupling parameters at a specific temperature. The WHAM equation for R simulations with the ith simulation performed at temperature, $T_i = {}^{1}/_{k_B\beta_i}$, with the coupling parameters set to $\{\lambda\}_i$ and the number of snapshots taken from the ith simulation represented as n_i are expressed as follows:

$$\mathrm{P}_{\{\lambda\},\beta}(\{V\},\zeta) = \frac{\sum_{k=1}^{N} N_k(\{V\},\zeta)\exp\left(-\beta\sum_{j=0}^{L}\lambda_j V_j\right)}{\sum_{m=1}^{R} n_m \exp\left(f_m - \beta_m\sum_{j=0}^{L}\lambda_{j,m}V_j\right)} \tag{2.26}$$

and

$$\exp(-f_j) = \sum_{\{V\},\zeta}\mathrm{P}_{\{\lambda\}_j,\beta_j}(\{V\},\zeta) \tag{2.27}$$

where $\mathrm{P}_{\{\lambda\},\beta}(\{V\},\zeta)$ is the (unnormalized) probability histogram, V_j is the restraining potential at the jth snapshot. $N_i(\{V\},\zeta)$ is the value taken by the histogram at $\{V\}$ and ζ during the ith simulation, and f_j is the free energy of the system. Equations 2.26 and 2.27 form a set of self-consistent equations that can be solved for $\mathrm{P}_{\{\lambda\},\beta}(\{V\},\zeta)$ and f_j iteratively[60]. The solution to equation 2.26 gives the best estimate for $\mathrm{P}_{\{\lambda\},\beta}(\{V\},\zeta)$, which in turn gives the best estimate for f_j to obtain the free energy profile along the reaction coordinate.

CHAPTER THREE

Insights into Key Interactions between Vancomycin and Bacterial Cell Wall Structures

This chapter reprinted with permission from: Feng Wang, Hongyu Zhou, Olatunde P. Olademehin, Sung Joon Kim, and Peng Tao. *Insights into Key Interactions between Vancomycin and Bacterial Cell Wall Structures*. ACS Omega 2018, 3, 37-45.

3.1 Abstract

Vancomycin is a glycopeptide antibiotic used for the treatment of serious infections by Gram-positive pathogens. Vancomycin inhibits cell wall biosynthesis by targeting the D-Ala-D-Ala terminus of peptidoglycan (PG). The highly cross-linked heptapeptide aglycon structure of vancomycin is the D-Ala-D-Ala binding site. The first residue of vancomycin is *N*-methyl-leucine, which is crucial for the dipeptide binding. The removal of *N*-methyl-leucine by Edman degradation results in desleucyl-vancomycin devoid of antimicrobial activities. To investigate the function of *N*-methyl-leucine for the dipeptide binding in vancomycin, molecular dynamics simulations of vancomycin and three *N*-terminus-modified vancomycin derivatives: desleucyl-vancomycin, vancomycinNtoC, and vancomycinSar, binding to a PG unit of the sequence L-Ala-D-iso-Gln-L-Lys-D-Ala-D-Ala with an intact pentaglycine bridge structure attached to the bridge link of L-Lys were carried out. Glycopeptide-PG binding interactions were characterized by root-mean-square-deviation contour analysis of atomic positions in vancomycin and its three analogues bound to a PG unit. The overall sampling space for four glycopeptide-PG complexes shows four distinct distributions with a continuous change between the

conformational spaces. The hydrogen bond analyses show that multiple hydrogen bonds between the D-Ala-D-Ala and the vancomycin aglycon structure strengthened the dipeptide binding. The simulations revealed that the removal or chemical modification of *N*-methyl-leucine significantly weakens the dipeptide binding to the aglycon structure and provides interesting structural insights into glycopeptide-PG binding interactions.

3.2 Introduction

Vancomycin (Figure 3.1a, R1) is a glycopeptide antibiotic isolated in 1956 from the fermentation of a soil actinomycete, *Amycolatopsis orientalis*. Since its discovery, vancomycin has been one of the most effective therapeutic agents for the treatment of serious infections by methicillin-resistant *Staphylococcus aureus*[61]. Vancomycin inhibits cell wall biosynthesis by binding with D-Ala-D-Ala dipeptide of peptidoglycan (PG)-stem unit (Figure 3.1b)[62]. The D-Ala-D-Ala dipeptide of PG binds to the aglycon structure of vancomycin, which is a highly cross-linked rigid cage-like structure formed by the phenolic ether linkages between the hydroxyphenylglycines at the second and sixth amino acid positions and between the phenolic hydroxyl residues at the fourth, fifth, and seventh positions (Figure 3.1a)[63]. The solution NMR structure of vancomycin complexed to acyl-L-Lys-D-Ala-D-Ala shows five hydrogen bonds between the heptapeptide backbone of aglycon to the D-Ala-D-Ala dipeptide are involved in the glycopeptide-PG binding[64]. In vancomycin-resistant enterococci, the D-Ala-D-Ala of the PG stem is replaced by a depsipeptide D-Ala-D-Lac, which replaces one of the hydrogen bonds with an electrostatic repulsion[65]. The depsipeptide substitution reduces the vancomycin binding affinity (K_d) from micromolar for the dipeptide to millimolar, enabling vancomycin resistance in enterococcal bacteria[66].

To investigate vancomycin-PG interactions, glycopeptide binding to a series of peptide analogues of bacterial cell wall were characterized using capillary electrophoresis, fluorescence correlation spectroscopy, and molecular dynamics (MD) simulations under different buffer systems.[67] One of the key residues that was identified as essential for the D-Ala-D-Ala binding was *N*-methylleucine found at the first position of the heptapeptide-core structure in vancomycin. *N*-methylleucine is not part of dipeptide binding site[64]. Nevertheless, the removal of *N*-methylleucine by Edman degradation[68] results in desleucyl-vancomycin (Figure 3.1a, R4) devoid of antimicrobial activity[69]. Because *N*-methylleucine is not directly involved in the dipeptide binding, the mechanism of loss dipeptide binding by desleucyl-vancomycin remains elusive. In this study, MD simulations of glycopeptide complexed to PG-peptide repeat unit (Figure 3.1b) were carried out to provide structural and dynamic insights for understanding the glycopeptide-PG interactions at atomic resolution[70]. The role of the *N*-methylleucine was elucidated by the MD simulations of PG binding by vancomycin and N-terminus modified vancomycin derivatives: vancomycin$_{NtoC}$, vancomycin$_{Sar}$, and desleucyl-vancomycin. In vancomycin$_{NtoC}$, the *N*-methyl in *N*-methylleucine of vancomycin is replaced with an ethyl moiety (Figure 3.1a, R2), and in vancomycin$_{Sar}$, the *N*-methylleucine is replaced by sarcosine (*N*-methylglycine) (Figure 3.1a, R3). Because the leucine sidechain substitution by sarcosine in vancomycin$_{Sar}$ significantly reduces the hydrophobicity, we hypothesized that the stability of glycopeptide-PG complex will gradually transition from vancomycin, vancomycin$_{NtoC}$, vancomycin$_{Sar}$, to desleucyl-vancomycin toward the unbound state.

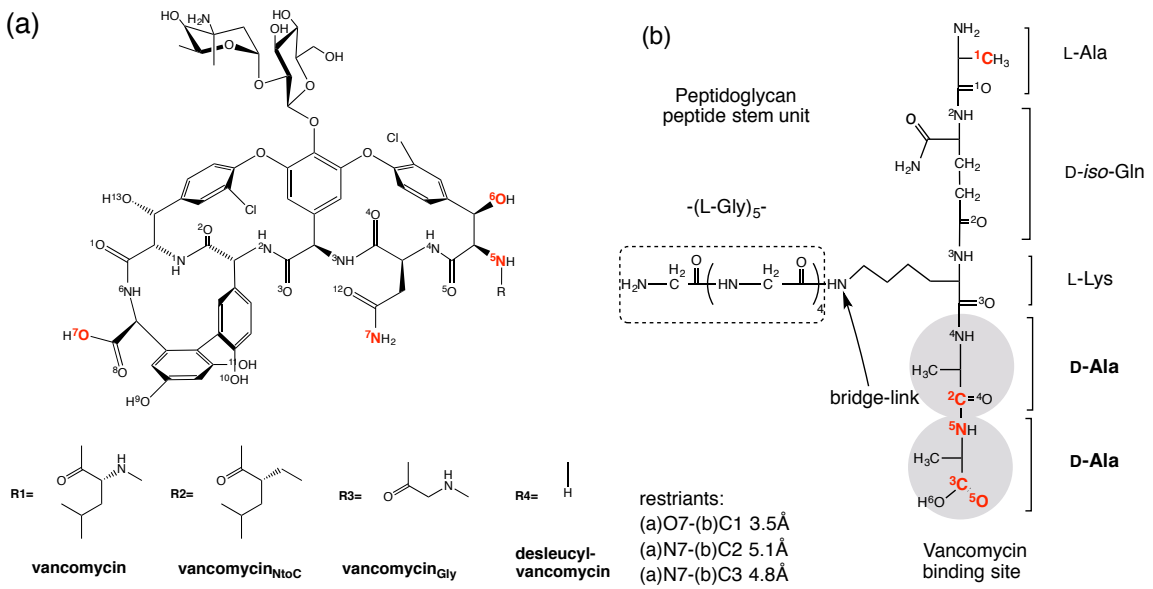

Figure 3.1. The chemical structure of vancomycin, vancomycin derivatives, and PG. (a) Chemical structures of vancomycin (R_n=R1), vancomycin$_{NtoC}$ (R_n=R2), vancomycin$_{Sar}$ (R_n =R3), and des-N-methylleucyl-vancomycin (R_n =R4). The key atoms are labeled with numbers shown in superscript. *(b)* The chemical *s*tructure of *S. aureus* PG-peptide stem unit without a disaccharide GlcNAc-MurNAc. A pentapeptides stem consists of the sequence L-Ala-D-iso-Gln-L-Lys-D-Ala-D-Ala, and a pentaglycine (dotted box) is attached to the ε-nitrogen side chain of L-Lys. The D-Ala-D-Ala (circles) of the PG stem is the known vancomycin-binding site. Three distance restraints were applied in the simulations: (1) "(a)O7-(b)C1 3.5 Å" which means that the distance between O7 in glycopeptide (a) and C1 in PG (b) is restrained to 3.5Å; (2) "(a)N7-(b)C2 5.1 Å" for the restrained distance of 5.1Å for internuclear distance between N7 in glycopeptide (a) and C2 in PG (b); and (3) "(a)N7-(b)C3 4.8 Å" for the restrained distance of 4.8Å between N7 in (a) and C3 in (b).

3.3 *Results*

3.3.1 Root-Mean-Square Deviation (RMSD) Analysis

The rmsd of vancomycin (V1) and its three analogues: vancomycin$_{NtoC}$ (V2), vancomycin$_{Sar}$ (V3) and desleucyl-vancomycin (V4) complexed with PG-peptide units for four independent simulations (s1 to s4) are plotted in Figure 3.2. The stability and flexibility of the complexes of vancomycin and its analogues bound to the peptide can be estimated by rmsd values, where a small rmsd indicates high stability and low flexibility, and vice versa for a large rmsd.

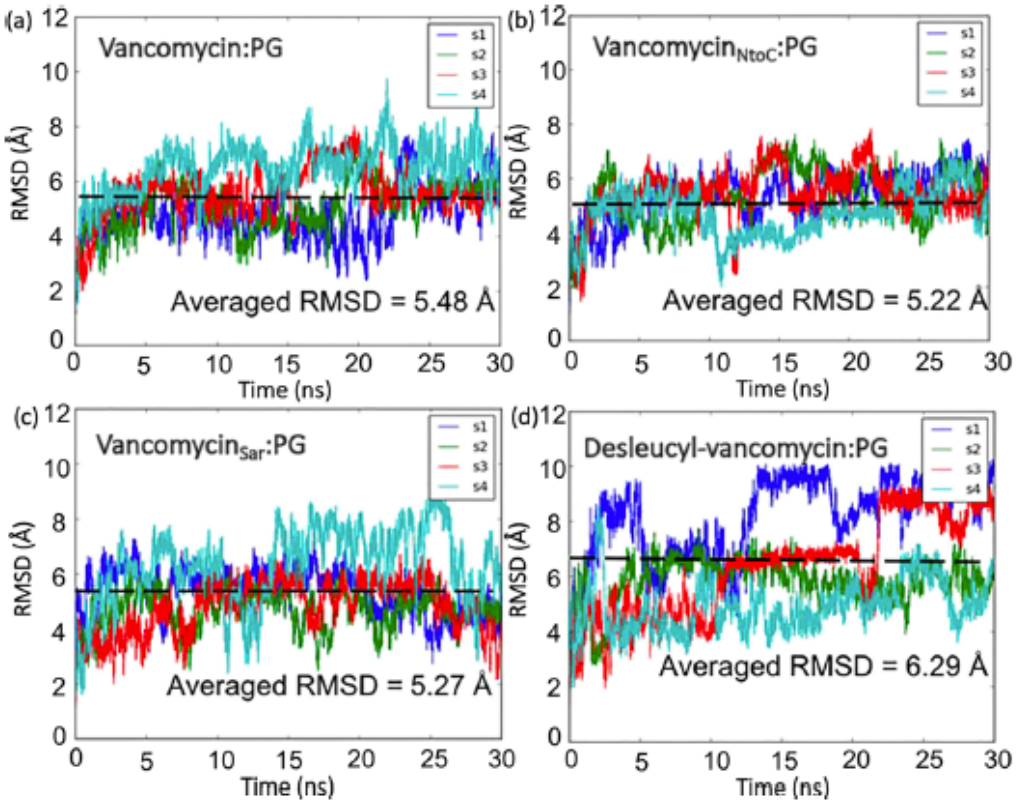

Figure 3.2. RMSD plots of MD simulations. The rmsd plots for the complexes of vancomycin/PG (a), vancomycinNtoC/PG (b), vancomycinSar/PG (c), and desleucyl-vancomycin/PG (d). Independent simulations for each system are labeled as s1, s2, s3, and s4. The black dashed line represents the averaged rmsd in each system.

Overall, vancomycin/PG and vancomycin$_{NtoC}$/PG complexes exhibit more fluctuation patterns and a lower rmsd range compared to the vancomycin$_{Sar}$/PG and desleucyl-vancomycin/PG, as shown in Figure 3.2, which suggests that the former two complexes have a lower flexibility and possibly a higher stability than the latter two. The averaged rmsd value for vancomycin/PG is 5.48 Å (Figure 3.2a). In comparison, the average rmsd value for desleucyl-vancomycin/PG was 6.29 Å (Figure 3.2d), for vancomycin$_{NtoC}$/PG is 5.22Å (Figure 3.2b), and for vancomycin$_{Sar}$/PG was 5.27Å (Figure 3.2c).

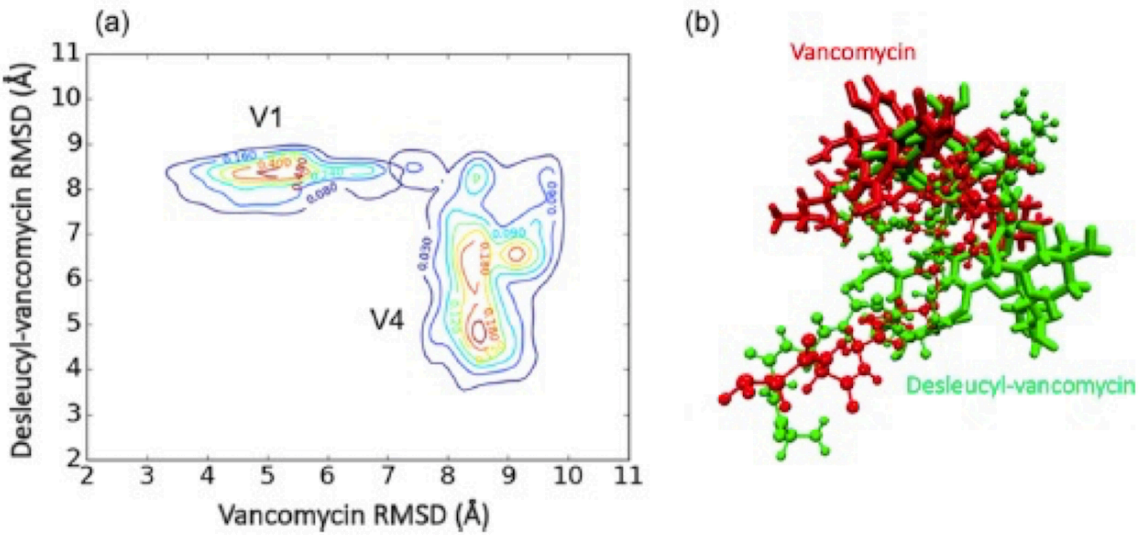

Figure 3.3. Comparison between simulations of vancomycin and desleucyl-vancomycin. (a) Two-dimensional (2D) rmsd (Å) contour plot of the vancomycin and desleucyl-vancomycin MD simulations. The contour lines represent the density of trajectories located in the area. (b) Initial structures for MD simulations of vancomycin (red) and desleucyl-vancomycin (green) complexes as references for rmsd (Å) calculation. For each frame of simulations of vancomycin and desleucyl-vancomycin, two rmsd (Å) values are calculated and plotted in regard to the reference vancomycin/PG complex and desleucyl-vancomycin/PG complex structures

To explore and compare the conformational distribution of MD simulations of vancomycin and desleucyl-vancomycin complexes, 2D contour plots are generated to illustrate the conformational distribution of these two complexes (Figure 3.3). The reference structures for vancomycin/PG (red) and desleucyl-vancomycin/PG (green) complexes are shown in Figure 3.3b with a shared aligned peptide structure. Vancomycin and desleucyl-vancomycin complexes have significantly different conformational space which is suggested by two completely different attraction basins on the 2D contour plot with very little overlap between the distributions (Figure 3.3a). In addition, the distribution for vancomycin/PG (V1) is much narrower than those/ of desleucyl-vancomycin/PG (V4). This is consistent with the observation that the simulations of vancomycin/PG complex have generally lower rmsd than that of desleucyl-vancomycin/PG complex (Figure 3.2).

For the vancomycin/PG rmsd distribution (V1), only a single attraction basin is observed at (5.5, 8.5Å). This is in contrast to multiple basins observed for the rmsd distribution of desleucyl-vancomycin/PG complex (V4) centered at (8.5, 4.5Å), (8.5, 6.5Å) and (9, 6.5Å) (Figure 3.3a). The broad distribution with multiple basins for the desleucyl-vancomycin/PG complex supports that the PG binding by desleucyl-vancomycin is more flexible than that by vancomycin.

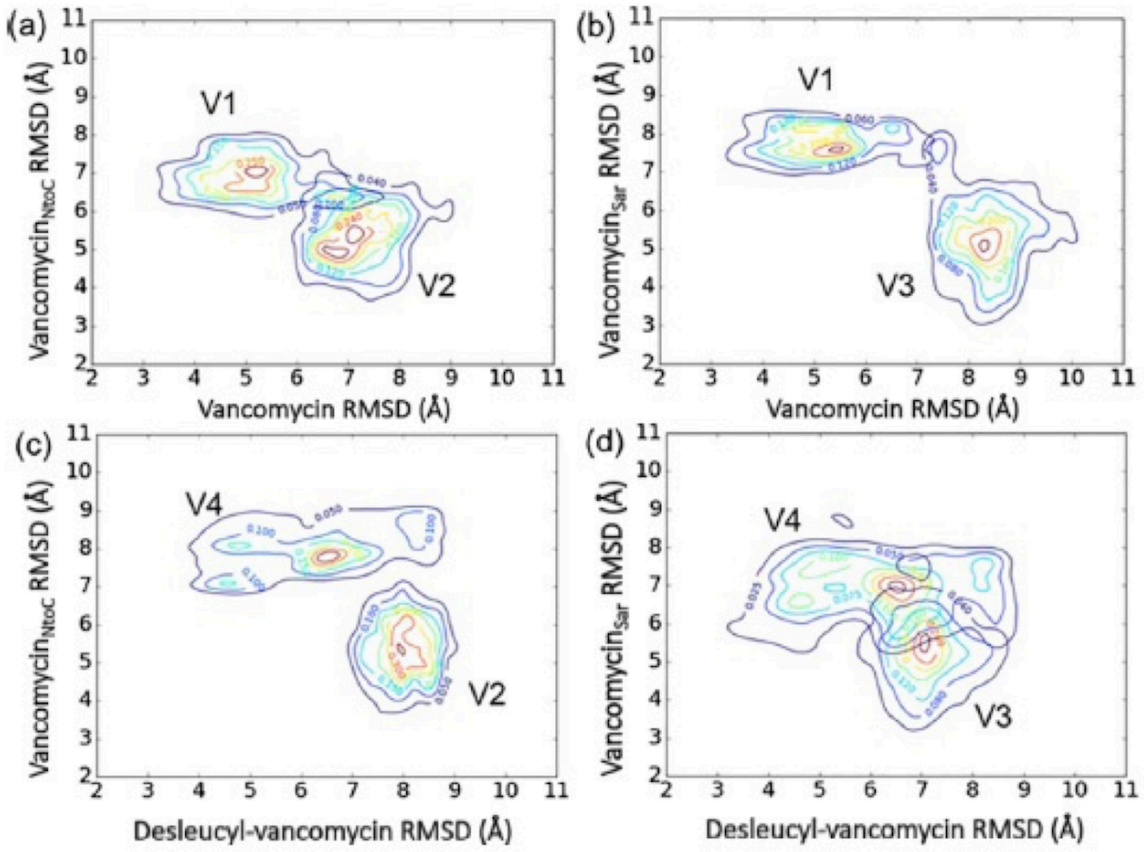

Figure 3.4. Comparative 2D rmsd (Å) contour plots of vancomycin/PG (V1) and desleucyl-vancomycin/PG (V4) complexes in regard to vancomycin$_{NtoC}$/PG (V2) and vancomycin$_{Sar}$/PG (V3) complexes. Comparative 2D rmsd contour plots of (a) vancomycin vs. vancomycin$_{NtoC}$, (b) vancomycin vs. vancomycin$_{Sar}$, (c) desleucyl-vancomycin vs. vancomycin$_{NtoC}$, and (d) desleucyl-vancomycin vs. vancomycin$_{Sar}$. The rmsd (Å) values for each plot were calculated in regard to the reference structure, which is the initial structure for the MD simulation of each complex. The contour lines represent the density of trajectories that are located within the area.

To further characterize all four glycopeptide-PG complexes, the comparative 2D rmsd distributions of vancomycin/PG (V1) and vancomycin$_{NtoC}$/PG complexes (V2) are shown in Figure 3.4a, V1 and vancomycins$_{Sar}$/PG (V3) in Figure 3.4b, desleucyl-vancomycin/PG (V4) and V2 in Figure 3.4c, and V4 and V3 in Figure 3.4d. While the rmsd distribution for V1 and V2 show a significant overlap with attraction basins of each complex being close to each other (Figure 3.4a), the V1 and V3 distributions show only a minimal overlap with increased separation between the basins (Figure 3.4b). This indicates that the binding mode of vancomycin$_{NtoC}$/PG complex resembles more closely to vancomycin/PG than that of vancomycin$_{Sar}$/PG complex. By contrast, the plots of vancomycin$_{NtoC}$/PG (V2) and desleucyl-vancomycin/PG (V4) complex distributions show no overlap (Figure 3.4c). This suggests that the binding mode of vancomycin$_{NtoC}$ and PG resembles more closely to vancomycin/PG complex than that of the desleucyl-vancomycin/PG complex. The desleucyl-vancomycin/PG complex distribution (V4), which overlaps with about one third of vancomycin$_{Sar}$/PG complex (V3) (Figure 3.4d) shows that these two complexes share significant conformational space.

3.3.2 Conformational Space for Glycopeptide-PG Complexes

To elucidate the relationship among these four glycopeptide-PG complexes, the simulations of all four complexes are plotted on a same 2D RMSD plot using vancomycin/PG and desleucyl-vancomycin/PG complexes as reference structures to characterize their distribution in overall conformational space. One of the advantages of this analysis is that it reveals the total conformational space for all glycopeptide-PG complexes. The overall shape of distributions is similar to the combined distribution of 2D rmsd plots shown in Figures 3.3 and 3.4. Four major clusters were identified from the

overall distribution using k-means clustering analysis[71] (Figure 3.5a). The shape and position of four clusters suggest some corresponding relations to the four glycopeptide-PG complexes.

The percentile contribution from the simulations of each glycopeptide-PG complex was calculated for each cluster and plotted in Figure 3.5b. Cluster "*a*" primarily corresponds to the conformational space of vancomycin/PG complex (V1), as shown in Figures 3.4 and 3.5a. Thus, vancomycin/PG complex distribution is the dominant contributor to cluster "*a*" (90%) with a minor contribution arising from the adjacent cluster "*b*". In cluster "*b*", vancomycin$_{NtoC}$/PG complex, which closely resembles vancomycin/PG complex more than any other analogues, is the major contributor (65%) with minor contributions from the adjacent clusters "*a*" and "*c*" (3% to each). In cluster "*c*", vancomycin$_{Sar}$/PG complex distribution is the dominant contributor (61%). The contribution from cluster "*d*" to the complex (21%) is significantly higher than that of cluster "*b*" (11%). Finally, in cluster "*d*", the desleucyl-vancomycin/PG complex is the dominant contributor (79%) with 21% contribution from the vancomycin$_{Sar}$/PG complex.

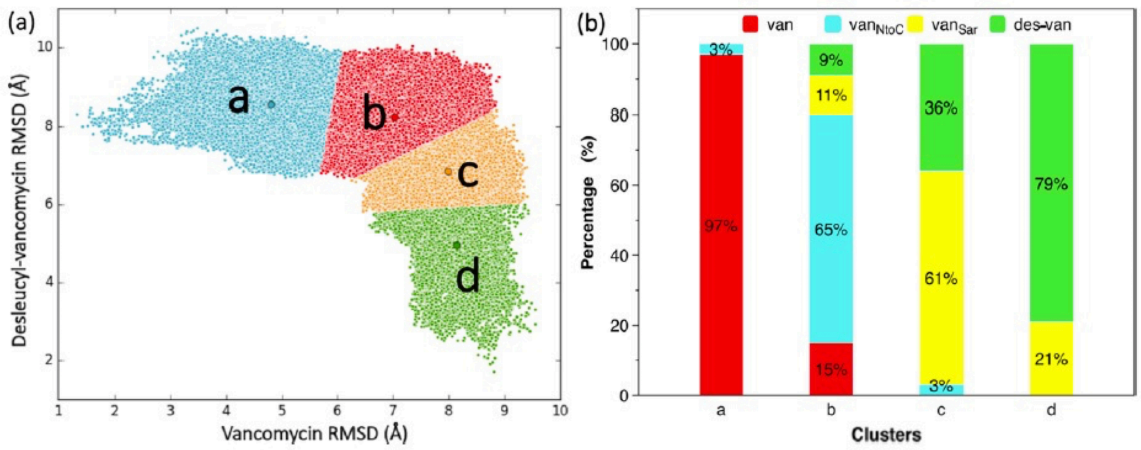

Figure 3.5. Overall sampling space and distribution of four glycopeptide-PG complexes. (a) Distribution of four glycopeptide-PG complexes in regard to vancomycin/PG and desleucyl-vancomycin/PG complexes as reference structures. The overall distribution is divided into four clusters (*a*, *b*, *c*, and *d*) using k-means clustering analysis. (b) Percentile of the contribution to each cluster in (a) from simulations of each glycopeptide-PG complex: van, red (vancomycin); des-van, green (desleucyl-vancomycin); van_{Sar}, yellow ($vancomycin_{Sar}$); and van_{NtoC}, blue ($vancomycin_{NtoC}$).

Interestingly, with an exception of vancomycin, which contributes to clusters "*a*" and "*b*" only, all three vancomycin analogues complexed with PG contribute to three clusters. For example, $vancomycin_{NtoC}$ contributes to clusters "*a*", "*b*", "*c*" and $vancomycin_{Sar}$ and desleucyl-vancomycin both contribute to clusters "*b*", "*c*", "*d*". This indicates that the vancomycin/PG complex has the narrowest distribution among all four complexes, and this suggests that it is also the most stable. This sequential distribution patterns exhibited by the vancomycin analogues, $vancomycin_{NtoC}$ and $vancomycin_{Sar}$ (Figure 3.5b), are consistent with the vancomycin analogues representing the intermediate states for progressive transition in PG binding from vancomycin to desleucyl-vancomycin that results in the loss of PG-dipeptide binding.

3.3.3 Interaction between PG and Vancomycin Analogues

A crucial insight into the molecular interaction for vancomycin and desleucyl-vancomycin with PG-peptide stem units is obtained from the detailed analysis of key atomic pairs found in the model structures. Model structures of vancomycin and desleucyl-vancomycin bound to the PG representing the centers of attraction basins in contour plots of these two simulations are illustrated in Figures 3.6a,b, respectively. The distribution of two pairs of key atomic distances, between N5 from desleucyl-vancomycin and N5 in D-Ala-D-Ala of PG (N5v-N5p), and between O6 from desleucyl-vancomycin and O5 in D-Ala-D-Ala of PG (O6v-O5p), from the simulations is co-plotted for both vancomycin/PG (V1) and desleucyl-vancomycin/PG complexes (V4) in Figure 3.6c. The N5v-N5p and O6v-O5p distances represent key interactions between the aglycon structure of vancomycin and the bound D-Ala-D-Ala dipeptide of PG. The distributions of V1 and V4 do not co-localize on the 2D contour plot, indicating that vancomycin and desleucyl vancomycin have an intrinsic difference in their interactions with D-Ala-D-Ala. The vancomycin/PG complex (V1) has a narrower distribution for N5v-N5p and O6v-O5p distances centered around (6.5, 6 Å) than desleucyl-vancomycin/PG (V4) centered around (9, 11 Å). The result from pair distance distribution simulations is consistent with the evidence that the conformational space distribution of vancomycin interaction with D-Ala-D-Ala moiety of PG is narrower and significantly stronger (Figure 3.5b) than that of desleucyl-vancomycin. This provides molecular insight into the loss of antimicrobial activity in desleucyl-vancomycin as evident in the model structures shown in Figure 3.6. While vancomycin adopts a binding pocket conformation that is favorable for binding the D-Ala-D-Ala moiety of PG (Figure 3.6a), the glycon structure of desleucyl-vancomycin

adopts an extended conformation that is not amenable for the dipeptide binding (Figure 3.6b).

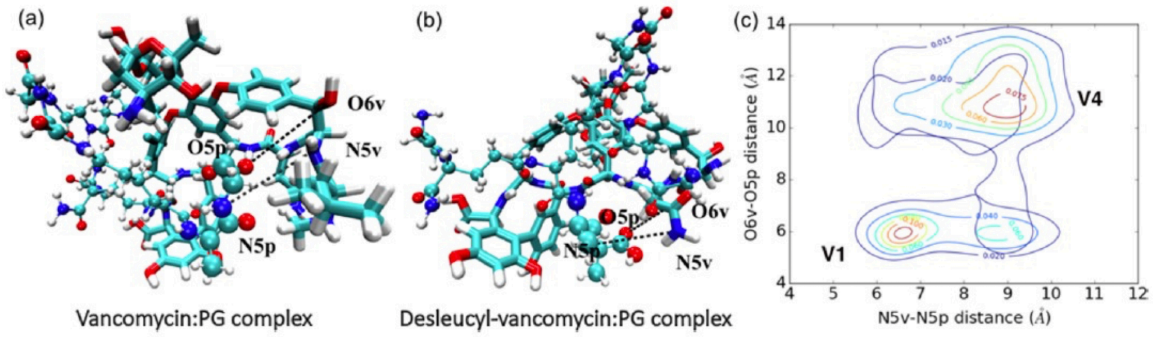

Figure 3.6. Key interaction between vancomycin and PG represented as atomic pair distance distributions. Model structures of vancomycin/PG (a) and desleucyl-vancomycin/PG (b) complexes. In (a,b), the stick structures represent (desleucyl-) vancomycin, and ball and stick structures represent PG units with D-Ala-D-Ala part represented by larger sphere. Color codes of ball and stick structure: oxygen (red), nitrogen (blue), hydrogen (white), carbon (cyan) and chlorine (green). The nomenclature, N5v and O6v refer to the amide nitrogen and the oxygen on the carbonyl carbon at the fifth residue in glycopeptides, respectively. N5p and O5p refer to the amide nitrogen and the oxygen from the D-Ala (fifth amino acid) in PG, respectively. (c) Contour plots of atomic pair distance distributions for the vancomycin/PG complex (V1) and desleucyl-vancomycin/PG complex (V4).

3.3.4 Hydrogen bonds, Entropy, and Binding Free Energy

The total number of hydrogen bonds (H-bonds) in each of four analogues/PG complexes was estimated using VMD 1.9.2 with the donor-acceptor distance defined as within 3 Å with the angle cutoff as 20° within linear (180°) configuration. Only the H-bonds with greater than 1% occupancy (stable for more than 1% of the simulations) were considered for the analysis. The total number of H-bonds formed during the simulations of four glycopeptide-PG complexes ranged from 10 to 13 (Figure 3.7a). Our simulations show that the vancomycin/PG complex had the largest number of H-bonds (five H-bonds) among all four complexes. The five H-bonds in vancomycin/PG complex showed high

occupancy (up to 27.97%) (Table 3.1), consistent with multiple H-bonds stabilizing the binding of the D-Ala-D-Ala to the aglycon of vancomycin. By contrast, desleucyl-vancomycin/PG complex had the least number of H-bonds (one H-bond) with a relatively low partial occupancy of only 13.12% (Table 3.2). The specific hydrogen bonds with occupancy higher than 3.00% are listed in the Table 3.1 and 3.2.

Table 3.1. Atom pairs of hydrogen bonds in vancomycin/PG complex

Donor[a]	Acceptor[a]	Occupancy[a] (%)
Van-Side-N6	Pep-Side-O2	27.97%
Pep-Side-O6	Van-Side-O3	6.95%
Van-Side-N6	Pep-Side-O3	6.15%
Van-Side-N6	Pep-Side-O1	5.71%
Van-Side-N3	Pep-Side-O5	4.87%
Van-Side-O7	Pep-Side-N1	3.54%

[a]The donors, acceptors, occupancy (>3.00%) and 59951 frames. "Van-Side" or "Pep-Side" represent where the atoms come from, van-side is for vancomycin and pep-side is for peptide units.

Table 3.2. The atoms pair of hydrogen bonds in desleucyl-vancomycin/PG complex[a]

Donor	Acceptor	Occupancy (%)
Des-van-Side-N6	Pep-Side-O2	14.74%
Pep-Side-N4	Des-van-Side-O3	13.12%
Des-van-Side-O11	Pep-Side-O3	6.55%

[a]The donors, acceptors, occupancy (>3.00%) and 59951 frames. "Des-van-Side" or "Pep-Side" represent where the atoms come from, "Des-van-side" is for desleucyl vancomycin and "Des-pep-side" is for peptide units

Table 3.3. Configurational entropies of glycopeptide-PG complexes[a]

Parameter	Vancomycin	$Vancomycin_{NtoC}$	$Vancomycin_{Sar}$	Desleucyl-vancomycin
Number of atoms	282	283	270	260
Molar mass of molecules	1450	1449	1394	1322
Configuration entropy[b]	836.6	788.9	715.1	706.4
Normalization entropy[b] (divided by the number of atoms)	2.97	2.79	2.65	2.72
Normalization entropy[b] (divided by atomic mass)	0.577	0.544	0.512	0.534

[a]The first row is the number of atoms from vancomycin, $vancomycin_{NtoC}$, $vancomycin_{Sar}$ and desleucyl vancomycin. [b]The unit of configuration entropy is calorie/mol•K.

We also calculated the configurational entropies of the four complexes (Figure 3.7b and Table 3.3). For the comparison, the configurational entropy for each of the vancomycin analogue and PG was calculated separately. Interestingly, vancomycin has the largest configurational entropy (836.6 cal/mol•K) among four analogues with desleucyl-vancomycin as the least (706.4 cal/mol•K). Although $vancomycin_{NtoC}$ has greater number of atoms than vancomycin, it has smaller entropy than vancomycin. The calculated entropies show the decreasing trend from vancomycin, $vancomycin_{NtoC}$, $vancomycin_{Sar}$, to desleucyl-vancomycin. A similar trend is also observed for the normalized entropies, where the calculated entropies are divided by the number of atoms or by the atomic mass of each analogue (Table 3.3), revealing intrinsic property of these analogues. The calculated entropies in Table 3.3 are for the glycopeptides only without PG binding; whereas, the calculated rmsd values in Figures 3.2 through 3.5 are for the glycopeptide-PG complexes. We observed that vancomycin with highest entropy when bound to PG results in a vancomycin/PG complex with the lowest rmsd. Likewise, the desleucyl-vancomycin with the lowest entropy when bound to PG results in a desleucyl-

vancomycin/PG complex with the highest rmsd. Hence, the low entropy of a glycopeptide does not necessarily correlate with the low rmsd in glycopeptide-PG complexes, and vice versa.

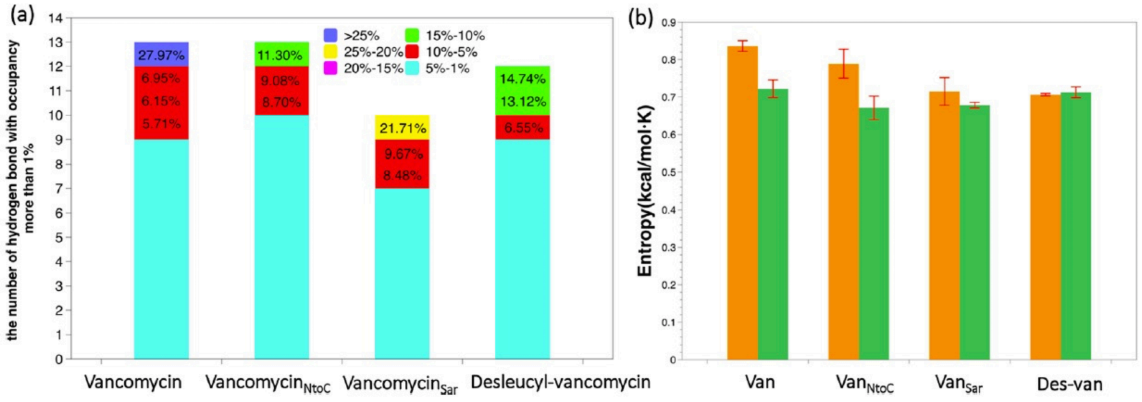

Figure 3.7. Number of hydrogen bonds and configurational entropies. (a) The number of hydrogen bonds found in the simulations of vancomycin, vancomycin$_{NtoC}$, vancomycin$_{Sar}$, desleucyl-vancomycin binding with PG. Only the hydrogen bonds that have more than 1% occupancy (being stable for more than 1% of the simulations for each complex) are considered in the analysis. (b) The configurational entropies of vancomycin, vancomycin$_{NtoC}$, vancomycin$_{Sar}$, desleucyl-vancomycin (orange bar) and PG in four complexes (green bar). Error bars represent the standard deviation from 4 independent simulations.

The binding free energy was calculated using the molecular mechanics/Poisson-Boltzmann surface area (MM/PBSA) method to further compare the stability of vancomycin and desleucyl-vancomycin binding with PG. The use of distance restraints during the simulations prevented the accurate calculation of the binding free energy; however, all simulations were subjected to the same distance restraints, and thus the effects of distance restraints on binding free energy are likely to be comparable for all complexes. The estimated binding free energy of vancomycin/PG and desleucyl-vancomycin/PG complexes are -37.84 ± 2.16 and -11.17 ± 16.07 kcal/mol, respectively. Hence PG binding

to vancomycin is significantly more favorably than desleucyl-vancomycin by a ΔΔG of approximately -27 kcal/mol. Despite the error in binding free energy calculation associated with large variance in trajectories, significant difference in ΔΔG is consistent with stable vancomycin/PG compared to desleucyl-vancomycin/PG complex.

3.4 Discussion

The X-ray crystal[72-73] and solution NMR structures of vancomycin and related glycopeptides, with an exception of ristocetin,[74-75] are found as dimers or oligomers. Hence drug dimerization is thought play an important role in glycopeptide mode of action.[76-77] However, *in situ* characterization of disaccharide-modified glycopeptides, including oritavancin that readily forms drug dimer in solution, when complexed to intact whole cells and isolated cell walls of *Staphylococcus aureus* are found as monomers without dimerization[78-85]. Glycopeptide antibiotics binding to PG in cell walls as a monomer is due to complex multivalent interactions among the cell wall glycans with drug sugar disaccharide and glycopeptide interactions with non-D-Ala-D-Ala segment of the PG-stem structure[86]. To characterize the monomeric glycopeptide-PG interactions, MD simulations of vancomycin and its three *N*-terminus modified vancomycin derivatives bound to a PG-stem unit, L-Ala-D-iso-Gln-L-Lys-D-Ala-D-Ala with a $(Gly)_5$ bridge attached, were carried out.

The first amino acid in type I glycopeptide antibiotics, which include vancomycin, chloroeremomycin, and eremomycin is *N*-methyl-leucine. *N*-methyl-leucine is essential for the dipeptide binding, where the removal by Edman degradation results in a hexapeptide[87] with 100-fold reduction in dipeptide binding affinity and the loss of antimicrobial activities[88]. Accordingly, our simulations show shat the desleucyl-

vancomycin/PG complex in general is less ordered than the vancomycin/PG complex. For example, the average rmsd value for desleucyl-vancomycin/PG simulation was significantly larger and had much broader rmsd distribution than that for vancomycin/PG simulation (Figure 3.2). This indicated that the desleucyl-vancomycin had greater conformational space with more flexible PG binding than vancomycin. Moreover, rmsd distributions in the 2D contour plot of desleucyl-vancomycin and vancomycin did not share a common space, indicating that desleucyl-vancomycin has a distinct binding structure. The desleucyl-vancomycin/PG complex, in comparison to the vancomycin/PG complex, showed reduced binding energy of approximately 27 kcal/mol (Figure 3.3). The key atomic distance distributions of selected atoms in the bound dipeptide to the aglycon structure of vancomycin and desleucyl-vancomycin (Figure 3.6c) further reveal that the D-Ala-D-Ala moiety of PG has a much tighter binding mode with vancomycin than desleucyl-vancomycin. The superimposed model structures of vancomycin and desleucyl-vancomycin bound to PG (Figure 3.6b) show that the binding cleft of desleucyl-vancomycin exhibits an extended conformation.

The peptide core of vancomycin is highly cross-linked to form a rigid structure. By contrast, the side chain of Asn and N-methyl-Leu is highly flexible in the absence of D-Ala-D-Ala binding. This flexibility is crucial for the dipeptide binding as these side chains are thought to function as "flaps" to swing into the ligand-binding site as a surrogate in the absence of a ligand[72]. The partial occupancy of the binding cleft by the Asn and *N*-methyl-Leu side chains is thought to prevent the hydration of the aglycon structure. In the presence of a ligand, the side chains of Asn and *N*-methyl-Leu facilitates the desolvation of the binding cleft necessary for the D-Ala-D-Ala binding.[73] Following the D-Ala-D-Ala binding,

the side chains of Asn and *N*-methyl-Leu become rigid.[89] Our rmsd distribution analysis shows that the replacement of *N*-methyl-Leu by shortened side-chain length significantly diminished PG binding and its stability. The order of most stable to least stable glycopeptide-PG complexes are: vancomycin, vancomycin$_{NtoC}$, vancomycin$_{Sar}$, and desleucyl-vancomycin. In the case of vancomycin$_{Sar}$, replacing the positively charged *N*-methyl-leucine with an ethyl moiety in aglycon interferes with the binding to the carboxyl terminus of the PG dipeptide.[89] The calculated glycopeptide stability correlated with the overall strength of hydrogen bonding interactions with the highest for the vancomycin/PG complex and the least for desleucyl-vancomycin/PG complex (Figure 3.7a). The changes in entropy, despite the shared hydrogen bonds, indicated that the highest entropy, corresponding to the lowest free energy, could be the crucial determinant for ligand binding. We anticipate that the glycopeptide-PG interactions are not local but involves multiple interactions between the aglycon structure and the non-D-Ala-D-Ala segment of PG-stem structure that are likely to be cooperative and critical for the overall effectiveness of PG binding by the glycopeptide antibiotics. Our study provides a new approach to characterize the complex interactions between the PG and glycopeptide antibiotics that will facilitate the design and development of novel antibiotics against the emerging multi-drug resistant Gram-positive pathogens.

3.5 Conclusion

In this study, we built simplified simulation models to study the molecular mechanism of vancomycin as an antibiotic through binding with bacteria cell wall structures. The Edman degradation of vancomycin cleaves the first residue from the aglycon structure, resulting in desleucyl-vancomycin with a damaged binding pocket and devoid of any

antimicrobial activities. To reveal the atomic details of vancomycin and cell wall peptide structure interactions, two vancomycin derivatives with chemical modification of the first residue in aglycon structure were built as intermediate analogues between vancomycin and desleucyl-vancomycin and referred to as vancomycin$_{NtoC}$ and vancomycin$_{Sar}$. Using MD simulations, we show that the binding in vancomycin/PG is the tightest among all four analogues. The rmsd distribution analyses revealed the continuous conformational distribution among these four analogues from vancomycin to desleucyl-vancomycin. Through atomic distance analyses, it is also suggested that the D-Ala-D-Ala segment of PG-stem structure binds more favorably with vancomycin than its desleucyl analogue. The calculated entropies and binding free energy of four complexes also displayed consistent trend from the most favorable binding of vancomycin against cell wall peptide to the least favorable of desleucyl-vancomycin. Overall, the MD simulations provide a new approach to provide insights for the development of novel glycopeptide antibiotics with improved antimicrobial activities against the evolving glycopeptide resistance in pathogens.

3.6 Computational Methods

3.6.1 MD Simulation

The structures of vancomycin and its derivatives (Figure 3.1) complexed with the PG-peptide repeat unit were based on the computational model from a previous study[86, 90] and optimized to B3LYP/6-311G(d,p) level of theory using the Gaussian09 program package[91]. The CHARMM General Force Field (CGenFF) for the simulation system was generated using the online server ParamChem (https://cgenff.paramchem.org/)[92]. Atomic charges of the simulation system were taken from the Gaussian calculations. All systems

were solvated in water box using a TIP3P model[93] with the addition of sodium and chlorine as charge balancing ions. Simulation box sizes, numbers of ions, and the ionic strength are listed in Table 3.4. The following equation was used to calculate the ionic strength based on the simulation box size and number of ions,

$$I = \frac{1}{2} \sum_{i=1}^{n} c_i z_i^2 \quad (3.1)$$

where i is the ion identification number, and z represents charge of the ion.

Table 3.4. Ionic strengths of vancomycin/PG, vancomycin$_{NtoC}$/PG, vancomycin$_{Sar}$/PG, and desleucyl-vancomycin/PG complexes

Parameter	Vancomycin	Vancomycin$_{NtoC}$	Vancomycin$_{Sar}$	Desleucyl-vancomycin
Ionic strength (mol.L^{-1})	84.9	84.8	85.2	71
Number of ions	4Cl$^-$, 6Na$^+$	4Cl$^-$, 6Na$^+$	4Cl$^-$, 6Na$^+$	4Cl$^-$, 6Na$^+$
Box size (Å)	46.1	46.1	46.0	48.9

The simulation boxes were subjected to 200 steps of the steepest descent energy minimization and then further energy minimized using the adopted basis Newton-Raphson method until the total gradient of the system was lower than 0.03 kcal/(mol·Å). Subsequently, the minimized simulation systems were subjected to 24 ps of the MD simulations at a temperature of 300 K as the equilibrium. Then the MD simulation of the system was run for 30 ns via isothermal-isobaric ensemble at 300 K and 1 atm. The time step for MD simulations is 2 fs, with all the bonds associated with hydrogen being fixed during the simulation. The cutoff distance for non-bonded interaction is 12 Å and using a Nosé–Hoover thermostat[94-95] to keep the temperature of system at 300K for 30ns. The leapfrog Verlet scheme was used for the integration of the atomic velocities and coordinates in simulations. All simulations used periodic boundary conditions, and electrostatic interactions were modeled using the particle mesh Ewald method[96]. Three

atomic pair distance restraints were applied during the simulations based on solid-state NMR experiments.[97-98] All simulations were carried out using MM simulation program, CHARMM version 40b1[99].

3.6.2 Root-Mean-Square Deviation (rmsd)

The rmsd is used to measure the difference of the conformation for each snapshot of the MD simulations from the reference structure. For a molecular structure represented by Cartesian coordinate vector r_i (i = 1 to N) of N atoms, the rmsd is calculated as follows:

$$\text{rmsd} = \sqrt{\frac{\sum_{i=1}^{N}(r_i^0 - Ur_i)^2}{N}} \tag{3.2}$$

The Cartesian coordinate vector r_i^0 is the *i*th atom in the reference structure. The transformation matrix U is defined as the best-fit alignment between the vancomycin-PG complex structures along trajectories in respect to the reference structure.

3.6.3 Cross-Correlation Matrix

The correlation of motion between all atomic pairs in each simulation was measured through cross-correlation matrix. The element C_{ij} of the cross-correlation matrix **C,** which measures the correlation between the movement of atoms *i* and *j* in the simulation is defined as

$$C_{ij} = \frac{\langle r_i r_j \rangle - \langle r_i \rangle \langle r_j \rangle}{\left[\left(\langle r_i^2 \rangle - \langle r_i \rangle^2\right)\left(\langle r_j^2 \rangle - \langle r_j \rangle^2\right)\right]^{1/2}} \tag{3.3}$$

where r_i and r_j are Cartesian coordinate vectors from the least-square fitted structures in MD simulation trajectories. It should be noted that the least-square fitting of the MD trajectory effectively projects out the translational and rotational motions of the

vancomycin and its analogues complexed with the peptide. The normalized matrix elements C_{ij} has its value ranging between -1 and 1. A positive C_{ij} value associates with an overall positive correlation between atoms *i* and *j*, and a negative value corresponds to a negative correlation.

3.6.4 Configurational Entropy

Entropy was estimated for the simulation systems using quasi-harmonic approximations based on MD simulations. Quasi-harmonic analysis was carried out through the inversion of cross-correlation matrix **C**

$$F_{ij} = k_B T[C^{-1}]_{ij} \quad (3.4)$$

In equation 3.4, F_{ij} is the element of the force constant matrix **F** describing the quasi-harmonic potential,[100] k_B is the Boltzmann constant, and *T* is the temperature.

Configurational entropy S_{config} of the simulation system could be calculated using the vibration frequency ω of the molecule with N atoms:

$$S_{config} = k_B \sum_i^{3N-6} \frac{\hbar\omega_i/k_B T}{e^{\hbar\omega_i/k_B T}-1} - \ln\left(1 - e^{-\hbar\omega_i/k_B T}\right) \quad (3.5)$$

$\hbar$ is the reduced Planck constant.

The vibration frequency ω in the quasi-harmonic model of the molecule on the effective quasi-harmonic potential can be calculated through the solution of the secular equation

$$\det(\mathbf{F} - \omega^2 \mathbf{M}) = 0 \quad (3.6)$$

where **M** is the mass matrix of the molecule.

3.6.5 MM/PBSA Binding Free Energy Calculation

Total free energy of binding $\Delta G_{binding}$ was computed using the MM/PBSA method. This method uses a thermodynamic cycle to calculate the free energy of binding for vancomycin

and its analogues against PG peptide. The free energies of binding are computed using the equation:

$$\Delta G_{binding}^{sol} = \Delta G_{complex}^{sol} - \Delta G_{van}^{sol} - \Delta G_{PG}^{sol} \quad (3.7)$$

where $\Delta G_{binding}^{sol}$ is the total free energy of binding in solution, and $\Delta G_{complex}^{sol}$, ΔG_{van}^{sol} and ΔG_{PG}^{sol} are free energies in solution of the complex, vancomycin/analogues, and PG, respectively. The free energy in solution of each entity (ΔG^{sol}) is calculated by the following equations:

$$\Delta G^{sol} = \Delta G^{gas} + \Delta G_{solvation} \quad (3.8)$$

$$\Delta G^{gas} = E_{internal} + E_{vdw} + E_{electrostatic} - T\Delta S \quad (3.9)$$

$$\Delta G_{solvation} = \Delta G_{PB} + \Delta G_{nonpolar} \quad (3.10)$$

where ΔG^{gas} is the free energy in gas phase, and $\Delta G_{solvation}$ is the solvation energy. ΔG^{gas} is the sum of the internal energy ($E_{internal}$), van der Waals (E_{vdw}) and Coulombic ($E_{electrostatic}$) interactions, as well as entropic contributions (ΔS). The internal energy includes bond stretching, bond angle, and torsional contributions to the total MM energies. The solvation energy $\Delta G_{solvation}$ includes polar (ΔG_{PB}) and nonpolar ($\Delta G_{nonpolar}$) contributions.

CHAPTER FOUR

Molecular Dynamics Simulation of Atomic Interactions in the Vancomycin Binding Site

This chapter reprinted with permission from: Olatunde P. Olademehin, Sung Joon Kim, and Kevin L. Shuford. *Molecular Dynamics Simulation of Atomic Interactions in the Vancomycin Binding Site*. ACS Omega 2021, 6, 775-785.

4.1 Abstract

Vancomycin is a glycopeptide antibiotic produced by *Amycolaptopsis orientalis* used to treat serious infections by Gram-positive pathogens including methicillin-resistant *Staphylococcus aureus*. Vancomycin inhibits cell wall biosynthesis by targeting the lipid II, which is the membrane-bound peptidoglycan precursor. The heptapeptide aglycon structure of vancomycin binds to the D-Ala-D-Ala of the pentapeptide stem structure in lipid II. The third residue of vancomycin aglycon is asparagine which is not directly involved in the dipeptide binding. Nonetheless, asparagine plays a crucial role in substrate recognition, as the vancomycin analogue with asparagine substituted by aspartic acid (V_D) shows a reduction in antibacterial activities. To characterize the function of asparagine, binding of vancomycin and its aspartic-acid-substituted analogue V_D to L-Lys-D-Ala-D-Ala and L-Lys-D-Ala-D-Lac was investigated using molecular dynamic simulations. Binding interactions were analyzed using root-mean-square deviation (RMSD), two-dimensional (2D) contour plots, hydrogen bond analysis, and free energy calculations of the complexes. The analysis shows that the aspartate substitution introduced a negative charge to the binding cleft of V_D which altered the aglycon conformation that minimized the repulsive

lone pair interaction in the binding of a depsipeptide. Our findings provide new insight for the development of novel glycopeptide antibiotics against the emerging vancomycin-resistant pathogens by chemical modification at the third residue in vancomycin to improve its binding affinity to the D-Ala-D-Lac terminated peptidoglycan in lipid II found in vancomycin-resistant enterococci and vancomycin-resistant *S. aureus*.

4.2 Introduction

Vancomycin is a glycopeptide antibiotic discovered in the 1950s[101] by Eli Lilly from the fermentation broth of a soil microbe *Amycolaptopsis orientalis*. The newly discovered antibiotic was named vancomycin, derived from the word "vanquish", because of its potent antibacterial activities. Vancomycin is highly active against a broad spectrum of Gram-positive pathogens including bacilli and all aerobic cocci including staphylococci, streptococci, and enterococci. Despite its early Food and Drug Administration (FDA) approval in 1958, vancomycin was not widely used due to the high cost and adverse side effects associated with purification. Instead, methicillin, a powerful semisynthetic β-lactam antibiotic that was developed in the 1950s became the antibiotic of choice against the penicillin-resistant pathogens. Then in the 1980s, vancomycin became one of the most important antibiotics due to the emergence of methicillin-resistant *Staphylococcus aureus* (MRSA) responsible for an alarming increase in mortality associated with serious nosocomial infections. MRSA is highly virulent, easily transmittable through contact, and it is typically resistant to multiple classes of antibiotics. Against MRSA, vancomycin was one of few remaining antibiotics that were highly effective, and thus, for a period vancomycin was considered as "the drug of last resort". Currently, there are more than a hundred different types of glycopeptide antibiotics produced by different organisms[102] and

even a greater number of chemically modified semisynthetic glycopeptides have been synthesized[103].

The mode of action of vancomycin and related glycopeptide antibiotics is that it inhibits peptidoglycan (PG) biosynthesis by binding to the membrane-bound PG precursor, lipid II. PG is the primary component of the cell wall in Gram-positive bacteria with a repeat unit consisting of a disaccharide (GlcNAc-MurNAc), a pentapeptide-stem structure consisting of L-Ala-D-iso-Glu-L-Lys-D-Ala-D-Ala, and a pentaglycine. Pentapeptide-stem is attached to MurNAc and the pentaglycine to the ε-nitrogen side of the Lys (Figure 4.1a). PG biosynthesis is catalyzed by two important enzymatic steps, transglycosylation and transpeptidation, which occur at the outside of the bacterial membrane[104]. Transglycosylation is the polymerization of the PG-repeat unit by forming a long glycan chain of repeating GlcNAc-MurNAc. Transpeptidation is a cross-linking between the two adjacent neighboring glycan chains. Unlike β-lactam antibiotics, which also target the cell wall by inhibiting the transpeptidation step of PG biosynthesis through binding to the penicillin-binding proteins, vancomycin binds to lipid II and thereby inhibits the transglycosylation step of PG biosynthesis[105]. The lipid II sequestration prevents the regeneration of the lipid transporter (C_{55}) from lipid II, which requires the transglycosylase activity. Since the number of C_{55} copies in bacterium is found in small numbers, vancomycin sequestration of lipid II is a potent means of inhibiting bacterial cell wall biosynthesis[106].

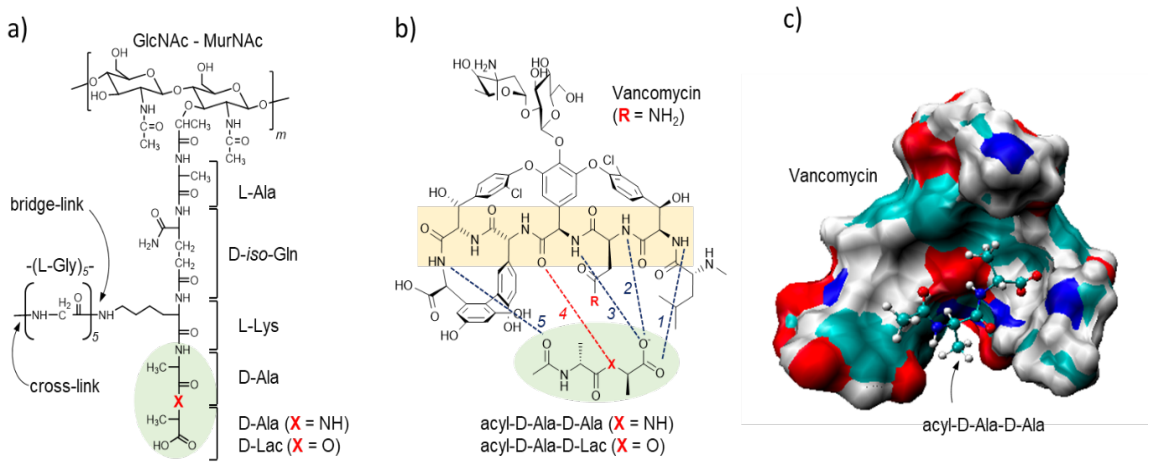

Figure 4.1. Chemical structure of *S. aureus* peptidoglycan (PG) and vancomycin. (a) The PG-repeat unit in *S. aureus* consists of a GlcNAc-MurNAc disaccharide, a pentapeptide stem with a sequence L-Ala-D-iso-Glu-L-Lys-D-Ala-D-Ala, and a pentaglycine bridge structure that is attached to the ε-nitrogen of the side chain L-Lys. Vancomycin binds to the D-Ala-D-Ala dipeptide of the PG-stem structure (green circle). In vancomycin-resistant pathogens, including vancomycin-resistant enterococci (VRE) and vancomycin-resistant *S. aureus* (VRSA), the dipeptide is replaced by a depsipeptide D-Ala-D-Lac. (b) Chemical structure of vancomycin and its interactions with the bound PG-stem structure. The vancomycin binding affinity to depsipeptide (X = O) is 1000-fold less than that to dipeptide (X = NH). The minimal inhibitory concentration of vancomycin against VRE and VRSA increases by 1000-fold. The lost efficacy is attributed to the depsipeptide substitution, which replaces a hydrogen bond with an electrostatic repulsion (red dotted line). (c) A model structure of vancomycin bound to an acyl-D-Ala-D-Ala. Vancomycin is shown as a space-filling model with an electrostatic surface and the dipeptide as a stick-and-ball model.

The structures of vancomycin bound to a tripeptide PG analogue, Acyl-L-Lys-D-Ala-D-Ala, have been well characterized since the early 1980s by solution-state nuclear magnetic resonance (NMR)[69] and X-ray crystallography[72]. The tripeptide-bound structures show that the D-Ala-D-Ala of PG stem is bound to a cleft formed by the vancomycin aglycon, and it is stabilized by five hydrogen bonds: three hydrogen bonds between the amide-protons of residues 1, 2, and 3 of vancomycin and the C-terminus of the dipeptide D-Ala-D-Ala, a fourth bond between the carbonyl of the 4th residue and an amide proton

of the terminal D-Ala, and a fifth hydrogen bond between the amide proton of the 7th residue of the aglycon and the carbonyl of the penultimate D-Ala from the C-terminal end (Figure 4.1b). The drug sugars, D-glucose and L-vancosamine, are attached to the phenolic moiety on the 4-hydroxyphenylglycine sidechain of the fourth amino acid and they are known to increase the vancomycin activity even though they do not participate in the dipeptide binding (Figure 4.1c).

Initially, the emergence of vancomycin resistance was thought to be highly unlikely. Then, in 1986, the first clinical case of infection by high-level vancomycin-resistant enterococci (VRE) was reported[107]. Since then, there has been a rapid increase in VRE-associated nosocomial infections worldwide. The mechanism of high-level vancomycin resistance in VRE involves the modification of the D-Ala-D-Ala terminus of PG stems from a dipeptide D-Ala-D-Ala to a depsipeptide D-Ala-D-Lac[65-66, 108-109]. The depsipeptide-terminated lipid II in VRE replaces an amide group of the terminal alanine with the oxygen of an ester bond. This modification replaces one of the hydrogen bonds by electrostatic repulsion (Figure 4.1b, red line) and reduces vancomycin binding affinity by a 1000-fold with K_D from 1μM to 1mM. The minimal inhibitory concentration (MIC) of vancomycin increases from 1 μg/ml against vancomycin-susceptible enterococci to approximately 1000 μg/ml for the VRE. Subsequently, in 2002, the first case of infection by vancomycin-resistant *S. aureus* (VRSA) with a MIC greater than 256 μg/ml was reported[110]. The genetic analysis confirmed that the mechanism of vancomycin resistance in VRSA was identical to that of VRE, possessing a transposal plasmid in VRSA containing the genetic determinants for vancomycin resistance in VRE[111].

There have been several important developments in glycopeptide antibiotics to overcome resistance through chemical modifications. Some of the developments include (1) C-terminus modifications[112], (2) homo- and hetero-dimerization of glycopeptide[103], (3) drug sugar modifications[113], and (4) aglycon modifications[114-115]. So far, the alkylation of hydrophobic adducts to the drug sugar has been the most effective, leading to the development of oritavancin (LY333328) by Eli Lilly,[116-117] which was FDA approved in 2014. Oritavancin is a lipoglycopeptide antibiotic that has potent bactericidal activities against a broad spectrum of multidrug-resistant pathogens including MRSA[118], and it is effective against vancomycin-resistant pathogens including VRE[119] and VRSA[120]. The mode of action of oritavancin differs from vancomycin by exhibiting dual inhibition of transglycosylase and transpeptidase activities[80, 85, 121-123].

Another exciting recent development is the chemical modification of the vancomycin aglycon structure to overcome the vancomycin resistance. Boger et al. have determined that the reduced vancomycin binding affinity to the depsipeptide terminated PG-stem is less affected by the loss of a hydrogen bond (Figure 4.1b), but more due to the electrostatic repulsion between the lone pair of a carbonyl oxygen atom at the 4th residue of vancomycin and the ester oxygen atom on the D-Ala-D-Lac.[114] A rational approach was taken to redesign the aglycon structure of vancomycin through total synthesis by replacing the carbonyl oxygen atom at the 4th residue of vancomycin with a protonated amidine nitrogen.[124] The incorporation of amidine nitrogen in the aglycon removes the destabilizing electron lone pair interactions and replaces it with stabilizing interactions between the proton of the amidine nitrogen and the oxygen on the ester of D-Lac when bound to D-Ala-D-Lac.[125] The modification on the glycopeptide resulted in a 600-fold

increase in binding affinity to the depsipeptide ligand and restored the activity against the VRE of VanA type with a MIC below 1 μg/ml.[126] This demonstrated a proof of principle that the rational approach to design glycopeptide aglycon will play an important role in the future development of novel antibiotics.

To facilitate the development through rational drug design, the function of each amino acid in the aglycon structure needs to be investigated. All amino acids in the vancomycin core are involved in the formation of a highly crosslinked core structure, except for the amino acids at positions 1 and 3 which are *N*-methylleucine and asparagine, respectively. These amino acids are not involved in the ridged cleft formation and do not participate in the dipeptide binding; nonetheless, they are essential for the activity of vancomycin. In the case of *N*-methylleucine, the removal by Edman degradation results in desleucyl-vancomycin which is devoid of any antimicrobial activity[127]. For the asparagine, the third amino acid of vancomycin substitution by aspartic acid or glutamine has been shown to reduce the antimicrobial activity against *S. aureus* by approximately 8 and 4-fold, respectively[63]. The introduction of the negative charge in the binding cleft by aspartic acid substitution or the lengthening of the sidechain by glutamine substitution is presumed to interfere with the dipeptide binding by electrostatic or steric interactions; however, the exact role of these core amino acids is not well understood.

In this study, we investigate the role and function of asparagine at the 3rd position of vancomycin using classical molecular dynamics (MD) simulations. MD simulations were carried out for vancomycin (V_N) and its aspartate-substituted analogue (V_D) bound to the PG tripeptide mimics representing vancomycin-susceptible and vancomycin-resistant bacteria. The four glycopeptide-PG complexes analyzed are (1) vancomycin bound to the

acyl-D-Ala-D-Ala (V_N-Ala), (2) vancomycin bound to the acyl-D-Ala-D-Lac (V_N-Lac), (3) aspartate-substituted vancomycin bound to the acyl-D-Ala-D-Ala (V_D-Ala), and (4) aspartate-substituted vancomycin bound to the acyl-D-Ala-D-Lac (V_D-Lac). From these simulations, we find that the aspartate-substituted analogue of vancomycin (V_D) shows improved binding to the acyl-D-Ala-D-Lac, the PG-stem structure found in VRE and VRSA. This indicates that the amino acids in the aglycon structure that do not directly participate in the PG-stem binding play a crucial role in stabilizing the glycopeptide-PG complex. Furthermore, the study provides a new insight for the chemical modifications of the aglycon structure for the development of new glycopeptide antibiotics to mediate the improvement in the binding to the D-Ala-D-Lac terminated PG precursors found in vancomycin-resistant pathogens.

4.3 Results and Discussion

4.3.1 Total Hydrogen Bonds and Binding Free Energies

The total number of hydrogen bonds formed between the glycopeptide and ligand as well as the total free energy of binding (ΔG_{bind}) during MD simulation are shown in Table 4.1. The contributions from van der Waals (ΔE_{vdw}) and electrostatic energy (ΔE_{ele}) to the ΔG_{bind} are also shown in the table. The average number of hydrogen bonds formed during MD simulation ranged from 2 to 5. The most stable complex was V_N-Ala, which has the maximum number of 5 stable hydrogen bonds[128], and the least stable complex was V_D-Ala with only 2 hydrogen bonds. The order of stability, ranked based on the overall free energy of binding from the most to least stable is as follows: V_N-Ala > V_D-Lac > V_N-Lac > V_D-Ala.

The strongest electrostatic attraction between the glycopeptide and its ligand was observed in the V_N-Ala complex with a ΔE_{ele} value of -80.53 kJ/mol (Table 4.1). This strong electrostatic attraction is attributed to the interactions between the C-terminus of the acyl-D-Ala-D-Ala and the aglycon structure[128]. In contrast, the weakest attraction was observed in the V_D-Ala complex with a ΔE_{ele} value of 31.55 kJ/mol, due to the loss of interaction by the displacement of the C-terminus of acyl-D-Ala-D-Ala out of the binding pocket (Figure 4.3b). It is interesting to note that the V_D-Lac complex is more stable (ΔG_{bind} of 9.60 kJ/mol) than the V_N-Lac complex (ΔG_{bind} of 14.31 kJ/mol) by -4.71 kJ/mol. This was surprising since the ΔE_{ele} of V_N-Lac complex (-65.45 kJ/mol) is much stronger than the V_D-Lac (23.27kJ/mol) complex with a difference $\Delta\Delta E_{ele}$ value of 88.42 kJ/mol. The van der Waals's contribution to the ΔG_{bind}, though some variations are observed between the complexes, nonetheless, all ranged between -32 to -45 kJ/mol. Thus, the difference in the van der Waals contributions between these two complexes ($\Delta\Delta E_{vdw}$) is only -13.02 kJ/mol, which is not enough to offset the large $\Delta\Delta E_{ele}$ value of 88.42 kJ/mol to attain the $\Delta\Delta G_{bind}$ of -4.71 kJ/mol. This led to the possibility that the increased binding stability of the V_D-Lac complex, compared to that of V_N-Lac, is not significantly dependent on the number of H-bonds formed or the interactions between the C-terminus of ligand and the aglycon of glycopeptide. Instead, V_D-Lac is more stable than V_N-Lac because of the conformation change associated with the aspartate substitution, which led to the minimization of the electrostatic repulsion between the electron lone pair on the carbonyl oxygen at the 4^{th} position of glycopeptide and the ester oxygen atom of the D-Ala-D-Lac.[114] It is worth noting that the molecular mechanics Poisson-Boltzmann surface area (MM/PBSA) binding energy method is not a reliable technique for calculating the absolute

binding free energies.[51]. However, the approach has been shown to be good for ranking the binding energies of similar ligands[129].

Table 4.1. Number of hydrogen bonds and binding energies of V_N-Ala, V_N-Lac, V_D-Lac, and V_D-Ala

Glycopeptide-PG Complex	Average Number of H-bonds	ΔE_{vdw} (kJ/mol)	ΔE_{ele} (kJ/mol)	ΔG_{bind} (kJ/mol)
V_N-Ala (R = NH_2, X = NH)	5.08 ± 0.19	-41.48 ± 1.36	-80.53 ± 5.33	-3.81 ± 0.33
V_N-Lac (R = NH_2, X = O)	4.33 ± 0.24	-32.32 ± 1.82	-65.45 ± 1.26	14.31 ± 0.68
V_D-Ala (R = O^-, X = NH)	2.10 ± 0.04	-35.38 ± 1.22	31.55 ± 0.59	15.82 ± 0.61
V_D-Lac (R = O^-, X = O)	3.39 ± 0.12	-45.34 ± 1.02	23.27 ± 2.11	9.60 ± 0.02

4.3.2 Root-Mean-Square Deviation

The time evolution of rmsd values for the four glycopeptide-PG complexes are shown in Figure 4.2. The rmsd for each glycopeptide-PG complex was calculated during the MD simulation by comparing the structures along the trajectories to the reference structure. The low fluctuation pattern in the rmsd plot of a complex indicates minimal changes in conformation which is indicative of a stable complex. In contrast, high fluctuation indicates the low stability of a complex during MD simulation. As expected, the unmodified vancomycin bound to acyl-D-Ala-D-Ala (V_N-Ala), which is the most stable complex of the four systems, had the lowest average rmsd value of 1.70 Å, followed by the V_D-Lac with 2.07 Å, V_N-Lac with 2.24 Å, and V_D-Ala with 2.90 Å. The stability of the complex, inferred from the rmsd plots, when ordered from the most to the least stable is V_N-Ala > V_D-Lac > V_N-Lac > V_D-Ala. An identical order was also observed when the overall binding energy (ΔG_{bind}) was calculated for the four complexes (Table 4.1). This indicated a direct correlation between the stability and binding energy of the complex.

Unexpectedly, the V_D-Lac complex shows increased stability (Figure 4.2c) compared to the V_N-Lac complex (Figure 4.2b), based on the smaller average rmsd value and the reduced fluctuating amplitudes of the rmsd plot. As stated previously, V_D-Lac had more stable binding energy than the V_N-Lac (Table 4.1). This suggests that the aspartate substitution, which introduces a negative change in the aglycon structure of V_D, diminished the effects of the electrostatic repulsion between the oxygen atom in the ester bond of the ligand D-Ala-D-Lac and the oxygen carbonyl carbon at the 4th residue of the glycopeptide that has been attributed as the primary cause of the loss in binding affinity to the depsipeptide[114].

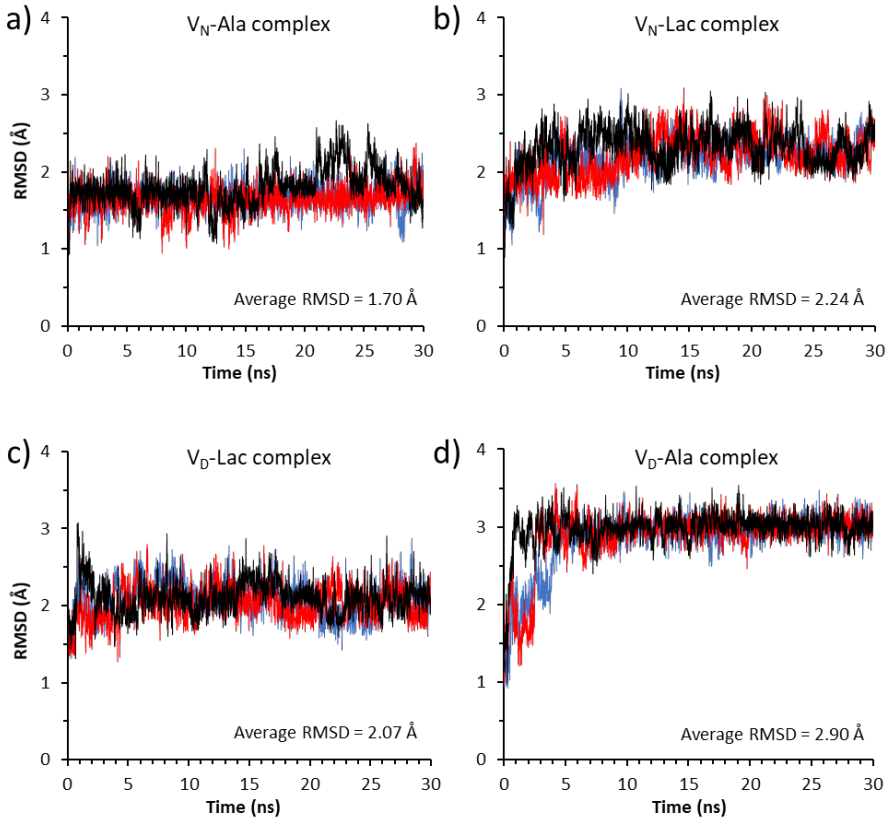

Figure 4.2. RMSD plots of three independent 30 ns MD simulations for the complex (a) V_N-Ala, (b) V_N-Lac, (c) V_D-Lac, and (d) V_D-Ala. The rmsd values of three independent simulations are plotted using colors red, blue, and black. The average rmsd value for each complex is shown as a figure inset.

The least-stable complex was V_D-Ala which shows an unusual rmsd fluctuating pattern (Figure 4.2d) that is not observed in other complexes. The initial structure of the V_D-Ala complex (Figure 4.3a) undergoes a large rmsd fluctuation during the first 3 ns of the MD simulation. Then, the rmsd amplitude rapidly stabilizes as the structure reaches the final conformation (Figure 4.3b) with an average rmsd value of 2.90 Å. Figure 4.3 shows the initial and final structure of the V_D-Ala complex, where V_D is represented as a space-filling model with an electrostatic surface and the bound-dipeptide ligand as a stick-and-ball model. The observed instability during the first 3 ns is associated with the rearrangement of the aglycon structure and its bound ligand, resulting in the partial displacement of the terminal D-Ala from the binding cleft (Figure 4.3b). The final structure of the V_D-Ala complex reveals the displacement of the D-Ala-D-Ala C-terminus from the binding cleft, which results in the loss of three hydrogen bonds between the C-terminus of the dipeptide and the amide protons of residues 1, 2, and 3 of the vancomycin peptide backbone (Figure 4.1b). This loss of three hydrogen bonds is consistent with the calculated 2.1 hydrogen bonds found in the V_D-Ala complex (Table 4.1).

The 2D rmsd contour plots shown in Figure 4.4 was used to further characterize the stability and conformational distribution of the different glycopeptide-ligand complexes during MD simulation. The V_N-Ala complex, which is the most stable complex, is used as a reference to compare the similarities of the binding distribution to that of other complexes (Figure 4.4). The numbers on the contour lines represent the density of the joint distribution between the conformational space of two different complexes along the rmsd trajectories.

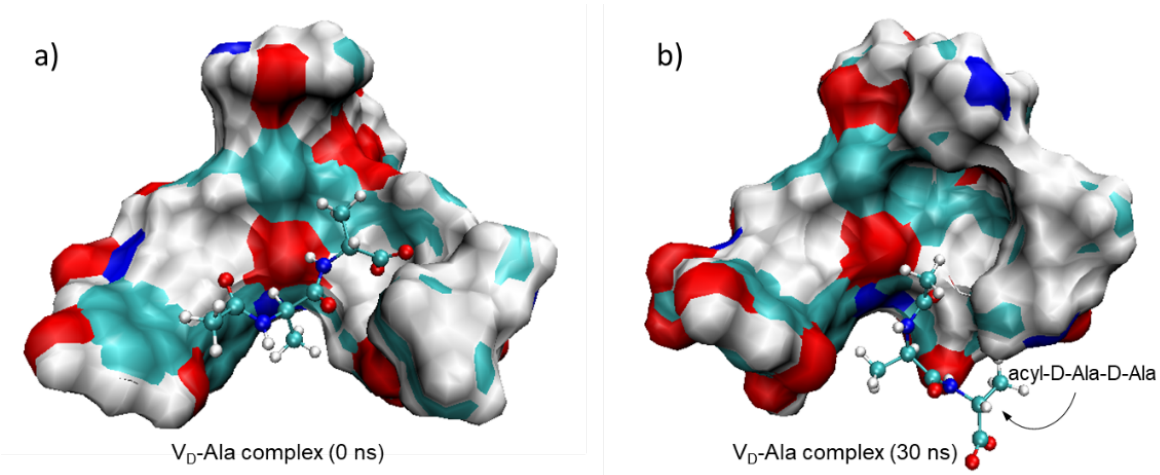

Figure 4.3. Initial structure of the V_D-Ala complex at t = 0 ns and the final structure at 30 ns MD simulation. (a) The initial structure of the V_D-Ala complex showing the acyl-D-Ala-D-Ala bound to the aglycon structure of glycopeptide. (b) The final structure of the V_D-Ala complex after 30 ns of MD simulation. The C-terminus of the D-Ala is displaced from the binding cleft, resulting in the loss of three hydrogen bonds between the C-terminus of D-Ala and the amide protons of residues 1, 2, and 3 of the aglycon.

The closer the attraction basin (area of highest density) for a distribution to be centered on the same points, the more similarity between the two different complexes under comparison. From Figure 4.4a, it can be seen that the binding distribution of V_D-Lac complex is closest to that of V_N-Ala due to their attraction basin centered at approximately (0.17, 0.20) Å and the presence of a single attraction basin. This is followed by the V_N-Lac complex (Figure 4.4b), whose joint distribution with V_N-Ala is centered at approximately (0.17, 0.23) Å, including a minor contribution at (0.17, 0.35) Å. The presence of multiple attraction basins in Figure 4.4b is indicative of greater differences between V_N-Lac and V_N-Ala complexes when compared to that of V_D-Lac and V_N-Ala complexes. The binding distribution of V_D-Ala complex is the least similar to that of V_N-Ala. This is shown by the high-density attraction basin centered at approximately (0.17, 0.30) Å, including an extension to about (0.18, 0.37) Å.

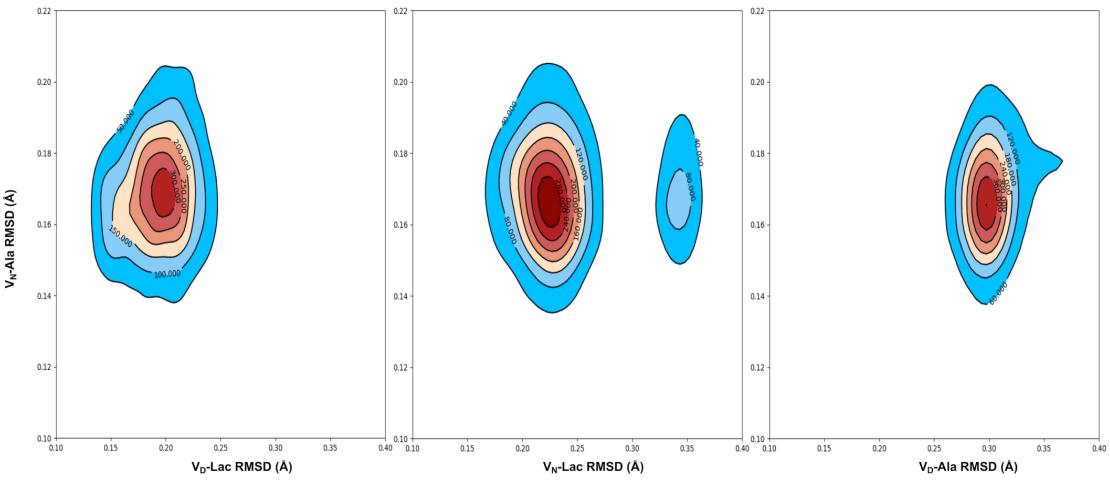

Figure 4.4. Comparative 2D rmsd (Å) contour plots of V_N-Ala complex relative to V_D-Lac, V_N-Lac, and V_D-Ala complexes. Comparative 2D rmsd contour plots of (a) V_N-Ala vs V_D-Lac, (b) V_N-Ala vs V_N-Lac, and (c) V_N-Ala vs V_D-Ala complexes. The contour lines represent the density of trajectories that are located within the area. The red color denotes the region of highest density and the blue color region of lowest density.

4.3.3 Glycopeptide Interactions with the C-terminus of Peptidoglycan Precursor

The interactions between the glycopeptide and the C-terminus of the bound ligand are summarized in Table 4.2. The average number of H-bonds formed with the C-terminus and the interaction energy is determined to gain insight into the C-terminus contribution to the ligand binding. The interaction energy (ΔE_{tot}) when ordered from the most stable to the least is as follows: V_N-Ala > V_N-Lac > V_D-Lac > V_D-Ala. This stability trend is identical to the trend observed for the average number of H-bonds shown in the table.

Table 4.2. Interactions between C-terminus of the peptidoglycan and glycopeptide

Glycopeptide-PG Complex	Average Number of H-bonds	ΔE_{vdw} (kJ/mol)	ΔE_{ele} (kJ/mol)	ΔE_{tot} (kJ/mol)
V_N-Ala (R = NH_2, X = NH)	3.28 ± 0.29	0.97 ± 3.32	-306.87 ± 26.31	-307.84 ± 26.52
V_N-Lac (R = NH_2, X = O)	2.73 ± 0.19	-3.79 ± 1.43	-254.93 ± 5.03	-258.72 ± 5.23
V_D-Ala (R = O^-, X = NH)	0.11 ± 0.05	-1.49 ± 0.74	-49.05 ± 4.11	-50.54 ± 4.18
V_D-Lac (R = O^-, X = O)	2.22 ± 0.03	-6.63 ± 0.29	-199.19 ± 6.41	-205.82 ± 6.42

In the V_N-Ala complex, the C-terminus of D-Ala-D-Ala forms approximately 3H-bonds per time frame (Figure 4.5a) with the aglycon during the simulation. From Table 4.2, the V_N-Ala complex has the most stable interaction energy followed by the V_N-Lac, V_D-Lac, and V_D-Ala complex. For vancomycin, the number of H-bonds formed between the aglycon structure to the C-terminus of D-Ala-D-Ala is 3.28 but reduces to 2.73 when bound to D-Ala-D-Lac. In the V_N-Lac complex, the replacement of an amide by ester oxygen in D-Ala-D-Lac replaces an H-bond (Figure 4.1b) with an electrostatic repulsion. This results in large rmsd fluctuation of V_N-Lac complex (Figure 4.2b) and it negatively impacted the H-bond interactions between the C-terminus of the bound ligand and the vancomycin aglycon. The V_D-Ala complex is the least stable without any H-bond interaction between the C-terminus of D-Ala-D-Ala and the glycopeptide (Table 4.2). An analysis of the number of H-bond formed per time frame between C-terminus of D-Ala-D-Ala and the modified vancomycin in the V_D-Ala complex (Figure 4.5d) shows that the number of H-bonds reduces from 3 to 0 within 3 ns of the simulation.

The H-bonds between the C-terminus of the D-Ala-D-Ala and the amide protons of aglycon residues 1, 2, and 3 are disrupted by the competing H-bond formed between the aspartate sidechain the glycopeptide and the hydrogen donor, the amide proton, of the C-terminus D-Ala. This preferential interaction between the aspartate sidechain of residue 3 in the glycopeptide with the D-Ala-D-Ala in the V_D-Ala complex was monitored by measuring the intermolecular distance between the amide nitrogen atom at the C-terminus of the dipeptide and the carbonyl oxygen atom of the aspartate side chain (Figure 4.6d).

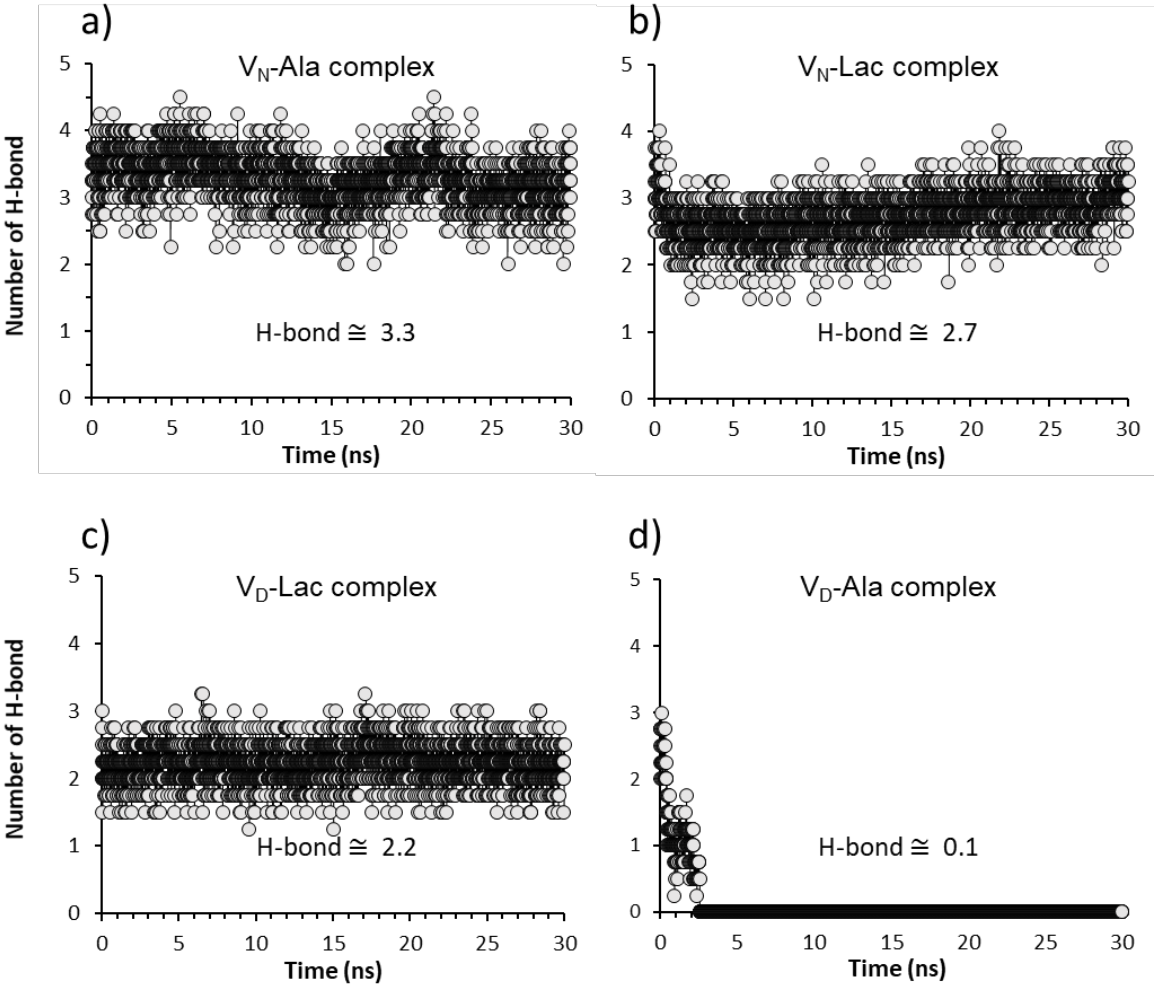

Figure 4.5. Number of intermolecular H-bonds formed per time frame between the C-terminus of the ligand and the glycopeptide. The number of stable H-bonds formed between (a) C-terminus of D-Ala-D-Ala and vancomycin in the V_N-Ala complex, (b) C-terminus of D-Ala-D-Lac and vancomycin in the V_N-Lac complex, (c) C-terminus of D-Ala-D-Lac and the modified vancomycin in the V_D-Lac complex, (d) C-terminus of D-Ala-D-Ala and the modified vancomycin in the V_D-Ala complex.

The intermolecular distance starting at 0.5 nm was rapidly reduced to an overall average of 0.29 nm within 3 ns and remained stable for the remaining duration of the simulation (Figure 4.6d). The replacement of asparagine at the 3rd amino acid position in vancomycin with an aspartate introduces a negative charge within the binding cleft. This destabilizes the D-Ala-D-Ala binding through the electrostatic repulsion between the negative charges of aspartic acid and the C-terminus of the dipeptide. The formation of a

new H-bond between the aspartate side chain and the amide proton of the terminal D-Ala of the dipeptide (Figure 4.6d) indicates a conformational change associated with the displacement of the bound C-terminal D-Ala out from the binding pocket (Figure 4.3b). The reduced binding stability in the V_D-Ala complex is consistent with the eightfold reduction in antimicrobial activity of V_D against *S. aureus* with PG-stems terminating in D-Ala-D-Ala [63].

In the case of the V_D-Lac complex, the aspartate side chain of glycopeptide does not form a destabilizing H-bond with the amide proton of the ligand due to ester oxygen in D-Lac (Figure 4.6c). The depsipeptide binding in the V_D-Lac complex with the overall ΔG_{bind} of 9.60 ± 0.02 kJ/mol is more stable than V_N-Lac with ΔG_{bind} of 14.31 ± 0.68 kJ/mol (Table 4.1). However, Table 4.2 shows that the localized C-terminus interaction of the bound ligand with the amide-protons of residues 1, 2, and 3 of the aglycon is less stable in V_D-Lac complex than V_N-Lac by approximately 53 kJ/mol. This indicates that the unaccounted interactions that involve non-C-terminus of ligand play an essential role in stabilizing the V_D-Lac complex.

In the V_D-Lac complex, the negatively charged carboxyl side chain of aspartate interacts constantly with the amide protons of the amino acids at positions 1, 2 and 3 of the aglycon with an interaction energy of -22.23 ± 5.65 kJ/mol. The measured interaction energy between the amide side chain of asparagine with the amide protons at position 1, 2 and 3 of the aglycon in the V_N-Lac complex is 32.11 ± 4.19 kJ/mol. The attraction of the aspartate sidechain to the neighboring amide protons in the aglycon of V_D-Lac complex makes the aspartate side chain less available for interaction with the non-C-terminus of the bound ligand, especially the ester oxygen. This is evident in the stable fluctuation pattern

shown in Figure 4.6c, where the intermolecular distance is measured between the carbonyl oxygen atom of the aspartate side chain and the C-terminus ester oxygen of D-Ala-D-Lac.

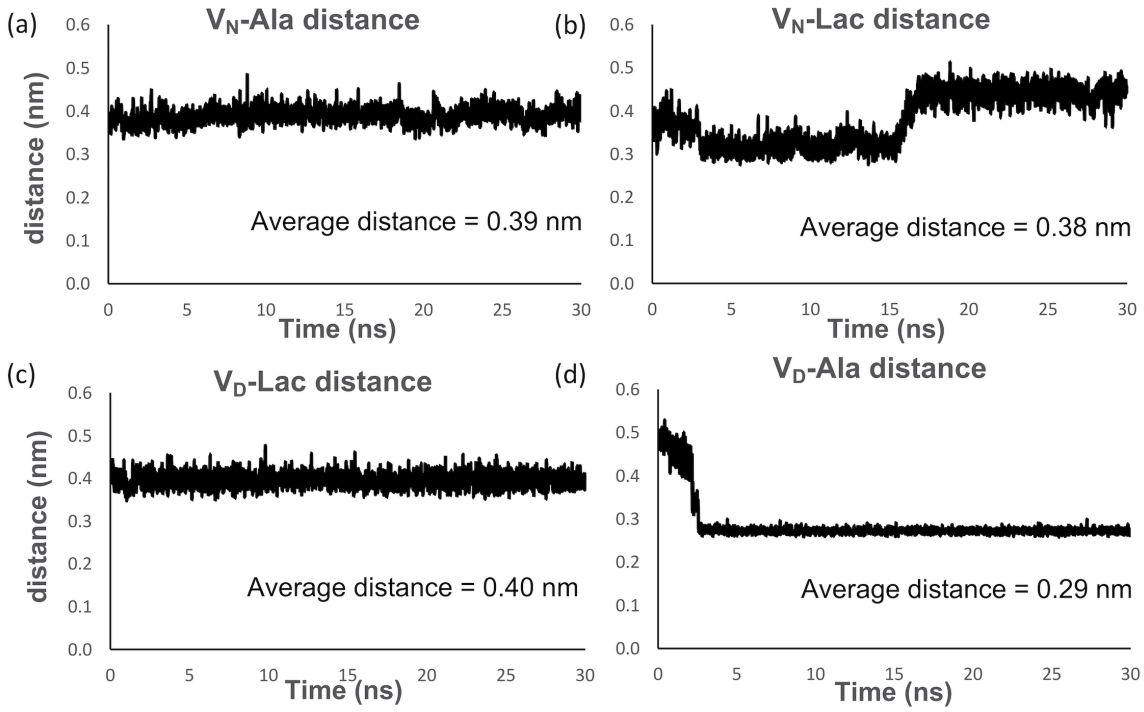

Figure 4.6. Monitoring intermolecular distance between the bound ligand and the side chain at the 3rd amino acid position in vancomycin per time frame during the 30 ns MD simulation. Intermolecular distances between the amide nitrogen of the asparagine side chain of residue 3 in vancomycin and (a) the C-terminus amide nitrogen of D-Ala-D-Ala for the V_N-Ala complex and (b) the ester oxygen of D-Ala-D-Lac for V_N-Lac complex. The fluctuating intermolecular distances in the V_N-Lac complex, compared to the V_N-Ala complex, indicate conformational changes associated with the depsipeptide binding. Intermolecular distances between the carbonyl oxygen atom of the aspartate side chain of residue 3 in the glycopeptide and (c) the C-terminus ester oxygen of D-Ala-D-Lac for the V_D-Lac complex, and (d) the C-terminus amide nitrogen of D-Ala-D-Ala for the V_D-Ala complex. In the V_D-Ala complex, the aspartate substitution in vancomycin introduces a negative charge which destabilizes the D-Ala-D-Ala binding through electrostatic repulsion with the C-terminus of the bound ligand. After 3 ns, the formation of a new H-bond between the aspartate side chain and the amide proton of the terminal D-Ala is associated with the removal of the terminal D-Ala out of the binding pocket (Figure 4.5d and Figure 4.3b).

On the other hand, the intermolecular distance between the amide nitrogen of the asparagine side chain and the ester oxygen of D-Ala-D-Lac in V_N-Lac complex shows an unstable fluctuation pattern implying more interaction (Figure 4.6b). Thus, the aspartate side chain in V_D-Lac complex competes for the amide protons of the amino acids at positions 1, 2 and 3 of the aglycon. The attraction of this negatively charged carboxyl side chain of aspartate for the neighboring amide protons in the V_D-Lac complex weakens the H-bond network between the aglycon and the C-terminus of the ligand D-Lac (Table 4.2). This results in conformational changes in both the aglycon and the bound depsipeptide, which stabilizes the depsipeptide binding cleft but weakens the aglycon interaction with the C-terminus of the ligand D-Lac. Both the bound ligand and the glycopeptide aglycon in the V_D-Lac complex undergo conformational rearrangements that stabilize the complex by minimization of the strong repulsive lone pair interaction which has been attributed to the loss of binding affinity in V_N-Lac complex. This conformational rearrangement that minimizes the strong repulsive lone pair interaction in the V_D-Lac complex is evident in Figure 4.7, which is a time-dependent plot of the intermolecular distance between the ester oxygen of D-Ala-D-Lac and the carbonyl oxygen of residue 4 in the glycopeptide during 30 ns MD simulation. The V_N-Lac complex shows greater atomic distance fluctuation than the V_D-Lac complex which is relatively more stable with a lower average distance value. The average distance value for the V_D-Lac complex is 3.9 Å and the V_N-Lac complex is 4.9 Å (Figure 4.7). We hypothesize that the conformational change caused by the substitution of aspartate for asparagine in the V_D-Lac complex leads to a reorientation of the amide carbonyl in the glycopeptide's residue 4. This reorientation minimizes the

repulsive lone pair interaction between the carbonyl oxygen of the glycopeptide and the D-Ala-D-Lac ester oxygen in the V_D-Lac complex relative to the V_N-Lac complex.

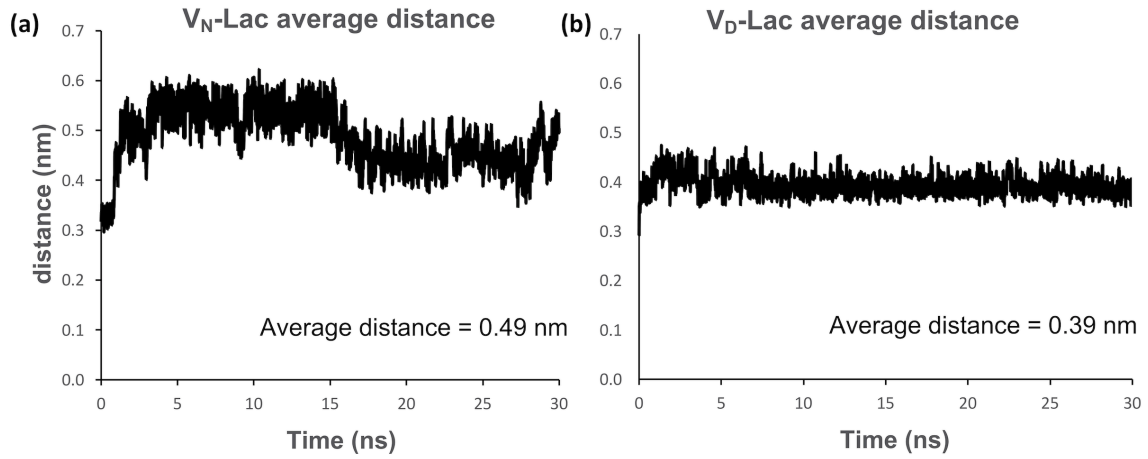

Figure 4.7. Average atomic distance per time frame during 30 ns MD simulation of oxygen-oxygen atoms involved in repulsive interactions between peptidoglycan precursor and the glycopeptide in the different complexes. Average atomic distance between (a) D-Ala-D-Lac ester oxygen of the ligand and carbonyl oxygen of residue 4 in vancomycin of the V_N-Lac complex and (b) D-Ala-D-Lac ester oxygen of the ligand and the carbonyl oxygen of residue 4 in the modified vancomycin of the V_D-Lac complex.

4.3.4 Intramolecular Interaction Between the Sidechain of Residue 3 of the Glycopeptide and Other Parts of the Glycopeptide

An analysis of the intramolecular interaction energy between the side-chain of residue 3 to the rest of the glycopeptide in various complexes was carried out during the MD simulation. Intramolecular interactions within the glycopeptide can be useful to yield conformational changes in the glycopeptide that can favor the binding of the glycopeptide to the D-Ala-D-Lac of peptidoglycan. In general, the glycopeptide with aspartate at residue 3 showed stronger intramolecular interaction energy (ΔE_{tot}) than the glycopeptide with asparagine (Table 4.3). The strongest intramolecular interaction was observed for the V_D-Ala complex followed by V_D-Lac, V_N-Ala, and V_N-Lac. In the case of V_D-Lac and V_N-

Lac complexes, the intramolecular interaction energy of V_D-Lac is greater than the V_N-Lac by approximately 60 kJ/mol (Table 4.3). This strong intramolecular interaction in the V_D-Lac complex stabilizes the binding cleft but weakens the intermolecular interaction with the C-terminus of the ligand (Table 2) allowing for the conformational rearrangement of the bound complex. The conformational changes minimize the lone pair/lone pair electrostatic repulsion, making the V_D-Lac complex more stable than the V_N-Lac. In the V_N-Lac complex, the opposite is observed where the intramolecular interaction is weaker but the intermolecular interaction with the C-terminus of the ligand is much stronger than the V_D-Lac complex (Table 4.2).

Table 4.3. Intramolecular interactions between the sidechain of Residue 3 in the Glycopeptide of the Different Complexes with Other Parts of the Glycopeptide.

Glycopeptide-PG Complex	ΔE_{vdw} (kJ/mol)	ΔE_{ele} (kJ/mol)	ΔE_{tot} (kJ/mol)
V_N-Ala (R = NH_2, X = NH)	-17.49 ± 1.02	-79.90 ± 2.82	-97.39 ± 3.00
V_N-Lac (R = NH_2, X = O)	-15.85 ± 0.65	-74.91 ± 4.82	-90.76 ± 4.86
V_D-Ala (R = O^-, X = NH)	-10.70 ± 0.20	-183.96 ± 1.26	-194.66 ± 1.28
V_D-Lac (R = O^-, X = O)	-14.03 ± 0.36	-136.03 ± 4.86	-150.06 ± 4.87

4.4 Conclusion

Vancomycin represents an important class of antibiotics reserved for the treatment of serious infection by multidrug-resistant Gram-positive pathogens. All side chains of amino acids in vancomycin, except for the residues at positions 1 and 3, are involved in cross-linking to form a binding cleft. The amino acids at 1 and 3 are N-methylleucine and asparagine, respectively. Although these residues are not directly involved in the PG-stem

binding, the removal or chemical modifications dramatically affects both the efficacy of the compound and its binding affinity to the PG-stem. For example, a natural product of vancomycin analogue that contains aspartate in place of asparagine at position 3 is known to have an eight-fold reduction in the antimicrobial activity against *S. aureus*[63]; however, the effects of aspartate substitution on the D-Ala-D-Ala binding is not well understood.

To investigate the role of the asparagine side chain of residue 3 in vancomycin, the following four glycopeptide-PG complexes were analyzed using molecular dynamics simulation: V_N-Ala, V_N-Lac, V_D-Ala, and V_D-Lac. While V_N-Ala was found to be the most stable complex, V_D-Lac showed greater stability over V_N-Lac and V_D-Ala. The V_D-Lac complex is more stable than the V_N-Lac complex by -4.71 kJ/mol ($\Delta\Delta G_{bind}$) and by -6.22 kJ/mol for the V_D-Ala complex. The reduced binding stability of the V_N-Lac and V_D-Ala complexes determined by MD simulations (Table 4.1) are consistent with the observed antimicrobial activities of the compounds. In the case of vancomycin (V_N), its activity against VRE is devoid of antimicrobial activity with MIC exceeding 1,000 μg/ml. For V_D, its activity against *S. aureus*, compared to vancomycin, is eight-fold reduced. Hence, the increased stability of the V_D-Lac complex strongly suggests that the aspartate-substituted analogue of vancomycin will exhibit antimicrobial activities against VRE and VRSA. Our analysis shows that the aspartate side chain in V_D is not directly involved in the depsipeptide binding. Instead, the aspartate substitution changed the conformations of both aglycon and its bound ligand such that it minimized the destabilizing lone pair interaction between the ester oxygen of the D-Lac and carbonyl oxygen at the 4th residue in V_D. The mechanism by which the aspartate side change affects the conformations of both aglycon and ligand is by forming transient intramolecular attraction with the amide protons at

positions 1, 2 and 3 of the aglycon. These intramolecular attractions compete with the intermolecular H-bonds between aglycon and the C-terminus of the D-Lac to allow rearrangement of the bound depsipeptide, which minimizes the electrostatic repulsion. The MD simulations of glycopeptide-PG complexes provided insight into the function of residue 3 in vancomycin aglycon and its effects on the conformational dynamics associated with the PG-stem binding necessary for the future development of novel glycopeptides to counter the continual emergence of glycopeptide resistance in pathogens.

4.5 Methods

4.5.1 Molecular Dynamics Simulation

The initial crystal structure of vancomycin complexed with the cell wall precursor analogue was obtained from the Protein Data Bank (PDB code: 1FVM)[130]. The structure was modified with GaussView 6.1.1 of the Gaussian16 software package[131] to generate the other complexes used in the simulations. The V_N-Ala complex represents the unmodified vancomycin and acyl-D-Ala-D-Ala, while V_N-Lac is the complex with acyl-D-Ala-D-Ala modified to acyl-D-Ala-D-Lac. In the V_D-Ala complex, the residue 3 of vancomycin is modified from Asparagine to Aspartate, and V_D-Lac is the complex with residue 3 of vancomycin modified to Aspartate and acyl-D-Ala-D-Ala modified to acyl-D-Ala-D-Lac. A CHARMM General Forcefield (CGenFF) was generated for the simulation system using the online paramchem/CGenFF-4.0 server[32-33]. Partial charges for the atoms were obtained from a series of Natural Population Analyses using density functional theory (DFT) at the B3LYP/6-311G(d,p) level of theory with the Gaussian16 software package[131]. All simulations were carried out under periodic boundary conditions using the GROMACS

version 2018.3[35]. A cubic box size of about 46.1 Å dimension was used. The number of atoms in the complexes range from 199 to 202. The system was solvated with transferable intermolecular potential with 3 points (TIP3P) explicit water molecules in a cubic periodic box and neutralized using sodium and chlorine ions in physiological conditions. Following energy minimization via steepest descent, constant volume and temperature (NVT) equilibration was performed for 200 ps at 1 fs time step using leap-frog integrator and modified Berendsen thermostat to equilibrate the system to a temperature of 300 K. Thereafter, constant pressure and temperature (NPT) equilibration was performed to stabilize the pressure of the system at 1 bar for 10 ns with 2 fs time step using Parrinello-Rahman barostats with the compressibility of 4.5 x 10^{-5} bar^{-1}. The pressure was controlled by the isotropic position scaling protocol applied in GROMACS. Initial velocities were assigned from a Maxwellian distribution. The particle mesh Ewald (PME) method was used for the electrostatic interactions, and the length of all covalent bonds was constrained using linear constraint solver (LINCS) algorithm[132]. A 30 ns molecular dynamics simulation was performed at a time step of 2 fs for each protein-ligand complex and the output saved after every 10 ps. The cutoff distance for the non-bonded interaction is 12 Å. Three simple harmonic distance restraints were applied to all of the systems during the MD simulation based on experimental solid-state NMR data[133]. The distances were defined and discussed in a previous publication[127].

4.5.2 Root-Mean-Square Deviation

The root-mean-squared deviation (rmsd) was used to quantitatively measure the conformational difference between the structures in the trajectories of the complex during MD simulations and a stable reference structure to estimate structural similarity. This was

done by least-squares fitting the dynamic structure to the reference structure. The calculation was done using GROMACS built-in functions, illustrated by the equation for a molecular structure represented by a cartesian coordinate vector $\mathbf{r}_i$ (i = 1 to N) of N atoms

$$\text{rmsd} = [\frac{1}{M}\sum_{i=1}^{N} m_i(\boldsymbol{r}_i^t - \boldsymbol{r}_i^0)^2]^{\frac{1}{2}} \quad (4.1)$$

where $M = \sum_{i=1}^{N} m_i$, $\boldsymbol{r}_i^0$ is the position of atom *i* in the reference structure, $\boldsymbol{r}_i^t$ is the position of atom *i* at time t, and m_i is the mass of atom *i*. The rmsd values for different complexes were obtained by comparing their structure at time t = 0 (i.e., following the complete equilibration process) with the various structures along the trajectories during MD simulations.

4.5.3 Hydrogen Bond Analysis

The hydrogen bond analysis monitored the stability of the hydrogen bonds formed between the glycopeptide and peptidoglycan analogues along the trajectory of the MD simulation. Hydrogen bond profiles between the selected glycopeptide and peptidoglycan precursor were calculated with the g_hbond utility in GROMACS. All possible donors and acceptors are considered in the hydrogen bond analysis. The donor-acceptor distance is defined within 3.5 Å and the angle cutoff as 30° within a linear configuration. The average number of hydrogen bonds per time frame for the different complexes can be used to compare their stability during the MD simulation.

4.5.4 Interaction Energy

The interaction energy was computed for each complex to characterize the nonbonded ligand-macromolecular interactions. The short-range nonbonded energies are decomposed using GROMACS g_energy analysis tool by defining the energy group of

interest to recalculate energies from the existing simulation trajectory. The short-range van der Waals (E_{vdw}) and electrostatic (E_{elec}) interactions were modeled using the Lennard-Jones short-range (LJ-SR) and Coulombic short-range interaction energy (Coul-SR), respectively. The total interaction energy (E_{tot}) is the sum of the short-range Lennard-Jones energy ($E_{LJ\text{-}SR}$) and the short-range Coulombic energy ($E_{Coul\text{-}SR}$).

$$E_{tot} = E_{LJ-SR} + E_{Coul-SR} \tag{4.2}$$

The measured *intermolecular* interaction energy is the interactions between the C-terminus of the bound ligand and the glycopeptide, while the intramolecular interaction energy was measured for the interactions within the glycopeptide, specifically between the side chain of residue 3 and other parts of the aglycon.

4.5.5 Binding Free Energy Calculations

The binding free energy between the glycopeptide and peptidoglycan analogues was computed using the molecular mechanics Poisson-Boltzmann surface area (MM/PBSA) method[51] to quantify the strength of the interaction in a complex between the glycopeptide and its bound ligand. This was implemented in GROMACS using an external tool, g_mmpbsa, which integrates high-throughput MD simulations with binding energy calculations[134]. The free energies of binding are described with the following set of equations

$$\begin{aligned} \Delta G_{bind} &= G_{complex} - G_{receptor} - G_{ligand} \\ &= \Delta E_{MM} + \Delta G_{sol} - T\Delta S \end{aligned} \tag{4.3}$$

$$\Delta E_{MM} = \Delta E_{internal} + \Delta E_{elec} + \Delta E_{vdW} \tag{4.4}$$

$$\Delta G_{sol} = \Delta G_{polar} + \Delta G_{nonpolar} \tag{4.5}$$

ΔG_{bind} is the total free energy of binding in solution, $G_{complex}$, $G_{receptor}$, and G_{ligand} are the free energies of the complex, glycopeptide, and ligand in the solution, respectively. ΔE_{MM} is the molecular mechanic's potential energy in a vacuum. ΔE_{MM} includes $\Delta E_{internal}$ (bond, angle, and dihedral energies), ΔE_{elec} (electrostatic), and ΔE_{vdW} (van der Waals) energies. ΔG_{sol} is the free energy of solvation, and T and S denote the temperature and entropy, respectively. ΔE_{MM} is evaluated directly from the force field terms and ΔG_{sol} can be decomposed into polar and nonpolar contribution states. The polar term is estimated by solving the Poisson-Boltzmann equation, whereas the nonpolar term is estimated using the solvent-accessible volume model. The current implementation of the MM/PBSA method within g-mmpbsa does not include entropic terms and thus is unable to provide the absolute binding free energy directly[134], although the tool is suited for calculating relative binding energies of similar systems[51, 53, 129, 134].

CHAPTER FIVE

Investigation of the Secondary-binding Site in Disaccharide-modified Glycopeptide by MD Simulations

5.1 Abstract

Oritavancin is a semisynthetic glycopeptide antibiotic used to treat severe infections by multidrug-resistant Gram-positive pathogens. Oritavancin is known to be a thousand times more potent than vancomycin against Gram-positive bacteria due to the additional interactions with bacterial peptidoglycan (PG) facilitated by a secondary-binding site. The presence of this secondary-binding site is evident in desleucyloritavancin, an Edman degradation product of oritavancin, still retaining its potency against Gram-positive bacteria, whereas desleucylvancomycin is devoid of any antimicrobial activities. Herein, using explicit solvent molecular dynamics (MD) simulations, steered MD simulations, and umbrella sampling, we show evidence of a secondary-binding site mediated by the disaccharide-modified hydrophobic sidechain of oritavancin interactions with the pentaglycyl bridge segment of the PG. The interactions were characterized through comparison to the interaction of PG with chloroeremomycin, vancomycin, and the desleucyl analogues of the glycopeptides. Our results show that the enhanced binding of oritavancin to PG over the binding of the other complexes studied is due to an increase in the hydrophobic effect, electrostatic and van der Waals interactions and not the average number of hydrogen bonding. Our ranking of the binding interactions of the biomolecular complexes directly correlates with the order based on their experimental minimum inhibitory concentrations (MIC). The results of our simulations provide insight into the

modification of glycopeptides to increase their antimicrobial activities or the design of novel antibiotics against pathogenic Gram-positive bacteria.

5.2 Introduction

Glycopeptide antibiotic consists of powerful antibiotics that are in clinical use including vancomycin, teicoplanin, telavancin, dalbavancin, and oritavancin (Fig. 5.1). All glycopeptide antibiotics target bacterial cell wall biosynthesis by binding to the D-Ala-D-Ala terminus[69] of the membrane-bound peptidoglycan (PG) precursor, lipid II. Lipid II refers to a PG-repeat unit attached to the lipid transporter (C_{55}). The PG-repeat unit in *Staphylococcus aureus* consists of a disaccharide (GlcNAc-MurNAc), a pentapeptide-stem structure of L-Ala-D-iso-Glu-L-Lys-D-Ala-D-Ala, and a pentaglycine attached to the ε-nitrogen side of the Lys (Figure 5.1d). Glycopeptide antibiotic binding to lipid II prevents the transglycosylation step of PG biosynthesis, which is required to regenerate the lipid transporter. Hence, the addition of vancomycin to *S. aureus* during the growth results in the accumulation of Park's Nucleotide which is a cytoplasmic PG-precursor.[105] Since C_{55} is found in a surprisingly low number of copies per bacterium[106, 135-136] and it is also a shared transporter used in wall-teichoic acid biosynthesis, vancomycin binding to lipid II is an effective means of inhibiting both PG and wall-teichoic acid biosynthesis in *S. aureus*.[121, 137]

In vancomycin-resistant pathogens, the D-Ala-D-Ala terminus of the PG stem is either cleaved or modified to prevent the glycopeptide binding. The D-Ala-D-Ala terminus modification to D-Ala-D-Ser is found in low-level vancomycin-resistant bacteria,[138-139] and modification to D-Ala-D-Lac is found in high-level vancomycin-resistant enterococci (VRE).[65-66, 138, 140] The depsipeptide substitution reduces the vancomycin binding affinity

(K_d) by a thousand fold from 1μM for a tripeptide acyl- L-Lys-D-Ala-D-Ala to 1mM for a tripeptide acyl-L-Lys-D-Ala-D-Lac, and increases the minimal inhibitory concentration (MIC) from 1 μg/ml against vancomycin-susceptible bacteria to greater than 1000 μg/ml against VRE. The replacement of the D-Ala-D-Ala by D-Ala-D-Lac substitutes an amide with an ester bond which replaces one of the hydrogen bonds with an electrostatic repulsion between the lone pair of a carbonyl oxygen atom at the 4th position of vancomycin aglycon and the ester oxygen atom on the D-Ala-D-Lac.[114, 141]

A series of chemical modifications by alkylation of the amine sugar (L-4-epi-vancosamine) of chloroeremomycin (Fig. 5.1b) with a hydrophobic group has led to the discovery of second-generation lipoglycopeptide antibiotics including oritavancin which exhibits potent activity against the VRE.[117, 142] Chloroeremomycin is the parent compound of oritavancin which differs from vancomycin by an additional 4-epi-vancosamine attached to the 6th amino acid of the heptapeptide core. While chloroeremomycin is only four times more potent than vancomycin, oritavancin shows a thousand-fold increase in the efficacy against the VRE. Oritavancin's potent antimicrobial activity against the VRE came as a surprise because the 4-chloro-biphenyl is attached to the vancosamine which is positioned far from the D-Ala-D-Ala binding site. Thus, an alkylated hydrophobic sidechain of oritavancin, despite a thousand-fold increase in activity, does not improve the glycopeptide binding affinity to the peptides terminating in either D-Ala-D-Ala or D-Ala-D-Lac. The dissociation constants for vancomycin and oritavancin to acyl-D-Ala-D-Lac are both on the order of 1 mM, suggesting that oritavancin has a distinct mode of action that involves more than D-Ala-D-Ala binding. Furthermore, oritavancin exhibits the following unique antimicrobial properties that are consistent with a new mode of action: 1) while

vancomycin is a biostatic agent, oritavancin is bactericidal achieving 3-log kill (99.9% reduction) within an hour of drug addition,[120, 143] 2) unlike vancomycin, oritavancin retains the potent killing kinetic against the VRE and vancomycin-resistant *S. aureus*,[120] and 3) while the Edman degradation product of vancomycin is devoid of activity, the Edman degradation product of oritavancin retains its potent activity.[85, 144-145]

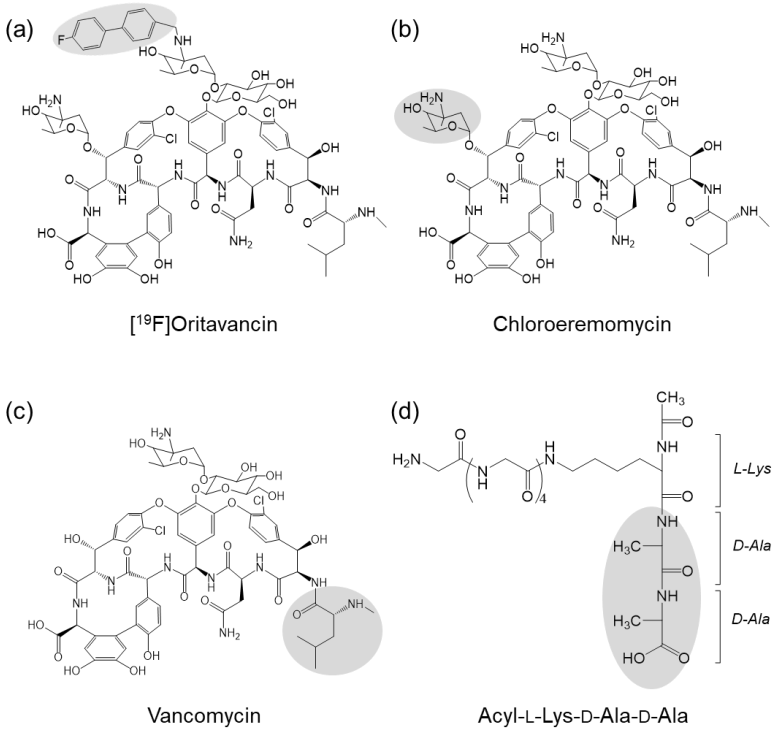

Figure 5.1. The chemical structures of the glycopeptides and a PG-repeat unit. (a) Chemical structure of [^{19}F]oritavancin with the biphenyl moiety highlighted in grey color. (b) Chemical structure of chloroeremomycin with the 4-epi-vancosamine highlighted in grey color. (c) Chemical structure of vancomycin with the first amino acid residue, N-methylleucine, shown in grey color. The cleavage of the N-methylleucine from [^{19}F]oritavancin, chloroeremomycin, and vancomycin by Edman degradation results in desleucyl-[^{19}F]oritavancin, desleucyl-chloroeremomycin, and desleucyl-vancomycin, respectively. (d) Chemical structure of the peptide portion of the PG-repeat unit in *S. aureus* with amino acid sequence acyl-L-Lys(Gly$_5$)-D-Ala-D-Ala. A pentaglycine is attached to the ε-nitrogen of the L-Lys. The D-Ala-D-Ala of the PG-repeat unit (grey color) is the primary binding site of the glycopeptide antibiotics. The PG disaccharide *N*-acetylglucosamine-*N*-acetylmuramic acid does not participate in binding to the glycopeptide antibiotics and was removed from the glycopeptide-PG complex.

The alkylated hydrophobic adducts of oritavancin and oritavancin-like lipoglycopeptide have been thought to act as membrane anchors through insertion into the bacterial lipid bilayer to localize the drug at the site of PG biosynthesis and to promote drug dimerization.[146] This is corroborated by a strong correlation between the lipophilicity indices of the alkylated hydrophobic adducts of the lipoglycopeptide and the MIC of the drug.[113] The co-localization of glycopeptide to its substrate at the membrane by membrane anchor is energetically favorable for intermolecular interaction and thereby overcoming weak binding to depsipeptide terminating lipid II.[147] This is supported by an observation that chloroeremomycin dissociation constant to a depsipeptide D-Ala-D-Lac in solution (1 mM)[148] decreases to 4 μM when a PG-mimic, docosanoyl-Gly-Ala-Glu-Lys-D-Ala-D-Lac, is anchored to the phosphatidyl-choline vesicle.[149] Drug dimerization is also thought to enhance the depsipeptide substituted lipid II bindings through positive cooperativity.[147] In solution, oritavancin dimerizes strongly with a dimerization constant approximately a thousand times greater than vancomycin.[113, 150] Hence, combined drug dimerization and membrane anchoring are thought to be the mode of action that pervades in all lipoglycopeptides to overcome the vancomycin resistance in VRE.

Although *in vitro* assays have shown that lipoglycopeptides dimerizes in solution and binds to lipid vesicles, *in situ* lipoglycopeptides exhibit a different mode of action.[78-85] Solid-state nuclear magnetic resonance (NMR) characterization of the ^{19}F-labeled oritavancin (Fig. 5.1a) bound to intact whole cells of *S. aureus* confirmed that [^{19}F]oritavancin preferentially binds to the PG as a monomer, not as a dimer, and oritavancin does not localize to the lipid bilayer of the bacterial membrane.[78] Even when [^{19}F]oritavancin was added to the protoplasts of *S. aureus*, where the cell wall is

enzymatically removed using lysostaphin to leave only a thin layer of nascent PG, oritavancin is still found bound to the PG but not to the membrane.[83] The absence [^{19}F]oritavancin membrane anchoring *in situ* was determined by ^{31}P{^{19}F} rotational-echo double resonance (REDOR) NMR, positioning the ^{19}F of oritavancin at least 14 Å or further away from the phosphate found in the lipid headgroup.[149] Solid-state NMR characterization of oritavancin and other lipoglycopeptide antibiotics with a varying hydrophobic sidechain length bound to intact whole cells has revealed that the positions of the drug hydrophobic sidechain are closely associated with the crosslinked PG-bridge structure.[79, 82, 84] The hydrophobic sidechain of lipoglycopeptide is thought to form a secondary-binding[84] to target partially crosslinked PG template to prevent the maturation of the nascent PG by inhibiting transpeptidase activity.[80] Hence, unlike vancomycin which inhibits transglycosylase activity, secondary-binding site in oritavancin enabled dual inhibition of both transglycosylase and transpeptidase activities in *S. aureus*.[80, 85, 121-123]

The significance of the secondary-binding site is evident when des-*N*-methylleucyl-oritavancin (desleucyl-oritavancin), an Edman degradation product of oritavancin, was complexed to whole cells of *S. aureus*.[80] For vancomycin, Edman degradation results in des-*N*-methylleucyl-vancomycin with the damaged D-Ala-D-Ala binding cleft which does not bind to PG and is devoid of any antimicrobial activities. However, desleucyl-oritavancin[80] and Edman degradation products of oritavancin-like vancomycin[145] retain potent antimicrobial activities. Despite the damage to the primary-binding site, the secondary-binding site in desleucyl-oritavancin[80] and desleucyl-chloro-biphenyl vancomycin[81] have been shown to enable binding to PG in intact whole cells of *S. aureus*. Furthermore, the addition of desleucyl-oritavancin to *S. aureus* during growth has been

shown to inhibit transpeptidase activity of cell wall biosynthesis which was confirmed by solid-state NMR[85] and by liquid chromatography-mass spectrometry analysis of the muropeptides.[122] The inhibition of transpeptidase activities by desleucyl-oritavancin showed that the secondary-binding site targeted the peptidoglycan template to induce cell wall disorder and to interfere with cell wall maturation. Despite the significance and relevance of the secondary-binding site in oritavancin, the structure and conformation of the oritavancin-PG complex remain unknown. This is because the secondary-binding site targets the crosslinked PG in the cell wall, which is not amenable to either x-ray diffraction or solution-state NMR for structural determination.

In this study, we investigate the role of the secondary-binding site in oritavancin complexed to the PG-repeat unit using molecular dynamics (MD) simulations, center-of-mass (COM) pulling simulations, and umbrella sampling. The simulations were carried out for the binding of PG with oritavancin, chloroeremomycin, vancomycin, and their desleucyl analogues (Figure 5.1). Our results show evidence of a secondary-binding site mediated by the disaccharide-modified hydrophobic sidechain of oritavancin interactions with the pentaglycyl bridge segment of the PG. These interactions contributed to the significant enhancement in oritavancin binding to PG compared to other glycopeptide antibiotics that do not have a secondary-binding site (chloroeremomycin and vancomycin). For the MD simulations, the experimentally determined solid-state NMR distance constraints[80, 85, 151] were utilized for the glycopeptide-PG and desleucyl-glycopeptide-PG complexes.

5.3 Results

5.3.1 Hydrogen Bonding, Experimental MIC and Binding Free Energy

For each glycopeptide-PG complex (Figure 5.2), the calculated average number of hydrogen bonds, free energy of binding, and the measured minimum inhibitory concentrations (MIC) of glycopeptides against *S. aureus*[152] are shown in Table 5.1. The heptapeptide-core structure of glycopeptide constitutes a primary-binding site which binds to the D-Ala-D-Ala dipeptide segment of the PG. The strength of this interaction is governed by electrostatic hydrogen bonding such that when vancomycin binds to the PG of vancomycin-susceptible *S. aureus*, five stable hydrogen bonds are formed between the heptapeptide-core structure of vancomycin and the D-Ala-D-Ala of the PG. Any chemical modification, to either glycopeptide antibiotic or PG, that affects this interaction results in loss of antimicrobial activity. For example, in the case of vancomycin-resistant *S. aureus* where D-Ala-D-Ala of the PG is mutated to a D-Ala-D-Lac, the depsipeptide substitution removes one of the hydrogen bonds and replaces it with an electrostatic repulsion. This results in a 1000-fold reduction in the binding affinity of vancomycin to PG accompanied by a thousand-fold increase in the MIC. All glycopeptide-PG complexes studied, including Ori-PG, Ceremo-PG, and Vanco-PG, show a minimum of five stable hydrogen bonds formed between the primary-binding pocket in glycopeptide to the PG (Table 5.1). In the case of desleucyl analogues of the glycopeptides that have a damaged primary-binding pocket due to the Edman degradation, the average number of stable hydrogen bonds between the glycopeptide and PG is less than five.

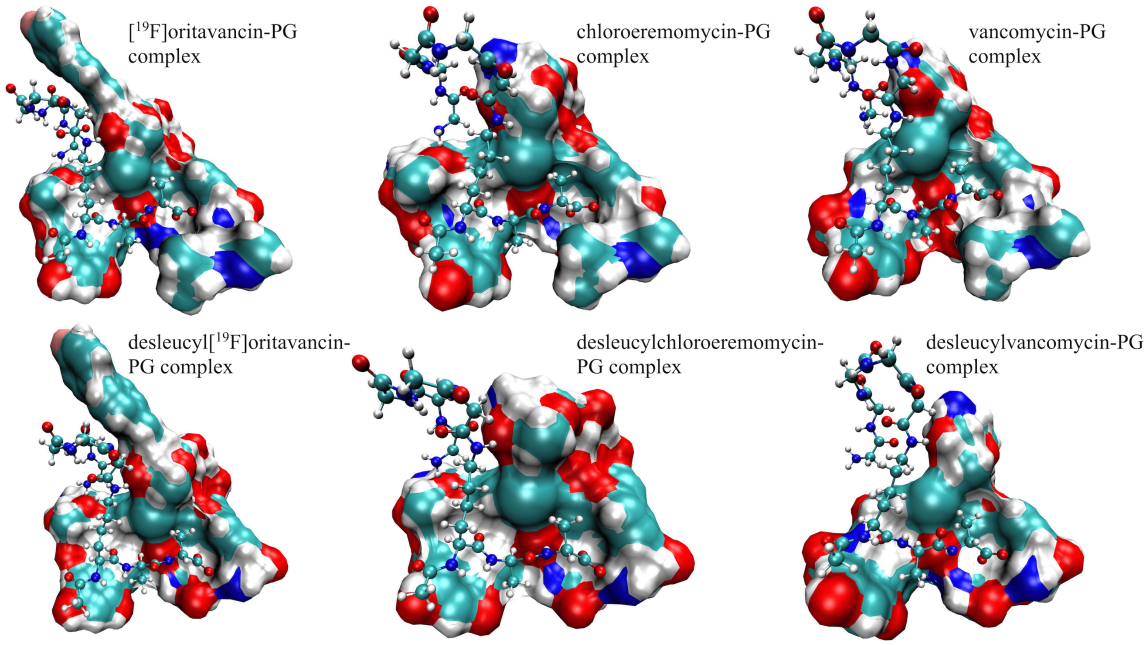

Figure 5.2. MD simulation model structures of the glycopeptide- and desleucylglycopeptide-PG complexes. The glycopeptides (top) and desleucylglycopeptides (bottom) are shown as a visual molecular dynamics (VMD)[153] solid surf model using a probe radius of 1.4 Å, while the CPK model represents the PG (Fig. 1d). The glycopeptide-PG complexes (top) include [^{19}F]oritavancin-PG complex (top left), chloroeremomycin-PG complex (top middle) and vancomycin-PG (top right). The desleucylglycopeptide-PG complexes (bottom) include desleucyl[^{19}F]oritavancin-PG complex (bottom left), desleucylchloroeremomycin-PG complex (bottom middle), and desleucylvancomycin-PG (bottom right).

Table 5.1. Average number of hydrogen bonds, experimental MIC[152], and free energy of binding for the (desleucyl)glycopeptide-PG complexes

Glycopeptide-PG Complex	Average number of H-bonds	MIC[a] (μM)	ΔG_{bind}[b] (Kcal/mol)	ΔG_{bind}[c] (Kcal/mol)
Ori-PG	5.50 ± 0.21	< 0.016	-15.04 ± 1.74	-125.89 ± 18.06
Des-Ori-PG	4.69 ± 0.16	0.30	-14.95 ± 1.76	-112.06 ± 20.98
Ceremo-PG	5.91 ± 0.07	0.29	-13.99 ± 0.61	-104.36 ± 16.35
Des-Ceremo-PG	4.89 ± 0.08	10.00	-12.56 ± 0.39	-91.96 ± 17.62
Vanco-PG	5.52 ± 0.37	0.84	-11.07 ± 1.64	-88.06 ± 18.14
Des-Vanco-PG	4.76 ± 0.07	> 673	-8.45 ± 1.80	-75.77 ± 17.77

[a] Experimental minimal inhibitory concentration

[b] Binding energy from umbrella sampling method

[c] Binding energy from MM/PBSA method

The log of MIC values directly correlates with the free energy of binding for all the complexes (Figure 5.3). The free energy of binding for the various complexes studied is calculated with both an end-point and a pathway method. The end-point free energy method is based on the molecular mechanics Poisson-Boltzmann surface area (MM/PBSA), while the more accurate pathway free energy calculation was obtained from the umbrella sampling (US) method. Both free energy calculation methods result in the same ranking of the stability of the (desleucyl)glycopeptide-PG complexes. Though the MM/PBSA free energy approach is considered less accurate than the umbrella sampling, it produced consistent results in ranking the binding interaction of biomolecular complexes, especially when similar ligands are involved in the binding.[129, 141] From the binding free energy values, the stability of the (desleucyl)glycopeptide-PG complexes is ranked as follows: Ori-PG > Des-Ori-PG > CEremo-PG > Des-CEremo-PG > Vanco-PG > Des-Vanco-PG. The Des-Vanco-PG complex is the least stable complex with a ΔG^{b}_{bind} value of -8.45 ± 1.80 kcal/mol while the Ori-PG complex is the most stable with a ΔG^{b}_{bind} of -15.04 ± 1.74 kcal/mol, both in excellent agreement with the antimicrobial activities measured by the MIC.[152]

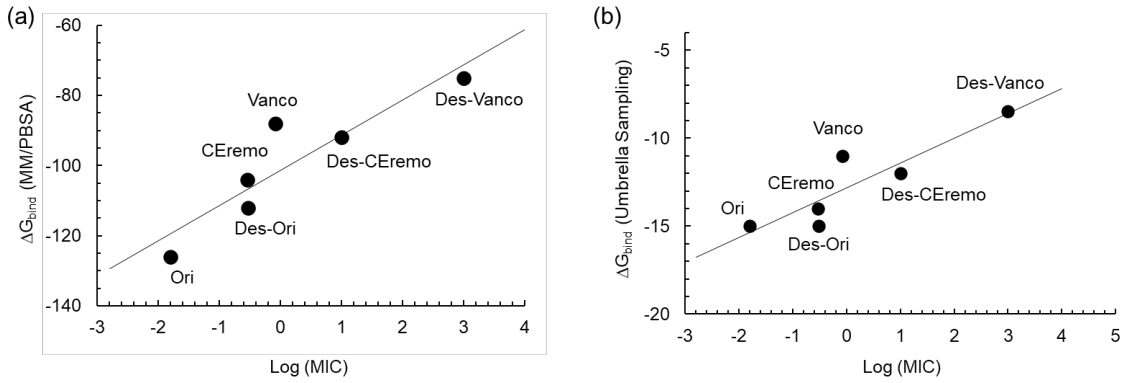

Figure 5.3. Plots of binding energy vs minimum inhibitory concentration for the (desleucyl)glycopeptide complexes. Plots of MM/PBSA binding energy vs Log (MIC) (top) and plots of umbrella sampling binding energy vs Log (MIC) (bottom) of the (desleucyl)glycopeptide complexes.

The decomposition of the MM/PBSA binding free energy into its electrostatic and van der Waals contribution to the total binding energy is given in Table 5.2. The increased binding of the Ori-PG complex compared to the other complexes can be seen as an overall increase in its electrostatic and van der Waals interactions. All the complexes that show comparatively increased binding based on the ΔG_{bind} values also show an increase in the electrostatic and van der Waals contribution to the free energy, except for the Des-CEremo-PG complex. The Des-CEremo-PG complex has a relatively lower van der Waals interaction than that of Vanco-PG but higher electrostatic interactions. From the error estimation shown for the van der Waals, electrostatic, and subsequently total binding energies of Des-CEremo-PG and Vanco-PG, there are no distinct differences in their energy values. Des-Vanco-PG with the least ΔG_{bind} value also has the least van der Waals and Electrostatic contribution to the total binding energy.

Table 5.2. MM/PBSA binding free energy decomposition

Glycopeptide-PG Complex	ΔE_{vdw} (Kcal/mol)	ΔE_{elec} (Kcal/mol)	ΔG_{bind}* (Kcal/mol)
Ori-PG	-62.08 ± 8.99	-117.29 ± 9.86	-125.89 ± 18.06
Des-Ori-PG	-54.37 ± 9.04	-111.90 ± 10.10	-112.06 ± 20.98
Ceremo-PG	-47.76 ± 8.86	-110.51 ± 10.17	-104.36 ± 16.35
Des-Ceremo-PG	-40.09 ± 8.76	-104.95 ± 10.43	-91.96 ± 17.62
Vanco-PG	-44.95 ± 8.46	-101.69 ± 9.82	-88.06 ± 18.14
Des-Vanco-PG	-35.97 ± 8.37	-99.35 ± 10.41	-75.77 ± 17.77

* MM/PBSA approach

5.3.2 Root-Mean-Square Deviation (RMSD) Analysis

The rmsd for each of the (desleucyl)glycopeptide-PG complex was calculated to gain insight into the stability of the complexes during the MD simulation (Figure 5.4). The rmsd value is obtained by comparing the structures of the complex along the trajectories of the simulation with a stable reference structure. Generally, a relatively lower rmsd value and a narrow rmsd fluctuation pattern indicate a stable binding and lower flexibility between the (desleucyl)glycopeptide and PG. The rmsd values for all the glycopeptide-PG complexes (approximately 3.00 Å) are all within the error estimation for the four independent MD simulations performed. This closeness in rmsd values limits the use of the absolute rmsd value to rank the overall stability of all the complexes. From observing the various rmsd fluctuation pattern, Ori-PG and Des-Ori-PG complexes appear to be the most stable complexes due to their narrow and less flexible fluctuation patterns. The CEremo-PG and the Vanco-PG complexes also show comparatively lower fluctuation patterns when compared to that of Des-CEremo-PG and Des-Vanco-PG complexes, which both have more flexible fluctuation patterns.

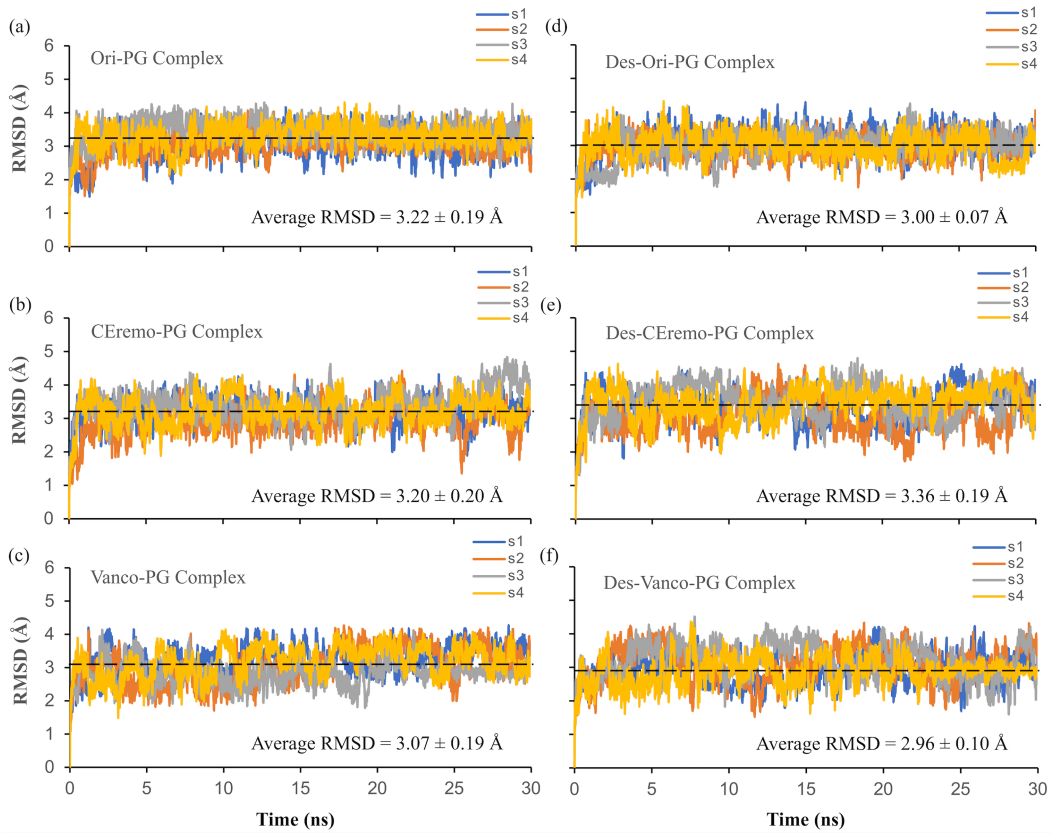

Figure 5.4. RMSD plots of MD simulations. The rmsd plots of the complexes of (a) [^{19}F]oritavancin-PG, (b) chloroeremomycin-PG, (c) vancomycin-PG, (d) desleucyl[^{19}F]oritavancin-PG, (e) desleucylchloroeremomycin-PG, and (f) desleucylvancomycin-PG. The rmsd plots are based on four independent simulations, labeled as s1, s2, s3, and s4. The average rmsd value for each complex is shown as a black dashed line.

The 2D rmsd (Å) contour plots was used to further characterize the binding distribution of the glycopeptide- and desleucylglycopeptide-PG complexes. The 2D contour plot compares the binding distribution between two complexes during MD simulation using their rmsd values. The presence of contour lines symmetric around a single attraction basin in a contour plot, indicates the similarities of binding distribution between the two complexes that are being compared. Multiple attraction basins in a contour plot implies that the binding distribution of the two complexes compared is distinct.

The binding distribution of the Ori-PG complex was used as a reference to generate the 2D contour plots shown in Figure 5.5. The binding distribution of the Des-Ori-PG complex (Figure 5.5c) with its contour lines most symmetric around a single attraction basin at (3.1, 3.2) Å and centered on the highest density of joint distribution indicates that the distribution is similar to that of Ori-PG complex despite the loss of its primary-binding site. We attribute this to the secondary-binding site which is present in both [^{19}F]oritavancin and desleucyl[^{19}F]oritavancin that contributes to the PG binding. This similarity in binding distribution between Ori-PG and Des-Ori-PG was also seen in their similar rmsd fluctuation pattern (Figure 5.4a and d).

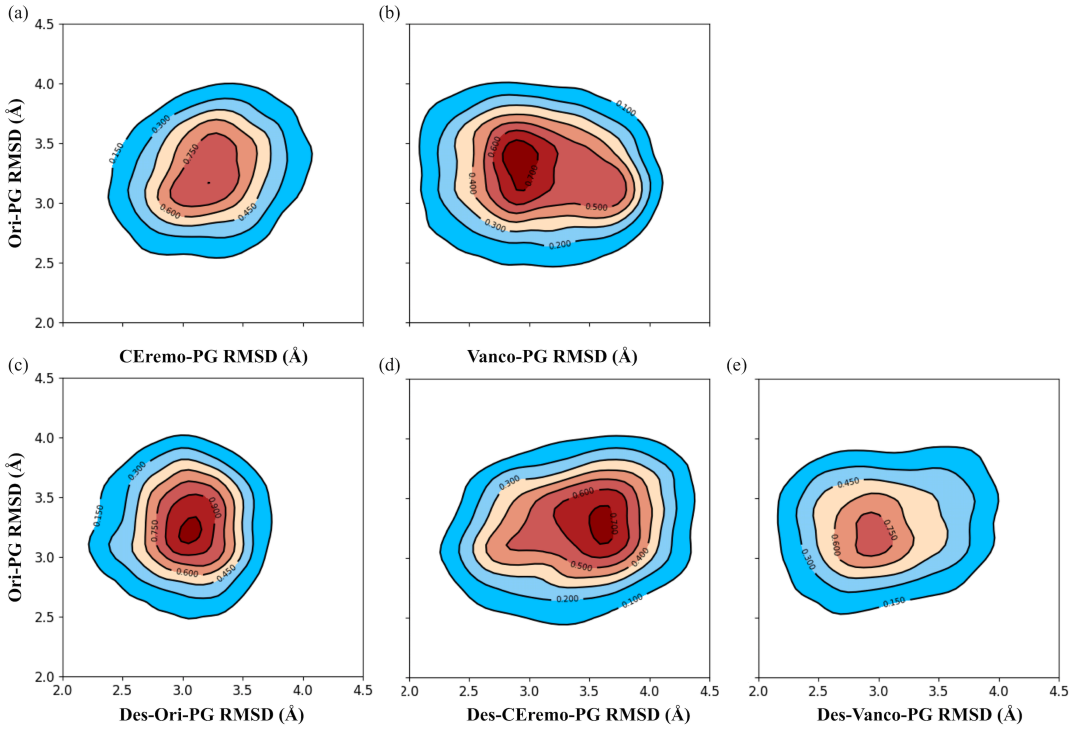

Figure 5.5. Comparative 2D rmsd (Å) contour plots of the Ori-PG complex relative to the other complexes. Comparative 2D rmsd contour plots of (a) Ori-PG vs. Ceremo-PG, (b) Ori-PG vs. Vanco-PG, (c) Ori-PG vs. Des-Ori-PG, (d) Ori-PG vs. Des-CEremo-PG, and (e) Ori-PG vs. Des-Vanco-PG complexes. The contour lines are the densities of trajectories located within an area. The region of the highest density of trajectories is denoted by the red color, while the blue colors represent regions of lower densities of trajectories.

The next complex with a similar binding distribution to that of the Ori-PG complex is the CEremo-PG complex (Figure 5.5a), based on the symmetrical contour lines. This is similar to the ranking of the complexes based on their binding energies and MIC values (Table 5.1) with Ori-PG > Des-Ori-PG > CEremo-PG. The 2D contour plots of Ori-PG vs. Vanco-PG, Des-CEremo-PG, and Des-Vanco-PG all show less symmetric contour lines, as well as a deviation from single attraction basins. All the complexes showed 2D contour plots with distinct binding distributions from that of Vanco-PG when the Vanco-PG was used as a reference for comparing other complexes (Figure S5.2).

5.3.3 Force-time Curve of Center-of-mass Pulling Simulation

The strength of the interaction between the (desleucyl)glycopeptide and PG can also be inferred from the force-time plot obtained from the center-of-mass (COM) pulling simulations for the various complexes (Figure 5.6). The magnitude of the pull, maximum force (F_{max}) required to pullout the bound PG from the glycopeptides, and the time required for dissociation of the complex can be used to infer the stability of the complex. This is especially true when the ligand-dissociation pathway is similar in the complexes compared[50]. In each glycopeptide-PG complex, the F_{max} required for pulling the PG away from the complex is higher than the corresponding desleucylglycopeptide-PG complex. Furthermore, a longer time is required to reach F_{max} and to achieve a major dissociation between the PG and the glycopeptide in glycopeptide-PG complex compared to the corresponding desleucylglycopeptide-PG complex. For example, the Ori-PG complex required a F_{max} of 645 kJ mol^{-1} nm^{-1} achieved in the duration of 91 ps (Fig. 5.6a, brown line), and a total of 215 ps to reach the major point of dissociation between the PG and [^{19}F]oritavancin (Fig. 5.6a, blue line). On the other hand, the Des-Ori-PG complex required

a F_{max} of 616 kJ mol^{-1} nm^{-1} for the duration of 141 ps, and a major dissociation between the PG and desleucyl[^{19}F]oritavancin was reached at 194 ps (Figure 5.6d). The values for the F_{max}, time to reach F_{max}, and time to reach a major dissociation point for all the complexes studied are shown in Table S5.1. The lower F_{max} and lesser time to reach a major dissociation point in the desleucylglycopeptide-PG complexes is due to the loss of binding in their primary binding pockets. Of the (desleucyl)glycopeptide complexes, the Des-Vanco-PG required the minimum magnitude of F_{max} (437 kJ mol^{-1} nm^{-1}) and took the least amount of time to reach the F_{max} (68 ps) and a major dissociation point (156 ps) (Figure 5.6f). This is consistent with the Des-Vanco-PG complex having the least stability based on the binding energy and the minimum antimicrobial activity of Des-Vanco measured by the MIC (Table 5.1).

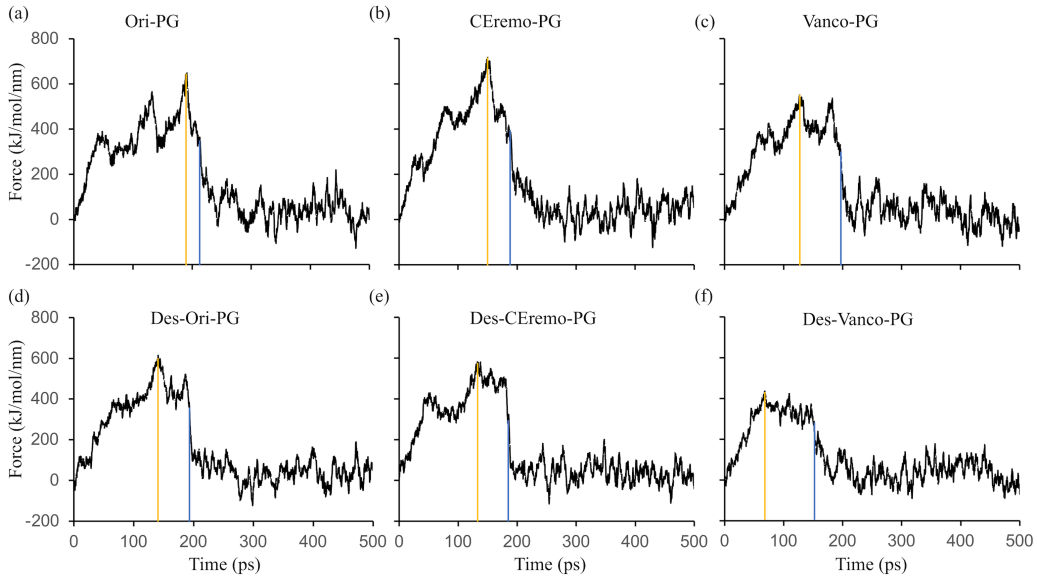

Figure 5.6. Plots of force vs time of the dissociation of the (desleucyl) glycopeptide and PG during center-of-mass (COM) pulling simulation. Plots of force vs time for (a) Ori-PG, (b) Ceremo-PG, (c) Vanco-PG, (d) Des-Ori-PG, (e) Des-Ceremo-PG, and (f) Des-Vanco-PG complexes. The yellow line in each figure corresponds to the point of maximum force and the blue line represents a major dissociation point between the (desleucyl)glycopeptide and PG

5.3.4 Potential of Mean Force (PMF) from Umbrella Sampling Simulation

The potential of mean force (PMF) along a reaction coordinate was obtained using umbrella sampling simulations[58]. Figure 5.7 shows the PMF leading to a ΔG_{bind}, and the corresponding umbrella histograms for the glycopeptide-PG complexes from the weighted histogram analysis method (WHAM)[60]. Umbrella sampling is commonly performed following an explicit solvent MD simulation and a steered MD simulation (SMD), also known as COM pulling simulation, as an effective way to obtain the PMF along a reaction coordinate. About 50 sampling windows are used to run the umbrella sampling simulations, each corresponding to a 10 ns simulation. The COM pulling simulation was performed to a total COM distance of about 5.5 nm. The Ori-PG complex is the most stable complex from the PMF curves, among all the (desleucyl)glycopeptide-PG complexes studied, with a ΔG_{bind} value of -15.04 ± 1.74 kcal/mol. The CEremo-PG complex has a ΔG_{bind} of -13.99 ± 0.61 kcal/mol, and the ΔG_{bind} of the Vanco-PG complex is -11.07 ± 1.64 kcal/mol (Figure 5.7). The PMF curves for the desleucylglycopeptide-PG complexes are shown in Figure S5.1.

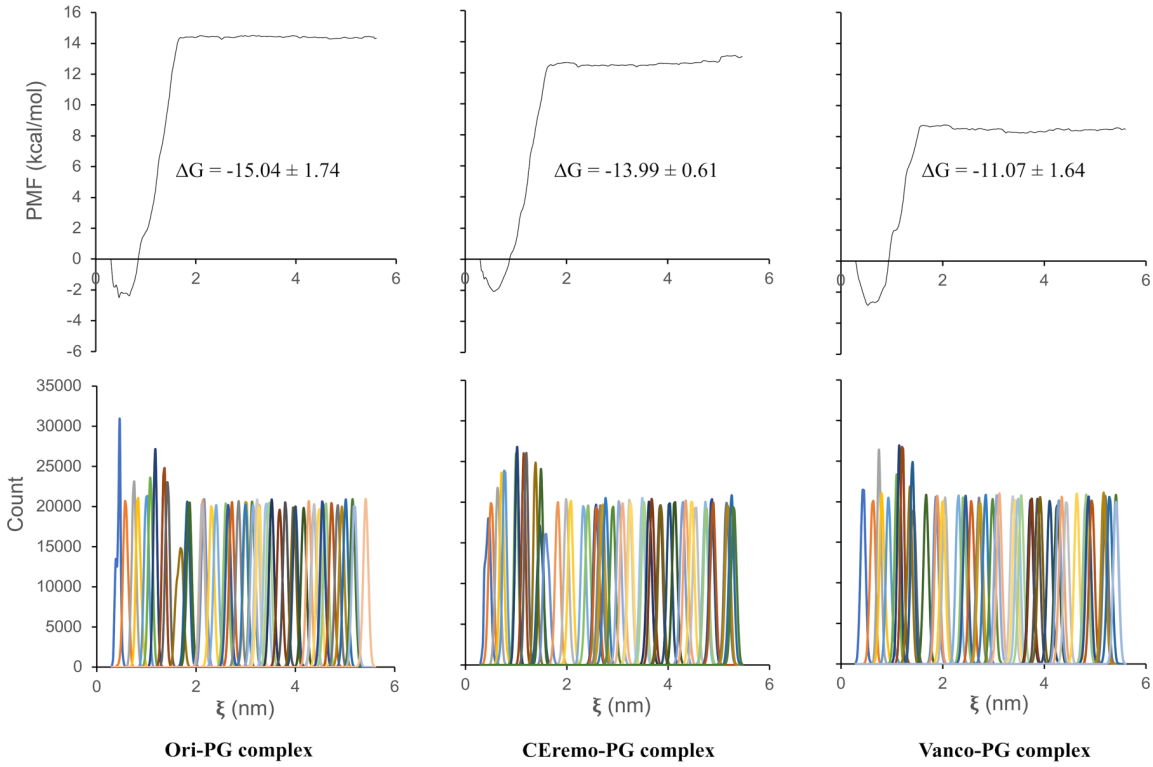

Figure 5.7. The potential of mean force (PMF) curve and corresponding umbrella histograms for complexes of [^{19}F]oritavancin-PG (left), chloroeremomycin-PG (middle), and vancomycin-PG (right). The ΔG values of the complexes obtained from the PMF curve are shown as an inset. The PMF for the desleucylglycopeptide-PG complexes is included in the S.I.

5.4 Discussion

Solid-state NMR has been used to confirm the existence of a secondary-binding site in the binding of [^{19}F]oritavancin to PG. This secondary-binding site (Figure 5.8) enhanced the binding of [^{19}F]oritavancin to PG as oritavancin is 1000-fold more potent than vancomycin against a broad range of Gram-positive bacteria. The removal of the first amino acid residue of vancomycin, *N*-methylleucine, by Edman degradation leads to the formation of desleucylvancomycin, which is devoid of antimicrobial activities due to a damaged primary binding pocket. On the other hand, the Edman degradation product of oritavancin, desleucyloritavancin, still maintains its potent antimicrobial activities despite

a damaged primary binding site. Despite the overwhelming experimental evidence and available NMR data showing the presence of a secondary-binding site in oritavancin, there is still a lack of computational study to compare the binding of oritavancin to PG with that of vancomycin or other glycopeptides. Herein, using explicit solvent MD simulation, COM pulling simulation, and umbrella sampling, we compare the binding of the PG-repeat unit to three different glycopeptides, including oritavancin, chloroeremomycin, and vancomycin, as well as their desleucyl analogues. The free energy of binding to predict the stability of the different (desleucyl)glycopeptide-PG complexes studied was computed through MM/PBSA and umbrella sampling methods. The ΔG_{bind} values obtained from both methods produced the same ranking for the stability of the (desleucyl)glycopeptide-PG complexes (Table 5.1). The order of stability of the complexes obtained is as follows: Ori-PG > Des-Ori-PG > CEremo-PG > Des-CEremo-PG > Vanco-PG > Des-Vanco-PG. This ranking pattern is also similar to that obtained from the experimental MIC[152] values, except for the Des-CEremo-PG complex, which showed lower stability than the Vanco-PG complex. Although, this difference in the ranking of Des-CEremo-PG and Vanco-PG complexes is insignificant considering the error estimations.

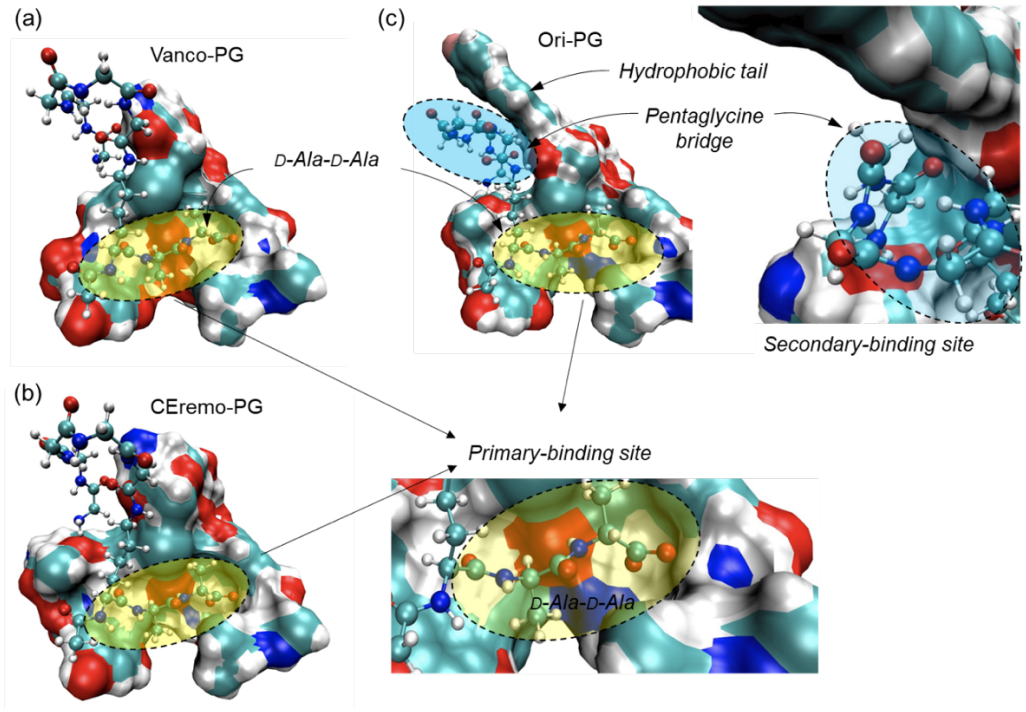

Figure 5.8. MD simulation model structures of the vancomycin-PG, chloroeremomycin-PG, and [^{19}F]oritavancin-PG complexes. (a) In the vancomycin-PG complex, the primary-binding site (yellow oval) at the heptapeptide-core of the aglycon is solely responsible for binding to the D-Ala-D-Ala terminus of the PG. (b) In the chloroeremomycin-PG complex, the presence of 4-epi-vancosamine attached to the 6th amino acid position enhances the PG binding. Even though chloroeremomycin does not have a secondary-binding site, the difference in the ΔG_{bind} of chloroeremomycin-PG to vancomycin-PG complex ($\Delta\Delta G_{bind}$) is -16.29 Kcal/mol. (c) In the oritavancin-PG complex, both primary and secondary-binding sites contribute to the PG binding. The total number of H-bonds formed between the PG and oritavancin is 5.5 which is identical to the number of H-bonds found in the vancomycin-PG complex. But, unlike vancomycin and chloroeremomycin, the secondary-binding site (blue oval) significantly enhances the binding of oritavancin to PG by $\Delta\Delta G_{bind}$ of -37.83 and -21.53 Kcal/mol in comparison to vancomycin and chloroeremomycin, respectively (Table 2). This enhancement is due to an increase in the ΔG_{bind} by electrostatic and van der Waals interactions between the drug hydrophobic sidechain with the pentaglycine-bridge structure of the bound PG.

The average number of hydrogen bonds, mainly responsible for the strength of interaction between the glycopeptide and PG at the primary binding pocket, formed between [^{19}F]oritavancin and the PG, is less than that formed between chloroeremomycin, vancomycin, and PG. This implies that the enhanced interaction between [^{19}F]oritavancin

and the PG are not due to an increase in the number of hydrogen bonds but other types of interactions, including hydrophobic effect due to the packing of the pentaglycyl bridge of the PG at the secondary-binding site of [^{19}F]oritavancin (Figure 5.8). A similar observation applies to the Des-Ori-PG complex with a lower average number of hydrogen bonds than Des-CEremo-PG and Des-Vanco-PG. Typically, five stable hydrogen bonds form at the primary binding site of [^{19}F]oritavancin, chloroeremomycin, and vancomycin. The desleucyl analogues of [^{19}F]oritavancin, chloroeremomycin, and vancomycin, formed by removing the first amino acid residue, N-methylleucine, show a reduction in the average number of hydrogen bonds formed (Table 5.1). This removal of N-methylleucine, which is not directly involved in the dipeptide binding, is thought to reduce the hydrophobicity of the primary binding pocket leading to a reduction in the strength of binding of the carboxylate anion of the PG to the three amide NH groups of residues 2-4 of the glycopeptide. The binding of the carboxylate anion of the PG to the neighboring amide hydrogen donors of the glycopeptide is mainly responsible for the strength of the interaction between the glycopeptide and PG at the primary binding site. The strength of this interaction is estimated to be about 20-30 kJ/mol[154]. The decomposition of the MM/PBSA total binding energy into its van der Waals and electrostatic contribution (Table 5.2) shows that the increase in the strength of the interaction between [^{19}F]oritavancin and PG is a result of a corresponding increase in both the electrostatic and van der Waals interactions, compared to that in the other complexes. The rmsd distribution analysis shows that Ori-PG and Des-Ori-PG complexes are most stable due to a less flexible and narrow rmsd fluctuation pattern. This stability trend is followed by the fluctuation pattern of the CEremo-PG complex. The other complexes, including Vanco-PG, Des-Vanco-PG, and

Des-CEremo-PG, show a more flexible rmsd fluctuation pattern in the time evolution of the MD simulation. A 2D rmsd contour plotted by comparing the binding distribution of the Ori-PG complex to that of the other complexes using their rmsd values (Figure 5.5) further confirmed that the Des-Ori-PG complex has a binding distribution is most similar to that of the Ori-PG complex. Both [^{19}F]oritavancin and desleucyl[^{19}F]oritavancin have a secondary-binding site that enhances their binding to the PG. The binding distribution of the CEremo-PG complex also shows the similarity of binding distribution to that of the Ori-PG complex but with less density of joint conformational distribution.

To further classify the interaction between the (desleucyl)glycopeptide and PG, a force-time curve is plotted after the COM pulling simulation for all the complexes studied. The force-time plot can be used to estimate the interaction between a receptor and ligand when their dissociation pathways are similar. Applying an external force to pull the ligand away from the receptor allows for the calculation of work, which is a path-dependent quantity. Since the dissociation is a path-dependent process, the magnitude of the maximum force applied to pull the PG away from the glycopeptide can be compared to that needed to pull the PG away from the corresponding desleucylglycopeptide, as both complexes only differ by N-methylleucine. Also, the time it takes to reach this maximum force and the time to reach a major dissociation point can give an insight into what it takes for the PG to escape the attractive pull of the (desleucyl)glycopeptide. The PG requires a comparative higher F_{max} and more time to reach a major dissociation point from the glycopeptide than that needed for the desleucylglycopeptide. This implies that the glycopeptides have a stronger attractive pull to the PG than the desleucylglycopeptides, mainly caused by the damaged primary binding pocket of the desleucylglycopeptides

(Figure 5.6). An observation of the force-time plots for all the complexes studied shows that it takes the least amount of time and least F_{max} to pull the PG away from desleucylvancomycin.

Overall, our study provides insight into the binding of PG to different glycopeptides, including [^{19}F]oritavancin, chloroeremomycin, and vancomycin, as well as their desleucyl analogues. This insight can be helpful in the modification of glycopeptides to increase their antimicrobial activities or the design of novel antibiotics against pathogenic Gram-positive bacteria.

5.5 Conclusion

In this study, we used explicit solvent MD simulation, COM pulling simulations, and umbrella sampling to characterize the binding of PG to three glycopeptide antibiotics and their desleucyl analogues. The glycopeptides simulated include [^{19}F]oritavancin, chloroeremomycin, and vancomycin. Their desleucyl analogues are formed by removing the first amino acid residue from the aglycon structure by Edman degradation. [^{19}F]oritavancin is known to be 1000-fold more potent than vancomycin against a vast majority of Gram-positive bacteria. This enhanced binding of [^{19}F]oritavancin has been shown, from solid-state NMR study, to be due to the presence of a secondary-binding site. As a result of this secondary-binding site, desleucyl [^{19}F]oritavancin is known to retain its potency against Gram-positive bacteria, whereas desleucylvancomycin is devoid of any antimicrobial activity. To reveal the enhanced binding of [^{19}F]oritavancin, MD simulation model structures of [^{19}F]oritavancin, chloroeremomycin, and vancomycin complexed with PG referred to as Ori-PG, CEremo-PG, and Vanco-PG respectively, as well as their corresponding desleucyl analogues, Des-Ori-PG, Des-CEremo-PG, and Des-Vanco-PG,

were made and used for the simulation studies. Our results show that the ranking of the stability of the (desleucyl)glycopeptide-PG complexes using the free energy of binding values agrees well with the ranking of their stability from the experimental MIC values. Ori-PG complex was shown to be the most stable of all the complexes studied. The average number of hydrogen bonds calculated shows that the enhanced binding of [^{19}F]oritavancin over the other complexes is not due to an increase in the electrostatic hydrogen bonding interactions, as [^{19}F]oritavancin showed a similar or comparatively lower average number of hydrogen bonding. A decomposition of the binding energy reveals an increase in both electrostatic and van der Waals interactions for [^{19}F]oritavancin compared to the other complexes. The rmsd distribution analyses showed that the stabilities of Ori-PG and Des-Ori-PG are higher than that of CEremo-PG, Des-CEremo-PG, Vanco-PG, and Des-Vanco-PG, based on the lower flexibility in their binding distribution. From the COM pulling simulation, the force-time plot was also used to confirm an increase in the attractive pull of the PG by [^{19}F]oritavancin and Desleucyl[^{19}F]oritavancin when compared to the other complexes. Overall, our MD simulations confirm the presence of a secondary-binding site in Ori-PG and Des-Ori-PG, which is mainly responsible for their enhanced stability of binding compared to the other (desleucyl)glycopeptide-PG complexes modeled. This insight can be useful in the modification of existing glycopeptides to improve their binding efficacy or the design of novel glycopeptides for improved antimicrobial activities against pathogenic Gram-positive bacteria.

5.6 Computational Methods

5.6.1 MD Simulation

The initial structure of [^{19}F]oritavancin complexed with the PG-repeat unit (Ori-PG) was based on a computational model reported in a previous study[155]. The Ori-PG complex was modified based on the solid-state NMR structure[78, 156] with GaussView 6.11 and optimized with a gaussian 16 program package using density functional (DFT) calculations at the B3LYP/6-311G (d,p) level of theory. The energy minimized structure obtained was modified to give the other complexes used in the simulation. The CEremo-PG complex, which represents chloroeremomycin complexed to PG-repeat unit, is the Ori-PG complex modified by removing the biphenyl moiety attached to the vancosamine sugar at the 4th residue of the heptapeptide core. The Vanco-PG, representing a complex of vancomycin and the PG-repeat unit, is obtained by modifying the Ori-PG complex through the removal of the biphenyl moiety on the vancosamine sugar at the 4th amino acid residue and the 4-epi-vancosamine attached to the 6th amino acid of the heptapeptide core. For each of the complexes, the desleucyl-glycopeptide-PG analogues are derived by removing the first amino acid residue of the aglycon, N-methylleucine. The initial stream file for the topology was generated using the CHARMM General Force field (CGenFF) through the online ParamChem/CGenFF-4.0 server[33] (https://cgenff.paramchem.org/). This was validated to ensure the reliability of the parameters and partial charges obtained.

Four independent simulations were carried out for each complex under periodic boundary conditions using GROMACS version 2018.3[35]. All the systems were solvated with transferable intermolecular potential with 3 points (TIP3P) explicit water molecules in a rhombic dodecahedral box, with the complex centered and placed at least 1.0 nm from

the box edge. Sodium and Chlorine ions were added as charge-balancing ions in physiological conditions. The simulation boxes were subjected to a maximum of 50,000 steps of the steepest descent energy minimization to guarantee the maximum force acting on each atom is below 1000 kJ/mol/nm. Thereafter, constant volume and temperature (NVT) equilibration was performed on the energy minimized system for 200 ps at a time-step of 1 fs using the leap-frog integrator and modified Berendsen thermostat for equilibrating the system to a temperature of 300 K. Initial velocities were assigned from a Maxwellian distribution. The NVT equilibration was followed by a constant pressure and temperature (NPT) equilibration for 10 ns with 2 fs time-step to stabilize the system's pressure at 1 bar using Parrinello-Rahman barostats with a compressibility of 4.5 x 10^{-5} bar^{-1}. The isotropic position scaling protocol was used to control the pressure. Long-range electrostatic interactions were modeled using the particle mesh Ewald (PME) model, and the length of all covalent bonds constrained with the linear constraint solver (LINCS) algorithm[132]. The molecular dynamics simulation was performed for 30 ns at a time-step of 2 fs and the output saved after every 10 ps for each simulation system. A 12 Å cut-off was used for short-range interactions. During the MD simulation, atomic pair distance constraints were applied based on solid-state NMR experiments[155].

5.6.2 Root-Mean-Square Deviation (RMSD)

The rmsd was used to quantitatively measure the conformational difference between the structures of each complex along the simulation trajectories and a stable reference structure of the complex, after NVT and NPT equilibration, to estimate the structural similarities. This was achieved by least-squares fitting of the dynamic structure to the reference structure using GROMACS built-in functions. The rmsd equation for a

molecular structure represented by a cartesian coordinate vector $\mathbf{r}_i$ $(i = 1 - N)$ of N atoms is illustrated by

$$\text{RMSD} = [\tfrac{1}{\text{M}} \sum_{i=1}^{N} m_i(\mathbf{r}_i^t - \mathbf{r}_i^0)^2]^{1/2} \quad (5.1)$$

where $\text{M} = \sum_{i=1}^{N} m_i$, $\mathbf{r}_i^t$ is the position of atom i along the trajectory at time t, $\mathbf{r}_i^0$ is the position of atom i for the stable reference structure, and m_i is the mass of atom i. The rmsd values for each of the glycopeptide-PG complex were obtained by comparing their configuration at $t = 0$ with the complex dynamic structure along the trajectories during MD simulation.

5.6.3 Hydrogen Bond Analysis

The stability of the moderate hydrogen bonds formed between the glycopeptide and PG-repeat unit in each complex along the trajectory of the MD simulation was monitored using the hydrogen bond analysis. The hydrogen bond profiles for the various complexes were obtained using the g_hbond utility in GROMACS, considering all possible hydrogen bond donors and acceptors. The criteria for the hydrogen bond formation are based on the donor-acceptor distance of 3.0 Å and the angle cut-off of 20^o within a linear configuration. The average number of hydrogen bonds formed in a particular complex during the simulation can be comparable to the stability of the complex along the simulation trajectories.

5.6.4 Binding Free Energy Calculations

The binding free energy of the different glycopeptide-PG complexes considered in the MD simulation study was obtained using both an end-point and pathway methods of binding energy computation. Specifically, we utilized the molecular mechanics Poisson-

Boltzmann surface area (MM/PBSA) for the end-point binding energy determination and the umbrella sampling method for the pathway binding energy computation.

5.6.4.1 Molecular mechanics Poisson-Boltzmann surface area (MM/PBSA) binding energy determination. In the MM/PBSA method, the free energy of binding, ΔG_{bind}, of the PG

to the glycopeptide (gly) to form a complex is given by the equation

$$\Delta G_{bind} = G_{complex} - G_{gly} - G_{PG} \tag{5.2}$$

The ΔG_{bind} can be decomposed into the contributions from the different interactions within the system as shown below

$$\Delta G_{bind} = \Delta E_{MM} + \Delta G_{sol} - T\Delta S \tag{5.3}$$

in which

$$\Delta E_{MM} = \Delta E_{int} + \Delta E_{elec} + \Delta E_{vdW} \tag{5.4}$$

$$\Delta G_{sol} = \Delta G_{polar} + \Delta G_{nonpolar} \tag{5.5}$$

where ΔE_{MM} is the change for the gas phase molecular mechanics (MM) energy, comprised of the changes in internal energies, ΔE_{int}, (bond, angle, and dihedral energies), electrostatic energies ΔE_{elec}, and the van der Waals energies ΔE_{vdW}; ΔG_{sol} is the sum of the polar (electrostatic) solvation energy, ΔG_{PB}, and the nonpolar contribution, $\Delta G_{nonpolar}$, between the solute and the continuum solvent. The polar contribution is calculated with the Poisson-Boltzmann model, while the nonpolar part is estimated with the solvent-accessible volume (SAV) model.

5.6.4.2 Umbrella sampling binding energy determination. Umbrella sampling is a useful tool in analyzing macromolecular interactions, and the binding energy from

umbrella sampling simulations is obtained from the potential of mean force (PMF)[50, 58]. The umbrella sampling simulations of the glycopeptide-PG complex were performed following a center-of-mass (COM) pulling simulation to generate a series of initial configurations. Each of these configurations generated corresponds to a point in space where the PG is harmonically restrained at increasing COM distance from the glycopeptide through an umbrella biasing potential. The biasing force is illustrated with the equation

$$F = \frac{k}{2}[\zeta - (\zeta_0 + vt)] \tag{5.6}$$

where v is the pulling velocity, t is time, and k is the force constant. ζ_0 is the reference coordinate point along the pulling path, and ζ is the coordinate point at a given time.

After the explicit solvent MD simulations reported in section 5.6.1, structures from the end of the trajectories were used for the pulling simulation. The glycopeptide complex was placed in a rectangular box with sufficient space for the PG to move along the z-axis during the pulling simulation and to satisfy the minimum image convention. Following solvation with TIP3P water and the addition of charge-balancing ions, the energy of the system was minimized with the steepest descent algorithm. Afterward, a 100 ps NPT equilibration at 2 fs time-step was performed using Berendsen weak coupling to maintain the pressure isotropically at 1.0 bar, with the complex heavy atoms position restrained. In the course of the pulling simulation, the restraints on the PG were removed while the glycopeptide remained as a stationary reference. The PG was pulled away from the glycopeptide along the z-axis for 500 ps at 2 fs time-step using a spring constant of 1000 kJ mol-1 nm-2 by applying a pulling rate of 0.01 nm ps-1. This pull rate was sufficient to maintain the integrity of the system and produce reliable results. At the end of the pulling simulation, a center-of-mass (COM) distance of about 5.5 nm was achieved. Snapshots

from the pulling simulation trajectories were taken as starting configurations for the umbrella sampling windows. A non-uniform window spacing ranging from 0.02 nm to 0.1 nm was used to ensure detailed sampling of configurations along the reaction coordinate and sufficient overlap of neighboring windows to obtain a continuous energy function. In total, about 50 windows were sampled on average. For the umbrella sampling, a 10 ns MD simulation was performed in each of the windows, resulting in a cumulative simulation time of 500 ns for one trial of each complex. The umbrella sampling simulations were carried out with the GROMACS version 2018.3. The WHAM[60] method was used to extract the equilibrium data (PMF) from the nonequilibrium umbrella sampling windows. For each (desleucyl)glycopeptide-PG complex, about three umbrella sampling simulation trials were performed to estimate the error in the free energy of binding.

CHAPTER SIX

Conclusion

In this dissertation, MD simulations have been applied to provide atomic details of the interactions between glycopeptide antibiotics and the PG of *S. aureus*. Chapter One is an introduction that includes the motivation for this work and essential information on cell-wall targeting antibiotics and *S. aureus* cell-wall biosynthesis and composition. The details on MD simulation methods and the data analyses performed after the simulations are given in Chapter Two. Chapter Three investigates the role of the first amino acid residue of vancomycin, N-methylleucine, in the binding of vancomycin to a PG pentapeptide stem of *S. aureus*. Although N-methylleucine is not directly involved in the binding of vancomycin with the PG dipeptide, its removal by Edman degradation of vancomycin yields desleucylvancomycin, devoid of any antimicrobial activities. To investigate the loss of binding of desleucylvancomycin, MD simulations of vancomycin and three N-terminus-modified vancomycin derivatives, including desleucylvancomycin, vancomycin$_{NtoC}$, and vancomycin$_{Sar}$, binding to a PG repeat unit of L-Ala-D-iso-Gln-L-Lys(Gly$_5$)-D-Ala-D-Ala were carried out. These binding interactions were characterized using root-mean-square deviations, 2D contour analysis, hydrogen bonding analysis, and the binding free energy estimation. Our results revealed that the leucine sidechain substitution by sarcosine in vancomycin$_{Sar}$ significantly reduces the hydrophobicity of the vancomycin primary binding pocket, and the stability of the glycopeptide-PG complex gradually transitions from vancomycin, vancomycin$_{NtoC}$, and vancomycin$_{Sar}$ to desleucylvancomycin towards the unbound state.

Chapter Four investigates the atomic interactions in the vancomycin binding site to gain insight into the binding of vancomycin to PG terminating in D-Ala-D-Ala (dipeptide) and D-Ala-D-Lac (depsipeptide). Five stable hydrogen bonds typically stabilize the binding of vancomycin to the PG dipeptide. The modification of the PG terminal from D-Ala-D-Ala to D-Ala-D-Lac results in a 1000-fold decrease in vancomycin binding affinity. The replacement of the D-Ala-D-Ala by D-Ala-D-Lac substitutes an amide with an ester bond resulting in the replacement of a single hydrogen bond in the binding of vancomycin to PG by electrostatic repulsion between the carbonyl oxygen atom at the 4th position of vancomycin and the ester oxygen atom on the D-Ala-D-Lac. The role of the asparagine sidechain at the 3rd residue of vancomycin in the binding of vancomycin to D-Ala-D-Ala and D-Ala-D-Lac was investigated by MD simulation of the dipeptide and depsipeptide binding to vancomycin and its aspartic-acid-substituted analogue, V_D. Our findings reveal that, even though the residue 3 sidechain of vancomycin is not directly involved in hydrogen bond formation for binding of PG, the substitution of asparagine for aspartate enhanced the binding of vancomycin to depsipeptide by altering the aglycon conformation, which results in the minimization of the repulsive interaction between the carbonyl oxygen atom at vancomycin residue 4 position and the ester oxygen atom on depsipeptide. This discovery provides great insight for the modification of vancomycin to improve its binding to D-Ala-D-Lac-terminated PG.

Chapter Five is a report on the investigation of the secondary-binding site in disaccharide-modified glycopeptide oritavancin. Oritavancin, a glycopeptide antibiotic, is a thousand times more potent than vancomycin. The removal of the first amino acid residue of oritavancin by Edman degradation results in desleucyloritavancin, which still retains its

potency against a vast majority of Gram-positive bacterial pathogens. In contrast, the Edman degradation product of vancomycin, desleucylvancomycin, is devoid of any antimicrobial activities. This implies that oritavancin remains potent despite damage to its primary-binding site in desleucyloritavancin. Solid-state NMR results have revealed the presence of a secondary-binding site at the disaccharide-modified hydrophobic sidechain of oritavancin that inhibits the transpeptidase activities of *S. aureus* through binding with the pentaglycyl bridge segment of PG. Herein, using explicit MD simulations, steered MD simulations, and umbrella sampling, we showed atomic-level details of the interactions of the secondary-binding site of oritavancin with the PG-repeat unit of *S. aureus*. The interactions of oritavancin with the acyl-L-Lys(Gly_5)-D-Ala-D-Ala of PG were characterized through comparison with the interactions of the PG with chloroeremomycin, vancomycin, and the desleucyl analogues of the glycopeptides. Our results show a direct correlation with the ranking of the stabilities of the glycopeptide- and desleucylglycopeptide-PG complexes based on their experimental minimum inhibitory concentrations (MIC). We also revealed that the improvements in the binding of oritavancin and desleucyloritavancin to PG over that of the other (desleucyl)glycopeptides are mainly due to hydrophobic effect, electrostatic and van der Waals interactions, and not based on the hydrogen bonding interactions.

In general, this work provides atomic-level details of various interactions between (desleucyl)glycopeptide antibiotics and bacterial cell wall structures. The results from our study are helpful towards providing insight into the modification of glycopeptides to improve their binding with the PG of *S. aureus* or the development of novel antibiotics to fight against the inevitable emergence of antibiotic resistance in pathogens. There is a need

for more work to be done to gain insight into other parts of the interactions between glycopeptides and bacterial cell wall structures not covered in this dissertation. Further research can be performed on the secondary-binding site of oritavancin by investigating the effect of hydrophobic sidechain length on the binding of oritavancin to PG. Also, the biphenyl moiety can be replaced with carborane of different lengths to explore how it compares with oritavancin binding as a function of hydrophobic sidechain length. We hypothesize that the binding of oritavancin at the secondary-binding site is governed mainly by the hydrophobic effect, and this investigation will give more insight into hydrophobicity at the secondary-binding site. Another interesting simulation that can be performed is the binding of C-terminus modified eremomycin with an oligomeric PG-lattice structure. Previous experimental result has shown that the carboxyl terminus of eremomycin facilitates binding to the non-D-Ala-D-Ala segment of the peptidoglycan pentapeptide stem. We hypothesize that the C-terminus interacts with the L-Ala segment of the PG-stem structure and the adjacent PG's disaccharide. In addition, there is also a need for improvement in forcefield parameters to capture better the effect of polarization in the various glycopeptide-PG interactions studied. *Ab initio* MD can be used to obtain forcefield parameters for glycopeptide-PG systems whose forces have not been parametrized.

APPENDICES

APPENDIX A

Supplemental Information for Chapter Four

Table S4.1: Cartesian coordinates for V_N-Ala complex

Atoms	X	Y	Z
H	-3.23000000	-5.21300000	2.24900000
H	-3.60800000	-6.88700000	2.65600000
H	-4.91100000	-5.74000000	2.34600000
H	-4.57500000	-7.21300000	0.34800000
H	-3.72600000	-4.93200000	-0.97400000
O	-1.58700000	-6.87900000	0.97500000
O	-2.27900000	-7.09700000	-1.06100000
C	-2.47200000	-6.82700000	0.12400000
C	-3.90900000	-6.04000000	2.04000000
C	-3.87900000	-6.40700000	0.55700000
N	-4.31200000	-5.28600000	-0.24900000
H	-6.42800000	-4.83800000	-2.63200000
H	-4.71400000	-4.42600000	-2.66400000
H	-5.92000000	-3.22400000	-3.12400000
H	-5.05800000	-2.78500000	-0.79100000
H	-7.85700000	-3.58400000	-0.33300000
O	-6.32700000	-5.10500000	0.81600000
C	-5.52100000	-4.74000000	-0.03100000
C	-5.70900000	-4.04200000	-2.43700000
C	-5.79600000	-3.57200000	-0.97900000
N	-7.12700000	-3.03100000	-0.73500000
O	-6.45100000	-1.05100000	-1.59000000
C	-7.32300000	-1.75300000	-1.10100000
C	-8.74500000	-1.21200000	-0.86300000
H	-8.92900000	-1.14500000	0.18900000
H	-8.83600000	-0.24100000	-1.30300000
H	-9.45800000	-1.87400000	-1.30800000
N	-3.38600000	-11.86300000	-0.17800000
C	-2.78200000	-12.15600000	1.11600000
C	-2.79600000	-10.65900000	-0.75200000
C	-1.28700000	-10.83300000	-0.93600000
O	-0.82800000	-11.67700000	-1.69500000
C	-3.40500000	-10.31500000	-2.11000000
C	-4.92700000	-10.19300000	-2.05900000
C	-5.35800000	-9.01500000	-1.18700000

Atoms	X	Y	Z
C	-5.49100000	-10.04500000	-3.47300000
H	-3.22600000	-12.66500000	-0.82200000
H	-3.23700000	-13.05800000	1.52500000
H	-1.71100000	-12.31000000	0.98200000
H	-2.95500000	-11.31600000	1.78800000
H	-2.97500000	-9.84200000	-0.05500000
H	-3.13300000	-11.09000000	-2.82700000
H	-2.97500000	-9.38300000	-2.47800000
H	-5.32500000	-11.10800000	-1.62000000
H	-5.00000000	-8.07400000	-1.60600000
H	-6.44400000	-8.95900000	-1.11800000
H	-4.96000000	-9.11200000	-0.17700000
H	-5.11300000	-9.14100000	-3.94900000
H	-5.21000000	-10.89600000	-4.09400000
H	-6.57900000	-9.98700000	-3.45300000
N	-0.54900000	-9.98300000	-0.19800000
C	0.89700000	-10.07300000	-0.31800000
C	1.42700000	-8.95900000	-1.24400000
O	2.44200000	-9.14200000	-1.90600000
C	1.56200000	-10.09900000	1.06700000
O	1.16300000	-11.25100000	1.76500000
C	1.17700000	-8.89300000	1.85900000
C	2.03000000	-7.73400000	1.85500000
C	-0.07200000	-8.86700000	2.58200000
C	1.59200000	-6.53800000	2.51300000
Cl	2.60200000	-5.13500000	2.49000000
C	-0.49900000	-7.66000000	3.24400000
C	0.31700000	-6.47800000	3.16700000
O	-0.15600000	-5.24000000	3.60000000
H	-0.98100000	-9.31000000	0.40200000
H	1.09400000	-11.02200000	-0.81900000
H	2.64700000	-10.13300000	0.96600000
H	1.60800000	-11.23000000	2.60200000
H	2.98000000	-7.75800000	1.34300000
H	-0.70000000	-9.74500000	2.60800000
H	-1.44700000	-7.62900000	3.76100000
N	0.71300000	-7.80600000	-1.28100000
C	1.21300000	-6.79600000	-2.20600000
C	1.10600000	-5.35800000	-1.67600000
O	2.09600000	-4.72200000	-1.33100000
C	0.42700000	-6.89500000	-3.51300000
C	0.42200000	-8.33600000	-4.02500000
O	1.44000000	-8.88700000	-4.42600000
N	-0.80000000	-8.89800000	-3.98200000
H	-0.12300000	-7.64400000	-0.75700000
H	2.25900000	-7.02800000	-2.39600000

Atoms	X	Y	Z
H	-0.60500000	-6.57900000	-3.35300000
H	0.85400000	-6.24600000	-4.27800000
H	-1.58300000	-8.37900000	-3.64100000
H	-0.95200000	-9.83900000	-4.28700000
N	-0.15300000	-4.88100000	-1.67300000
C	-0.35500000	-3.50700000	-1.23100000
C	-1.51400000	-2.86100000	-2.00900000
O	-2.51300000	-3.48600000	-2.34300000
C	-0.59800000	-3.35400000	0.25800000
C	-1.22200000	-2.17600000	0.78900000
C	-1.45800000	-1.98500000	2.21400000
C	-1.07500000	-3.06100000	3.10100000
O	-1.33300000	-3.00100000	4.45700000
C	-0.45300000	-4.26500000	2.61100000
C	-0.21300000	-4.37800000	1.17600000
H	-0.91100000	-5.49100000	-1.90800000
H	0.56600000	-2.98300000	-1.48700000
H	-1.56400000	-1.42100000	0.09400000
H	0.26000000	-5.26800000	0.79200000
N	-1.28500000	-1.55600000	-2.25400000
C	-2.30700000	-0.76600000	-2.90700000
C	-1.92000000	0.72200000	-2.94900000
O	-0.75700000	1.02800000	-3.16900000
C	-2.74700000	-1.17900000	-4.27700000
C	-4.13800000	-1.45900000	-4.44400000
C	-4.71500000	-1.70000000	-5.71300000
C	-3.87100000	-1.71000000	-6.86900000
O	-4.41200000	-1.96300000	-8.11300000
C	-2.45300000	-1.45100000	-6.74100000
C	-1.89200000	-1.18000000	-5.43800000
H	-0.42800000	-1.13200000	-1.96200000
H	-3.13300000	-0.91600000	-2.22300000
H	-4.77600000	-1.45800000	-3.57400000
H	-5.34500000	-2.11000000	-8.02700000
H	-1.81900000	-1.45700000	-7.61600000
H	-0.83900000	-0.96300000	-5.33600000
N	-2.89100000	1.65500000	-2.74800000
C	-4.31200000	1.44300000	-2.47900000
O	-2.02900000	-0.82000000	2.79700000
C	-2.25800000	1.37200000	1.64300000
C	-3.93600000	-0.42600000	1.33200000
C	-2.74500000	0.05400000	1.96600000
C	-4.07000000	1.62700000	-0.06400000
C	-2.91700000	2.15900000	0.62500000
C	-4.60100000	0.34900000	0.32800000
C	-4.69400000	2.29200000	-1.26400000

Atoms	X	Y	Z
Cl	-4.55800000	-1.98400000	1.75500000
O	-5.04200000	2.67300000	-4.44900000
C	-5.14900000	1.67100000	-3.75100000
O	-4.25700000	3.62400000	-1.41700000
H	-2.59000000	2.60900000	-2.78300000
H	-4.46300000	0.40400000	-2.21400000
H	-1.38000000	1.74800000	2.14200000
H	-2.53100000	3.13400000	0.36200000
H	-5.48000000	-0.03900000	-0.15500000
H	-5.77600000	2.26800000	-1.15800000
H	-4.66800000	4.25600000	-0.68600000
N	-5.97700000	0.62600000	-3.97700000
O	-5.58200000	-4.21800000	-6.36900000
C	-6.55800000	-3.28200000	-6.09200000
C	-6.17900000	-1.94500000	-5.77200000
C	-7.93600000	-3.66900000	-6.11900000
C	-8.95700000	-2.70500000	-5.83200000
O	-10.28700000	-3.07400000	-5.85400000
C	-8.58600000	-1.35600000	-5.51500000
C	-7.19500000	-0.94800000	-5.47600000
C	-6.83800000	0.50800000	-5.12300000
C	-8.05900000	1.40100000	-4.81900000
O	-8.62700000	1.96300000	-5.75400000
O	-8.41400000	1.52000000	-3.64100000
H	-5.97500000	-0.12600000	-3.32400000
H	-6.23600000	0.93300000	-5.92100000
H	-4.72800000	-3.81200000	-6.30700000
H	-8.18500000	-4.69700000	-6.32800000
H	-10.82600000	-2.32400000	-5.64100000
H	-9.35500000	-0.63600000	-5.27800000
C	-1.08900000	-1.98300000	6.56800000
C	-0.26500000	-1.02300000	7.41900000
C	1.22200000	-1.28100000	7.20500000
C	1.55700000	-1.31200000	5.71200000
C	3.02200000	-1.70800000	5.49800000
C	-0.63600000	-1.96700000	5.10700000
O	-2.45400000	-1.64400000	6.65600000
O	-0.59500000	-1.22600000	8.77000000
O	1.96400000	-0.24700000	7.80100000
O	0.74300000	-2.26000000	5.05700000
O	3.28900000	-2.93400000	6.13000000
H	-0.95700000	-2.99500000	6.95000000
H	-0.50300000	0.00700000	7.16200000
H	1.51400000	-2.22200000	7.67100000
H	1.36100000	-0.32400000	5.29100000
H	3.69200000	-0.95900000	5.91800000

Atoms	X	Y	Z
H	3.26200000	-1.82400000	4.44000000
H	-0.83600000	-1.00800000	4.63000000
H	-1.25500000	-0.58100000	8.98900000
H	2.20300000	-0.54700000	8.66700000
H	4.20300000	-3.12900000	5.97100000
C	-3.12500000	-2.41200000	7.62800000
C	-4.56400000	-1.92000000	7.81700000
C	-5.43700000	-2.19300000	6.59100000
N	-6.83600000	-1.97400000	6.94000000
C	-5.06700000	-1.24400000	5.45100000
C	-5.24800000	-3.64400000	6.15300000
O	-5.93000000	-3.86500000	4.94400000
C	-3.76200000	-3.94800000	5.98100000
O	-3.13200000	-3.76200000	7.22600000
C	-3.51200000	-5.37600000	5.49300000
H	-2.58600000	-2.32500000	8.57100000
H	-4.99600000	-2.43400000	8.67500000
H	-4.57200000	-0.85600000	8.05500000
H	-7.41500000	-2.57800000	6.39200000
H	-4.02800000	-1.37600000	5.15000000
H	-5.69400000	-1.42500000	4.57700000
H	-5.20300000	-0.20600000	5.75200000
H	-5.67300000	-4.31600000	6.89800000
H	-6.78300000	-4.21200000	5.17200000
H	-3.34500000	-3.24500000	5.26400000
H	-3.98700000	-5.54500000	4.52700000
H	-2.44500000	-5.56700000	5.38300000
H	-3.91400000	-6.10300000	6.19800000
H	-6.97200000	-2.17200000	7.91100000

Table S4.2: Cartesian coordinates for V_N-Lac complex

Atoms	X	Y	Z
H	-3.23000000	-5.21300000	2.24900000
H	-3.60800000	-6.88700000	2.65600000
H	-4.91100000	-5.74000000	2.34600000
H	-4.57500000	-7.21300000	0.34800000
O	-1.58700000	-6.87900000	0.97500000
O	-2.27900000	-7.09700000	-1.06100000
C	-2.47200000	-6.82700000	0.12400000
C	-3.90900000	-6.04000000	2.04000000
C	-3.87900000	-6.40700000	0.55700000
O	-4.31200000	-5.28600000	-0.24900000

Atoms	X	Y	Z
H	-6.42800000	-4.83800000	-2.63200000
H	-4.71400000	-4.42600000	-2.66400000
H	-5.92000000	-3.22400000	-3.12400000
H	-5.05800000	-2.78500000	-0.79100000
H	-7.85700000	-3.58400000	-0.33300000
O	-6.32700000	-5.10500000	0.81600000
C	-5.52100000	-4.74000000	-0.03100000
C	-5.70900000	-4.04200000	-2.43700000
C	-5.79600000	-3.57200000	-0.97900000
N	-7.12700000	-3.03100000	-0.73500000
O	-6.45100000	-1.05100000	-1.59000000
C	-7.32300000	-1.75300000	-1.10100000
C	-8.74500000	-1.21200000	-0.86300000
H	-8.92900000	-1.14500000	0.18900000
H	-8.83600000	-0.24100000	-1.30300000
H	-9.45800000	-1.87400000	-1.30800000
N	-3.38600000	-11.86300000	-0.17800000
C	-2.78200000	-12.15600000	1.11600000
C	-2.79600000	-10.65900000	-0.75200000
C	-1.28700000	-10.83300000	-0.93600000
O	-0.82800000	-11.67700000	-1.69500000
C	-3.40500000	-10.31500000	-2.11000000
C	-4.92700000	-10.19300000	-2.05900000
C	-5.35800000	-9.01500000	-1.18700000
C	-5.49100000	-10.04500000	-3.47300000
H	-3.22600000	-12.66500000	-0.82200000
H	-3.23700000	-13.05800000	1.52500000
H	-1.71100000	-12.31000000	0.98200000
H	-2.95500000	-11.31600000	1.78800000
H	-2.97500000	-9.84200000	-0.05500000
H	-3.13300000	-11.09000000	-2.82700000
H	-2.97500000	-9.38300000	-2.47800000
H	-5.32500000	-11.10800000	-1.62000000
H	-5.00000000	-8.07400000	-1.60600000
H	-6.44400000	-8.95900000	-1.11800000
H	-4.96000000	-9.11200000	-0.17700000
H	-5.11300000	-9.14100000	-3.94900000
H	-5.21000000	-10.89600000	-4.09400000
H	-6.57900000	-9.98700000	-3.45300000
N	-0.54900000	-9.98300000	-0.19800000
C	0.89700000	-10.07300000	-0.31800000
C	1.42700000	-8.95900000	-1.24400000
O	2.44200000	-9.14200000	-1.90600000
C	1.56200000	-10.09900000	1.06700000
O	1.16300000	-11.25100000	1.76500000
C	1.17700000	-8.89300000	1.85900000

Atoms	X	Y	Z
C	2.03000000	-7.73400000	1.85500000
C	-0.07200000	-8.86700000	2.58200000
C	1.59200000	-6.53800000	2.51300000
Cl	2.60200000	-5.13500000	2.49000000
C	-0.49900000	-7.66000000	3.24400000
C	0.31700000	-6.47800000	3.16700000
O	-0.15600000	-5.24000000	3.60000000
H	-0.98100000	-9.31000000	0.40200000
H	1.09400000	-11.02200000	-0.81900000
H	2.64700000	-10.13300000	0.96600000
H	1.60800000	-11.23000000	2.60200000
H	2.98000000	-7.75800000	1.34300000
H	-0.70000000	-9.74500000	2.60800000
H	-1.44700000	-7.62900000	3.76100000
N	0.71300000	-7.80600000	-1.28100000
C	1.21300000	-6.79600000	-2.20600000
C	1.10600000	-5.35800000	-1.67600000
O	2.09600000	-4.72200000	-1.33100000
C	0.42700000	-6.89500000	-3.51300000
C	0.42200000	-8.33600000	-4.02500000
O	1.44000000	-8.88700000	-4.42600000
N	-0.80000000	-8.89800000	-3.98200000
H	-0.12300000	-7.64400000	-0.75700000
H	2.25900000	-7.02800000	-2.39600000
H	-0.60500000	-6.57900000	-3.35300000
H	0.85400000	-6.24600000	-4.27800000
H	-1.58300000	-8.37900000	-3.64100000
H	-0.95200000	-9.83900000	-4.28700000
N	-0.15300000	-4.88100000	-1.67300000
C	-0.35500000	-3.50700000	-1.23100000
C	-1.51400000	-2.86100000	-2.00900000
O	-2.51300000	-3.48600000	-2.34300000
C	-0.59800000	-3.35400000	0.25800000
C	-1.22200000	-2.17600000	0.78900000
C	-1.45800000	-1.98500000	2.21400000
C	-1.07500000	-3.06100000	3.10100000
O	-1.33300000	-3.00100000	4.45700000
C	-0.45300000	-4.26500000	2.61100000
C	-0.21300000	-4.37800000	1.17600000
H	-0.91100000	-5.49100000	-1.90800000
H	0.56600000	-2.98300000	-1.48700000
H	-1.56400000	-1.42100000	0.09400000
H	0.26000000	-5.26800000	0.79200000
N	-1.28500000	-1.55600000	-2.25400000
C	-2.30700000	-0.76600000	-2.90700000
C	-1.92000000	0.72200000	-2.94900000

Atoms	X	Y	Z
O	-0.75700000	1.02800000	-3.16900000
C	-2.74700000	-1.17900000	-4.27700000
C	-4.13800000	-1.45900000	-4.44400000
C	-4.71500000	-1.70000000	-5.71300000
C	-3.87100000	-1.71000000	-6.86900000
O	-4.41200000	-1.96300000	-8.11300000
C	-2.45300000	-1.45100000	-6.74100000
C	-1.89200000	-1.18000000	-5.43800000
H	-0.42800000	-1.13200000	-1.96200000
H	-3.13300000	-0.91600000	-2.22300000
H	-4.77600000	-1.45800000	-3.57400000
H	-5.34500000	-2.11000000	-8.02700000
H	-1.81900000	-1.45700000	-7.61600000
H	-0.83900000	-0.96300000	-5.33600000
N	-2.89100000	1.65500000	-2.74800000
C	-4.31200000	1.44300000	-2.47900000
O	-2.02900000	-0.82000000	2.79700000
C	-2.25800000	1.37200000	1.64300000
C	-3.93600000	-0.42600000	1.33200000
C	-2.74500000	0.05400000	1.96600000
C	-4.07000000	1.62700000	-0.06400000
C	-2.91700000	2.15900000	0.62500000
C	-4.60100000	0.34900000	0.32800000
C	-4.69400000	2.29200000	-1.26400000
Cl	-4.55800000	-1.98400000	1.75500000
O	-5.04200000	2.67300000	-4.44900000
C	-5.14900000	1.67100000	-3.75100000
O	-4.25700000	3.62400000	-1.41700000
H	-2.59000000	2.60900000	-2.78300000
H	-4.46300000	0.40400000	-2.21400000
H	-1.38000000	1.74800000	2.14200000
H	-2.53100000	3.13400000	0.36200000
H	-5.48000000	-0.03900000	-0.15500000
H	-5.77600000	2.26800000	-1.15800000
H	-4.66800000	4.25600000	-0.68600000
N	-5.97700000	0.62600000	-3.97700000
O	-5.58200000	-4.21800000	-6.36900000
C	-6.55800000	-3.28200000	-6.09200000
C	-6.17900000	-1.94500000	-5.77200000
C	-7.93600000	-3.66900000	-6.11900000
C	-8.95700000	-2.70500000	-5.83200000
O	-10.28700000	-3.07400000	-5.85400000
C	-8.58600000	-1.35600000	-5.51500000
C	-7.19500000	-0.94800000	-5.47600000
C	-6.83800000	0.50800000	-5.12300000
C	-8.05900000	1.40100000	-4.81900000

Atoms	X	Y	Z
O	-8.62700000	1.96300000	-5.75400000
O	-8.41400000	1.52000000	-3.64100000
H	-5.97500000	-0.12600000	-3.32400000
H	-6.23600000	0.93300000	-5.92100000
H	-4.72800000	-3.81200000	-6.30700000
H	-8.18500000	-4.69700000	-6.32800000
H	-10.82600000	-2.32400000	-5.641000000
H	-9.35500000	-0.63600000	-5.27800000
C	-1.08900000	-1.98300000	6.56800000
C	-0.26500000	-1.02300000	7.41900000
C	1.22200000	-1.28100000	7.20500000
C	1.55700000	-1.31200000	5.71200000
C	3.02200000	-1.70800000	5.49800000
C	-0.63600000	-1.96700000	5.10700000
O	-2.45400000	-1.64400000	6.65600000
O	-0.59500000	-1.22600000	8.77000000
O	1.96400000	-0.24700000	7.80100000
O	0.74300000	-2.26000000	5.05700000
O	3.28900000	-2.93400000	6.13000000
H	-0.95700000	-2.99500000	6.95000000
H	-0.50300000	0.00700000	7.16200000
H	1.51400000	-2.22200000	7.67100000
H	1.36100000	-0.32400000	5.29100000
H	3.69200000	-0.95900000	5.91800000
H	3.26200000	-1.82400000	4.44000000
H	-0.83600000	-1.00800000	4.63000000
H	-1.25500000	-0.58100000	8.98900000
H	2.20300000	-0.54700000	8.66700000
H	4.20300000	-3.12900000	5.97100000
C	-3.12500000	-2.41200000	7.62800000
C	-4.56400000	-1.92000000	7.81700000
C	-5.43700000	-2.19300000	6.59100000
N	-6.83600000	-1.97400000	6.94000000
C	-5.06700000	-1.24400000	5.45100000
C	-5.24800000	-3.64400000	6.15300000
O	-5.93000000	-3.86500000	4.94400000
C	-3.76200000	-3.94800000	5.98100000
O	-3.13200000	-3.76200000	7.22600000
C	-3.51200000	-5.37600000	5.49300000
H	-2.58600000	-2.32500000	8.57100000
H	-4.99600000	-2.43400000	8.67500000
H	-4.57200000	-0.85600000	8.05500000
H	-7.41500000	-2.57800000	6.39200000
H	-4.02800000	-1.37600000	5.15000000
H	-5.69400000	-1.42500000	4.57700000
H	-5.20300000	-0.20600000	5.75200000

Atoms	X	Y	Z
H	-5.67300000	-4.31600000	6.89800000
H	-6.78300000	-4.21200000	5.17200000
H	-3.34500000	-3.24500000	5.26400000
H	-3.98700000	-5.54500000	4.52700000
H	-2.44500000	-5.56700000	5.38300000
H	-3.91400000	-6.10300000	6.19800000
H	-6.97200000	-2.17200000	7.91100000

Table S4.3: Cartesian coordinates for V_D-Lac complex

Atoms	X	Y	Z
H	-3.23000000	-5.21300000	2.24900000
H	-3.60800000	-6.88700000	2.65600000
H	-4.91100000	-5.74000000	2.34600000
H	-4.57500000	-7.21300000	0.34800000
O	-1.58700000	-6.87900000	0.97500000
O	-2.27900000	-7.09700000	-1.06100000
C	-2.47200000	-6.82700000	0.12400000
C	-3.90900000	-6.04000000	2.04000000
C	-3.87900000	-6.40700000	0.55700000
O	-4.31200000	-5.28600000	-0.24900000
H	-6.42800000	-4.83800000	-2.63200000
H	-4.71400000	-4.42600000	-2.66400000
H	-5.92000000	-3.22400000	-3.12400000
H	-5.05800000	-2.78500000	-0.79100000
H	-7.85700000	-3.58400000	-0.33300000
O	-6.32700000	-5.10500000	0.81600000
C	-5.52100000	-4.74000000	-0.03100000
C	-5.70900000	-4.04200000	-2.43700000
C	-5.79600000	-3.57200000	-0.97900000
N	-7.12700000	-3.03100000	-0.73500000
O	-6.45100000	-1.05100000	-1.59000000
C	-7.32300000	-1.75300000	-1.10100000
C	-8.74500000	-1.21200000	-0.86300000
H	-8.92900000	-1.14500000	0.18900000
H	-8.83600000	-0.24100000	-1.30300000
H	-9.45800000	-1.87400000	-1.30800000
N	-3.38600000	-11.86300000	-0.17800000
C	-2.78200000	-12.15600000	1.11600000
C	-2.79600000	-10.65900000	-0.75200000
C	-1.28700000	-10.83300000	-0.93600000
O	-0.82800000	-11.67700000	-1.69500000
C	-3.40500000	-10.31500000	-2.11000000

Atoms	X	Y	Z
C	-4.92700000	-10.19300000	-2.05900000
C	-5.35800000	-9.01500000	-1.18700000
C	-5.49100000	-10.04500000	-3.47300000
H	-3.22600000	-12.66500000	-0.82200000
H	-3.23700000	-13.05800000	1.52500000
H	-1.71100000	-12.31000000	0.98200000
H	-2.95500000	-11.31600000	1.78800000
H	-2.97500000	-9.84200000	-0.05500000
H	-3.13300000	-11.09000000	-2.82700000
H	-2.97500000	-9.38300000	-2.47800000
H	-5.32500000	-11.10800000	-1.62000000
H	-5.00000000	-8.07400000	-1.60600000
H	-6.44400000	-8.95900000	-1.11800000
H	-4.96000000	-9.11200000	-0.17700000
H	-5.11300000	-9.14100000	-3.94900000
H	-5.21000000	-10.89600000	-4.09400000
H	-6.57900000	-9.98700000	-3.45300000
N	-0.54900000	-9.98300000	-0.19800000
C	0.89700000	-10.07300000	-0.31800000
C	1.42700000	-8.95900000	-1.24400000
O	2.44200000	-9.14200000	-1.90600000
C	1.56200000	-10.09900000	1.06700000
O	1.16300000	-11.25100000	1.76500000
C	1.17700000	-8.89300000	1.85900000
C	2.03000000	-7.73400000	1.85500000
C	-0.07200000	-8.86700000	2.58200000
C	1.59200000	-6.53800000	2.51300000
Cl	2.60200000	-5.13500000	2.49000000
C	-0.49900000	-7.66000000	3.24400000
C	0.31700000	-6.47800000	3.16700000
O	-0.15600000	-5.24000000	3.60000000
H	-0.98100000	-9.31000000	0.40200000
H	1.09400000	-11.02200000	-0.81900000
H	2.64700000	-10.13300000	0.96600000
H	1.60800000	-11.23000000	2.60200000
H	2.98000000	-7.75800000	1.34300000
H	-0.70000000	-9.74500000	2.60800000
H	-1.44700000	-7.62900000	3.76100000
N	0.71300000	-7.80600000	-1.28100000
C	1.21300000	-6.79600000	-2.20600000
C	1.10600000	-5.35800000	-1.67600000
O	2.09600000	-4.72200000	-1.33100000
C	0.42700000	-6.89500000	-3.51300000
C	0.42200000	-8.33600000	-4.02500000
O	1.44000000	-8.88700000	-4.42600000
H	-0.12300000	-7.64400000	-0.75700000

Atoms	X	Y	Z
H	2.25900000	-7.02800000	-2.39600000
H	-0.60500000	-6.57900000	-3.35300000
H	0.85400000	-6.24600000	-4.27800000
N	-0.15300000	-4.88100000	-1.67300000
C	-0.35500000	-3.50700000	-1.23100000
C	-1.51400000	-2.86100000	-2.00900000
O	-2.51300000	-3.48600000	-2.34300000
C	-0.59800000	-3.35400000	0.25800000
C	-1.22200000	-2.17600000	0.78900000
C	-1.45800000	-1.98500000	2.21400000
C	-1.07500000	-3.06100000	3.10100000
O	-1.33300000	-3.00100000	4.45700000
C	-0.45300000	-4.26500000	2.61100000
C	-0.21300000	-4.37800000	1.17600000
H	-0.91100000	-5.49100000	-1.90800000
H	0.56600000	-2.98300000	-1.48700000
H	-1.56400000	-1.42100000	0.09400000
H	0.26000000	-5.26800000	0.79200000
N	-1.28500000	-1.55600000	-2.25400000
C	-2.30700000	-0.76600000	-2.90700000
C	-1.92000000	0.72200000	-2.94900000
O	-0.75700000	1.02800000	-3.16900000
C	-2.74700000	-1.17900000	-4.27700000
C	-4.13800000	-1.45900000	-4.44400000
C	-4.71500000	-1.70000000	-5.71300000
C	-3.87100000	-1.71000000	-6.86900000
O	-4.41200000	-1.96300000	-8.11300000
C	-2.45300000	-1.45100000	-6.74100000
C	-1.89200000	-1.18000000	-5.43800000
H	-0.42800000	-1.13200000	-1.96200000
H	-3.13300000	-0.91600000	-2.22300000
H	-4.77600000	-1.45800000	-3.57400000
H	-5.34500000	-2.11000000	-8.02700000
H	-1.81900000	-1.45700000	-7.61600000
H	-0.83900000	-0.96300000	-5.33600000
N	-2.89100000	1.65500000	-2.74800000
C	-4.31200000	1.44300000	-2.47900000
O	-2.02900000	-0.82000000	2.79700000
C	-2.25800000	1.37200000	1.64300000
C	-3.93600000	-0.42600000	1.33200000
C	-2.74500000	0.05400000	1.96600000
C	-4.07000000	1.62700000	-0.06400000
C	-2.91700000	2.15900000	0.62500000
C	-4.60100000	0.34900000	0.32800000
C	-4.69400000	2.29200000	-1.26400000
Cl	-4.55800000	-1.98400000	1.75500000

Atoms	X	Y	Z
O	-5.04200000	2.67300000	-4.44900000
C	-5.14900000	1.67100000	-3.75100000
O	-4.25700000	3.62400000	-1.41700000
H	-2.59000000	2.60900000	-2.78300000
H	-4.46300000	0.40400000	-2.21400000
H	-1.38000000	1.74800000	2.14200000
H	-2.53100000	3.13400000	0.36200000
H	-5.48000000	-0.03900000	-0.15500000
H	-5.77600000	2.26800000	-1.15800000
H	-4.66800000	4.25600000	-0.68600000
N	-5.97700000	0.62600000	-3.97700000
O	-5.58200000	-4.21800000	-6.36900000
C	-6.55800000	-3.28200000	-6.09200000
C	-6.17900000	-1.94500000	-5.77200000
C	-7.93600000	-3.66900000	-6.11900000
C	-8.95700000	-2.70500000	-5.83200000
O	-10.28700000	-3.07400000	-5.85400000
C	-8.58600000	-1.35600000	-5.51500000
C	-7.19500000	-0.94800000	-5.47600000
C	-6.83800000	0.50800000	-5.12300000
C	-8.05900000	1.40100000	-4.81900000
O	-8.62700000	1.96300000	-5.75400000
O	-8.41400000	1.52000000	-3.64100000
H	-5.97500000	-0.12600000	-3.32400000
H	-6.23600000	0.93300000	-5.92100000
H	-4.72800000	-3.81200000	-6.30700000
H	-8.18500000	-4.69700000	-6.32800000
H	-10.82600000	-2.32400000	-5.64100000
H	-9.35500000	-0.63600000	-5.27800000
C	-1.08900000	-1.98300000	6.56800000
C	-0.26500000	-1.02300000	7.41900000
C	1.22200000	-1.28100000	7.20500000
C	1.55700000	-1.31200000	5.71200000
C	3.02200000	-1.70800000	5.49800000
C	-0.63600000	-1.96700000	5.10700000
O	-2.45400000	-1.64400000	6.65600000
O	-0.59500000	-1.22600000	8.77000000
O	1.96400000	-0.24700000	7.80100000
O	0.74300000	-2.26000000	5.05700000
O	3.28900000	-2.93400000	6.13000000
H	-0.95700000	-2.99500000	6.95000000
H	-0.50300000	0.00700000	7.16200000
H	1.51400000	-2.22200000	7.67100000
H	1.36100000	-0.32400000	5.29100000
H	3.69200000	-0.95900000	5.91800000
H	3.26200000	-1.82400000	4.44000000

Atoms	X	Y	Z
H	-0.83600000	-1.00800000	4.63000000
H	-1.25500000	-0.58100000	8.98900000
H	2.20300000	-0.54700000	8.66700000
H	4.20300000	-3.12900000	5.97100000
C	-3.12500000	-2.41200000	7.62800000
C	-4.56400000	-1.92000000	7.81700000
C	-5.43700000	-2.19300000	6.59100000
N	-6.83600000	-1.97400000	6.94000000
C	-5.06700000	-1.24400000	5.45100000
C	-5.24800000	-3.64400000	6.15300000
O	-5.93000000	-3.86500000	4.94400000
C	-3.76200000	-3.94800000	5.98100000
O	-3.13200000	-3.76200000	7.22600000
C	-3.51200000	-5.37600000	5.49300000
H	-2.58600000	-2.32500000	8.57100000
H	-4.99600000	-2.43400000	8.67500000
H	-4.57200000	-0.85600000	8.05500000
H	-7.41500000	-2.57800000	6.39200000
H	-4.02800000	-1.37600000	5.15000000
H	-5.69400000	-1.42500000	4.57700000
H	-5.20300000	-0.20600000	5.75200000
H	-5.67300000	-4.31600000	6.89800000
H	-6.78300000	-4.21200000	5.17200000
H	-3.34500000	-3.24500000	5.26400000
H	-3.98700000	-5.54500000	4.52700000
H	-2.44500000	-5.56700000	5.38300000
H	-3.91400000	-6.10300000	6.19800000
H	-6.97200000	-2.17200000	7.91100000
O	-0.76000000	-8.87900000	-3.98300000

Table S4.4: Cartesian coordinates for V_D-Ala complex

Atoms	X	Y	Z
H	-3.23000000	-5.21300000	2.24900000
H	-3.60800000	-6.88700000	2.65600000
H	-4.91100000	-5.74000000	2.34600000
H	-4.57500000	-7.21300000	0.34800000
H	-3.72600000	-4.93200000	-0.97400000
O	-1.58700000	-6.87900000	0.97500000
O	-2.27900000	-7.09700000	-1.06100000
C	-2.47200000	-6.82700000	0.12400000
C	-3.90900000	-6.04000000	2.04000000
C	-3.87900000	-6.40700000	0.55700000

Atoms	X	Y	Z
N	-4.31200000	-5.28600000	-0.24900000
H	-6.42800000	-4.83800000	-2.63200000
H	-4.71400000	-4.42600000	-2.66400000
H	-5.92000000	-3.22400000	-3.12400000
H	-5.05800000	-2.78500000	-0.79100000
H	-7.85700000	-3.58400000	-0.33300000
O	-6.32700000	-5.10500000	0.81600000
C	-5.52100000	-4.74000000	-0.03100000
C	-5.70900000	-4.04200000	-2.43700000
C	-5.79600000	-3.57200000	-0.97900000
N	-7.12700000	-3.03100000	-0.73500000
O	-6.45100000	-1.05100000	-1.59000000
C	-7.32300000	-1.75300000	-1.10100000
C	-8.74500000	-1.21200000	-0.86300000
H	-8.92900000	-1.14500000	0.18900000
H	-8.83600000	-0.24100000	-1.30300000
H	-9.45800000	-1.87400000	-1.30800000
N	-3.38600000	-11.86300000	-0.17800000
C	-2.78200000	-12.15600000	1.11600000
C	-2.79600000	-10.65900000	-0.75200000
C	-1.28700000	-10.83300000	-0.93600000
O	-0.82800000	-11.67700000	-1.69500000
C	-3.40500000	-10.31500000	-2.11000000
C	-4.92700000	-10.19300000	-2.05900000
C	-5.35800000	-9.01500000	-1.18700000
C	-5.49100000	-10.04500000	-3.47300000
H	-3.22600000	-12.66500000	-0.82200000
H	-3.23700000	-13.05800000	1.52500000
H	-1.71100000	-12.31000000	0.98200000
H	-2.95500000	-11.31600000	1.78800000
H	-2.97500000	-9.84200000	-0.05500000
H	-3.13300000	-11.09000000	-2.82700000
H	-2.97500000	-9.38300000	-2.47800000
H	-5.32500000	-11.10800000	-1.62000000
H	-5.00000000	-8.07400000	-1.60600000
H	-6.44400000	-8.95900000	-1.11800000
H	-4.96000000	-9.11200000	-0.17700000
H	-5.11300000	-9.14100000	-3.94900000
H	-5.21000000	-10.89600000	-4.09400000
H	-6.57900000	-9.98700000	-3.45300000
N	-0.54900000	-9.98300000	-0.19800000
C	0.89700000	-10.07300000	-0.31800000
C	1.42700000	-8.95900000	-1.24400000
O	2.44200000	-9.14200000	-1.90600000
C	1.56200000	-10.09900000	1.06700000
O	1.16300000	-11.25100000	1.76500000

Atoms	X	Y	Z
C	1.17700000	-8.89300000	1.85900000
C	2.03000000	-7.73400000	1.85500000
C	-0.07200000	-8.86700000	2.58200000
C	1.59200000	-6.53800000	2.51300000
Cl	2.60200000	-5.13500000	2.49000000
C	-0.49900000	-7.66000000	3.24400000
C	0.31700000	-6.47800000	3.16700000
O	-0.15600000	-5.24000000	3.60000000
H	-0.98100000	-9.31000000	0.40200000
H	1.09400000	-11.02200000	-0.81900000
H	2.64700000	-10.13300000	0.96600000
H	1.60800000	-11.23000000	2.60200000
H	2.98000000	-7.75800000	1.34300000
H	-0.70000000	-9.74500000	2.60800000
H	-1.44700000	-7.62900000	3.76100000
N	0.71300000	-7.80600000	-1.28100000
C	1.21300000	-6.79600000	-2.20600000
C	1.10600000	-5.35800000	-1.67600000
O	2.09600000	-4.72200000	-1.33100000
C	0.42700000	-6.89500000	-3.51300000
C	0.42200000	-8.33600000	-4.02500000
O	1.44000000	-8.88700000	-4.42600000
H	-0.12300000	-7.64400000	-0.75700000
H	2.25900000	-7.02800000	-2.39600000
H	-0.60500000	-6.57900000	-3.35300000
H	0.85400000	-6.24600000	-4.27800000
N	-0.15300000	-4.88100000	-1.67300000
C	-0.35500000	-3.50700000	-1.23100000
C	-1.51400000	-2.86100000	-2.00900000
O	-2.51300000	-3.48600000	-2.34300000
C	-0.59800000	-3.35400000	0.25800000
C	-1.22200000	-2.17600000	0.78900000
C	-1.45800000	-1.98500000	2.21400000
C	-1.07500000	-3.06100000	3.10100000
O	-1.33300000	-3.00100000	4.45700000
C	-0.45300000	-4.26500000	2.61100000
C	-0.21300000	-4.37800000	1.17600000
H	-0.91100000	-5.49100000	-1.90800000
H	0.56600000	-2.98300000	-1.48700000
H	-1.56400000	-1.42100000	0.09400000
H	0.26000000	-5.26800000	0.79200000
N	-1.28500000	-1.55600000	-2.25400000
C	-2.30700000	-0.76600000	-2.90700000
C	-1.92000000	0.72200000	-2.94900000
O	-0.75700000	1.02800000	-3.16900000
C	-2.74700000	-1.17900000	-4.27700000

Atoms	X	Y	Z
C	-4.13800000	-1.45900000	-4.44400000
C	-4.71500000	-1.70000000	-5.71300000
C	-3.87100000	-1.71000000	-6.86900000
O	-4.41200000	-1.96300000	-8.11300000
C	-2.45300000	-1.45100000	-6.74100000
C	-1.89200000	-1.18000000	-5.43800000
H	-0.42800000	-1.13200000	-1.96200000
H	-3.13300000	-0.91600000	-2.22300000
H	-4.77600000	-1.45800000	-3.57400000
H	-5.34500000	-2.11000000	-8.02700000
H	-1.81900000	-1.45700000	-7.61600000
H	-0.83900000	-0.96300000	-5.33600000
N	-2.89100000	1.65500000	-2.74800000
C	-4.31200000	1.44300000	-2.47900000
O	-2.02900000	-0.82000000	2.79700000
C	-2.25800000	1.37200000	1.64300000
C	-3.93600000	-0.42600000	1.33200000
C	-2.74500000	0.05400000	1.96600000
C	-4.07000000	1.62700000	-0.06400000
C	-2.91700000	2.15900000	0.62500000
C	-4.60100000	0.34900000	0.32800000
C	-4.69400000	2.29200000	-1.26400000
Cl	-4.55800000	-1.98400000	1.75500000
O	-5.04200000	2.67300000	-4.44900000
C	-5.14900000	1.67100000	-3.75100000
O	-4.25700000	3.62400000	-1.41700000
H	-2.59000000	2.60900000	-2.78300000
H	-4.46300000	0.40400000	-2.21400000
H	-1.38000000	1.74800000	2.14200000
H	-2.53100000	3.13400000	0.36200000
H	-5.48000000	-0.03900000	-0.15500000
H	-5.77600000	2.26800000	-1.15800000
H	-4.66800000	4.25600000	-0.68600000
N	-5.97700000	0.62600000	-3.97700000
O	-5.58200000	-4.21800000	-6.36900000
C	-6.55800000	-3.28200000	-6.09200000
C	-6.17900000	-1.94500000	-5.77200000
C	-7.93600000	-3.66900000	-6.11900000
C	-8.95700000	-2.70500000	-5.83200000
O	-10.28700000	-3.07400000	-5.85400000
C	-8.58600000	-1.35600000	-5.51500000
C	-7.19500000	-0.94800000	-5.47600000
C	-6.83800000	0.50800000	-5.12300000
C	-8.05900000	1.40100000	-4.81900000
O	-8.62700000	1.96300000	-5.75400000
O	-8.41400000	1.52000000	-3.64100000

Atoms	X	Y	Z
H	-5.97500000	-0.12600000	-3.32400000
H	-6.23600000	0.93300000	-5.92100000
H	-4.72800000	-3.81200000	-6.30700000
H	-8.18500000	-4.69700000	-6.32800000
H	-10.82600000	-2.32400000	-5.64100000
H	-9.35500000	-0.63600000	-5.27800000
C	-1.08900000	-1.98300000	6.56800000
C	-0.26500000	-1.02300000	7.41900000
C	1.22200000	-1.28100000	7.20500000
C	1.55700000	-1.31200000	5.71200000
C	3.02200000	-1.70800000	5.49800000
C	-0.63600000	-1.96700000	5.10700000
O	-2.45400000	-1.64400000	6.65600000
O	-0.59500000	-1.22600000	8.77000000
O	1.96400000	-0.24700000	7.80100000
O	0.74300000	-2.26000000	5.05700000
O	3.28900000	-2.93400000	6.13000000
H	-0.95700000	-2.99500000	6.95000000
H	-0.50300000	0.00700000	7.16200000
H	1.51400000	-2.22200000	7.67100000
H	1.36100000	-0.32400000	5.29100000
H	3.69200000	-0.95900000	5.91800000
H	3.26200000	-1.82400000	4.44000000
H	-0.83600000	-1.00800000	4.63000000
H	-1.25500000	-0.58100000	8.98900000
H	2.20300000	-0.54700000	8.66700000
H	4.20300000	-3.12900000	5.97100000
C	-3.12500000	-2.41200000	7.62800000
C	-4.56400000	-1.92000000	7.81700000
C	-5.43700000	-2.19300000	6.59100000
N	-6.83600000	-1.97400000	6.94000000
C	-5.06700000	-1.24400000	5.45100000
C	-5.24800000	-3.64400000	6.15300000
O	-5.93000000	-3.86500000	4.94400000
C	-3.76200000	-3.94800000	5.98100000
O	-3.13200000	-3.76200000	7.22600000
C	-3.51200000	-5.37600000	5.49300000
H	-2.58600000	-2.32500000	8.57100000
H	-4.99600000	-2.43400000	8.67500000
H	-4.57200000	-0.85600000	8.05500000
H	-7.41500000	-2.57800000	6.39200000
H	-4.02800000	-1.37600000	5.15000000
H	-5.69400000	-1.42500000	4.57700000
H	-5.20300000	-0.20600000	5.75200000
H	-5.67300000	-4.31600000	6.89800000
H	-6.78300000	-4.21200000	5.17200000

Atoms	X	Y	Z
H	-3.34500000	-3.24500000	5.26400000
H	-3.98700000	-5.54500000	4.52700000
H	-2.44500000	-5.56700000	5.38300000
H	-3.91400000	-6.10300000	6.19800000
H	-6.97200000	-2.17200000	7.91100000
O	-0.76000000	-8.87900000	-3.98300000

APPENDIX B

Supplemental Information for Chapter Five

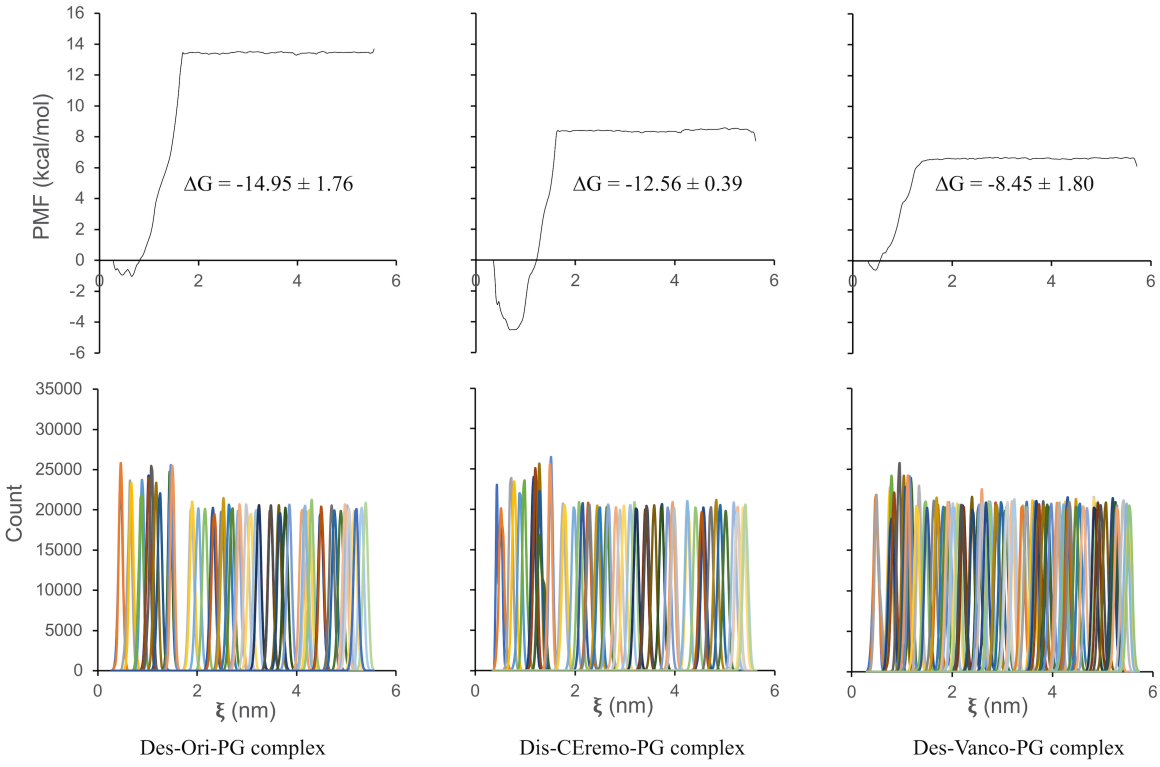

Figure S5.1. The potential of mean force (PMF) curve and corresponding umbrella histograms for complexes of desleucyl[^{19}F]oritavancin-PG (left), desleucylchloroeremomycin-PG (middle), and desleucylvancomycin-PG (right). The ΔG values of the complexes obtained from the PMF curve are shown as an inset.

Table S5.1. Center-of-mass (COM) pulling simulation data containing time taken to reach major dissociation between PG and (desleucyl)glycopeptide, magnitude of the maximum force applied in pulling PG away from the (desleucyl)glycopeptide, and the time to reach the maximum force.

Complex	*Major transition time (ps)*	F_{max} *(kJ/mol/nm)*	*Time to reach* F_{max} *(ps)*
Ori-PG	215	645	191
Des-Ori-PG	194	616	141
CEremo-PG	191	719	150
Des-CEremo-PG	186	579	134
Vanco-PG	198	552	127
Des-Vanco-PG	156	437	68

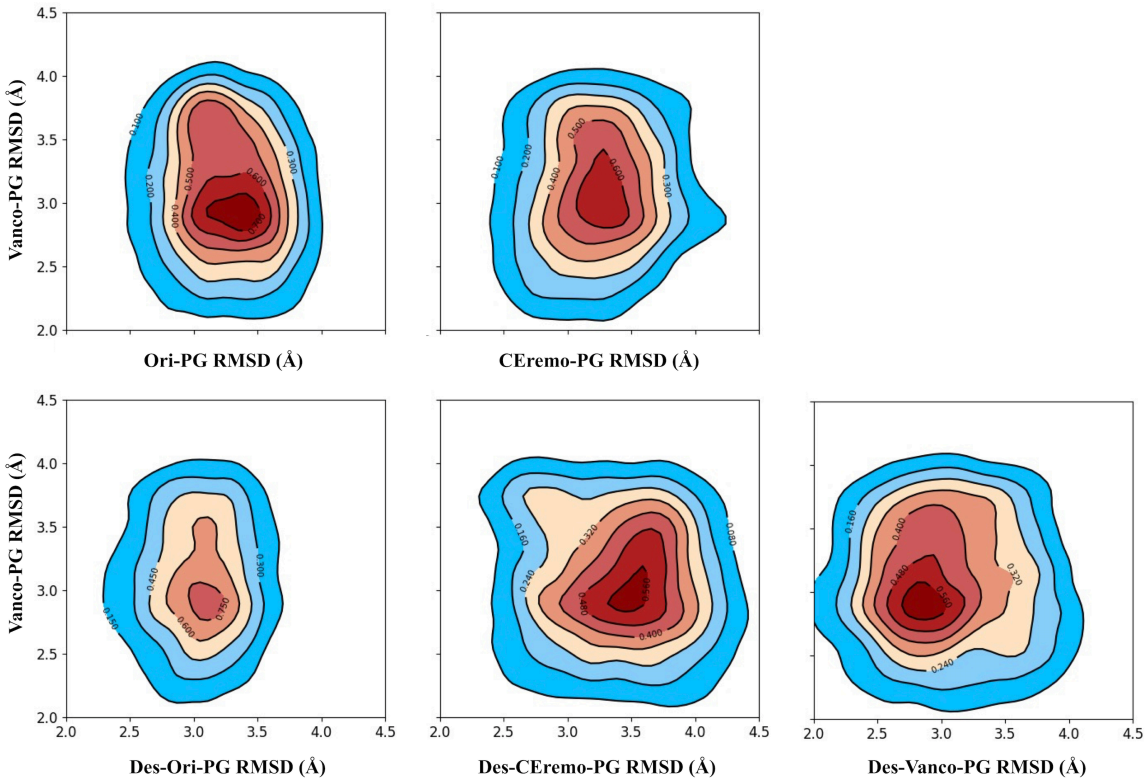

Figure S5.2. Comparative 2D rmsd (Å) contour plots of the Vanco-PG complex relative to the other complexes. Comparative 2D rmsd contour plots of Vanco-PG vs. Ori-PG (top left), Vanco-PG vs. CEremo-PG (top right), Vanco-PG vs. Des-Ori-PG (bottom left), Vanco-PG vs. Des-CEremo-PG (bottom middle), and Vanco-PG vs. Des-Vanco-PG complexes. The contour lines are the densities of trajectories located within an area. The region of the highest density of trajectories is denoted by the red color, while the blue colors represent regions of lower densities of trajectories.

Table S5.2. Cartesian coordinates for Ori-PG complex

Atoms	X	Y	Z
C	-1.661539	7.465033	5.120902
C	-0.662690	6.589786	4.381976
O	0.539481	6.796426	4.410927
N	-1.219273	5.556919	3.674659
C	-0.431340	4.736709	2.746723
C	0.514016	3.775857	3.503744
C	1.431474	2.986551	2.566460
C	2.261357	1.915459	3.281676
C	3.211037	1.217834	2.302248
N	3.927489	0.079239	2.873217
C	-1.384038	3.957227	1.824245
O	-1.255446	3.979825	0.596042

Atoms	X	Y	Z
N	-2.332114	3.258461	2.476998
C	-3.269869	2.317096	1.874207
C	-4.679945	2.916261	1.750028
C	-3.299407	1.086752	2.807690
O	-2.872057	1.183265	3.961343
N	-3.853389	-0.018380	2.292017
C	-4.116635	-1.207467	3.095341
C	-2.887148	-2.123671	3.190287
C	-5.343578	-1.975024	2.550200
O	-5.748570	-2.914616	3.276361
O	-5.838640	-1.612202	1.449705
N	5.636608	2.436592	-1.791507
C	5.144247	1.289494	-1.032094
C	6.261663	0.546984	-0.293763
O	6.086827	-0.574875	0.197393
N	7.424129	1.223228	-0.230248
C	8.678776	0.652038	0.219668
C	9.439718	1.442871	1.291022
O	10.657834	1.428670	1.298170
N	8.685474	2.104006	2.214637
C	9.315975	2.832853	3.310191
C	9.496320	1.986153	4.585579
O	10.584431	1.801835	5.100364
N	8.334944	1.456490	5.062413
C	8.291674	0.445281	6.105640
C	7.178369	-0.565434	5.803835
O	6.434450	-0.981195	6.668177
N	7.073297	-0.923405	4.472567
C	5.752879	-1.143633	3.917135
C	5.144648	0.186234	3.425032
O	5.752905	1.257144	3.544348
H	-4.370080	-0.873657	4.103915
H	-2.056880	-1.584080	3.650494
H	-3.129042	-2.995629	3.799978
H	-2.579654	-2.458677	2.195473
H	-4.199688	-0.019761	1.335403
H	-2.907118	2.031598	0.888438
H	-4.653677	3.845472	1.179813
H	-5.338296	2.210379	1.242693
H	-5.093287	3.130757	2.739161
H	-2.235924	3.110339	3.478708
H	0.163503	5.390485	2.104276
H	-2.220732	5.559083	3.551543
H	-2.529087	6.900338	5.470711
H	-2.013854	8.254453	4.450267
H	-1.156408	7.923670	5.970022

Atoms	X	Y	Z
H	1.110101	4.381580	4.188646
H	-0.084541	3.086545	4.109202
H	0.833438	2.497202	1.789915
H	2.098301	3.685714	2.046516
H	2.846075	2.360135	4.093489
H	1.595465	1.172719	3.733740
H	2.649311	0.842070	1.443504
H	3.950957	1.937560	1.944444
H	3.608117	-0.850358	2.618483
H	5.783032	-1.849668	3.085253
H	5.123825	-1.569664	4.700004
H	7.676752	-0.388283	3.863208
H	9.272925	-0.035616	6.155675
H	8.073008	0.862732	7.091196
H	7.455380	1.659853	4.593595
H	10.311213	3.133186	2.990633
H	8.719696	3.721585	3.534997
H	7.676678	2.041754	2.172035
H	8.468348	-0.347408	0.608052
H	9.376225	0.543159	-0.613811
H	7.399638	2.107075	-0.736405
H	4.437698	1.636270	-0.275169
H	4.610060	0.538724	-1.626346
H	5.863694	2.169571	-2.743234
H	4.938985	3.178393	-1.848068
N	-9.281012	-2.782320	5.983592
C	-8.783729	-2.442612	4.648427
C	-9.240243	-3.473707	3.598984
O	-10.397888	-3.876434	3.595515
C	-9.334935	-1.071140	4.208388
C	-8.887703	0.125330	5.066589
C	-9.702955	1.369124	4.681383
C	-7.385344	0.405330	4.924692
H	-7.089283	1.271246	5.525774
H	-7.130157	0.614991	3.880900
H	-6.779569	-0.442855	5.252297
H	-9.406129	2.237301	5.279671
H	-10.774335	1.204334	4.837362
H	-9.553798	1.614198	3.625205
C	-8.659163	-3.972723	6.557080
N	-8.295271	-3.874187	2.687992
C	-8.690598	-4.691075	1.556652
C	-8.679028	-4.018234	0.174400
O	-9.220683	-4.611422	-0.753851
C	-7.974967	-6.087162	1.531453
O	-7.965284	-6.634007	2.840104

Atoms	X	Y	Z
C	-6.587353	-6.071834	0.906653
C	-5.466075	-5.630081	1.614286
C	-6.429750	-6.486718	-0.416811
C	-4.236341	-5.516688	0.980019
C	-5.191622	-6.389827	-1.042510
Cl	-5.023701	-6.901644	-2.715873
C	-4.096911	-5.862405	-0.360635
O	-2.893684	-5.624932	-1.009510
N	-8.118434	-2.782749	0.049145
C	-8.347874	-2.022230	-1.167985
C	-7.125487	-1.497924	-1.939863
O	-7.322196	-1.001008	-3.049464
C	-9.376758	-0.870724	-0.975677
C	-8.857486	0.315465	-0.168613
O	-9.094414	0.459826	1.019459
N	-8.120951	1.215005	-0.886882
H	-7.630636	1.931582	-0.374119
H	-7.820432	1.004143	-1.827254
N	-5.892092	-1.605034	-1.390776
C	-4.734462	-1.171843	-2.157471
C	-4.326416	0.275946	-1.806018
O	-4.131554	0.629414	-0.648968
C	-3.542437	-2.121805	-1.979206
C	-3.762899	-3.426702	-1.556678
C	-2.241382	-1.711577	-2.274244
C	-2.704733	-4.328374	-1.436621
C	-1.182676	-2.603251	-2.125108
C	-1.397079	-3.930330	-1.735856
O	-0.340100	-4.807035	-1.575334
N	-4.145375	1.101445	-2.866106
C	-3.354741	2.322928	-2.760326
C	-2.493047	2.391673	-4.047339
O	-2.905919	1.863002	-5.073798
C	-4.098491	3.654507	-2.657648
C	-3.729593	4.554002	-1.658641
C	-4.131690	5.895721	-1.672426
C	-5.443899	5.399335	-3.661924
C	-4.980813	4.092323	-3.654363
C	-4.995404	6.312931	-2.700217
O	-5.421139	7.600486	-2.799629
N	-1.330357	3.085097	-4.007265
C	-0.729052	3.778207	-2.883037
C	-0.981829	5.298574	-3.046731
O	-1.170041	5.772721	-4.157779
C	0.766251	3.387589	-2.718980
O	1.483071	3.928686	-3.819980

Atoms	X	Y	Z
C	0.850110	1.872606	-2.603588
C	0.978196	1.052131	-3.725944
C	0.595465	1.283588	-1.364148
C	0.767141	-0.319111	-3.623455
C	0.394730	-0.088010	-1.258387
Cl	0.040724	-0.782343	0.306791
C	0.429638	-0.894134	-2.402044
O	0.140035	-2.243044	-2.354516
N	-1.068776	5.979255	-1.889803
C	-1.450229	7.387067	-1.847822
C	-0.200957	8.368541	-1.881629
C	-2.443403	7.597387	-0.697252
C	-2.130399	8.486911	0.330339
C	-3.665081	6.875467	-0.632518
C	-2.988906	8.662726	1.412986
O	-2.685100	9.536110	2.428418
C	-4.506807	7.073315	0.481937
O	-5.688174	6.397719	0.609388
C	-4.178868	7.953824	1.509253
O	-0.470492	9.571549	-1.777637
O	0.911577	7.804459	-2.051317
C	0.163345	-5.348341	-2.766913
C	1.363219	-6.245553	-2.457397
O	2.489293	-5.483288	-2.020934
C	1.797452	-6.981861	-3.737175
O	2.844903	-7.903816	-3.465151
C	0.648197	-7.710267	-4.423407
O	1.033841	-8.268178	-5.676093
C	-0.530160	-6.736955	-4.598289
O	-0.862023	-6.136614	-3.348177
C	-1.799995	-7.422810	-5.092188
O	-2.292127	-8.369510	-4.162469
H	0.449441	-4.543101	-3.460315
H	-2.549985	-6.652784	-5.314309
H	-1.567722	-7.964952	-6.010329
C	3.141487	-5.924427	-0.829377
C	4.588076	-5.424352	-0.857744
C	4.756929	-3.922676	-0.538449
N	6.202470	-3.639349	-0.372930
C	4.300913	-3.055046	-1.725003
C	3.922838	-3.633153	0.742077
C	2.468419	-4.121044	0.612582
O	2.470575	-5.538451	0.335771
C	1.665259	-3.947204	1.889058
H	3.121489	-7.018425	-0.805859
H	5.042275	-5.636549	-1.829149

Atoms	X	Y	Z
H	5.128516	-6.012146	-0.110790
H	4.422162	-1.994850	-1.494741
H	3.262826	-3.238911	-1.989562
H	4.924697	-3.287569	-2.591661
H	0.658119	-4.340506	1.742611
H	1.593227	-2.891759	2.151691
H	2.133974	-4.490848	2.714696
O	3.910599	-2.250323	1.103185
H	6.363333	-2.641967	-0.476453
C	9.083242	-4.265080	-0.438554
C	8.390622	-3.874531	0.712304
C	9.118349	-3.291903	1.752598
C	10.496234	-3.110817	1.653110
C	11.194816	-3.513189	0.507751
C	10.457902	-4.092684	-0.537081
C	13.502332	-3.550689	1.503434
C	12.664220	-3.333384	0.399607
C	13.259630	-2.944236	-0.809602
C	14.636895	-2.781625	-0.920727
C	15.426698	-3.009097	0.194777
C	14.881114	-3.390027	1.410097
F	16.769621	-2.854264	0.094255
C	6.895166	-4.098010	0.830227
C	2.905190	3.903336	-3.711968
C	3.504381	4.717672	-4.853176
C	3.412763	6.268225	-4.721170
N	4.403385	6.910947	-5.609959
C	2.039530	6.793708	-5.147610
C	3.770819	6.682615	-3.255756
C	3.122752	5.772419	-2.193350
O	3.370587	4.356323	-2.463719
C	3.660989	6.039936	-0.799653
H	3.242125	2.859578	-3.760684
H	3.058748	4.400440	-5.801914
H	4.565662	4.442851	-4.888985
H	2.039630	7.880586	-5.079291
H	1.225146	6.403966	-4.543502
H	1.845288	6.508637	-6.188799
H	3.158583	5.405027	-0.065046
H	3.478295	7.081741	-0.540699
H	4.738373	5.847547	-0.753248
O	3.480705	8.027627	-2.965464
H	-9.095590	-0.123251	6.113390
H	-9.063799	-0.882935	3.164514
H	-10.429501	-1.142650	4.228104
H	-7.691957	-2.419961	4.679583

Atoms	X	Y	Z
H	-9.083160	-4.161397	7.547725
H	-8.786268	-4.890513	5.957242
H	-7.586617	-3.799152	6.681961
H	-10.280032	-2.949329	5.888155
H	-7.329924	-3.509318	2.794977
H	-9.746046	-4.912958	1.731575
H	-7.886845	-5.887571	3.449308
H	-8.605681	-6.735771	0.921160
H	-5.556806	-5.307617	2.642230
H	-3.376710	-5.112906	1.500977
H	-7.281448	-6.845390	-0.980707
H	-4.765226	-3.744382	-1.316620
H	-2.039058	-0.700219	-2.596162
H	-5.052665	-1.194496	-3.202923
H	-5.786170	-1.752231	-0.380639
H	-8.806775	-2.732212	-1.859241
H	-7.589814	-2.364733	0.816975
H	-9.679853	-0.537607	-1.970255
H	-10.244049	-1.271523	-0.452473
H	-2.537356	-7.881552	-3.366026
H	-0.240793	-5.959113	-5.327753
H	0.316556	-8.551387	-3.811500
H	1.558527	-7.610505	-6.144986
H	3.605379	-7.383191	-3.187193
H	2.163301	-6.205792	-4.433673
H	1.054601	-6.958875	-1.687440
H	1.969691	-3.596640	-0.206613
H	4.368915	-4.209523	1.565555
H	4.651388	-1.770918	0.693512
H	6.546007	-3.620286	1.758510
H	6.712001	-5.171096	0.955575
H	8.602528	-2.962406	2.649590
H	8.526041	-4.699498	-1.260115
H	11.027568	-2.617820	2.459264
H	10.973859	-4.433615	-1.428213
H	15.531001	-3.561398	2.259313
H	13.071421	-3.868700	2.445279
H	12.633906	-2.739062	-1.669987
H	15.098453	-2.468826	-1.849217
H	-4.247627	0.752230	-3.812343
H	0.487011	1.902198	-0.481012
H	1.179731	1.497839	-4.691531
H	0.802116	-0.958306	-4.497523
H	1.121889	3.838365	-1.789181
H	2.046393	5.952079	-2.200624
H	4.863062	6.571024	-3.161978

Atoms	X	Y	Z
H	2.535658	8.104924	-2.687425
H	5.333889	6.545666	-5.421933
H	4.186850	6.685253	-6.577699
H	-0.970646	3.350671	-4.915607
H	-1.206205	3.448274	-1.964149
H	-0.905477	5.497655	-1.013609
H	-1.964789	7.578819	-2.794608
H	-4.851095	8.090605	2.346188
H	-1.236566	9.091597	0.234836
H	-1.849348	9.964990	2.211770
H	-5.779728	5.806319	-0.150657
H	-4.966779	8.117362	-2.118192
H	-6.113644	5.752718	-4.436606
H	-5.275450	3.417498	-4.450312
H	-3.062112	4.233286	-0.867949
H	-2.741094	2.215837	-1.866728

Table S5.3. Cartesian coordinates for Des-Ori-PG complex

Atoms	X	Y	Z
C	-2.144910	7.475828	5.278923
C	-1.167289	6.630927	4.478818
O	0.014171	6.916654	4.372678
N	-1.718987	5.529230	3.879829
C	-0.973698	4.715787	2.911583
C	0.108547	3.858472	3.607120
C	0.979260	3.083787	2.614671
C	1.950397	2.106953	3.285615
C	2.842389	1.423582	2.243882
N	3.691061	0.364722	2.786356
C	-1.958065	3.829813	2.129110
O	-1.956594	3.798000	0.894397
N	-2.783751	3.105009	2.907641
C	-3.709525	2.075005	2.448358
C	-5.163424	2.573911	2.446136
C	-3.557961	0.894621	3.433107
O	-3.023636	1.077548	4.530328
N	-4.082580	-0.269139	3.027435
C	-4.179032	-1.430278	3.905505
C	-2.885095	-2.258393	3.911550
C	-5.398121	-2.302967	3.526102
O	-5.660546	-3.228642	4.331348
O	-6.026436	-2.029832	2.468542

Atoms	X	Y	Z
N	4.748901	2.587154	-2.130922
C	4.417685	1.450691	-1.274353
C	5.653483	0.821224	-0.625010
O	5.608398	-0.283098	-0.069303
N	6.766142	1.574122	-0.713348
C	8.096871	1.109601	-0.372464
C	8.905247	2.001995	0.577488
O	10.115794	2.067565	0.457747
N	8.204098	2.658884	1.544925
C	8.889826	3.482243	2.535302
C	9.257465	2.715317	3.820878
O	10.402399	2.628803	4.226592
N	8.190416	2.136158	4.439497
C	8.324128	1.178866	5.525063
C	7.259526	0.083681	5.386244
O	6.638068	-0.334985	6.341163
N	7.045328	-0.347880	4.090354
C	5.694083	-0.681734	3.686391
C	4.947402	0.578819	3.202520
O	5.488083	1.691773	3.210227
H	-4.351650	-1.062628	4.919370
H	-2.052296	-1.643066	4.258123
H	-3.002216	-3.111987	4.581032
H	-2.657361	-2.623011	2.905753
H	-4.523155	-0.341919	2.113306
H	-3.429507	1.763786	1.443584
H	-5.260293	3.472530	1.835916
H	-5.818745	1.801658	2.042077
H	-5.488331	2.811247	3.462675
H	-2.576328	3.014808	3.899335
H	-0.494354	5.373269	2.182237
H	-2.725446	5.459858	3.862210
H	-2.930799	6.874413	5.742136
H	-2.617864	8.205345	4.614709
H	-1.589655	8.009154	6.049485
H	0.727102	4.535920	4.198527
H	-0.375744	3.163445	4.301671
H	0.341320	2.517507	1.927290
H	1.539282	3.797445	1.997503
H	2.581827	2.629646	4.011397
H	1.387472	1.346463	3.837164
H	2.224187	0.968666	1.466029
H	3.489949	2.170773	1.779251
H	3.413427	-0.595498	2.607650
H	5.689112	-1.425856	2.887843
H	5.179072	-1.107311	4.548796

Atoms	X	Y	Z
H	7.544888	0.193606	3.398209
H	9.336666	0.766099	5.493282
H	8.177828	1.630960	6.508733
H	7.255766	2.257585	4.056791
H	9.824022	3.830066	2.100432
H	8.258620	4.340557	2.781891
H	7.203037	2.528950	1.610906
H	7.997465	0.119706	0.079467
H	8.712104	1.003975	-1.268739
H	6.628576	2.427496	-1.252613
H	3.768989	1.788896	-0.463667
H	3.879912	0.637355	-1.775782
H	4.896446	2.287249	-3.088492
H	3.998885	3.278074	-2.146801
N	-8.180258	-4.380872	4.055561
C	-8.630065	-5.278476	3.008900
C	-8.805908	-4.677767	1.604729
O	-9.396006	-5.351602	0.765299
C	-7.824625	-6.624438	2.970493
O	-7.643984	-7.101958	4.293764
C	-6.512031	-6.550665	2.203853
C	-5.358493	-6.001249	2.770111
C	-6.460777	-7.021433	0.890737
C	-4.210406	-5.840517	2.006265
C	-5.302335	-6.876162	0.135252
Cl	-5.269535	-7.460723	-1.522309
C	-4.183777	-6.244417	0.674924
O	-3.072170	-5.962503	-0.106129
N	-8.348861	-3.416396	1.367182
C	-8.753274	-2.735579	0.148422
C	-7.655226	-2.172849	-0.769481
O	-7.997782	-1.747108	-1.873218
C	-9.835493	-1.645234	0.396414
C	-9.321448	-0.388079	1.091654
O	-9.446198	-0.198987	2.290475
N	-8.726403	0.519684	0.261320
H	-8.238035	1.291925	0.687884
H	-8.508767	0.281109	-0.695127
N	-6.368047	-2.171203	-0.348293
C	-5.327352	-1.703229	-1.250256
C	-4.988220	-0.215880	-1.007568
O	-4.702270	0.208147	0.106033
C	-4.059776	-2.563172	-1.156023
C	-4.144274	-3.856380	-0.655661
C	-2.827309	-2.084657	-1.603376
C	-3.018824	-4.679892	-0.607380

Atoms	X	Y	Z
C	-1.699074	-2.896684	-1.526702
C	-1.779379	-4.213303	-1.059057
O	-0.652752	-5.009944	-0.971549
N	-4.973909	0.564453	-2.116120
C	-4.264165	1.838653	-2.147580
C	-3.544381	1.897586	-3.519470
O	-4.021158	1.291422	-4.472792
C	-5.085132	3.122453	-2.026411
C	-4.680761	4.093902	-1.112101
C	-5.175202	5.404117	-1.142840
C	-6.644385	4.722367	-2.960286
C	-6.092483	3.450394	-2.943642
C	-6.165795	5.711149	-2.091986
O	-6.688582	6.961475	-2.202937
N	-2.435081	2.666422	-3.631878
C	-1.772915	3.453729	-2.608383
C	-2.146895	4.944053	-2.811558
O	-2.479570	5.347583	-3.916618
C	-0.245007	3.170243	-2.584649
O	0.316775	3.699966	-3.777382
C	-0.043933	1.671813	-2.412024
C	0.026844	0.805192	-3.504373
C	-0.129667	1.131511	-1.127999
C	-0.076127	-0.569862	-3.320041
C	-0.222040	-0.243057	-0.941480
Cl	-0.365964	-0.878154	0.681215
C	-0.246897	-1.102535	-2.045874
O	-0.434955	-2.463256	-1.908911
N	-2.163545	5.675806	-1.683006
C	-2.636475	7.056080	-1.663412
C	-1.468929	8.113846	-1.870975
C	-3.520128	7.259723	-0.425621
C	-3.167626	8.219053	0.523376
C	-4.675340	6.463996	-0.201655
C	-3.922110	8.393614	1.681113
O	-3.578839	9.335640	2.619703
C	-5.411488	6.663232	0.984957
O	-6.523582	5.919500	1.264975
C	-5.043562	7.614538	1.932515
O	-1.810156	9.300476	-1.792458
O	-0.342564	7.615514	-2.131130
C	-0.236061	-5.577435	-2.184253
C	1.048918	-6.377597	-1.962764
O	2.157257	-5.522302	-1.680547
C	1.401645	-7.148433	-3.247262
O	2.533295	-7.985097	-3.045982

Atoms	X	Y	Z
C	0.242599	-7.984249	-3.776698
O	0.537354	-8.579082	-5.037056
C	-1.012706	-7.099972	-3.870029
O	-1.257324	-6.459482	-2.619726
C	-2.274888	-7.891418	-4.197633
O	-2.602646	-8.819460	-3.180714
H	-0.078890	-4.791725	-2.938590
H	-3.095639	-7.184235	-4.373765
H	-2.099511	-8.463447	-5.110254
C	2.956228	-5.858599	-0.545506
C	4.353868	-5.267447	-0.747101
C	4.448594	-3.743621	-0.513708
N	5.880044	-3.358642	-0.513010
C	3.814929	-2.969260	-1.683100
C	3.730441	-3.444048	0.833062
C	2.308167	-4.031628	0.878098
O	2.381550	-5.458164	0.665307
C	1.628404	-3.845532	2.222705
H	3.015422	-6.948945	-0.471843
H	4.720958	-5.498925	-1.750403
H	5.007124	-5.779877	-0.035631
H	3.884318	-1.893047	-1.513730
H	2.770812	-3.233631	-1.829217
H	4.362357	-3.204599	-2.599182
H	0.641651	-4.310574	2.199926
H	1.509602	-2.784992	2.444672
H	2.215368	-4.314619	3.017910
O	3.658023	-2.048322	1.132185
H	5.959297	-2.359489	-0.676644
C	8.776036	-3.797903	-0.852092
C	8.178046	-3.395055	0.346593
C	8.964899	-2.713900	1.278335
C	10.309498	-2.448750	1.027325
C	10.914791	-2.862712	-0.166000
C	10.118141	-3.541574	-1.101428
C	13.308313	-2.698917	0.583430
C	12.349423	-2.593318	-0.435131
C	12.790394	-2.228457	-1.715973
C	14.134492	-1.982353	-1.977667
C	15.047338	-2.100635	-0.942001
C	14.655857	-2.453748	0.339336
F	16.358976	-1.863978	-1.189224
C	6.721612	-3.709170	0.630090
C	1.740779	3.772864	-3.817767
C	2.162606	4.565173	-5.050178
C	1.976429	6.111177	-4.977760

Atoms	X	Y	Z
N	2.824326	6.770849	-5.992784
C	0.533602	6.523621	-5.280897
C	2.451332	6.622293	-3.577550
C	1.979726	5.727246	-2.414093
O	2.297476	4.318351	-2.646251
C	2.636454	6.100071	-1.097519
H	2.143339	2.752151	-3.855435
H	1.646385	4.171556	-5.932170
H	3.231418	4.358606	-5.184703
H	0.464473	7.610264	-5.260921
H	-0.185998	6.113006	-4.578302
H	0.255224	6.173712	-6.282466
H	2.256866	5.472118	-0.287114
H	2.408417	7.139621	-0.867027
H	3.723808	5.980900	-1.155679
O	2.098627	7.958612	-3.318042
H	-7.529977	-3.723707	3.674420
H	-8.965323	-3.891232	4.434935
H	-9.644177	-5.559426	3.302914
H	-7.556663	-6.321868	4.857930
H	-8.466974	-7.343072	2.458726
H	-5.366879	-5.633317	3.786693
H	-3.332791	-5.355518	2.416108
H	-7.338035	-7.463152	0.435416
H	-5.092353	-4.226012	-0.298270
H	-2.730039	-1.080025	-1.988948
H	-5.747564	-1.799914	-2.254651
H	-6.150177	-2.259418	0.650714
H	-9.229030	-3.508316	-0.459059
H	-7.775693	-2.926172	2.056311
H	-10.260482	-1.383788	-0.574693
H	-10.615026	-2.074445	1.024652
H	-2.799425	-8.308487	-2.385260
H	-0.854026	-6.343194	-4.659330
H	0.034479	-8.812844	-3.096982
H	0.964404	-7.913426	-5.586800
H	3.279680	-7.402523	-2.872341
H	1.639691	-6.386756	-4.011735
H	0.870720	-7.069263	-1.134060
H	1.693420	-3.583341	0.093283
H	4.297013	-3.947333	1.629932
H	4.318025	-1.543220	0.626518
H	6.435784	-3.208435	1.567858
H	6.627746	-4.784107	0.821078
H	8.520892	-2.373339	2.208985
H	8.170206	-4.309078	-1.590891

Atoms	X	Y	Z
H	10.883992	-1.881669	1.750942
H	10.563678	-3.893222	-2.025766
H	15.398918	-2.538833	1.122605
H	12.998487	-2.995819	1.578288
H	12.067811	-2.108682	-2.514357
H	14.476451	-1.687966	-2.962234
H	-5.146874	0.161461	-3.030150
H	-0.191077	1.786025	-0.266482
H	0.097687	1.213198	-4.504444
H	-0.085274	-1.249214	-4.163952
H	0.170628	3.690115	-1.717940
H	0.898250	5.835797	-2.316602
H	3.552575	6.587030	-3.593758
H	1.183568	7.988273	-2.946314
H	3.792397	6.477041	-5.887250
H	2.527114	6.482411	-6.921662
H	-2.188840	2.908140	-4.583689
H	-2.130123	3.140760	-1.630968
H	-1.878888	5.251234	-0.808346
H	-3.256564	7.165310	-2.558679
H	-5.635370	7.749789	2.828355
H	-2.332665	8.875019	0.308313
H	-2.801483	9.806434	2.298102
H	-6.650079	5.285357	0.545484
H	-6.204797	7.540971	-1.596228
H	-7.412347	4.991351	-3.675444
H	-6.418310	2.718050	-3.673877
H	-3.915711	3.858143	-0.382238
H	-3.557071	1.817533	-1.319257

Table S5.4. Cartesian coordinates for CEremo-PG complex

Atoms	X	Y	Z
C	2.616910	6.853786	4.982632
C	3.114222	5.594022	4.293106
O	4.276137	5.226634	4.354195
N	2.157440	4.909300	3.591237
C	2.496038	3.789015	2.705256
C	2.880682	2.526834	3.510838
C	3.348654	1.374229	2.618797
C	3.580814	0.065805	3.381429
C	4.120268	-1.021574	2.446310
N	4.223171	-2.342592	3.062777

Atoms	X	Y	Z
C	1.307729	3.504021	1.770969
O	1.453494	3.424804	0.547038
N	0.133441	3.340198	2.409262
C	-1.121531	2.915099	1.798325
C	-2.095991	4.090212	1.618688
C	-1.729437	1.866916	2.756329
O	-1.325532	1.794261	3.920133
N	-2.720436	1.123122	2.247582
C	-3.514643	0.214574	3.067540
C	-2.845764	-1.160084	3.219191
C	-4.947489	0.078414	2.501744
O	-5.751534	-0.546092	3.235000
O	-5.201285	0.591702	1.379274
N	6.904868	-1.187042	-1.596736
C	5.927285	-1.954586	-0.828511
C	6.565394	-3.102505	-0.041001
O	5.885979	-4.002177	0.468266
N	7.907327	-3.033606	0.043474
C	8.751017	-4.101864	0.543309
C	9.771711	-3.713896	1.620302
O	10.846644	-4.285387	1.664765
N	9.389977	-2.750448	2.506358
C	10.265938	-2.356848	3.604884
C	10.014844	-3.149550	4.902811
O	10.887382	-3.795765	5.454214
N	8.731933	-3.071099	5.355242
C	8.210673	-3.914827	6.417856
C	6.762753	-4.311055	6.103833
O	5.896180	-4.310391	6.953780
N	6.527882	-4.624279	4.777867
C	5.263813	-4.231936	4.187353
C	5.343565	-2.788189	3.648936
O	6.373865	-2.112682	3.763973
H	-3.603641	0.660330	4.060650
H	-1.868458	-1.047029	3.692885
H	-3.471892	-1.803222	3.839581
H	-2.709561	-1.631259	2.241500
H	-3.012044	1.249493	1.281130
H	-0.913663	2.462812	0.830303
H	-1.635684	4.884448	1.029981
H	-2.996276	3.749064	1.106645
H	-2.381475	4.502793	2.590037
H	0.133472	3.197372	3.416345
H	3.335826	4.075367	2.067480
H	1.271349	5.366857	3.437725
H	1.580983	6.762103	5.317797

Atoms	X	Y	Z
H	2.678541	7.694389	4.285030
H	3.261596	7.056953	5.836806
H	3.676574	2.813459	4.200556
H	2.021899	2.209425	4.112291
H	2.606106	1.188817	1.834976
H	4.271107	1.671851	2.104666
H	4.290393	0.218824	4.201036
H	2.640331	-0.273160	3.828678
H	3.463592	-1.125503	1.579044
H	5.114276	-0.733931	2.095994
H	3.516673	-3.029674	2.818201
H	4.980393	-4.899882	3.371913
H	4.495916	-4.295783	4.959592
H	7.320202	-4.446140	4.175931
H	8.860018	-4.790538	6.507863
H	8.191401	-3.411531	7.387249
H	8.052528	-2.502193	4.855708
H	11.293198	-2.557492	3.309429
H	10.141147	-1.286743	3.792591
H	8.466370	-2.344075	2.434447
H	8.098044	-4.879886	0.946200
H	9.334628	-4.545978	-0.266097
H	8.300606	-2.254248	-0.481800
H	5.446272	-1.297591	-0.100922
H	5.118113	-2.395428	-1.422687
H	7.000182	-1.559539	-2.535253
H	6.627406	-0.210092	-1.690171
N	-8.873956	1.281493	5.830220
C	-8.253208	1.311081	4.503888
C	-9.114418	0.570786	3.463131
O	-10.327376	0.744480	3.433014
C	-8.104597	2.767297	4.018351
C	-7.172308	3.652409	4.864213
C	-7.317785	5.118264	4.428151
C	-5.707180	3.206766	4.762139
H	-5.056631	3.859362	5.353465
H	-5.366203	3.241567	3.722378
H	-5.564853	2.186408	5.125894
H	-6.665469	5.772424	5.016660
H	-8.347523	5.468835	4.554954
H	-7.054461	5.232767	3.372040
C	-8.878911	-0.042016	6.447426
N	-8.443733	-0.248374	2.589965
C	-9.150733	-0.829259	1.464690
C	-8.807310	-0.282506	0.069487
O	-9.544911	-0.590961	-0.862024

Atoms	X	Y	Z
C	-9.156634	-2.398049	1.490826
O	-9.421998	-2.845106	2.810456
C	-7.906720	-3.041836	0.908300
C	-6.720267	-3.141108	1.640166
C	-7.934655	-3.525901	-0.400679
C	-5.565295	-3.625673	1.041305
C	-6.779964	-4.028689	-0.990374
Cl	-6.837256	-4.615018	-2.646644
C	-5.577275	-4.040551	-0.286869
O	-4.388549	-4.403266	-0.903763
N	-7.739457	0.552977	-0.064814
C	-7.572577	1.293610	-1.304190
C	-6.232864	1.172728	-2.049495
O	-6.159951	1.667826	-3.174838
C	-7.960131	2.794514	-1.167672
C	-6.967721	3.635756	-0.370505
O	-7.132238	3.911615	0.806493
N	-5.887840	4.072782	-1.084951
H	-5.131934	4.500733	-0.572817
H	-5.701704	3.716812	-2.011078
N	-5.196427	0.529500	-1.461033
C	-3.956186	0.357617	-2.201197
C	-2.934418	1.467234	-1.868250
O	-2.618884	1.729536	-0.713559
C	-3.337526	-1.027087	-1.966708
C	-4.140408	-2.070573	-1.523531
C	-1.988632	-1.269730	-2.230693
C	-3.617400	-3.352870	-1.352300
C	-1.461051	-2.542445	-2.030599
C	-2.268175	-3.609497	-1.620021
O	-1.735443	-4.867756	-1.408919
N	-2.375905	2.082294	-2.939593
C	-1.114221	2.807329	-2.835730
C	-0.295295	2.430661	-4.097129
O	-0.887196	2.117156	-5.124233
C	-1.164277	4.334294	-2.783929
C	-0.440487	4.996312	-1.793449
C	-0.180513	6.371643	-1.847863
C	-1.539486	6.468033	-3.865360
C	-1.729246	5.095318	-3.816047
C	-0.737895	7.104813	-2.910033
O	-0.522330	8.440099	-3.049587
N	1.055138	2.513941	-4.036435
C	1.888254	2.890154	-2.909386
C	2.365520	4.350643	-3.112852
O	2.435536	4.821578	-4.238900

Atoms	X	Y	Z
C	3.033565	1.862383	-2.691726
O	3.937776	1.977677	-3.781647
C	2.409622	0.482625	-2.541776
C	2.165565	-0.341396	-3.642091
C	1.891366	0.117184	-1.298449
C	1.346061	-1.458594	-3.517042
C	1.080806	-1.004959	-1.169810
Cl	0.420292	-1.407619	0.398242
C	0.760979	-1.774169	-2.294547
O	-0.117055	-2.837287	-2.227282
N	2.581248	5.032801	-1.973778
C	2.888971	6.459163	-1.973236
C	4.449969	6.756021	-1.989843
C	2.083939	7.139472	-0.858093
C	2.753023	7.819230	0.159464
C	0.666221	7.061402	-0.815240
C	2.052875	8.404865	1.211554
O	2.706582	9.074117	2.217023
C	-0.009449	7.659939	0.268680
O	-1.371162	7.606550	0.374451
C	0.668757	8.324829	1.286607
O	4.761852	7.951214	-1.919594
O	5.181436	5.738995	-2.113657
C	-1.516690	-5.618482	-2.572915
C	-0.869077	-6.955653	-2.208143
O	0.473648	-6.781454	-1.753904
C	-0.799895	-7.850630	-3.458251
O	-0.298348	-9.141035	-3.135054
C	-2.143328	-7.992314	-4.163510
O	-2.035750	-8.705714	-5.391799
C	-2.739177	-6.593042	-4.394698
O	-2.779453	-5.866741	-3.168245
C	-4.173434	-6.635298	-4.912321
O	-5.061634	-7.219445	-3.978144
H	-0.880538	-5.057610	-3.274202
H	-4.481561	-5.614679	-5.173392
H	-4.200562	-7.253335	-5.811290
C	0.829392	-7.433414	-0.534001
C	2.344207	-7.654348	-0.528978
C	3.178917	-6.388152	-0.236577
N	4.589819	-6.794685	-0.033243
C	3.193326	-5.447422	-1.454553
C	2.549302	-5.706284	1.011589
C	1.035861	-5.476113	0.848317
O	0.390996	-6.744593	0.601783
C	0.380603	-4.911283	2.095827

Atoms	X	Y	Z
H	0.308338	-8.394749	-0.487935
H	2.666720	-8.083060	-1.481419
H	2.540981	-8.399789	0.246337
H	3.784364	-4.554254	-1.243219
H	2.191639	-5.142851	-1.746583
H	3.655265	-5.968587	-2.296734
H	-0.691919	-4.802990	1.927204
H	0.797281	-3.932555	2.333736
H	0.532629	-5.582026	2.946657
O	3.167865	-4.461112	1.342788
H	5.109738	-6.022740	0.332523
H	4.627194	-7.557524	0.612265
C	5.186981	1.305957	-3.629953
C	6.113044	1.716515	-4.769417
C	6.742178	3.139523	-4.673128
N	7.932555	3.226324	-5.544815
C	5.771778	4.222402	-5.152138
C	7.225298	3.391114	-3.206615
C	6.213131	2.915300	-2.145355
O	5.786900	1.535428	-2.378012
C	6.789959	2.951439	-0.741923
H	5.007194	0.223026	-3.646289
H	5.587908	1.608317	-5.724327
H	6.929660	0.984218	-4.767128
H	6.270307	5.189559	-5.106883
H	4.859090	4.269981	-4.564939
H	5.486236	4.024338	-6.192477
H	6.039330	2.642430	-0.009641
H	7.102172	3.968730	-0.510765
H	7.657347	2.287630	-0.658733
O	7.580969	4.727935	-2.953827
H	-7.489230	3.561442	5.909243
H	-7.759320	2.775725	2.979447
H	-9.109691	3.206862	4.006305
H	-7.273932	0.831088	4.567722
H	-9.359213	0.017559	7.428502
H	-9.403309	-0.818177	5.863576
H	-7.848949	-0.376121	6.601139
H	-9.836125	1.588641	5.708025
H	-7.420709	-0.364021	2.718485
H	-10.192896	-0.536068	1.612117
H	-9.019742	-2.198434	3.405815
H	-10.004276	-2.704409	0.875522
H	-6.670339	-2.779476	2.657817
H	-4.625396	-3.644679	1.579477
H	-8.846034	-3.471893	-0.982474

Atoms	X	Y	Z
H	-5.180565	-1.884682	-1.307370
H	-1.338526	-0.475233	-2.567663
H	-4.231093	0.449294	-3.255122
H	-5.187475	0.383304	-0.445253
H	-8.294478	0.851245	-1.993880
H	-7.091185	0.706634	0.709700
H	-8.058960	3.196788	-2.177834
H	-8.923483	2.853909	-0.662695
H	-5.068817	-6.647556	-3.200036
H	-2.112093	-6.059179	-5.131342
H	-2.835006	-8.566806	-3.544286
H	-1.259459	-8.378012	-5.858355
H	0.611416	-9.018757	-2.845203
H	-0.106285	-7.352366	-4.159591
H	-1.484294	-7.422070	-1.432985
H	0.848230	-4.808465	0.003421
H	2.666221	-6.395763	1.860266
H	4.053068	-4.388932	0.945755
H	-2.610893	1.788170	-3.880891
H	2.064190	0.745131	-0.432318
H	2.566061	-0.069837	-4.610331
H	1.098375	-2.070793	-4.375909
H	3.540508	2.129833	-1.761305
H	5.340127	3.568619	-2.189139
H	8.142202	2.793773	-3.077345
H	6.772580	5.239453	-2.706336
H	8.587606	2.481076	-5.320903
H	7.653245	3.093616	-6.513691
H	1.512289	2.554846	-4.938847
H	1.297058	2.846361	-1.998641
H	2.489738	4.558986	-1.083022
H	2.536571	6.834558	-2.939071
H	0.120307	8.782253	2.099641
H	3.826283	7.942688	0.078382
H	3.649547	9.064178	2.016838
H	-1.711193	7.098599	-0.375328
H	0.106941	8.712781	-2.365757
H	-1.958349	7.063800	-4.667348
H	-2.287326	4.605338	-4.606111
H	-0.008894	4.431112	-0.976222
H	-0.634005	2.459875	-1.921828

Table S5.5. Cartesian coordinates for Des-CEremo-PG complex

Atoms	X	Y	Z
C	3.956268	6.065362	5.362953
C	4.133964	4.811579	4.522584
O	5.214648	4.263022	4.381303
N	2.987515	4.351809	3.929994
C	3.006430	3.277942	2.929445
C	3.281765	1.902966	3.580326
C	3.420663	0.777637	2.551941
C	3.533440	-0.615058	3.180559
C	3.747067	-1.683483	2.103210
N	3.711249	-3.055017	2.606520
C	1.668873	3.268703	2.169807
O	1.627541	3.279690	0.935424
N	0.584140	3.232941	2.966853
C	-0.797035	3.066829	2.526773
C	-1.575529	4.391275	2.576998
C	-1.433173	2.043591	3.493377
O	-0.889300	1.802788	4.574614
N	-2.596075	1.513453	3.092449
C	-3.409765	0.669269	3.960675
C	-2.966918	-0.801094	3.915921
C	-4.909691	0.811013	3.611617
O	-5.697309	0.255627	4.414963
O	-5.227271	1.457928	2.577954
N	5.874315	-1.912656	-2.318316
C	4.898166	-2.584774	-1.463710
C	5.437549	-3.885356	-0.861526
O	4.694154	-4.710409	-0.316529
N	6.770488	-4.035115	-0.977774
C	7.483865	-5.263244	-0.685175
C	8.695002	-5.139548	0.247614
O	9.654185	-5.873719	0.089437
N	8.607644	-4.213189	1.244246
C	9.681477	-4.063290	2.220667
C	9.483781	-4.922074	3.485360
O	10.303413	-5.744349	3.852824
N	8.307900	-4.685622	4.131968
C	7.805234	-5.530875	5.202300
C	6.281917	-5.665519	5.086296
O	5.554574	-5.606936	6.056296
N	5.815597	-5.815850	3.793468
C	4.565761	-5.178467	3.429926
C	4.811316	-3.721913	2.984045
O	5.946324	-3.229152	2.986175
H	-3.283547	1.030952	4.983485

Atoms	X	Y	Z
H	-1.928255	-0.885933	4.241919
H	-3.599738	-1.392322	4.579649
H	-3.049196	-1.196564	2.899422
H	-2.993874	1.771519	2.192341
H	-0.804855	2.677848	1.510176
H	-1.074736	5.154140	1.979911
H	-2.582695	4.243248	2.186115
H	-1.649667	4.753038	3.606015
H	0.700272	3.000573	3.950283
H	3.785384	3.486460	2.192051
H	2.178306	4.954354	3.944241
H	2.976515	6.106578	5.844898
H	4.060632	6.946098	4.722270
H	4.738400	6.086432	6.120802
H	4.202607	1.997479	4.158621
H	2.474000	1.670188	4.282702
H	2.555797	0.782910	1.879548
H	4.299386	0.973031	1.924649
H	4.365665	-0.650299	3.891074
H	2.620868	-0.842190	3.741862
H	2.968090	-1.603885	1.340954
H	4.716734	-1.524039	1.625890
H	2.872277	-3.597968	2.426609
H	4.063472	-5.716654	2.624021
H	3.913065	-5.191667	4.303944
H	6.535028	-5.709606	3.091354
H	8.304291	-6.501855	5.133313
H	8.005869	-5.121339	6.194986
H	7.670974	-3.974307	3.781060
H	10.609170	-4.394271	1.759523
H	9.765642	-3.008483	2.496766
H	7.764574	-3.662563	1.341218
H	6.771920	-5.963084	-0.240907
H	7.866178	-5.717409	-1.601989
H	7.212192	-3.282191	-1.503115
H	4.640373	-1.929822	-0.628856
H	3.951738	-2.837599	-1.956154
H	5.774167	-2.208259	-3.283325
H	5.754720	-0.899940	-2.302481
N	-8.364361	1.028210	4.208590
C	-9.308499	0.670146	3.167478
C	-9.075564	1.281485	1.776265
O	-9.976826	1.178452	0.949208
C	-9.574265	-0.874186	3.088566
O	-9.724781	-1.392786	4.400092
C	-8.543692	-1.649603	2.280649

Atoms	X	Y	Z
C	-7.300685	-1.999521	2.815107
C	-8.834408	-2.001857	0.961586
C	-6.338282	-2.602012	2.016244
C	-7.874066	-2.623063	0.170578
Cl	-8.258933	-3.039610	-1.493352
C	-6.604470	-2.886965	0.680482
O	-5.591157	-3.373251	-0.133096
N	-7.911711	1.948461	1.537585
C	-7.796805	2.763859	0.339937
C	-6.613365	2.503521	-0.606961
O	-6.615561	3.081728	-1.694392
C	-7.903797	4.288101	0.634535
C	-6.683016	4.887538	1.326207
O	-6.633467	5.077158	2.530399
N	-5.655097	5.213698	0.486821
H	-4.774232	5.469660	0.905604
H	-5.662110	4.919018	-0.478677
N	-5.628125	1.655176	-0.227692
C	-4.549617	1.359762	-1.157818
C	-3.319666	2.260911	-0.910300
O	-2.807011	2.364178	0.197940
C	-4.145943	-0.120187	-1.113923
C	-5.043194	-1.061343	-0.624988
C	-2.907045	-0.545631	-1.595802
C	-4.724460	-2.419850	-0.622024
C	-2.578222	-1.898064	-1.564427
C	-3.488109	-2.858758	-1.108578
O	-3.150297	-4.198783	-1.066159
N	-2.820288	2.876247	-2.010298
C	-1.452700	3.382561	-2.051059
C	-0.892287	2.999181	-3.444832
O	-1.665506	2.877124	-4.388659
C	-1.237730	4.887395	-1.889596
C	-0.282324	5.334929	-0.978495
C	0.194949	6.651854	-0.979145
C	-1.395763	7.143226	-2.755259
C	-1.804783	5.818361	-2.770147
C	-0.373562	7.556982	-1.892358
O	0.041797	8.849236	-1.972899
N	0.448056	2.864408	-3.584856
C	1.481122	3.001303	-2.574959
C	2.164028	4.381606	-2.749915
O	2.154845	4.936567	-3.839227
C	2.456403	1.791582	-2.603770
O	3.206579	1.863055	-3.808321
C	1.636476	0.518491	-2.453833

Atoms	X	Y	Z
C	1.106741	-0.153352	-3.557136
C	1.242260	0.126662	-1.173575
C	0.136624	-1.135372	-3.384327
C	0.280539	-0.861948	-0.998919
Cl	-0.213586	-1.297771	0.620679
C	-0.317326	-1.465810	-2.111085
O	-1.343513	-2.380220	-1.982709
N	2.647666	4.914822	-1.613630
C	3.187760	6.269456	-1.563921
C	4.758734	6.318862	-1.797833
C	2.671587	6.962632	-0.296044
C	3.580353	7.433694	0.651274
C	1.280861	7.103602	-0.043328
C	3.141855	8.023117	1.834647
O	4.032167	8.487354	2.771678
C	0.872849	7.698981	1.168574
O	-0.450320	7.849726	1.476471
C	1.788070	8.153961	2.113869
O	5.273735	7.439134	-1.695579
O	5.284439	5.215574	-2.099666
C	-3.224911	-4.865091	-2.297742
C	-2.766870	-6.314708	-2.126587
O	-1.364020	-6.394773	-1.871258
C	-3.023674	-7.091641	-3.430031
O	-2.706104	-8.468634	-3.274499
C	-4.456672	-6.956583	-3.930584
O	-4.642454	-7.562933	-5.206136
C	-4.835176	-5.466174	-3.973714
O	-4.581800	-4.857491	-2.709345
C	-6.313997	-5.236252	-4.268736
O	-7.149007	-5.757122	-3.251749
H	-2.607389	-4.348955	-3.048301
H	-6.479501	-4.160497	-4.410595
H	-6.569400	-5.757804	-5.192643
C	-0.956698	-7.202899	-0.766365
C	0.485196	-7.657481	-1.006770
C	1.553269	-6.569395	-0.760233
N	2.890152	-7.208360	-0.801771
C	1.555981	-5.535319	-1.900112
C	1.227056	-5.914250	0.612228
C	-0.233962	-5.436357	0.697001
O	-1.110765	-6.560558	0.466653
C	-0.604960	-4.892247	2.064840
H	-1.620349	-8.071087	-0.706359
H	0.595390	-8.042623	-2.023861
H	0.659817	-8.492121	-0.322371

Atoms	X	Y	Z
H	2.312284	-4.768601	-1.721543
H	0.588981	-5.052519	-2.015162
H	1.802044	-6.043247	-2.835918
H	-1.656906	-4.602668	2.069046
H	-0.000741	-4.016547	2.301902
H	-0.450951	-5.653316	2.835537
O	2.086052	-4.816585	0.928495
H	3.578161	-6.563835	-0.468258
H	2.888230	-8.023341	-0.222287
C	4.333910	0.993278	-3.894025
C	5.148140	1.356240	-5.130882
C	6.014659	2.648585	-5.035890
N	7.069680	2.627379	-6.070709
C	5.182978	3.909004	-5.287692
C	6.732443	2.686663	-3.646394
C	5.812337	2.280120	-2.477941
O	5.132111	1.010919	-2.735370
C	6.576588	2.097410	-1.179406
H	3.974190	-0.042160	-3.955660
H	4.484624	1.419071	-5.999862
H	5.822337	0.508156	-5.302163
H	5.838329	4.778107	-5.253831
H	4.381962	4.044913	-4.566603
H	4.726297	3.853789	-6.283414
H	5.893984	1.844046	-0.363914
H	7.084400	3.027985	-0.930509
H	7.323098	1.301363	-1.274029
O	7.339373	3.922719	-3.361277
H	-7.449771	1.115119	3.813659
H	-8.634637	1.899409	4.618424
H	-10.255776	1.107982	3.491155
H	-9.140712	-0.874018	4.969470
H	-10.538575	-0.986809	2.590194
H	-7.049611	-1.744533	3.835316
H	-5.349347	-2.816766	2.402625
H	-9.795696	-1.753158	0.530206
H	-5.996983	-0.735619	-0.241063
H	-2.185959	0.164843	-1.973521
H	-4.949116	1.589079	-2.149055
H	-5.502643	1.417305	0.762730
H	-8.671607	2.504607	-0.260070
H	-7.145482	1.927546	2.213007
H	-8.073174	4.791359	-0.319436
H	-8.763709	4.451055	1.283052
H	-6.951658	-5.264563	-2.444903
H	-4.235961	-4.971956	-4.759576

Atoms	X	Y	Z
H	-5.142089	-7.469945	-3.253412
H	-3.894699	-7.319444	-5.762252
H	-1.757383	-8.517067	-3.118884
H	-2.360607	-6.646057	-4.193599
H	-3.337812	-6.747964	-1.300014
H	-0.422412	-4.673306	-0.062636
H	1.343356	-6.688060	1.384883
H	2.906827	-4.847770	0.407164
H	-3.229997	2.709617	-2.922517
H	1.636946	0.638177	-0.303550
H	1.408525	0.139457	-4.554542
H	-0.327464	-1.620358	-4.234738
H	3.125520	1.890450	-1.745451
H	5.064065	3.063135	-2.344313
H	7.544858	1.944037	-3.698640
H	6.670851	4.529593	-2.959808
H	7.614860	1.771596	-5.999745
H	6.640007	2.628946	-6.992514
H	0.775525	2.915508	-4.541496
H	1.023510	2.967560	-1.589901
H	2.602656	4.381861	-0.753254
H	2.772569	6.781879	-2.437411
H	1.442813	8.615386	3.029807
H	4.637227	7.394708	0.416329
H	4.922898	8.348414	2.430137
H	-0.971832	7.471749	0.754694
H	0.796869	8.956625	-1.375996
H	-1.815987	7.867821	-3.442241
H	-2.541677	5.495826	-3.497260
H	0.157580	4.637015	-0.276366
H	-0.915301	2.882371	-1.246347

Table S5.6. Cartesian coordinates for Vanco-PG complex

Atoms	X	Y	Z
C	2.034396	7.972911	3.761789
C	2.708747	6.764658	3.133183
O	3.921143	6.630815	3.102581
N	1.848650	5.843130	2.596607
C	2.323434	4.720870	1.778218
C	3.018080	3.644048	2.643051
C	3.625048	2.513937	1.807782
C	4.176192	1.358808	2.650037

Atoms	X	Y	Z
C	4.836347	0.301385	1.759025
N	5.251067	-0.905519	2.471133
C	1.138186	4.122077	1.001799
O	1.189870	3.945258	-0.219509
N	0.079278	3.807287	1.771754
C	-1.115336	3.092637	1.334626
C	-2.314385	4.038330	1.159470
C	-1.418891	2.053853	2.436802
O	-0.909083	2.179543	3.553564
N	-2.283972	1.088214	2.100191
C	-2.808991	0.136439	3.073348
C	-1.871386	-1.064541	3.269883
C	-4.230398	-0.324809	2.675144
O	-4.828609	-1.010014	3.539319
O	-4.676998	0.012377	1.546131
N	7.237008	0.244622	-2.525973
C	6.500607	-0.609310	-1.596739
C	7.418637	-1.528717	-0.786194
O	6.976978	-2.482432	-0.133712
N	8.722746	-1.200163	-0.849610
C	9.800818	-2.032909	-0.352501
C	10.814464	-1.350292	0.574216
O	11.980759	-1.701564	0.553623
N	10.328517	-0.389316	1.410534
C	11.201593	0.273801	2.373343
C	11.225557	-0.413089	3.753071
O	12.252988	-0.822872	4.262412
N	9.996629	-0.530969	4.329739
C	9.746416	-1.342924	5.509087
C	8.383479	-2.034903	5.384007
O	7.610966	-2.109203	6.317315
N	8.100800	-2.522465	4.121536
C	6.737754	-2.438354	3.636211
C	6.483950	-1.069127	2.971789
O	7.366694	-0.203599	2.919966
H	-2.897625	0.657992	4.028864
H	-0.898243	-0.721123	3.626747
H	-2.301988	-1.746165	4.005081
H	-1.730303	-1.600439	2.326832
H	-2.677588	1.056575	1.162587
H	-0.907162	2.589673	0.392008
H	-2.072771	4.839606	0.460294
H	-3.170635	3.482662	0.775863
H	-2.590226	4.488255	2.116927
H	0.194950	3.772202	2.781707
H	3.031573	5.092440	1.033587

Atoms	X	Y	Z
H	0.879770	6.107357	2.498944
H	1.070034	7.723188	4.210711
H	1.868104	8.733166	2.992751
H	2.698000	8.381191	4.523004
H	3.798582	4.145240	3.218318
H	2.294368	3.234806	3.356327
H	2.868489	2.111876	1.125069
H	4.422421	2.924887	1.176002
H	4.910057	1.726738	3.374428
H	3.363565	0.897155	3.220957
H	4.140314	-0.013587	0.977676
H	5.719787	0.733035	1.282869
H	4.675544	-1.734851	2.361502
H	6.522007	-3.228568	2.914797
H	6.067580	-2.565148	4.487612
H	8.787057	-2.261798	3.426599
H	10.561126	-2.066672	5.604247
H	9.712454	-0.754512	6.428880
H	9.177550	-0.154971	3.858023
H	12.218632	0.240508	1.989495
H	10.884852	1.314897	2.481625
H	9.340191	-0.173677	1.402016
H	9.351733	-2.873866	0.181472
H	10.388060	-2.440745	-1.178209
H	8.907352	-0.419454	-1.477617
H	5.964433	0.017261	-0.880968
H	5.745869	-1.253713	-2.062853
H	7.322092	-0.198534	-3.434282
H	6.765157	1.136866	-2.672271
N	-8.012895	0.456400	6.284260
C	-7.527766	0.464606	4.902254
C	-8.313001	-0.528345	4.024560
O	-9.534322	-0.590067	4.107663
C	-7.712199	1.864451	4.281919
C	-6.903061	2.992008	4.946733
C	-7.372271	4.351057	4.405559
C	-5.393310	2.821876	4.729191
H	-4.835502	3.642946	5.191204
H	-5.157514	2.812237	3.660132
H	-5.021374	1.889832	5.161237
H	-6.813291	5.173696	4.864462
H	-8.435963	4.512827	4.609839
H	-7.229451	4.402953	3.321709
C	-7.702940	-0.773155	7.008667
N	-7.572254	-1.292697	3.158347
C	-8.245706	-2.109704	2.167144

Atoms	X	Y	Z
C	-8.139422	-1.655731	0.702193
O	-8.879693	-2.192342	-0.116929
C	-7.939597	-3.640265	2.326832
O	-7.995896	-3.990016	3.700224
C	-6.642617	-4.094217	1.672727
C	-5.400924	-3.892051	2.281399
C	-6.688036	-4.707932	0.419805
C	-4.229494	-4.210057	1.607587
C	-5.512487	-5.042838	-0.243348
Cl	-5.596550	-5.797956	-1.828601
C	-4.274653	-4.755189	0.328092
O	-3.095877	-4.949707	-0.377482
N	-7.273232	-0.652745	0.385790
C	-7.364068	-0.026486	-0.922638
C	-6.096733	0.030281	-1.791868
O	-6.220967	0.410880	-2.956576
C	-8.026856	1.380602	-0.873983
C	-7.154582	2.471578	-0.260022
O	-7.267460	2.832054	0.900066
N	-6.248391	3.027534	-1.118683
H	-5.550247	3.640819	-0.727155
H	-6.076807	2.618892	-2.025680
N	-4.906630	-0.341902	-1.263317
C	-3.725915	-0.353130	-2.112652
C	-2.918251	0.957356	-1.984518
O	-2.561631	1.392608	-0.895916
C	-2.828171	-1.564783	-1.827900
C	-3.367751	-2.689038	-1.215695
C	-1.486043	-1.575310	-2.210862
C	-2.589113	-3.825231	-0.992244
C	-0.702324	-2.698293	-1.960107
C	-1.244226	-3.849741	-1.377755
O	-0.457374	-4.956494	-1.117863
N	-2.587293	1.552086	-3.157025
C	-1.489350	2.508366	-3.248481
C	-0.724891	2.163822	-4.552527
O	-1.330192	1.639786	-5.481274
C	-1.835078	3.995628	-3.321506
C	-1.172949	4.881061	-2.472515
C	-1.195237	6.267556	-2.670545
C	-2.716468	5.896837	-4.534631
C	-2.626576	4.525580	-4.349270
C	-1.976440	6.768616	-3.726519
O	-2.041583	8.098819	-4.000832
N	0.582615	2.505556	-4.641622
C	1.419761	3.146585	-3.644564

Atoms	X	Y	Z
C	1.579905	4.641685	-4.020380
O	1.457549	4.998067	-5.183431
C	2.759867	2.380884	-3.462226
O	3.525408	2.550641	-4.647109
C	2.435918	0.931482	-3.130847
C	2.264671	-0.033287	-4.125413
C	2.109942	0.605946	-1.813363
C	1.695782	-1.265638	-3.820408
C	1.551073	-0.629180	-1.505322
Cl	1.121730	-0.984172	0.152040
C	1.292901	-1.557207	-2.520762
O	0.651168	-2.753745	-2.271438
N	1.754851	5.466592	-2.972385
C	1.773890	6.917609	-3.125323
C	3.238145	7.499540	-3.331304
C	0.950373	7.546155	-1.993427
C	1.557933	8.441427	-1.113355
C	-0.414871	7.207584	-1.795096
C	0.850041	8.990709	-0.046938
O	1.443610	9.871573	0.823668
C	-1.098642	7.777373	-0.700814
O	-2.408606	7.479968	-0.448133
C	-0.479208	8.659879	0.179927
O	3.312920	8.732795	-3.395990
O	4.142366	6.631063	-3.444650
C	-0.196691	-5.769196	-2.230468
C	0.731258	-6.915472	-1.823713
O	2.047469	-6.445596	-1.529783
C	0.866878	-7.906128	-2.993648
O	1.639357	-9.038525	-2.616679
C	-0.478240	-8.370404	-3.538977
O	-0.339066	-9.174236	-4.706750
C	-1.356297	-7.139889	-3.824096
O	-1.432457	-6.310983	-2.666323
C	-2.793431	-7.504696	-4.182392
O	-3.464333	-8.145491	-3.113709
H	0.252910	-5.174418	-3.039892
H	-3.318402	-6.592951	-4.495265
H	-2.776017	-8.206600	-5.017784
C	2.629446	-6.888932	-0.303193
C	4.152669	-6.819149	-0.438928
C	4.743253	-5.395142	-0.344567
N	6.218857	-5.505620	-0.257118
C	4.465901	-4.599929	-1.632727
C	4.102271	-4.718275	0.900532
C	2.564824	-4.795183	0.878542

Atoms	X	Y	Z
O	2.164054	-6.180944	0.809836
C	1.921842	-4.237514	2.135625
H	2.314369	-7.921090	-0.121093
H	4.469493	-7.275901	-1.380178
H	4.559257	-7.429786	0.371829
H	4.885123	-3.594494	-1.561373
H	3.402308	-4.521227	-1.842481
H	4.946692	-5.109309	-2.471560
H	0.838532	-4.351043	2.072263
H	2.156227	-3.178571	2.244402
H	2.276550	-4.775788	3.019573
O	4.489311	-3.351450	1.057872
H	6.605966	-4.615950	-0.014973
H	6.461955	-6.176697	0.443281
H	-7.103826	2.951865	6.023247
H	-7.466925	1.829952	3.215495
H	-8.781447	2.103378	4.338476
H	-6.471253	0.186704	4.903158
H	-8.098505	-0.703644	8.026236
H	-8.112529	-1.690393	6.551271
H	-6.617919	-0.889720	7.080905
H	-9.023660	0.562661	6.238404
H	-6.539309	-1.199822	3.187809
H	-9.308416	-2.004175	2.398039
H	-7.679021	-3.221033	4.192875
H	-8.760274	-4.162755	1.832419
H	-5.335166	-3.423973	3.253748
H	-3.261215	-3.995972	2.043485
H	-7.639160	-4.886988	-0.065289
H	-4.401357	-2.680800	-0.907801
H	-1.037285	-0.711969	-2.680616
H	-4.103971	-0.424578	-3.135738
H	-4.780826	-0.377698	-0.245399
H	-8.041581	-0.665856	-1.492446
H	-6.603273	-0.300402	1.071902
H	-8.290472	1.650167	-1.898610
H	-8.935418	1.309689	-0.277274
H	-3.516639	-7.507643	-2.390538
H	-0.913291	-6.576860	-4.665305
H	-0.986499	-8.997440	-2.803861
H	0.313777	-8.756479	-5.278558
H	2.528761	-8.717867	-2.435642
H	1.384936	-7.361689	-3.803858
H	0.289873	-7.406404	-0.951318
H	2.176476	-4.266016	0.004484
H	4.426208	-5.281676	1.787633

Atoms	X	Y	Z
H	5.304970	-3.155549	0.565173
H	-2.840450	1.123032	-4.039972
H	2.229989	1.341539	-1.026686
H	2.518072	0.206918	-5.149972
H	1.500155	-1.999185	-4.593343
H	3.282902	2.833932	-2.616421
H	2.976149	2.943541	-5.329417
H	0.942574	2.537977	-5.587341
H	0.930203	3.086985	-2.676232
H	1.836355	5.078962	-2.039958
H	1.271822	7.117805	-4.077055
H	-1.034427	9.087706	1.004399
H	2.574544	8.755548	-1.317155
H	2.348973	10.018548	0.526899
H	-2.705505	6.842168	-1.112111
H	-1.421543	8.554431	-3.412675
H	-3.312699	6.316739	-5.335732
H	-3.143441	3.860126	-5.031733
H	-0.568997	4.494987	-1.660251
H	-0.872496	2.354125	-2.364033

Table S5.7. Cartesian coordinates for Des-Vanco-PG complex

Atoms	X	Y	Z
C	3.122686	7.575430	4.131396
C	3.536587	6.333278	3.359702
O	4.703884	6.057263	3.136123
N	2.495984	5.553686	2.928104
C	2.696790	4.431556	2.003361
C	3.370216	3.231432	2.707786
C	3.697123	2.086669	1.745558
C	4.216511	0.827404	2.446961
C	4.596490	-0.248478	1.424245
N	4.956094	-1.535252	2.016365
C	1.342555	4.024541	1.397905
O	1.188465	3.913275	0.177493
N	0.379120	3.795042	2.310227
C	-0.948377	3.254821	2.036691
C	-2.030136	4.345723	2.086325
C	-1.213524	2.198238	3.131834
O	-0.530940	2.197629	4.159909
N	-2.234771	1.364033	2.896703
C	-2.725287	0.427610	3.902218

Atoms	X	Y	Z
C	-1.929148	-0.886255	3.904453
C	-4.237166	0.163457	3.712062
O	-4.781847	-0.493733	4.631619
O	-4.800779	0.615983	2.679892
N	6.303749	-0.345874	-3.180467
C	5.611829	-1.157495	-2.181728
C	6.516205	-2.225217	-1.559516
O	6.059318	-3.155115	-0.883562
N	7.827294	-2.052020	-1.811932
C	8.852833	-3.034993	-1.520632
C	10.071882	-2.532993	-0.736946
O	11.167838	-3.019569	-0.951853
N	9.842312	-1.570413	0.201022
C	10.926428	-1.072989	1.041408
C	11.068591	-1.835942	2.373224
O	12.100043	-2.394338	2.700735
N	9.934605	-1.838818	3.128720
C	9.762108	-2.681399	4.300489
C	8.319013	-3.196931	4.361986
O	7.691360	-3.231735	5.400350
N	7.791418	-3.573804	3.140893
C	6.393063	-3.299405	2.876661
C	6.218997	-1.873745	2.312878
O	7.186863	-1.118561	2.157982
H	-2.603299	0.900252	4.879261
H	-0.877979	-0.682860	4.118859
H	-2.328270	-1.552547	4.670809
H	-1.999667	-1.380110	2.931020
H	-2.764724	1.433660	2.031060
H	-0.948856	2.785554	1.054537
H	-1.795754	5.151159	1.389470
H	-2.997642	3.919503	1.819207
H	-2.100535	4.769668	3.091590
H	0.638842	3.688392	3.287870
H	3.327257	4.757862	1.172677
H	1.564901	5.937153	2.992281
H	2.212311	7.417551	4.714644
H	2.941435	8.393046	3.427327
H	3.938919	7.856930	4.795497
H	4.285130	3.601713	3.173761
H	2.715011	2.871453	3.508488
H	2.802246	1.817949	1.173617
H	4.436941	2.434841	1.013934
H	5.091019	1.062617	3.062252
H	3.446206	0.434300	3.118926
H	3.757307	-0.432457	0.748894

Atoms	X	Y	Z
H	5.446564	0.100968	0.833677
H	4.269987	-2.282057	1.965584
H	5.973404	-4.015349	2.167624
H	5.846866	-3.393781	3.816266
H	8.393752	-3.357655	2.358393
H	10.483247	-3.501722	4.240095
H	9.940870	-2.146980	5.236353
H	9.108785	-1.341008	2.804703
H	11.862207	-1.205664	0.503328
H	10.764289	-0.009420	1.237527
H	8.899292	-1.237899	0.354345
H	8.385305	-3.845435	-0.956171
H	9.253606	-3.462065	-2.442570
H	8.013785	-1.264235	-2.430475
H	5.272519	-0.513423	-1.367824
H	4.720274	-1.679075	-2.549465
H	6.195289	-0.743102	-4.107343
H	5.932595	0.603354	-3.217298
N	-7.565048	-0.423629	4.670617
C	-8.477206	-1.095844	3.765291
C	-8.533966	-0.574439	2.320167
O	-9.450330	-0.970629	1.605868
C	-8.347692	-2.658670	3.816510
O	-8.242339	-3.077498	5.167504
C	-7.231197	-3.226258	2.952007
C	-5.897051	-3.209477	3.367852
C	-7.540740	-3.757114	1.698652
C	-4.889337	-3.626163	2.508617
C	-6.529544	-4.191656	0.848649
Cl	-6.944557	-4.838943	-0.732199
C	-5.193877	-4.087547	1.231631
O	-4.168009	-4.380893	0.344654
N	-7.604359	0.334171	1.911955
C	-7.809159	1.040938	0.658570
C	-6.688946	0.995455	-0.394036
O	-6.936259	1.454475	-1.509818
C	-8.273023	2.512103	0.863634
C	-7.187396	3.453739	1.376250
O	-7.079114	3.757879	2.552798
N	-6.356311	3.945645	0.409352
H	-5.535339	4.447442	0.711051
H	-6.375368	3.572197	-0.528330
N	-5.490333	0.453750	-0.071369
C	-4.460731	0.350100	-1.093504
C	-3.483085	1.544950	-1.041984
O	-2.915583	1.871116	-0.006015

Atoms	X	Y	Z
C	-3.691868	-0.974641	-0.998411
C	-4.272458	-2.059535	-0.353577
C	-2.434282	-1.123714	-1.585209
C	-3.619952	-3.291705	-0.297601
C	-1.771039	-2.344968	-1.502562
C	-2.361818	-3.454821	-0.887882
O	-1.692076	-4.660889	-0.796076
N	-3.257992	2.162171	-2.227894
C	-2.073487	2.983824	-2.451831
C	-1.562293	2.625758	-3.871026
O	-2.361072	2.232175	-4.714007
C	-2.234418	4.503497	-2.413017
C	-1.345895	5.253058	-1.643682
C	-1.221126	6.641324	-1.782354
C	-3.038197	6.563074	-3.400539
C	-3.096629	5.182546	-3.284281
C	-2.081123	7.292127	-2.684175
O	-2.016917	8.634112	-2.893661
N	-0.250030	2.813087	-4.148811
C	0.801159	3.290952	-3.269889
C	1.092084	4.775241	-3.608202
O	0.843782	5.209939	-4.723572
C	2.045182	2.361152	-3.327408
O	2.640577	2.505857	-4.609353
C	1.592803	0.944316	-3.005771
C	1.153828	0.065730	-3.998069
C	1.428443	0.584979	-1.667167
C	0.484906	-1.105144	-3.656088
C	0.769448	-0.590020	-1.323852
Cl	0.550715	-0.985707	0.365168
C	0.246786	-1.420584	-2.321846
O	-0.497326	-2.544044	-2.022144
N	1.524889	5.511690	-2.569120
C	1.705114	6.956369	-2.667214
C	3.184160	7.369724	-3.075474
C	1.146400	7.612884	-1.397857
C	1.987302	8.376942	-0.588990
C	-0.205774	7.429325	-1.003156
C	1.522124	8.944818	0.594732
O	2.346063	9.696815	1.395872
C	-0.640533	8.013037	0.205116
O	-1.925155	7.860539	0.646468
C	0.210490	8.762982	1.012308
O	3.404541	8.586827	-3.103483
O	3.943559	6.407219	-3.361154
C	-1.705798	-5.433670	-1.966098

Atoms	X	Y	Z
C	-0.880798	-6.704238	-1.752746
O	0.513458	-6.412952	-1.648859
C	-1.048327	-7.635135	-2.966791
O	-0.378462	-8.871626	-2.758171
C	-2.507742	-7.902966	-3.314137
O	-2.647724	-8.649243	-4.519411
C	-3.254959	-6.561866	-3.411924
O	-3.051493	-5.797706	-2.225339
C	-4.764047	-6.730842	-3.556533
O	-5.343840	-7.347066	-2.422108
H	-1.310162	-4.851464	-2.812015
H	-5.209677	-5.746357	-3.748797
H	-4.960860	-7.380617	-4.410880
C	1.210898	-6.992498	-0.545467
C	2.693173	-7.097853	-0.913246
C	3.467335	-5.762563	-0.856996
N	4.913324	-6.053707	-1.004006
C	3.104134	-4.867178	-2.054916
C	3.110653	-5.086508	0.497628
C	1.589981	-4.977450	0.711647
O	1.010639	-6.299026	0.652724
C	1.217980	-4.419987	2.073824
H	0.797957	-7.988269	-0.356511
H	2.805312	-7.534401	-1.909139
H	3.135297	-7.798333	-0.199543
H	3.653635	-3.924922	-2.010878
H	2.039868	-4.649816	-2.093822
H	3.385658	-5.381398	-2.977191
H	0.131804	-4.399206	2.175091
H	1.598616	-3.404724	2.185558
H	1.629350	-5.046741	2.870614
O	3.687354	-3.787150	0.645447
H	5.442118	-5.232161	-0.790844
H	5.170977	-6.788183	-0.376185
H	-6.742128	-0.150286	4.172534
H	-8.009736	0.387585	5.050333
H	-9.471422	-0.877318	4.162256
H	-7.760360	-2.381556	5.634206
H	-9.292639	-3.049897	3.435766
H	-5.627949	-2.809282	4.335484
H	-3.847575	-3.554915	2.796819
H	-8.568572	-3.792870	1.360573
H	-5.239004	-1.945346	0.111134
H	-1.954643	-0.294738	-2.085365
H	-4.993244	0.383319	-2.047476
H	-5.219577	0.344726	0.912535

Atoms	X	Y	Z
H	-8.639826	0.521061	0.176678
H	-6.800212	0.563783	2.498782
H	-8.650213	2.869708	-0.096504
H	-9.083899	2.516281	1.590985
H	-5.206133	-6.750156	-1.675584
H	-2.874568	-6.008512	-4.289415
H	-2.976090	-8.505855	-2.533705
H	-2.039814	-8.280470	-5.169136
H	0.561454	-8.670665	-2.705204
H	-0.592075	-7.110971	-3.826049
H	-1.245782	-7.188119	-0.841948
H	1.145941	-4.356264	-0.070508
H	3.489128	-5.734665	1.301341
H	4.438537	-3.662302	0.040000
H	-3.692553	1.817949	-3.076681
H	1.757060	1.254491	-0.880951
H	1.279903	0.332347	-5.039534
H	0.084488	-1.764370	-4.416926
H	2.741889	2.698987	-2.556260
H	2.050055	3.000225	-5.182488
H	-0.034100	2.856474	-5.136990
H	0.458066	3.234838	-2.240314
H	1.694736	5.064161	-1.676264
H	1.096163	7.269571	-3.521046
H	-0.156525	9.206105	1.928824
H	2.993684	8.578312	-0.935905
H	3.208239	9.751174	0.968024
H	-2.396451	7.302073	0.012590
H	-1.263219	8.977682	-2.391806
H	-3.689079	7.096651	-4.082607
H	-3.789895	4.624061	-3.903321
H	-0.681476	4.751443	-0.950491
H	-1.356181	2.706297	-1.680468

BIBLIOGRAPHY

1. Grundmann, H.; Aires-de-Sousa, M.; Boyce, J.; Tiemersma, E., Emergence and resurgence of meticillin-resistant Staphylococcus aureus as a public-health threat. *Lancet* **2006,** *368* (9538), 874-85.

2. Hubbard, B. K.; Walsh, C. T., Vancomycin assembly: nature's way. *Angew Chem Int Ed Engl* **2003,** *42* (7), 730-65.

3. Boucher, H. W.; Corey, G. R., Epidemiology of methicillin-resistant Staphylococcus aureus. *Clin Infect Dis* **2008,** *46 Suppl 5*, S344-9.

4. Gorwitz, R. J.; Kruszon-Moran, D.; McAllister, S. K.; McQuillan, G.; McDougal, L. K.; Fosheim, G. E.; Jensen, B. J.; Killgore, G.; Tenover, F. C.; Kuehnert, M. J., Changes in the prevalence of nasal colonization with Staphylococcus aureus in the United States, 2001-2004. *J Infect Dis* **2008,** *197* (9), 1226-34.

5. Kluytmans, J.; van Belkum, A.; Verbrugh, H., Nasal carriage of Staphylococcus aureus: epidemiology, underlying mechanisms, and associated risks. *Clin Microbiol Rev* **1997,** *10* (3), 505-20.

6. Levy, S. B., The challenge of antibiotic resistance. *Sci Am* **1998,** *278* (3), 46-53.

7. Darrow, J. J.; Kesselheim, A. S., Incentivizing Antibiotic Development: Why Isn't the Generating Antibiotic Incentives Now (GAIN) Act Working? *Open Forum Infect Dis* **2020,** *7* (1), ofaa001.

8. Walsh, C., Molecular mechanisms that confer antibacterial drug resistance. *Nature* **2000,** *406* (6797), 775-81.

9. Ling, L. L.; Schneider, T.; Peoples, A. J.; Spoering, A. L.; Engels, I.; Conlon, B. P.; Mueller, A.; Schäberle, T. F.; Hughes, D. E.; Epstein, S.; Jones, M.; Lazarides, L.; Steadman, V. A.; Cohen, D. R.; Felix, C. R.; Fetterman, K. A.; Millett, W. P.; Nitti, A. G.; Zullo, A. M.; Chen, C.; Lewis, K., A new antibiotic kills pathogens without detectable resistance. *Nature* **2015,** *517* (7535), 455-9.

10. Piddock, L. J., Teixobactin, the first of a new class of antibiotics discovered by iChip technology? *J Antimicrob Chemother* **2015,** *70* (10), 2679-80.

11. Walsh, C., *Antibiotics_ Actions, Origins, Resistance*. ASM Press: Washington, D.C., 2003.

12. Fischbach, M. A.; Walsh, C. T., Antibiotics for emerging pathogens. *Science* **2009,** *325* (5944), 1089-93.

13. Hamad, B., The antibiotics market. *Nat Rev Drug Discov* **2010,** *9* (9), 675-6.

14. Neidhardt, F., Ingraham, J., and Schaechter, M., *The Physiology of the Bacterial Cell*. Sinauer Associates, Inc.: Sunderland, 1990.

15. Martínez-Carmona, M.; Gun'ko, Y. K.; Vallet-Regí, M., Mesoporous Silica Materials as Drug Delivery: "The Nightmare" of Bacterial Infection. *Pharmaceutics* **2018,** *10* (4).

16. Dramsi, S.; Magnet, S.; Davison, S.; Arthur, M., Covalent attachment of proteins to peptidoglycan. *FEMS Microbiol Rev* **2008,** *32* (2), 307-20.

17. Kim, S. J.; Chang, J.; Singh, M., Peptidoglycan architecture of Gram-positive bacteria by solid-state NMR. *Biochim Biophys Acta* **2015,** *1848* (1 Pt B), 350-62.

18. Boneca, I. G.; Huang, Z. H.; Gage, D. A.; Tomasz, A., Characterization of Staphylococcus aureus cell wall glycan strands, evidence for a new beta-N-acetylglucosaminidase activity. *J Biol Chem* **2000,** *275* (14), 9910-8.

19. Vollmer, W.; Blanot, D.; de Pedro, M. A., Peptidoglycan structure and architecture. *FEMS Microbiol Rev* **2008,** *32* (2), 149-67.

20. Rogers, H. J., Ward, J. B., and Perkins, H. R. , *Microbial cell walls and membranes*. Chapman and Hall, London: New York, 1980.

21. Navarre, W. W.; Schneewind, O., Surface proteins of gram-positive bacteria and mechanisms of their targeting to the cell wall envelope. *Microbiol Mol Biol Rev* **1999,** *63* (1), 174-229.

22. van Heijenoort, J., Formation of the glycan chains in the synthesis of bacterial peptidoglycan. *Glycobiology* **2001,** *11* (3), 25r-36r.

23. Ghuysen, J., and Hakenbeck, R., *Bacterial Cell Wall*. Elsevier: 1994; Vol. 27.

24. Marraffini, L. A.; Dedent, A. C.; Schneewind, O., Sortases and the art of anchoring proteins to the envelopes of gram-positive bacteria. *Microbiol Mol Biol Rev* **2006,** *70* (1), 192-221.

25. Tomasz, A., The mechanism of the irreversible antimicrobial effects of penicillins: how the beta-lactam antibiotics kill and lyse bacteria. *Annu Rev Microbiol* **1979,** *33*, 113-37.

26. Reynolds, P. E.; Somner, E. A., Comparison of the target sites and mechanisms of action of glycopeptide and lipoglycodepsipeptide antibiotics. *Drugs Exp Clin Res* **1990,** *16* (8), 385-9.

27. Maki, H.; Miura, K.; Yamano, Y., Katanosin B and plusbacin A(3), inhibitors of peptidoglycan synthesis in methicillin-resistant Staphylococcus aureus. *Antimicrob Agents Chemother* **2001,** *45* (6), 1823-7.

28. Patti, G. J.; Kim, S. J.; Yu, T. Y.; Dietrich, E.; Tanaka, K. S.; Parr, T. R., Jr.; Far, A. R.; Schaefer, J., Vancomycin and oritavancin have different modes of action in Enterococcus faecium. *J Mol Biol* **2009,** *392* (5), 1178-91.

29. Karplus, M.; McCammon, J. A., Molecular dynamics simulations of biomolecules. *Nat Struct Biol* **2002,** *9* (9), 646-52.

30. Hollingsworth, S. A.; Dror, R. O., Molecular Dynamics Simulation for All. *Neuron* **2018,** *99* (6), 1129-1143.

31. Lin, F. Y.; MacKerell, A. D., Jr., Force Fields for Small Molecules. *Methods Mol Biol* **2019,** *2022*, 21-54.

32. Guvench, O.; Mallajosyula, S. S.; Raman, E. P.; Hatcher, E.; Vanommeslaeghe, K.; Foster, T. J.; Jamison, F. W., 2nd; Mackerell, A. D., Jr., CHARMM additive all-atom force field for carbohydrate derivatives and its utility in polysaccharide and carbohydrate-protein modeling. *J Chem Theory Comput* **2011,** *7* (10), 3162-3180.

33. Vanommeslaeghe, K.; Raman, E. P.; MacKerell, A. D., Jr., Automation of the CHARMM General Force Field (CGenFF) II: assignment of bonded parameters and partial atomic charges. *J Chem Inf Model* **2012,** *52* (12), 3155-68.

34. Gavezzotti, A., *Molecular Aggregation: Structure Analysis and Molecular Simulation of Crystals and Liquids*. Oxford University Press: New York, USA, 2006.

35. Hess, B.; Kutzner, C.; van der Spoel, D.; Lindahl, E., GROMACS 4: Algorithms for Highly Efficient, Load-Balanced, and Scalable Molecular Simulation. *J Chem Theory Comput* **2008,** *4* (3), 435-47.

36. Berendsen, H. J. C.; Postma, J. P. M.; van Gunsteren, W. F.; DiNola, A.; Haak, J. R., Molecular dynamics with coupling to an external bath. *The Journal of Chemical Physics* **1984,** *81* (8), 3684-3690.

37. Nosé, S., A molecular dynamics method for simulations in the canonical ensemble. *Molecular Physics* **2006,** *52* (2), 255-268.

38. Hoover, W. G., Canonical dynamics: Equilibrium phase-space distributions. *Phys Rev A Gen Phys* **1985,** *31* (3), 1695-1697.

39. Bussi, G.; Donadio, D.; Parrinello, M., Canonical sampling through velocity rescaling. *J Chem Phys* **2007,** *126* (1), 014101.

40. Parrinello, M., Rahman, A., Polymorphic transitions in single crystals: A new molecular dynamics method. *J. Appl. Phys.* **1981,** *52*, 7182-7190.

41. Nosé, S.; Klein, M. L., Constant pressure molecular dynamics for molecular systems. *Molecular Physics* **2006,** *50* (5), 1055-1076.

42. Williams-Noonan, B. J.; Yuriev, E.; Chalmers, D. K., Free Energy Methods in Drug Design: Prospects of "Alchemical Perturbation" in Medicinal Chemistry. *J Med Chem* **2018,** *61* (3), 638-649.

43. Chodera, J. D.; Mobley, D. L.; Shirts, M. R.; Dixon, R. W.; Branson, K.; Pande, V. S., Alchemical free energy methods for drug discovery: progress and challenges. *Curr Opin Struct Biol* **2011,** *21* (2), 150-60.

44. Clark, A. J.; Gindin, T.; Zhang, B.; Wang, L.; Abel, R.; Murret, C. S.; Xu, F.; Bao, A.; Lu, N. J.; Zhou, T.; Kwong, P. D.; Shapiro, L.; Honig, B.; Friesner, R. A., Free Energy Perturbation Calculation of Relative Binding Free Energy between Broadly Neutralizing Antibodies and the gp120 Glycoprotein of HIV-1. *J Mol Biol* **2017,** *429* (7), 930-947.

45. Mutyala, R.; Reddy, R. N.; Sumakanth, M.; Reddanna, P.; Reddy, M. R., Calculation of relative binding affinities of fructose 1,6-bisphosphatase mutants with adenosine monophosphate using free energy perturbation method. *J Comput Chem* **2007,** *28* (5), 932-7.

46. Wu, K. W.; Chen, P. C.; Wang, J.; Sun, Y. C., Computation of relative binding free energy for an inhibitor and its analogs binding with Erk kinase using thermodynamic integration MD simulation. *J Comput Aided Mol Des* **2012,** *26* (10), 1159-69.

47. Lawrenz, M.; Baron, R.; Wang, Y.; McCammon, J. A., Independent-Trajectory Thermodynamic Integration: a practical guide to protein-drug binding free energy calculations using distributed computing. *Methods Mol Biol* **2012,** *819*, 469-86.

48. Bowman, J. D.; Lindert, S., Molecular Dynamics and Umbrella Sampling Simulations Elucidate Differences in Troponin C Isoform and Mutant Hydrophobic Patch Exposure. *J Phys Chem B* **2018,** *122* (32), 7874-7883.

49. Akhshi, P.; Wu, G., Umbrella sampling molecular dynamics simulations reveal concerted ion movement through G-quadruplex DNA channels. *Phys Chem Chem Phys* **2017,** *19* (18), 11017-11025.

50. Lemkul, J. A.; Bevan, D. R., Assessing the stability of Alzheimer's amyloid protofibrils using molecular dynamics. *J Phys Chem B* **2010,** *114* (4), 1652-60.

51. Hou, T.; Wang, J.; Li, Y.; Wang, W., Assessing the performance of the MM/PBSA and MM/GBSA methods. 1. The accuracy of binding free energy calculations based on molecular dynamics simulations. *J Chem Inf Model* **2011,** *51* (1), 69-82.

52. Srinivasan, J.; Miller, J.; Kollman, P. A.; Case, D. A., Continuum solvent studies of the stability of RNA hairpin loops and helices. *J Biomol Struct Dyn* **1998,** *16* (3), 671-82.

53. Kollman, P. A.; Massova, I.; Reyes, C.; Kuhn, B.; Huo, S.; Chong, L.; Lee, M.; Lee, T.; Duan, Y.; Wang, W.; Donini, O.; Cieplak, P.; Srinivasan, J.; Case, D. A.; Cheatham, T. E., 3rd, Calculating structures and free energies of complex molecules: combining molecular mechanics and continuum models. *Acc Chem Res* **2000,** *33* (12), 889-97.

54. Wang, E.; Sun, H.; Wang, J.; Wang, Z.; Liu, H.; Zhang, J. Z. H.; Hou, T., End-Point Binding Free Energy Calculation with MM/PBSA and MM/GBSA: Strategies and Applications in Drug Design. *Chem Rev* **2019,** *119* (16), 9478-9508.

55. Hansson, T.; Marelius, J.; Aqvist, J., Ligand binding affinity prediction by linear interaction energy methods. *J Comput Aided Mol Des* **1998,** *12* (1), 27-35.

56. Weis, A.; Katebzadeh, K.; Söderhjelm, P.; Nilsson, I.; Ryde, U., Ligand affinities predicted with the MM/PBSA method: dependence on the simulation method and the force field. *J Med Chem* **2006,** *49* (22), 6596-606.

57. Genheden, S.; Ryde, U., Comparison of end-point continuum-solvation methods for the calculation of protein-ligand binding free energies. *Proteins* **2012,** *80* (5), 1326-42.

58. G. M., T., and J. P., Valleau, Nonphysical sampling distributions in Monte Carlo free-energy estimation: Umbrella sampling. *Journal of Computational Physics* **1977,** *23*, 187-199.

59. Jarzynski, C., Nonequilibrium Equality for Free Energy Differences. *Physical Review Letters* **1997,** *78* (14), 2690 - 2693.

60. Kumar, S., Rosenberg, J. M., Bouzida, D., Swendsen, R. H., and Kollman, P. A., The Weighted Histogram Analysis Method for Free-Energy Calculations on Biomolecules. I. The Method *Journal of Computational Chemistry* **1992,** *13* (8), 1011 - 1021.

61. Walsh, G. D. W. a. C. T., D-Alanyl-D-alanine Ligases and the Molecular Mechanism of Vancomycin Resistance. *Acc. Chem .Res.* **1992,** *25*, 468-473.

62. Gokhale, R. S.; Tsuji, S. Y.; Cane, D. E.; Khosla, C., Dissecting and exploiting intermodular communication in polyketide synthases. *Science* **1999,** *284* (5413), 482-485.

63. Nagarajan, R., Structure-activity relationships of vancomycin-type glycopeptide antibiotics. *J. Antibiot.* **1993,** *46* (8), 1181-95.

64. Barna, J.; Williams, D., The structure and mode of action of glycopeptide antibiotics of the vancomycin group. *Annual Reviews in Microbiology* **1984,** *38* (1), 339-357.

65. Arthur, M.; Molinas, C.; Bugg, T. D.; Wright, G. D.; Walsh, C. T.; Courvalin, P., Evidence for in vivo incorporation of D-lactate into peptidoglycan precursors of vancomycin-resistant enterococci. *Antimicrob. Agents Chemother.* **1992,** *36* (4), 867-869.

66. Bugg, T. D.; Wright, G. D.; Dutka-Malen, S.; Arthur, M.; Courvalin, P.; Walsh, C. T., Molecular basis for vancomycin resistance in *Enterococcus faecium* BM4147: biosynthesis of a depsipeptide peptidoglycan precursor by vancomycin resistance proteins VanH and VanA. *Biochemistry* **1991,** *30* (43), 10408-10415.

67. Xing, B.; Jiang, T.; Wu, X.; Liew, R.; Zhou, J.; Zhang, D.; Yeow, E. K., Molecular interactions between glycopeptide vancomycin and bacterial cell wall peptide analogues. *Chemistry-A European Journal* **2011,** *17* (50), 14170-14177.

68. Bischoff, D.; Pelzer, S.; Höltzel, A.; Nicholson, G. J.; Stockert, S.; Wohlleben, W.; Jung, G.; Süssmuth, R. D., The Biosynthesis of Vancomycin-Type Glycopeptide Antibiotics-New Insights into the Cyclization Steps This work was supported by the Deutsche Forschungsgemeinschaft (SFB 323). We thank M. Schierle, Dr. S. Stevanovic and Prof. H.-G. Rammensee for help with Edman degradation and J. Turner, Prof. B. List and Prof. D. Boger (La Jolla, USA) for discussions on the work. *Angew Chem Int Ed Engl* **2001,** *40* (9), 1693-1696.

69. Sheldrick, G. M.; Jones, P. G.; Kennard, O.; Williams, D. H.; Smith, G. A., Structure of vancomycin and its complex with acetyl-D-alanyl-D-alanine. *Nature* **1978,** *271* (5642), 223-225.

70. Gokhale, R. S.; Tsuji, S. Y.; Cane, D. E.; Khosla, C., Dissecting and exploiting intermodular communication in polyketide synthases. *Science* **1999,** *284* (5413), 482-5.

71. Lloyd, S., Least squares quantization in PCM. *IEEE transactions on information theory* **1982,** *28* (2), 129-137.

72. Schäfer, M.; Schneider, T. R.; Sheldrick, G. M., Crystal structure of vancomycin. *Structure* **1996,** *4* (12), 1509-15.

73. Loll, P. J.; Bevivino, A. E.; Korty, B. D.; Axelsen, P. H., Simultaneous recognition of a carboxylate-containing ligand and an intramolecular aurrogate ligand in the crystal structure of an asymmetric vancomycin dimer. *J. Am. Chem. Soc.* **1997,** *119* (7), 1516-1522.

74. Batta, G.; Sztaricskai, F.; Kövér, K. E.; Rüdel, C.; Berdnikova, T. F., An NMR study of eremomycin and its derivatives. Full 1H and 13C assignment, motional behavior, dimerization and complexation with Ac-D-Ala-D-Ala. *J Antibiot (Tokyo)* **1991,** *44* (11), 1208-21.

75. Groves, P.; Searle, M. S.; Mackay, J. P.; Williams, D. H., The structure of an asymmetric dimer relevant to the mode of action of the glycopeptide antibiotics. *Structure* **1994,** *2* (8), 747-54.

76. Cristofaro, M. F.; Beauregard, D. A.; Yan, H.; Osborn, N. J.; Williams, D. H., Cooperativity between non-polar and ionic forces in the binding of bacterial cell wall analogues by vancomycin in aqueous solution. *J Antibiot (Tokyo)* **1995,** *48* (8), 805-10.

77. Jia, Z.; O'Mara, M. L.; Zuegg, J.; Cooper, M. A.; Mark, A. E., Vancomycin: ligand recognition, dimerization and super-complex formation. *FEBS J* **2013,** *280* (5), 1294-307.

78. Kim, S. J.; Cegelski, L.; Studelska, D. R.; O'Connor, R. D.; Mehta, A. K.; Schaefer, J., Rotational-echo double resonance characterization of vancomycin binding sites in *Staphylococcus aureus*. *Biochemistry* **2002,** *41* (22), 6967-6977.

79. Kim, S. J.; Cegelski, L.; Preobrazhenskaya, M.; Schaefer, J., Structures of *Staphylococcus aureus* cell-wall complexes with vancomycin, eremomycin, and chloroeremomycin derivatives by $^{13}C\{^{19}F\}$ and $^{15}N\{^{19}F\}$ rotational-echo double resonance. *Biochemistry* **2006,** *45* (16), 5235-5250.

80. Kim, S. J.; Cegelski, L.; Stueber, D.; Singh, M.; Dietrich, E.; Tanaka, K. S.; Parr, T. R.; Far, A. R.; Schaefer, J., Oritavancin exhibits dual mode of action to inhibit cell-wall biosynthesis in *Staphylococcus aureus*. *J. Mol. Biol.* **2008,** *377* (1), 281-293.

81. Kim, S. J.; Matsuoka, S.; Patti, G. J.; Schaefer, J., Vancomycin derivative with damaged D-Ala-D-Ala binding cleft binds to cross-linked peptidoglycan in the cell wall of *Staphylococcus aureus*. *Biochemistry* **2008,** *47* (12), 3822-3831.

82. Kim, S. J.; Schaefer, J., Hydrophobic side-chain length determines activity and conformational heterogeneity of a vancomycin derivative bound to the cell wall of *Staphylococcus aureus*. *Biochemistry* **2008,** *47* (38), 10155-10161.

83. Kim, S. J.; Singh, M.; Schaefer, J., Oritavancin binds to isolated protoplast membranes but not intact protoplasts of *Staphylococcus aureus*. *J. Mol. Biol.* **2009,** *391* (2), 414-425.

84. Kim, S. J.; Tanaka, K. S.; Dietrich, E.; Rafai Far, A.; Schaefer, J., Locations of the hydrophobic side chains of lipoglycopeptides bound to the peptidoglycan of *Staphylococcus aureus*. *Biochemistry* **2013,** *52* (20), 3405-3414.

85. Kim, S. J.; Singh, M.; Sharif, S.; Schaefer, J., Desleucyl-Oritavancin with a Damaged d-Ala-d-Ala Binding Site Inhibits the Transpeptidation Step of Cell-Wall Biosynthesis in Whole Cells of Staphylococcus aureus. *Biochemistry* **2017,** *56* (10), 1529-1535.

86. Chang, J.; Zhou, H.; Preobrazhenskaya, M.; Tao, P.; Kim, S. J., The carboxyl terminus of eremomycin facilitates binding to the non-d-Ala-d-Ala segment of the peptidoglycan pentapeptide stem. *Biochemistry* **2016,** *55* (24), 3383-3391.

87. Booth, P. M.; Williams, D. H., Preparation and conformational analysis of vancomycin hexapeptide and aglucovancomycin hexapeptide. *Journal of the Chemical Society, Perkin Transactions 1* **1989,** (12), 2335-2339.

88. Allen, N. E.; LeTourneau, D. L.; Hobbs, J. N., Jr.; Thompson, R. C., Hexapeptide derivatives of glycopeptide antibiotics: tools for mechanism of action studies. *Antimicrob. Agents Chemother.* **2002,** *46* (8), 2344-8.

89. Jia, Z.; O'Mara, M. L.; Zuegg, J.; Cooper, M. A.; Mark, A. E., Vancomycin: ligand recognition, dimerization and super-complex formation. *FEBS J* **2013,** *280* (5), 1294-1307.

90. Jusuf, S.; Axelsen, P. H., Synchronized conformational fluctuations and binding site desolvation during molecular recognition. *Biochemistry* **2004,** *43* (49), 15446-15452.

91. Frisch, M.; Trucks, G.; Schlegel, H. B.; Scuseria, G.; Robb, M.; Cheeseman, J.; Scalmani, G.; Barone, V.; Mennucci, B.; Petersson, G., Gaussian 09, revision a. 02, gaussian. *Inc., Wallingford, CT* **2009,** *200*.

92. Vanommeslaeghe, K.; Hatcher, E.; Acharya, C.; Kundu, S.; Zhong, S.; Shim, J.; Darian, E.; Guvench, O.; Lopes, P.; Vorobyov, I., CHARMM general force field: A force field for drug-like molecules compatible with the CHARMM all-atom additive biological force fields. *Journal of computational chemistry* **2010,** *31* (4), 671-690.

93. Jorgensen, W. L.; Chandrasekhar, J.; Madura, J. D.; Impey, R. W.; Klein, M. L., Comparison of simple potential functions for simulating liquid water. *The Journal of chemical physics* **1983,** *79* (2), 926-935.

94. Evans, D. J.; Holian, B. L., The nose–hoover thermostat. *The Journal of chemical physics* **1985,** *83* (8), 4069-4074.

95. Tobias, D. J.; Martyna, G. J.; Klein, M. L., Molecular dynamics simulations of a protein in the canonical ensemble. *The Journal of Physical Chemistry* **1993,** *97* (49), 12959-12966.

96. Brooks, B. R.; Bruccoleri, R. E.; Olafson, B. D.; States, D. J.; Swaminathan, S. a.; Karplus, M., CHARMM: a program for macromolecular energy, minimization, and dynamics calculations. *Journal of computational chemistry* **1983,** *4* (2), 187-217.

97. Singh, M.; Kim, S. J.; Sharif, S.; Preobrazhenskaya, M.; Schaefer, J., REDOR constraints on the peptidoglycan lattice architecture of *Staphylococcus aureus* and its FemA mutant. *Biochim. Biophys. Acta* **2015,** *1848* (1 Pt B), 363-368.

98. Kim, S. J.; Chang, J.; Singh, M., Peptidoglycan architecture of Gram-positive bacteria by solid-state NMR. *Biochim. Biophys. Acta* **2015,** *1848* (1 Pt B), 350-362.

99. Halgren, T. A., The representation of van der Waals (vdW) interactions in molecular mechanics force fields: potential form, combination rules, and vdW parameters. *Journal of the American Chemical Society* **1992,** *114* (20), 7827-7843.

100. Levy, R. M.; Srinivasan, A. R.; Olson, W. K.; McCammon, J. A., Quasi-harmonic Method for Studying Very Low-Frequency Modes in Proteins. *Biopolymers* **1984,** *23* (6), 1099-1112.

101. McCormick, M. H.; McGuire, J. M.; Pittenger, G. E.; Pittenger, R. C.; Stark, W. M., Vancomycin, a new antibiotic. I. Chemical and biologic properties. *Antibiotics annual* **1955,** *3*, 606-11.

102. Nagarajan, R., *Glycopeptide Antibiotics*. Marcel Dekker: New York, 1994; Vol. 63.

103. Nicolaou, K. C.; Hughes, R.; Cho, S. Y.; Winssinger, N.; Labischinski, H.; Endermann, R., Synthesis and biological evaluation of vancomycin dimers with potent activity against vancomycin-resistant bacteria: target-accelerated combinatorial synthesis. *Chemistry* **2001,** *7* (17), 3824-43.

104. van Heijenoort, J., Formation of the glycan chains in the synthesis of bacterial peptidoglycan. *Glycobiology* **2001,** *11* (3), 25R-36R.

105. Cegelski, L.; Kim, S. J.; Hing, A. W.; Studelska, D. R.; O'Connor, R. D.; Mehta, A. K.; Schaefer, J., Rotational-echo double resonance characterization of the effects of vancomycin on cell wall synthesis in Staphylococcus aureus. *Biochemistry* **2002,** *41* (43), 13053-8.

106. Müller, A.; Klöckner, A.; Schneider, T., Targeting a cell wall biosynthesis hot spot. *Nat Prod Rep* **2017,** *34* (7), 909-932.

107. Leclercq, R.; Derlot, E.; Duval, J.; Courvalin, P., Plasmid-mediated resistance to vancomycin and teicoplanin in Enterococcus faecium. *N Engl J Med* **1988,** *319* (3), 157-61.

108. Bugg, T. D.; Dutka-Malen, S.; Arthur, M.; Courvalin, P.; Walsh, C. T., Identification of vancomycin resistance protein VanA as a D-alanine:D-alanine ligase of altered substrate specificity. *Biochemistry* **1991,** *30* (8), 2017-21.

109. Derlot, E.; Courvalin, P., Mechanisms and implications of glycopeptide resistance in enterococci. *Am. J. Med.* **1991,** *91* (3B), 82S-85S.

110. Chang, S.; Sievert, D. M.; Hageman, J. C.; Boulton, M. L.; Tenover, F. C.; Downes, F. P.; Shah, S.; Rudrik, J. T.; Pupp, G. R.; Brown, W. J.; Cardo, D.; Fridkin, S. K.; Vancomycin-Resistant *Staphylococcus aureus* Investigative, T., Infection with vancomycin-resistant *Staphylococcus aureus* containing the *vanA* resistance gene. *N Engl J Med* **2003,** *348* (14), 1342-1347.

111. Perichon, B.; Courvalin, P., Synergism between beta-lactams and glycopeptides against VanA-type methicillin-resistant *Staphylococcus aureus* and heterologous expression of the vanA operon. *Antimicrob. Agents Chemother.* **2006,** *50* (11), 3622-3630.

112. Miroshnikova, O. V.; Printsevskaya, S. S.; Olsufyeva, E. N.; Pavlov, A. Y.; Nilius, A.; Hensey-Rudloff, D.; Preobrazhenskaya, M. N., Structure-activity relationships in the series of eremomycin carboxamides. *J. Antibiot.* **2000,** *53* (3), 286-293.

113. Allen, N. E.; LeTourneau, D. L.; Hobbs, J. N., Jr., The role of hydrophobic side chains as determinants of antibacterial activity of semisynthetic glycopeptide antibiotics. *J. Antibiot.* **1997,** *50* (8), 677-684.

114. McComas, C. C.; Crowley, B. M.; Boger, D. L., Partitioning the loss in vancomycin binding affinity for D-Ala-D-Lac into lost H-bond and repulsive lone pair contributions. *J Am Chem Soc* **2003,** *125* (31), 9314-5.

115. Olsufyeva, E. N.; Berdnikova, T. F.; Miroshnikova, O. V.; Reznikova, M. I.; Preobrazhenskaya, M. N., Chemical modification of antibiotic eremomycin at the asparagine side chain. *J. Antibiot.* **1999,** *52* (3), 319-24.

116. Butler, M. S.; Hansford, K. A.; Blaskovich, M. A.; Halai, R.; Cooper, M. A., Glycopeptide antibiotics: back to the future. *J Antibiot (Tokyo)* **2014,** *67* (9), 631-44.

117. Cooper, R. D.; Snyder, N. J.; Zweifel, M. J.; Staszak, M. A.; Wilkie, S. C.; Nicas, T. I.; Mullen, D. L.; Butler, T. F.; Rodriguez, M. J.; Huff, B. E.; Thompson, R. C., Reductive alkylation of glycopeptide antibiotics: synthesis and antibacterial activity. *J Antibiot (Tokyo)* **1996,** *49* (6), 575-81.

118. Vaudaux, P.; Huggler, E.; Arhin, F. F.; Moeck, G.; Renzoni, A.; Lew, D. P., Comparative activity of oritavancin against meticillin-resistant Staphylococcus aureus (MRSA) bloodstream isolates from Geneva University Hospital. *Int J Antimicrob Agents* **2009,** *34* (6), 540-3.

119. Sweeney, D.; Stoneburner, A.; Shinabarger, D. L.; Arhin, F. F.; Belley, A.; Moeck, G.; Pillar, C. M., Comparative in vitro activity of oritavancin and other agents against vancomycin-susceptible and -resistant enterococci. *J. Antimicrob. Chemother.* **2016,** *72*, 622-624.

120. McKay, G. A.; Beaulieu, S.; Arhin, F. F.; Belley, A.; Sarmiento, I.; Parr, T., Jr.; Moeck, G., Time-kill kinetics of oritavancin and comparator agents against Staphylococcus aureus, Enterococcus faecalis and Enterococcus faecium. *J Antimicrob Chemother* **2009,** *63* (6), 1191-9.

121. Singh, M.; Chang, J.; Coffman, L.; Kim, S. J., Hidden mode of action of glycopeptide antibiotics: inhibition of wall teichoic acid biosynthesis. *J. Phys. Chem. B* **2017,** *121* (16), 3925-3932.

122. Chang, J. D.; Foster, E. E.; Thadani, A. N.; Ramirez, A. J.; Kim, S. J., Inhibition of *Staphylococcus aureus* cell wall biosynthesis by desleucyl-oritavancin: a quantitative peptidoglycan composition analysis by mass spectrometry. *J. Bacteriol.* **2017,** *199* (15).

123. Patti, G. J.; Kim, S. J.; Yu, T. Y.; Dietrich, E.; Tanaka, K. S.; Parr, T. R., Jr.; Far, A. R.; Schaefer, J., Vancomycin and oritavancin have different modes of action in *Enterococcus faecium*. *J. Mol. Biol.* **2009,** *392* (5), 1178-1191.

124. James, R. C.; Pierce, J. G.; Okano, A.; Xie, J.; Boger, D. L., Redesign of glycopeptide antibiotics: back to the future. *ACS Chem Biol* **2012,** *7* (5), 797-804.

125. Xie, J.; Okano, A.; Pierce, J. G.; James, R. C.; Stamm, S.; Crane, C. M.; Boger, D. L., Total synthesis of [Psi[C(horizontal lineS)NH]Tpg4]vancomycin aglycon, [Psi[C(horizontal lineNH)NH]Tpg4]vancomycin aglycon, and related key compounds: reengineering vancomycin for dual D-Ala-D-Ala and D-Ala-D-Lac binding. *J Am Chem Soc* **2012,** *134* (2), 1284-97.

126. Xie, J.; Pierce, J. G.; James, R. C.; Okano, A.; Boger, D. L., A redesigned vancomycin engineered for dual D-Ala-D-ala And D-Ala-D-Lac binding exhibits potent antimicrobial activity against vancomycin-resistant bacteria. *J Am Chem Soc* **2011,** *133* (35), 13946-9.

127. Wang, F.; Zhou, H.; Olademehin, O. P.; Kim, S. J.; Tao, P., Insights into Key Interactions between Vancomycin and Bacterial Cell Wall Structures. *ACS Omega* **2018,** *3* (1), 37-45.

128. Williams, D. H.; Bardsley, B., The Vancomycin Group of Antibiotics and the Fight against Resistant Bacteria. *Angew Chem Int Ed Engl* **1999,** *38* (9), 1172-1193.

129. Wang, W.; Kollman, P. A., Free energy calculations on dimer stability of the HIV protease using molecular dynamics and a continuum solvent model. *J Mol Biol* **2000,** *303* (4), 567-82.

130. Nitanai, Y.; Kikuchi, T.; Kakoi, K.; Hanamaki, S.; Fujisawa, I.; Aoki, K., Crystal structures of the complexes between vancomycin and cell-wall precursor analogs. *J Mol Biol* **2009,** *385* (5), 1422-32.

131. Frisch, M. J.; Trucks, G. W.; Schlegel, H. B.; Scuseria, G. E.; Robb, M. A.; Cheeseman, J. R.; Scalmani, G.; Barone, V.; Petersson, G. A.; Nakatsuji, H.; Li, X.; Caricato, M.; Marenich, A. V.; Bloino, J.; Janesko, B. G.; Gomperts, R.; Mennucci, B.; Hratchian, H. P.; Ortiz, J. V.; Izmaylov, A. F.; Sonnenberg, J. L.; Williams; Ding, F.; Lipparini, F.; Egidi, F.; Goings, J.; Peng, B.; Petrone, A.; Henderson, T.; Ranasinghe, D.; Zakrzewski, V. G.; Gao, J.; Rega, N.; Zheng, G.; Liang, W.; Hada, M.; Ehara, M.; Toyota, K.; Fukuda, R.; Hasegawa, J.; Ishida, M.; Nakajima, T.; Honda, Y.; Kitao, O.; Nakai, H.; Vreven, T.; Throssell, K.; Montgomery Jr., J. A.; Peralta, J. E.; Ogliaro, F.; Bearpark, M. J.; Heyd, J. J.; Brothers, E. N.; Kudin, K. N.; Staroverov, V. N.; Keith, T. A.; Kobayashi, R.; Normand, J.; Raghavachari, K.; Rendell, A. P.; Burant, J. C.; Iyengar, S. S.; Tomasi, J.; Cossi, M.; Millam, J. M.; Klene, M.; Adamo, C.; Cammi, R.; Ochterski, J. W.; Martin, R. L.; Morokuma, K.; Farkas, O.; Foresman, J. B.; Fox, D. J. *Gaussian 16 Rev. C.01*, Wallingford, CT, 2016.

132. Hess, B., P-LINCS: A Parallel Linear Constraint Solver for Molecular Simulation. *J Chem Theory Comput* **2008,** *4* (1), 116-22.

133. Singh, M.; Kim, S. J.; Sharif, S.; Preobrazhenskaya, M.; Schaefer, J., REDOR constraints on the peptidoglycan lattice architecture of Staphylococcus aureus and its FemA mutant. *Biochim Biophys Acta* **2015,** *1848* (1 Pt B), 363-8.

134. Kumari, R.; Kumar, R.; Lynn, A., g_mmpbsa--a GROMACS tool for high-throughput MM-PBSA calculations. *J Chem Inf Model* **2014,** *54* (7), 1951-62.

135. Vollmerhaus, P. J.; Breukink, E.; Heck, A. J., Getting closer to the real bacterial cell wall target: biomolecular interactions of water-soluble lipid II with glycopeptide antibiotics. *Chem. Eur. J.* **2003,** *9* (7), 1556-1565.

136. Schneider, T.; Sahl, H. G., Lipid II and other bactoprenol-bound cell wall precursors as drug targets. *Curr. Opin. Investig. Drugs* **2010,** *11* (2), 157-164.

137. Chang, J.; Coffman, L.; Kim, S. J., Inhibition of d-Ala incorporation into wall teichoic acid in *Staphylococcus aureus* by desleucyl-oritavancin. *Chem. Commun.* **2017,** *53* (41), 5649-5652.

138. Billot-Klein, D.; Gutmann, L.; Sable, S.; Guittet, E.; van Heijenoort, J., Modification of peptidoglycan precursors is a common feature of the low-level vancomycin-resistant VANB-type Enterococcus D366 and of the naturally glycopeptide-resistant species *Lactobacillus casei, Pediococcus pentosaceus, Leuconostoc mesenteroides,* and *Enterococcus gallinarum*. *J. Bacteriol.* **1994,** *176* (8), 2398-2405.

139. Meziane-Cherif, D.; Stogios, P. J.; Evdokimova, E.; Savchenko, A.; Courvalin, P., Structural basis for the evolution of vancomycin resistance D,D-peptidases. *Proc. Natl. Acad. Sci. U. S. A.* **2014,** *111* (16), 5872-5877.

140. Evers, S.; Reynolds, P. E.; Courvalin, P., Sequence of the vanB and ddl genes encoding D-alanine:D-lactate and D-alanine: D-alanine ligases in vancomycin-resistant *Enterococcus faecalis* V583. *Gene* **1994,** *140* (1), 97-102.

141. Olademehin, O. P.; Kim, S. J.; Shuford, K. L., Molecular Dynamics Simulation of Atomic Interactions in the Vancomycin Binding Site. *ACS Omega* **2021,** *6* (1), 775-785.

142. Barrett, J. F., Oritavancin. Eli Lilly & Co. *Curr. Opin. Investig. Drugs* **2001,** *2* (8), 1039-44.

143. Arhin, F. F.; McKay, G. A.; Beaulieu, S.; Sarmiento, I.; Parr, T. R., Jr.; Moeck, G., Time-kill kinetics of oritavancin and comparator agents against Streptococcus pyogenes. *Int J Antimicrob Agents* **2009,** *34* (6), 550-4.

144. Goldman, R. C.; Baizman, E. R.; Longley, C. B.; Branstrom, A. A., Chlorobiphenyl-desleucyl-vancomycin inhibits the transglycosylation process required for peptidoglycan synthesis in bacteria in the absence of dipeptide binding. *FEMS Microbiol. Lett.* **2000,** *183* (2), 209-214.

145. Ge, M.; Chen, Z.; Onishi, H. R.; Kohler, J.; Silver, L. L.; Kerns, R.; Fukuzawa, S.; Thompson, C.; Kahne, D., Vancomycin derivatives that inhibit peptidoglycan biosynthesis without binding D-Ala-D-Ala. *Science* **1999,** *284* (5413), 507-511.

146. Beauregard, D. A.; Williams, D. H.; Gwynn, M. N.; Knowles, D. J., Dimerization and membrane anchors in extracellular targeting of vancomycin group antibiotics. *Antimicrob. Agents Chemother.* **1995,** *39* (3), 781-785.

147. Westwell, M. S.; Bardsley, B.; Dancer, R. J.; Try, A. C.; Williams, D. H., Cooperativity in ligand binding expressed at a model cell membrane by the vancomycin group antibioitcs. *Chem. Commun.* **1996**, 580-590.

148. Allen, N. E.; Nicas, T. I., Mechanism of action of oritavancin and related glycopeptide antibiotics. *FEMS Microbiol Rev* **2003,** *26* (5), 511-32.

149. Entress, R. M.; Dancer, R. J.; O'Brien, D. P.; Try, A. C.; Cooper, M. A.; Williams, D. H., 19F NMR in the measurement of binding affinities of chloroeremomycin to model bacterial cell-wall surfaces that mimic VanA and VanB resistance. *Chem. Biol.* **1998,** *5* (6), 329-337.

150. LeTourneau, D. L.; Allen, N. E., Use of capillary electrophoresis to measure dimerization of glycopeptide antibiotics. *Analytical Biochemistry* **1997,** *246* (1), 62-6.

151. Cegelski, L.; Steuber, D.; Mehta, A. K.; Kulp, D. W.; Axelsen, P. H.; Schaefer, J., Conformational and quantitative characterization of oritavancin-peptidoglycan complexes in whole cells of *Staphylococcus aureus* by in vivo ^{13}C and ^{15}N labeling. *J. Mol. Biol.* **2006,** *357* (4), 1253-62.

152. Kim, S. J.; Cegelski, L.; Stueber, D.; Singh, M.; Dietrich, E.; Tanaka, K. S.; Parr, T. R., Jr.; Far, A. R.; Schaefer, J., Oritavancin exhibits dual mode of action to inhibit cell-wall biosynthesis in Staphylococcus aureus. *J Mol Biol* **2008,** *377* (1), 281-93.

153. Humphrey, W.; Dalke, A.; Schulten, K., VMD: visual molecular dynamics. *J Mol Graph* **1996,** *14* (1), 33-8, 27-8.

154. D. H., W., M. S., Searle, M. S., Westwell, U. Gerhard, S. E., Holroyd,, Towards a semi-quantitative description of a bimolecular association involving weak interactions in aqueous solution. *Philox. Trans. R. Soc. London A* **1993,** *345*, 11-21.

155. Cegelski, L.; Steuber, D.; Mehta, A. K.; Kulp, D. W.; Axelsen, P. H.; Schaefer, J., Conformational and quantitative characterization of oritavancin-peptidoglycan complexes in whole cells of Staphylococcus aureus by in vivo 13C and 15N labeling. *J Mol Biol* **2006,** *357* (4), 1253-62.

156. Mehta, A. K.; Cegelski, L.; O'Connor, R. D.; Schaefer, J., REDOR with a relative full-echo reference. *J Magn Reson* **2003,** *163* (1), 182-7.